Evaluation of Long-Hole Mine Design Influences on Unplanned Ore Dilution

By

John Gordon Henning

A thesis submitted to the Faculty of Graduate Studies and Research

in partial fulfillment of the requirements of the degree

Doctor of Philosophy of Engineering

Department of Mining, Metals and Materials Engineering

McGill University

Montreal, Canada

January 2007

Your file Votre référence
ISBN: 978-0-494-32193-5
Our file Notre référence
ISBN: 978-0-494-32193-5

ABSTRACT

Unplanned ore dilution or stope overbreak, which has a direct and large influence on the cost of a stope, and ultimately on the profitability of a mining operation, can be attributed to both the mining process and to geologic setting. The research undertaken in this document, applicable to a wide range of underground mines employing the blasthole mining method to extract tabular orebodies, focuses on examining factors attributable to the generation of unstable stope hanging-walls.

The primary objective of the research undertaken is to establish new models for stope and orezone design, with respect to anticipated stope overbreak, focusing on the position and type of stope within the orezone extraction sequence. Identified factors influencing unplanned dilution, such as: induced stress environment, stope geometry, and the setting of individual stopes are considered.

The research undertaken incorporates a variety of components, including (i) parametric 3-D numerical modelling to examine influences of individual factors on hanging-wall overbreak, (ii) case example analysis, and (iii) orezone extraction sequence simulation, using 3-D elastic numerical modelling. Design criteria, developed from the parametric modelling, was applied to the orezone sequence modelling to develop trends for stope dilution, as functions of stope design and construction.

It was found that hanging-wall overbreak is not significantly influenced by depth alone, and that stopes with large vertical and short horizontal dimensions or stopes having long horizontal and short vertical dimensions are more stable than large square-like stopes. Also, through parametric and case studies, it was demonstrated that, in addition to stope dimension, the amount of unplanned dilution differed according to stope type. Five stope types were identified, based on their position within a tabular blasthole mining sequence. Measured overbreak varies with stope type, with secondary stopes generating a greater volume of

hanging-wall dilution than do primary stopes. A pillarless mining sequence will generate less overall dilution than a primary stope : secondary pillar mining sequence.

RÉSUMÉ

La planification de la dilution des minerais ou du bris hors-profile d'un chantier a une grande influence sur les coûts et la rentabilité du travail dans la mine et ses chantiers. Cette influence peut être attribuée au processus d'excavation et les structures géologiques. Cette recherche peut s'appliquer à plusieurs autres mines qui utilise le même processus d'excavation des minerais (l'abattage par trou de mine profound) pour extraire les gisements de minerai tabulaires. La recherce dans ce document étudie les facteurs qui peuvent être la cause d'instabilité de l'éponte supérieure des chantiers.

Le but ultime de cette recherche est d'établir de nouveaux et de meilleurs modèles pour la conception de chantier en respectant la possibilité du bris hors-profile et en misant sur le type de chantiers et l'ordre d'excavation de la zone minéralisée. Les facteurs qui peuvent influencer la dilution ou le bris hors-profile sont les suivants; les contraintes induites par l'environnement, la géométrie du chantier et l'emplacement des différents chantiers.

La recherche entreprise incorpore une variété de composante, y compri, la modélisation paramétrique en 3-D, afin d'examiner les influences des différents facteurs du bris hors-profile de l'éponte supérieure, l'analyse d'étude de cas et la simulation dans l'ordre d'excavation des minerais en utilisant un modéle numérique en 3-D. Les critères développés à partir de la modélisation paramétrique en 3-D, ont été appliqué à l'ordre d'excavation de la zone mineralisée et les tendances de la dilution des chantiers comme fonction dans la conceptualisation et la construction d'un chantier.

On a constaté que le bris hors-profile de l'éponte supérieure n'est pas sensiblement influencé par seulement la profondeur. Les chantiers ayant de grandes dimensions horizontale et une dimension verticale courte ou les chantiers ayant une grande dimension verticale et une dimension horizontale courte sont

plus stable que celui des chantiers en forme de carres. En outre, par des études de cas et des etudes paramétriques on a démontré qu'en plus de la dimension de chantier, la quantité de la dilution des minerais diffère selon le type de chantier. Cinq types de chantiers ont été identifiés, basé sur leur position et de l'ordre d'excavation des minerais. Le volume du bris hors-profil dépend du type de chantier. En effect, les chantiers secondaires produisent un plus grand volume de dilution que les chantiers primaires. De plus, l'ordre ou la séquence d'excavation sans pilier produit moins de dilution globale que l'excavation de la séquence d'un chantier primaire et d'un chantier secondaire.

TABLE OF CONTENTS

LIST OF TABLES

LIST OF FIGURES

ACKNOWLEDGEMENTS

I wish to express my appreciation to my supervisor Dr. Hani S. Mitri for his continuing guidance and direction throughout the period of my study. Without his encouragement, this work would not have come to its current state of development.

Thanks are also due to Agnico-Eagle Mines Limited for allowing me to make use of the data gathered at the Bousquet #2 Mine.

Finally, I would like to thank my wife Anne and daughters Kimberly and Cynthia for their patience and encouragement throughout the study.

CHAPTER 1

INTRODUCTION

1.1 Background

In a global competitive market, there is pressure on mines to maximize production, increase revenue and reduce costs. Unplanned ore dilution, illustrated in Figures 1.1 and 1.2, has a direct and large influence on the cost of a stope, and ultimately on the profitability of a mining operation. The economic impact of dilution is due to costs associated with the mucking, haulage, crushing, hoisting, milling, and treatment of waste or low grade rock having little or no value, displacing profitable ore and processing capacity. The additional time required for excavation and backfilling of the larger stope volumes produced by the extraction of waste rock can also lead to unscheduled delays, changes to the mining schedule, and potentially, development rehabilitation costs.

As will be shown later in this report, stope overbreak can be attributed to both the mining process (engineering design, stope sequencing, drilling and blasting), and to geologic setting (rockmass quality and stress environment). Efforts to reduce unplanned dilution require an understanding of all the influences that directly or indirectly provoke wall rock caving into a stope.

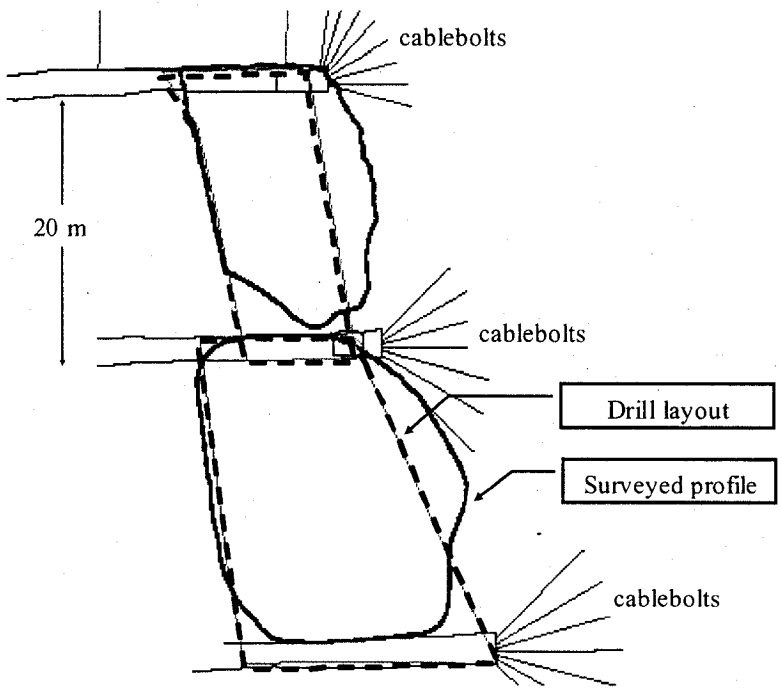

Figure 1.1 Surveyed stope overbreak, Kidd Creek mine, after Tannant et al., 1998.

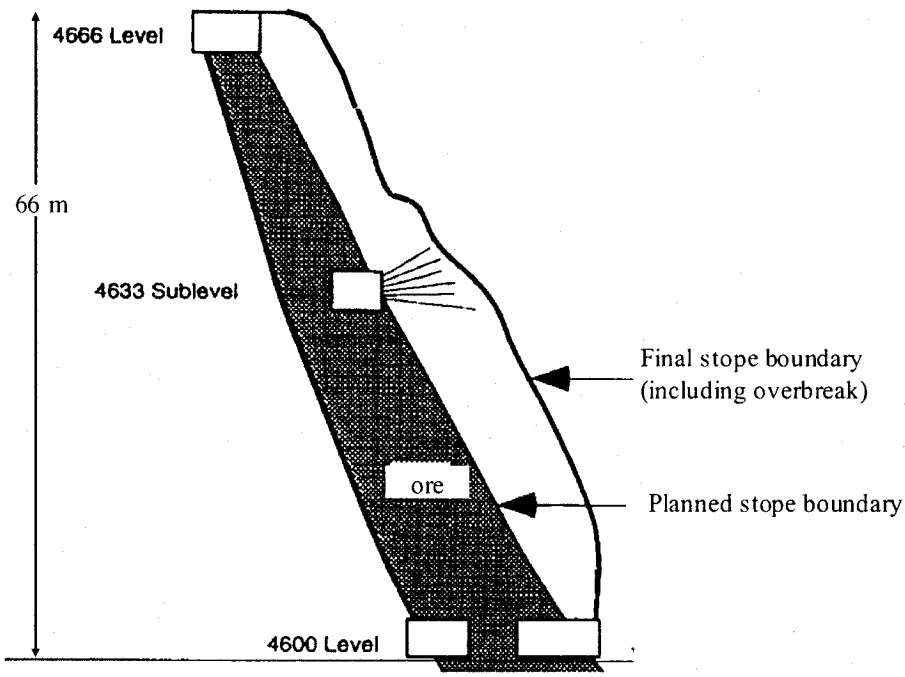

Figure 1.2 Stope dilution surveyed, Golden Giant mine, after Anderson and Grebenc, 1995

1.2 Research objective

Rock mechanics can play an important role in reducing or controlling the effects of dilution. The extent and source of stope wall shoughage can be measured and quantified. This observed overbreak can be linked to the prediction of the stability of an exposed rock surface by empirical or numerical modelling techniques. As a result, predicted overbreak departing from the initial stope design can be controlled through improved stope design. It is intended that, through the research described in this thesis, to establish relationships between the parameters identified as influencing stope overbreak, and to assess alternatives for orezone sequencing and stope dimensioning.

Dilution can occur from any surface exposed by stope extraction, such as footwall, sidewalls, and roof. This thesis places emphasis on hanging-wall dilution, which is the dominant source of dilution in tabular orebodies. The focus of this research is on factors attributable to the generation of unstable stope hanging-walls, such as stope extraction and effectiveness of stope hanging-wall reinforcement. The primary objective of the tasks undertaken in this research is to establish new models for stope and orezone design, with respect to anticipated stope overbreak, focusing on the position and type of stope within the orezone extraction sequence. Identified factors influencing unplanned dilution, such as: induced stress environment, stope geometry, and the stope setting within the orezone extraction sequence are considered.

Additional goals of this work are:

- Enhance understanding of factors contributing to ore dilution on metal mines,
- Review and compile currently available mathematical and empirical models, for the estimation of variation of ore dilution,
- Increase the value of stope recovery information for (1) mine design, and (2) operational decision-making,
- Develop a Canadian mine-based geomechanical data bank, and

- Construct fundamental models to characterize the stoping environment most frequently encountered in longhole mines. Such model will serve as a tool for a quantitative evaluation of ore dilution, taking into account factors such as mining variability and various mining methods.

This work described in this thesis will be applicable to a wide range of underground mines employing the blasthole mining method. Orezones at these mines are generally tabular, with ore widths of 4 to 15 meters. Numerous Canadian mines use the blasthole mining method. Examples from Ontario and Quebec include: Agnico-Eagle, Bouchard-Hébert, Bousquet, Creighton, Doyon, Garson, Golden Giant, Kidd Creek, Louvicourt, Musselwhite and Williams mines, (Canadian Mining Journal, 2002).

1.3 Thesis structure

This thesis is organized into seven chapters, which by themselves can stand alone. Thesis structure progresses from the general to the specific. This introductory chapter is followed by Chapter 2, which reviews dilution sources, the impact of dilution on the mine operation and empirical approaches for estimating of unplanned dilution. Chapter 3 reviews blasthole mining methods, and examines parameters influencing ore dilution in the blasthole stoping environment.

In Chapter 4, numerical modelling tools are discussed, followed by an examination of model design parameters, such as stope geometry, stress setting, stope type and rockmass quality, appropriate to a typical Canadian blasthole mine environment. Numerical modelling input parameters are analysed in a series of parametric studies, presented in Chapter 5. Chapter 5 defines two new terms used in the research to quantify overbreak: Dilution Density (DD) and measured Dilution Density (DD_{cms}).

Chapter 6 introduces the mine and orezones where the case histories are compiled. Stope geometry, construction, and setting are described in detail. Stope excavation details, including measurements of stope dilution, stope sequencing

and stope type, obtained from a comprehensive database of 172 stope histories are analysed. 3-D numerical modelling of the extraction sequence of the two orezones, is then described. The chapter concludes with discussions of dilution severity associated with identified stope types and draws comparisons between modelled dilution estimates and measured values.

Chapter 7 presents concluding remarks and provides suggestions for future research.

CHAPTER 2

METHODS OF ORE DILUTION ESTIMATION

2.1 Definition of dilution

The term 'dilution' refers to any waste material within the mining block, including barren and subgrade rock and backfill. Mine dilution, defined as "the contamination of ore with barren (or below-cutoff-grade) waste wall rock", Tatman (2001), is a common and devastating mine disease, (Miller et al., 1992). Tintor (1988) and Knoll (1989) reported that many operations have closed because of uncontrolled dilution, including some in their first year of production. According to Taylor (1994), dilution tends to be the most consistently underestimated factor in mine planning.

Increasing ore dilution results in a decrease of hoisted grade in comparison with the mining reserves, (Planeta et al., 1990). Dilution negatively influences the profitability of mining operations. Dilution lowers the quantity of mineral or metal that can be produced from each tonne of ore processed in mining/milling operations. Metal losses reduce the recovery and the economic return from a non-renewable resource, (Vallée et al., 1992).

Dilution is a qualitative parameter that enables the mine operator to evaluate quality of design, (Pakalnis, 1986). Traditionally, the mining industry has used the dilution concept to define the negative differences between forecasts and production results (Vallée et al., 1992). Dilution and sacrifice of ore tend to be inseparable factors, with a trade-off between optimum recovery and impairment

of grade. Inadequate attention to stope design can quickly eliminate profitability from high productivity bulk mining methods, Bawden (1993) and Pelley (1994).

2.1.1 Dilution Type: planned and unplanned dilution

Dilution can refer to either a measure of external waste (unplanned dilution) that has sloughed from the stope wall, or to material that is of lower grade than cut-off, but which is included in the mineral deposit, reserve or stope outline and extracted with the mining of ore (planned dilution). Only unplanned dilution is considered in this study.

Scoble and Moss (1994) define "total dilution" as the sum of planned dilution plus unplanned dilution, illustrated in Figure 2.1. Planned (or internal) dilution is defined as non-ore material (below cut-off grade) that lies within the designed stope boundaries as determined by: selectivity of mining method, orebody continuity (along strike and dip), or complexity of orebody shape. Planned dilution is a factor considered when estimating ore reserve blocks (Tatman, 2001).

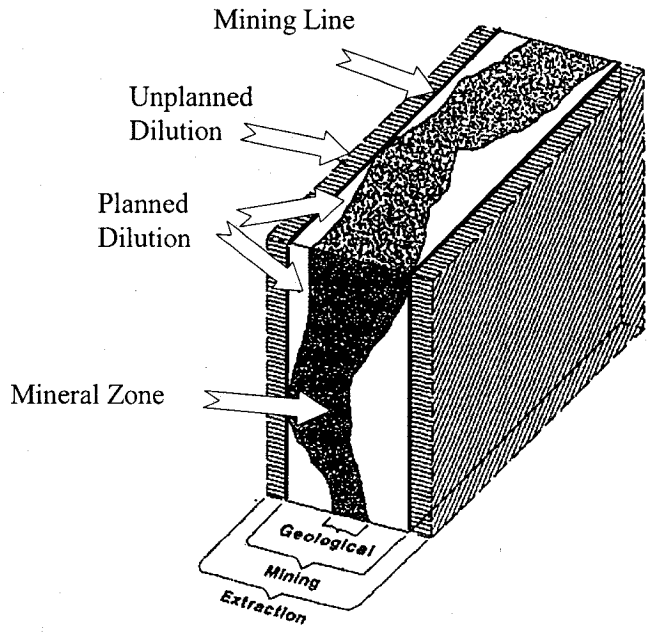

Figure 2.1 Illustration of planned and unplanned dilution, after Scoble and Moss (1994)

Unplanned dilution refers to additional non-ore material derived from rock or backfill outside the stope boundaries due to blast induced overbreak, sloughage of unstable wall rock, or sloughing of backfill, (Scoble and Moss, 1994). Components of dilution, including unplanned dilution from the stope hanging-wall and footwall, are illustrated in Figure 2.2. The term 'overbreak' is synonymous with unplanned wall dilution (Yao et al., 1999).

Other terms used to describe dilution type are: intentional and unintentional dilution (Annels, 1996), primary and secondary dilution (Olsson and Thorshag, 1986), and planned and additional dilution (Planeta et al., 1990). Unplanned dilution has also been referred to as accidental dilution (Corlett, 1970). Accidental dilution results from failure to appreciate the conditions that bring it about, or the effectiveness of the precautions taken to prevent it. External dilution refers to rock or fill outside the ore envelope that is removed with the ore: either planned or unplanned.

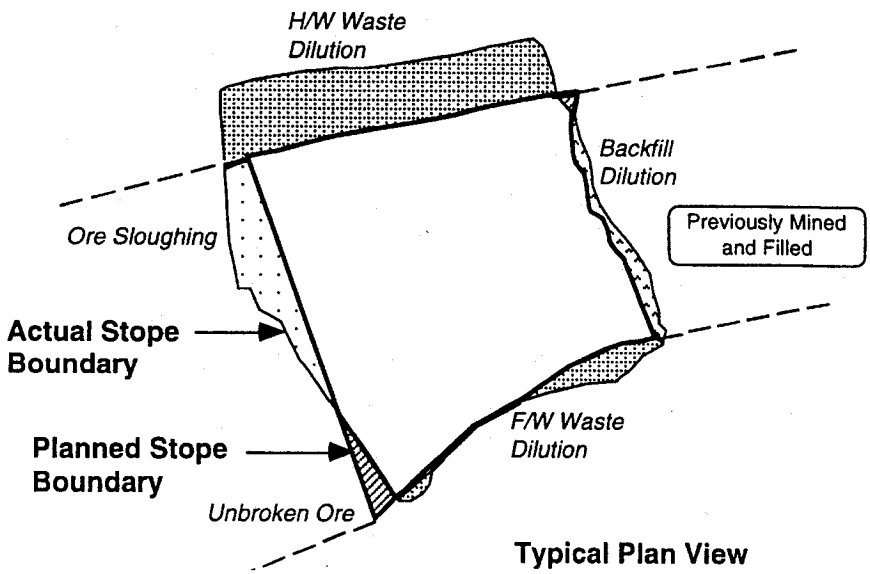

Figure 2.2 Plan view of stope showing the components of dilution, (Anderson and Grebenc, 1995)

2.1.2 Dilution reporting

Production control has traditionally been based on weight of rock hoisted, rather than the weight of metal. As a result of poor accessibility to data, many mines are unable to collect adequate data to calculate dilution with any precision (Scoble and Moss, 1994).

A value of dilution is recorded by most mines, (Canadian Mining Journal, 2002), although not in an identical manner. A survey of mines throughout Canada by Pakalnis (1986) identified nine variations on a definition of dilution. These are presented in Table 2.1.

Table 2.1 Definitions of Dilution (Pakalnis, 1986)

Definitions of Dilution:	
Dilution = (Tons waste mined) / (Tons ore mined)	(2-1)
Dilution = (Tons waste mined) / (Tons ore mined + tons waste mined)	(2-2)
Dilution = (Undiluted in-situ grade as derived from drill holes) / (Sample assay grade at drawpoint)	(2-3)
Dilution = (Undiluted in-situ grade of reserves) / (mill head grades obtained from same tonnage)	(2-4)
Dilution = (Tonnage mucked – tonnage blasted) / (Tonnage blasted)	(2-5)
Dilution = Difference between backfill tonnage actually placed and theoretically required to fill void	(2-6)
Dilution = Dilution visually observed and assessed	(2-7)
Dilution = ("x" amount of meters of footwall slough + "y" amount of hanging-wall slough) / (ore width)	(2-8)
Dilution = (Tons drawn from stopes) / (Calculated reserve tonnage) over the last 10 years	(2-9)

Dilution is usually calculated as a percentage:

$$\text{Percent dilution} = (\text{units of dilution} \cdot 100)/\text{units of ore} \qquad (2\text{-}10)$$

In their review of Canadian mining practices, Scoble and Moss (1994) reported that Equations 2-1 and 2-2 were the most widely used. Of these two, Equation 2-1 was recommended as a standard measure of dilution (Pakalnis et al., 1995), as it was more sensitive to wall sloughage. For example, a 2:1 sloughage-to-ore ratio produces a 66% dilution factor according to Equation 2-2, whereas Equation 2-1 produces a dilution factor of 200%.

Common variations of Equation 2-1 include:

- Dilution = (Tons waste milled) / (Tons ore milled), where waste is wall rock outside of the planned stope boundary, and ore refers to rock planned, drilled and blasted within the stope boundary, (Gauthier, 2001).
- Dilution = (External Dilution + Internal Dilution + Fill Dilution) / Recovered Ore, (INCO, 2002).
- Dilution = (Waste tonnes + Backfill tonnes) / Planned tonnes, (Anderson and Grebenc, 1995).
- Dilution = volume of wall slough beyond the planned mining outline / volume of ore mined within the planned mining outline, (Yao et al., 1999).
- Dilution = (CMS area – ore reserves)/ore reserve, (Mah et al., 1995). Ore reserve refers to the designed stope outline; CMS is discussed in Section 2.6.

2.2 Sources of dilution

Most underground mines experience some form of dilution. Dilution values volunteered by industry in a survey of Canadian underground mines, revealed typical amounts in the range of 10% to 25%, with extremes in excess of 60%, (Canadian Mining Journal, 2002). A survey of open stope dilution severity, undertaken by Pakalnis (1986) found that, of the fifteen mines surveyed, 47% of the operations reported dilution exceeding 20%, 21% of the mines had dilution amounts exceeding 35%.

2.2.1 Planned dilution sources

2.2.1.1 Design of the mining method

Dilution takes place wherever the ore contours are irregular. Irregular walls may also be the cause of metal loss (Vallée et al., 1992). Production stopes are the main sources of dilution when mining irregular, small thickness or narrow vein deposits, (Elbrond, 1994), or when unsuitablely sized equipment has been selected (Trevor, 1991). In the case of narrow veins, it may be necessary to widen the working place and include some waste material in the stream of production if this material cannot be moved separately (Planeta et al., 1990).

For unique situations when stope width exceeds the deposit thickness, mining methods specifically designed to minimize planned dilution (Xishan, 1998; Whiteway, 1988) have not been embraced by underground mine operations, which tend to prefer traditional stoping methods, such as blasthole stoping (Canadian Mining Journal, 2002).

2.2.1.2 The mining operation

The contact between ore and subgrade material cannot be followed in detail due to a lack of flexibility of the drilling machines and blasting utilized by the mining operation (Elbrond, 1994). Some ore (above the cut-off grade) will be lost and some material below cut-off grade will be drilled, blasted, loaded and transported to the concentrator with the valuable ore.

2.2.2 Unplanned dilution sources

2.2.2.1 Stope wall instability

Stope wall stability is adversely affected by blasting damage (Vallée et al., 1992). When overbreak causes the rupture of an individual bed or structural feature on the stope hanging-wall it is difficult to prevent failure of the remainder of that feature into the open stope (Pelley, 1994).

Dilution takes place wherever the ore contours are irregular, or the low mechanical strength of the wall results in additional material being dropped into the stope. Incompetent walls can cause extreme dilution, (Elbrond, 1994). Graham (1968) describes 100% dilution in the presence of incompetent walls (chlorite walls). Mechanical wall dilution may be reduced by not emptying the stope completely before blasting new rounds, (Vallée et al., 1992).

2.2.2.2 The mining operation

Unplanned dilution can be created by wall delimitation errors due to drill set-up errors, such as blast-drillhole angle or drillhole deviation (Vallée et al., 1992).

2.2.2.3 Handling of material

Mucking errors in ore and waste handling, such as dispatching of waste rock into the ore passes (Vallée et al., 1992; Trevor, 1991) are identified as another source of unplanned dilution. Sources of waste rock include waste rock from lateral and vertical development, backfill failures into a stope during mining, and the caving of barren rock into the stope during mining (Planeta et al., 1990).

2.2.2.4 Backfill dilution

Backfill dilution can occur in two ways (Pelley 1994): (i) If overbreak reduces the size of the secondary stope the backfill now contained within the original volume is often designated into the system, and (ii) Failure of free standing fill faces. The type of material and the method of emplacement may be factors in how much backfill contributes to dilution, (Trevor, 1991).

2.2.2.5 Dilution as a function of mine age

As an ore body is progressively mined, from initial development through to primary stope mining, pillar recovery and closure, the source and amount of dilution increases. The dilution / mine age relationship, as suggested by (Trevor, 1991), is illustrated in Figure 2.3.

During early mining, dilution is associated with a learning curve associated with mining operations in a new environment and a lack of knowledge about the orebody, (Scoble and Moss, 1994). Dilution stabilizes with primary stoping. At the late stages of mining, associated with pillar recovery and deteriorating ground conditions, the amount of dilution increases.

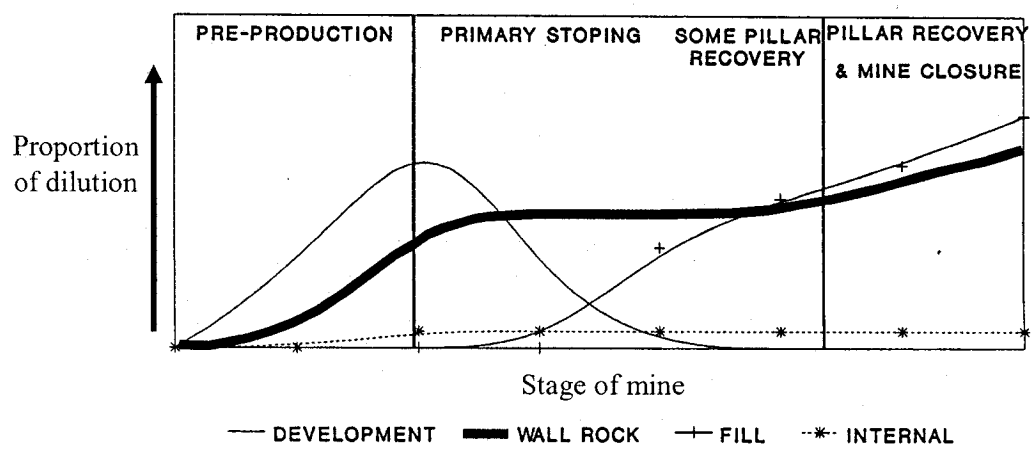

Figure 2.3 Schematic illustration of dilution source as a function of mine age. Relative amount of unplanned dilution is plotted on vertical axis, (Trevor, 1991)

2.3 Orezone width

Narrow stopes, mined by longhole method, are generally victims of considerable dilution: the narrower the zone is, the more important the border effects, (Vallée et al., 1992). For example, if both the hanging-wall and footwall of a steeply dipping 1.5m wide tabular deposit contributes 0.3m of overbreak, then an unplanned mining dilution of 40% results. If this orezone was 3.0m thick, mined in the same conditions, the resulting dilution factor becomes 20%. Dilution relationships between stope wall sloughage and stope width are described in (Pakalnis et al., 1995), and illustrated in Figure 2.4.

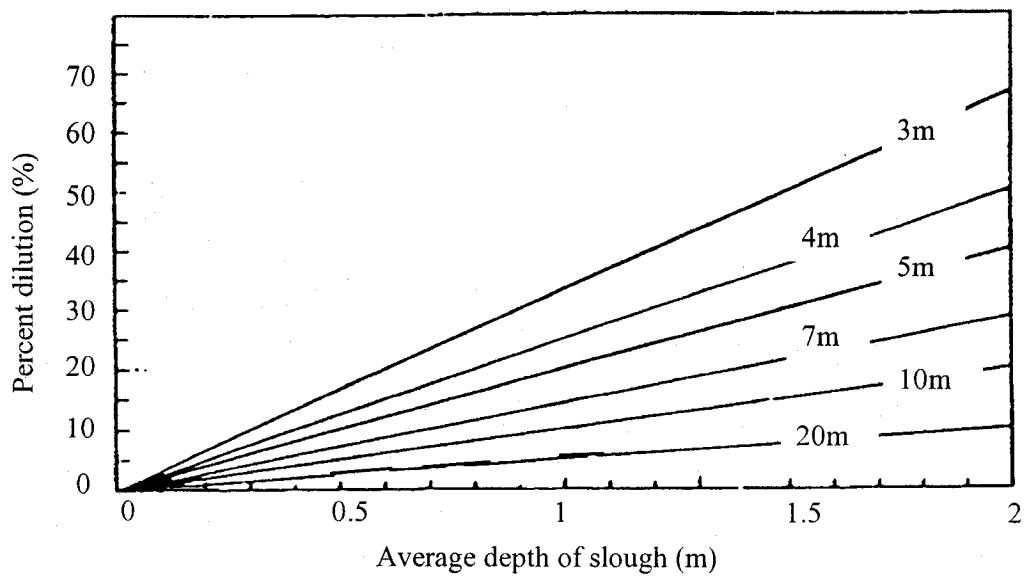

Figure 2.4 Dilution as a function of stope width, (Pakalnis et al., 1995)

O'Hara (1980) compared stope width against stope wall sloughage as functions of stoping method, stope dip angle, and stope wall rock competence. Plotted results, shown in Figure 2.5, illustrate dilution increase due to stope width. Of the three mining methods compared (blasthole, shrinkage, and cut and fill), overbreak was more severe with the blasthole stopes.

The angle at which the stope dipped influenced dilution. Vertical stopes had lower dilution amounts. For blasthole stopes, O'Hara (1980) predicted dilution by the following relationship:

$$\% \text{ Dilution} = 100/W^{0.5}\sin A^{\circ} \qquad (2\text{-}11)$$

where W = stope width (ft), and A° = Orebody dip angle

The curves of Figure 2.5 shifted up or down to reflect stope wall rock competence (O'Hara, 1980). When stope wall rock is regular and competent, dilution may be 70% of that plotted. Dilution may increase to 150% of the plotted data when stope wall rock is unusually weak and incompetent.

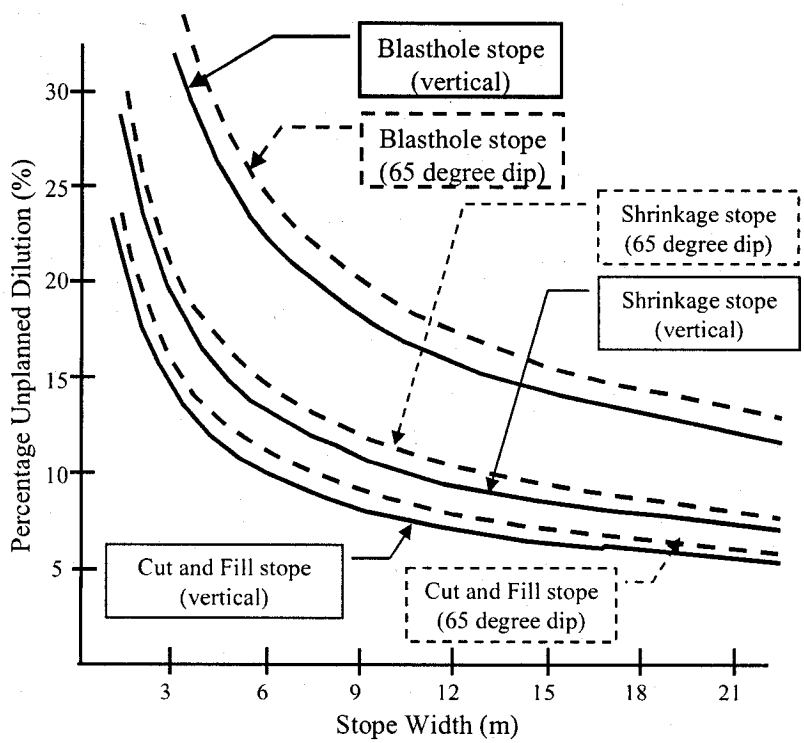

Figure 2.5 Comparison of stope width against stope wall sloughage as functions of stoping method and stope dip angle, modified from O'Hara (1980)

2.4 Equivalent Linear Overbreak/Slough

To express dilution independently of stope width, Dunne and Pakalnis (1996) suggested that dilution values be calculated average metres of wall slough per square metre of wall (m/m2), rather than percent dilution.

Equivalent Linear Overbreak/Slough (ELOS) is a method of converting the volumetric CMS measurement into an average sloughage depth over the entire stope surface. A schematic diagram of ELOS is presented in Figure 2.6. For a given stope surface, ELOS is calculated as follows, (Connors et al., 1996):

$$\text{ELOS} = \frac{\text{Volume of slough (overbreak) from stope surface}}{\text{stope height} \cdot \text{wall strike length}} \qquad (2\text{-}12)$$

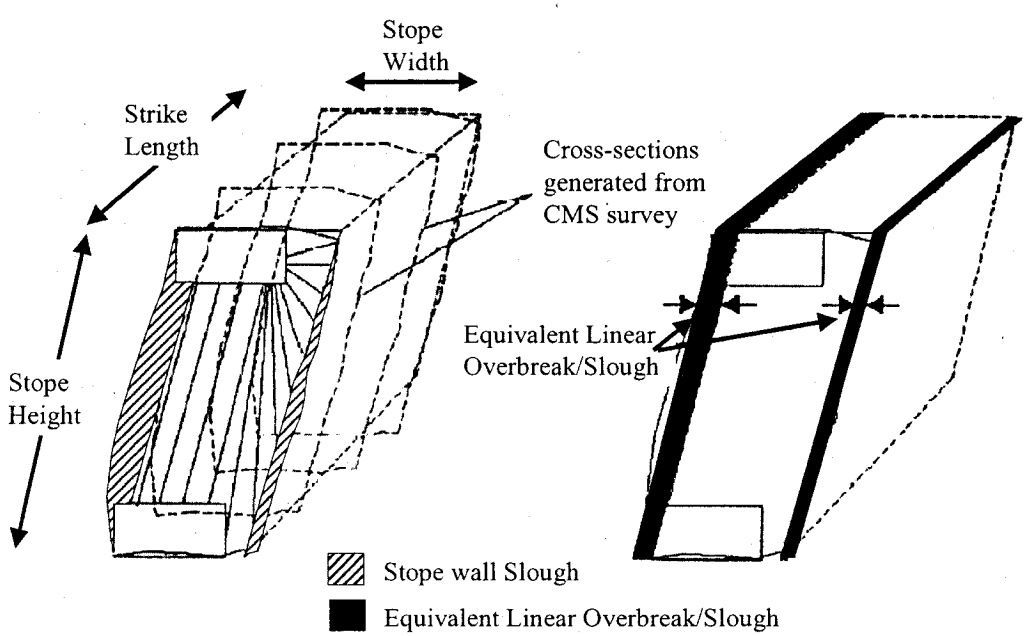

Figure 2.6 Schematic illustration of ELOS parameter, modified from Clark and Pakalnis (1997)

In a blasthole stoping example reported by Gauthier (2001), dilution associated with a 10 meter-wide stopes were compared against narrower 5 meter-wide stopes. The higher percent dilution of the narrower stopes reflects the influence

of stope width on dilution calculation. To calculate dilution independently of stope width, the ELOS approach was used. ELOS values, representing average metres of sloughage per square metre from both stope walls are provided in Table 2.2.

Table 2.2 Comparison of surveyed stope dilution with average sloughage depth over the entire stope surface, Gauthier (2001)

Stope width	Total Dilution	Total ELOS
10 meter-wide stopes	22% to 25%	1.9 to 2.3 m/m^2
5 meter-wide stopes	32 %	1.9 m/m^2

An advantage of reporting stope sloughage in terms of ELOS is that its meaning in terms of dilution is readily apparent. For example, a predicted ELOS of 2 meters for a 6 meter wide stope corresponds to an unplanned dilution of 33%, assuming that the slough rock has no economic grade. A second advantage is that the source of unplanned dilution can be associated with individual stope walls, such as hanging-wall and footwall.

2.5 Dilution impact on the mine operation

Length of mine life, net present value, cost of producing metal and loss of metal are all affected by dilution (Elbrond, 1994; Tatman, 2001). The realized grade from a mineral deposit rarely measures up to the pre-production estimate, (Trevor, 1991). Dilution constitutes a severe constraint on economical result of a mine by increasing production cost and by reducing the mineral base and the net present value. Ore dilution larger than foreseen may jeopardize the feasibility of the mining investment decision (Elbrond, 1994; Clow, 1991; Germain et al., 1996).

There is an inverse correlation between dilution severity and the final grade of ore, as illustrated in Figure 2.7. The level of acceptable dilution is highly

dependant upon grade since a higher grade stope can be economical, whereas a lower grade stope with the same dilution may no longer be mineable, (Pakalnis, 1986).

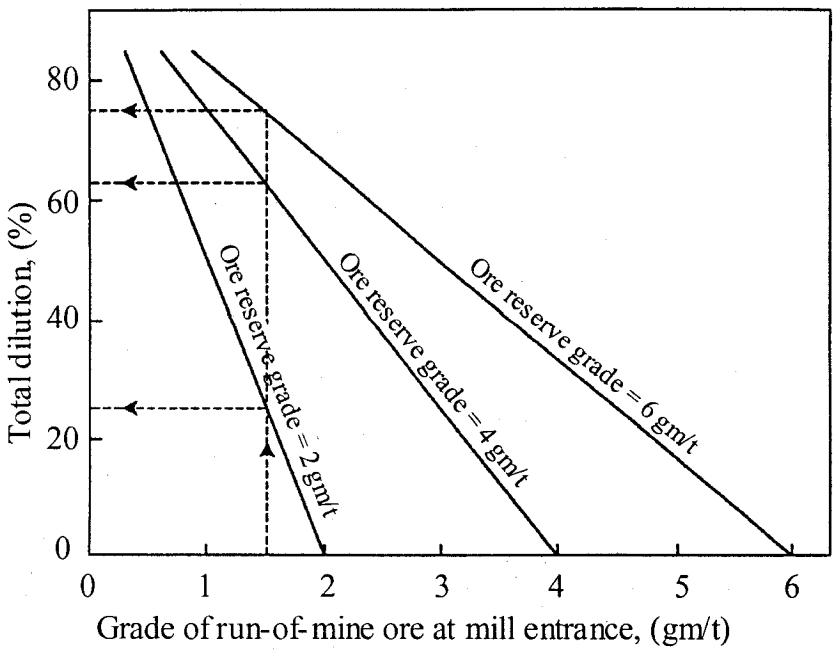

Figure 2.7 Influence of dilution on ore reserve grade, (Planeta et al., 1990)

Ore losses and dilution are significant and have considerable effects on the economical results of a mining operation. The most serious economic consequence of dilution is when this prevents the operator from milling ore. Anderson and Grebenc (1995), report 13.6% overall dilution at the Golden Giant Mine. As a result of this unplanned dilution, the mine was operating at 86.4% capacity despite producing at maximum possible milling rate. The direct cost of mining, milling and administration to handle the unplanned dilution was reported as $5.4 million annually.

Dilution in open stopes reduces over-all grade and adds to haulage and milling costs. In some cases this can result in significant loss of reserves. Values presented in Bawden et al. (1989), revealed that stope wall dilution, hoisted and

milled, reduced stope profitability in a base metal mine by approximately $8 per tonne.

Dilution also has an adverse effect on operating costs, as more tons must be mined to yield the same metal content as the undiluted ore. Metal grade of each ton of diluted ore is reduced and mill recovery will consequently be lower (O'Hara, 1980). A case study from a zinc orebody by Bawden et al. (1989) illustrated the importance of dilution on the Rate of Return. The case study showed dilution in the order of 30% resulted in a negligible rate of return for the orebody with grade of 20% zinc. An economically attractive property can result in economic failure due strictly to what many would consider "moderate" dilution. Trends from the case study are shown in Figure 2.8.

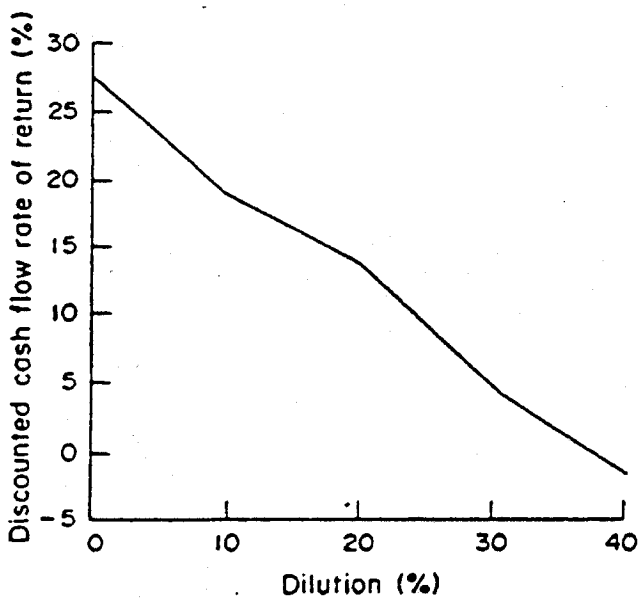

Figure 2.8 Influence of dilution on rate of return, (Bawden, 1993)

Every tonne of dilution costs in the neighbourhood of $20 to $30, (Trevor, 1991), and Miller et al. (1992). The presence of low grades of metals in the waste rock can reduce the net cost of unplanned dilution. Effective dilution control offers very real financial benefits as the only revenue a mine has is generated by ore.

Relationships between dilution reduction and increase in profit are shown in Figure 2.9. Bawden (1993) described that a 10% decrease in dilution would mean an increase of approximately 6% on the Rate of Return of the property. In an example provided by Dunne and Pakalnis (1996), where the cost of dilution was reported as $30/tonne, a 1% decrease in dilution from a mine design budgeted at 500,000 tonnes would yield a cost saving of $150,000.

Another form of dilution occurs when backfill fails and falls into adjacent stopes as they are being mined. This form of dilution is very costly to a mine because the failed backfill has no mineralization that can help to offset the cost, and the mine must essentially pay twice for the cost of placing the fill. Usually with fill failure there are few problems with oversize so that secondary blasting costs are not included in the cost for fill failure. The cost for dilution from backfill is in the range of $55 per tonne, (Board et al., 1996).

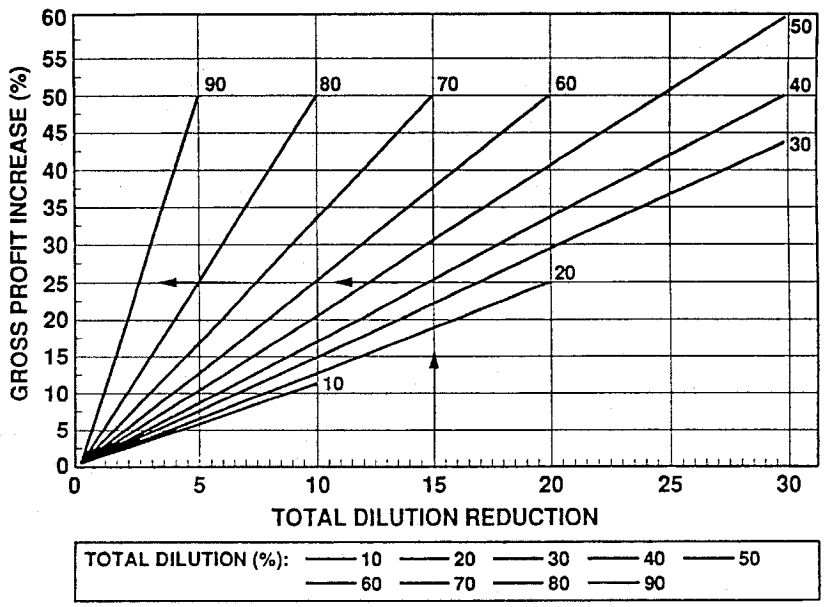

Figure 2.9 Gross profit increase as a function of total dilution reduction, (Planeta et al., 1990)

2.5.1 Indirect dilution costs

Dilution has both direct costs (dilution tons displace ore tons in the ore handling and process circuits) and indirect costs: each ton of sterile rock or backfill that circulates through the mill carries mineral values with it to the tailings, De la Vergne, (2000).

Dilution generally enters the stope as oversize sloughed or caved waste wall rock, requiring secondary drilling and blasting. If dilution results in the plugging of drawpoints, serious production delays may be incurred. In the worst case the stope may be lost, (Bawden et al., 1989).

With unplanned dilution, stope mucking time may be extended due to: (i) the increased tonnage to be mucked from the stope due to the additional dilution tonnage, and (ii) stope brow hang-ups due to oversize muck. Increased length of time required to muck out a stope affects the mine schedule by postponing the development and mining of adjacent stope panels. Anderson and Grebenc (1995) documented a case example of the relationship between unplanned dilution and stope mucking cycle. Their results, illustrated in Figure 2.10, indicate that stope mucking time increased by 50% above the planned mucking time, in what many would consider "moderate" dilution conditions of 20% dilution.

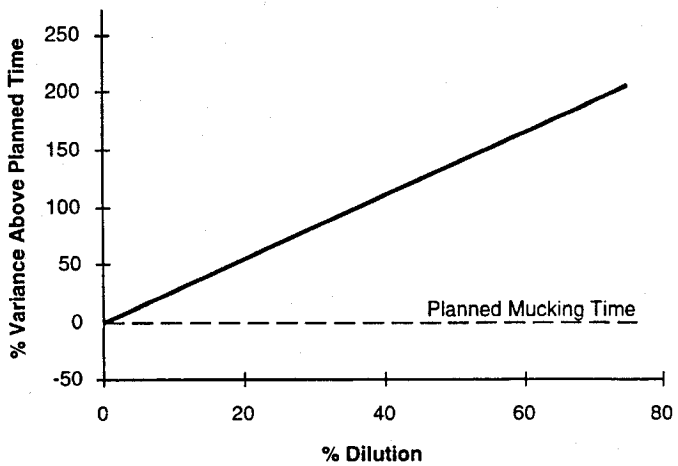

Figure 2.10 Increased length in time required to muck a stope due to unplanned dilution, Anderson and Grebenc (1995)

2.6 Quantification of dilution

The measurement of mined stope profiles has traditionally been difficult, due to the non-entry nature of the open stope mining method. The dimensions of mined stope walls have been estimated from visual observations, drilling test holes to break through into a stope, and with hand-held or tripod mounted rangefinders. Skeeles and Semier (1991) describe open stope surveys using a theodolite and laser range finder. Other methods include stope mucking calculations, back-calculation from mill recovery, and rules of thumb.

2.6.1 Laser measurement of mined stope profiles (the Cavity Monitoring System)

In recent years, accurate surveying of excavated stope surfaces has been made possible with the application of automated non-contact laser rangefinders. The Cavity Monitoring System, (CMS), was developed jointly by the Noranda Technology Center and Optech Systems. The CMS, described by Miller et al., (1992), consists of reflectorless laser rangefinder, which is extended up to 5 metres into the stope cavity at the end of a boom support, as shown in Figure 2.11.

The CMS offers a volume-based technique for directly measuring stope performance. First implemented by the Canadian mining industry, (Anderson and Grebenc, 1995; Mah et al., 1995; Germain et al., 1996; Yao et al., 1999), it is now adopted by mines world-wide (Calvert et al., 2000; Uggalla, S., 2001).

The rangefinder is housed in a motorized assembly capable of rotating 360 degrees about the boom axis and up to 135 degrees about the pivot axis, defining a sphere of 270 degrees. The CMS has the capacity to survey stope voids up to 100 metres high when visibility within the stope is clear. In complex-shaped stopes, effective range of the CMS is in the range of 20 metres (Mah et al., 1995).

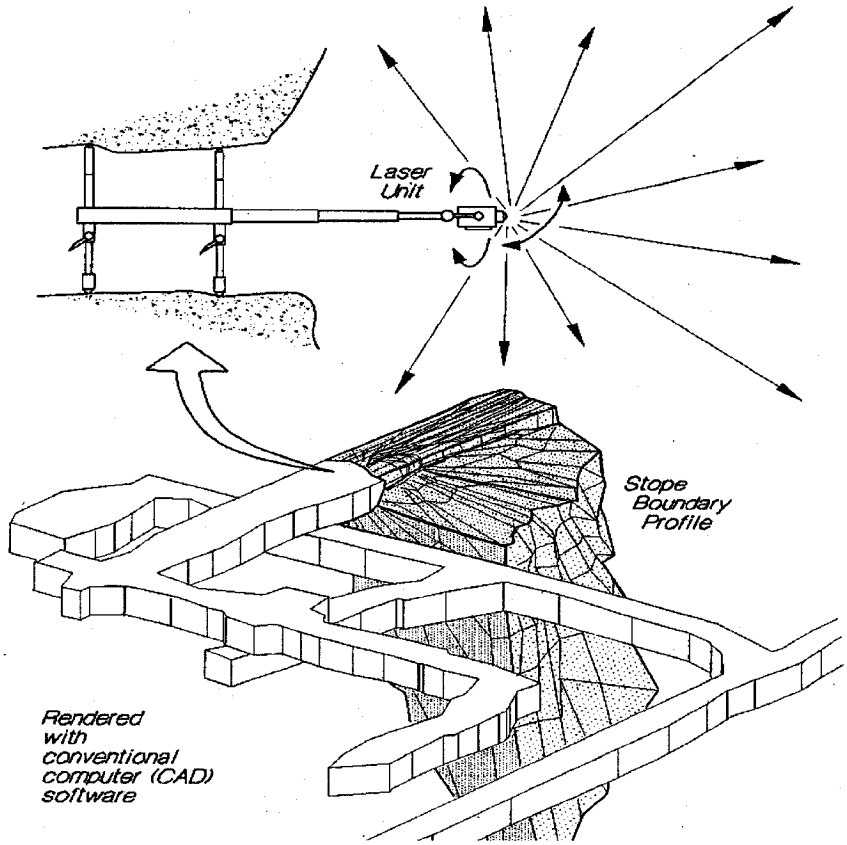

Figure 2.11 Cavity Monitoring System, (Hutchinson and Diederichs, 1996)

The CMS is programmed and activated remotely with a hand-held controller and data logger. Output from the CMS can be converted to a three-dimensional (3-D) polyline mesh, containing up to 50,000 points in space, for input into AutoCAD software to produce 2-D or 3-D data visualization. 2-D sections generated can be compared against the mining plans to identify areas of unplanned dilution (overbreak) or unmined ore (underbreak). The major advantage of the system is that it gives the true volume of the void, allowing stope reconciliation and stope performance evaluation. Shortcomings of CMS include: muck left at the base of the stope, set-up errors, hidden or blind spots in the geometry of the stope, distance (range of scanner), and occurrences suspended dust, blasting smoke, and humidity (fog) inside the stope.

2.7 Empirical analysis

CMS data provides a record of how different stope geometries perform in a particular quality rockmass, or mining induced stress environment. Empirical back-analysis of CMS stope stability data can provide useful predictions of dilution or sloughage for particular stope design.

An approach reported by Connors et al. (1996), employs rockmass classification and the Stability Graph method to predict the extent or severity of Equivalent Linear Overbreak/Slough (ELOS) is described below. Other approaches at quantifying hanging-wall behaviour using the Stability Graph method are reported by Milne et al. (1996) and by Germain et al. (1996).

2.7.1 Stability Graph method

The Stability Graph method for open stope design, developed by Mathews et al. (1981), and modified by others, including Potvin (1988), Nickson (1992), and Mawdesley et al. (2001), combines information about rockmass strength and structure, the stresses around the opening and the size, shape and orientation of the opening to predict stope stability. A widely employed version of the Stability Graph is provided in Figure 2.12.

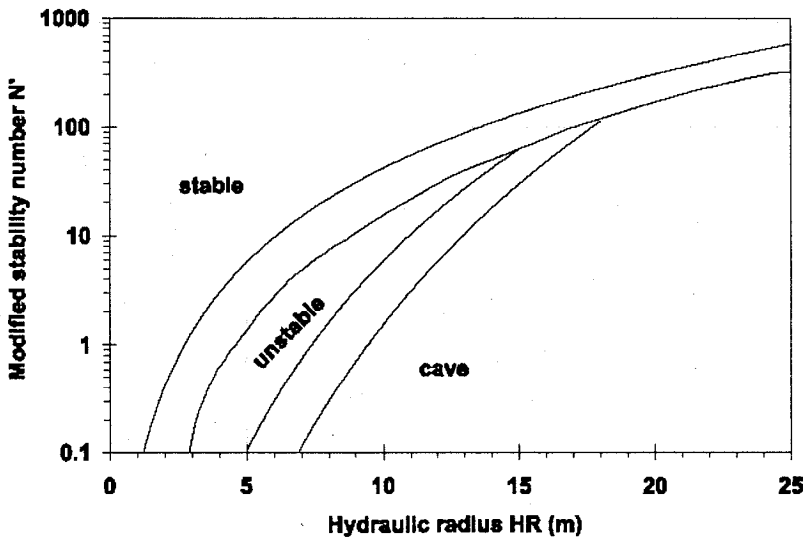

Figure 2.12 Stability Graph for open stope design, after Nickson (1992)

Two parameters are needed to assess stope wall stability: the Stability Index number (N'), which is a measure of the rockmass ability to stand up under a given stress condition, and the "hydraulic radius" (HR), which represents the dimensions of the stope face. The Stability Index, N', is defined as:

$$N' = Q' \cdot A \cdot B \cdot C = \frac{RQD}{Jn} \cdot \frac{Jr}{Ja} \cdot A \cdot B \cdot C \qquad (2\text{-}13)$$

Where Q', the modified Rock Tunneling Quality Index, corresponds to the first four terms from Q classification system (Barton et al., 1974). A is the rock stress factor, accounting for stresses acting at the free surfaces of open stopes at depth. B is the joint orientation adjustment factor, which represents the destabilizing influence of oblique structure. A, B and C are defined in Figure 2.13. The gravity adjustment factor, C, depends on the inclination of the stope surface, is determined from the following relationship (Hoek et al., 1995):

$$C = 8 - 6 \cdot \cos\alpha \qquad (2\text{-}14)$$

where α = the stope surface inclination

The second parameter required for a stability analysis is the hydraulic radius, HR, is equivalent to the face area divided by the face perimeter, as indicated in Equation 2-15.

$$HR = \frac{\text{Area of surface analyzed}}{\text{Perimeter of surface analyzed}} \qquad (2\text{-}15)$$

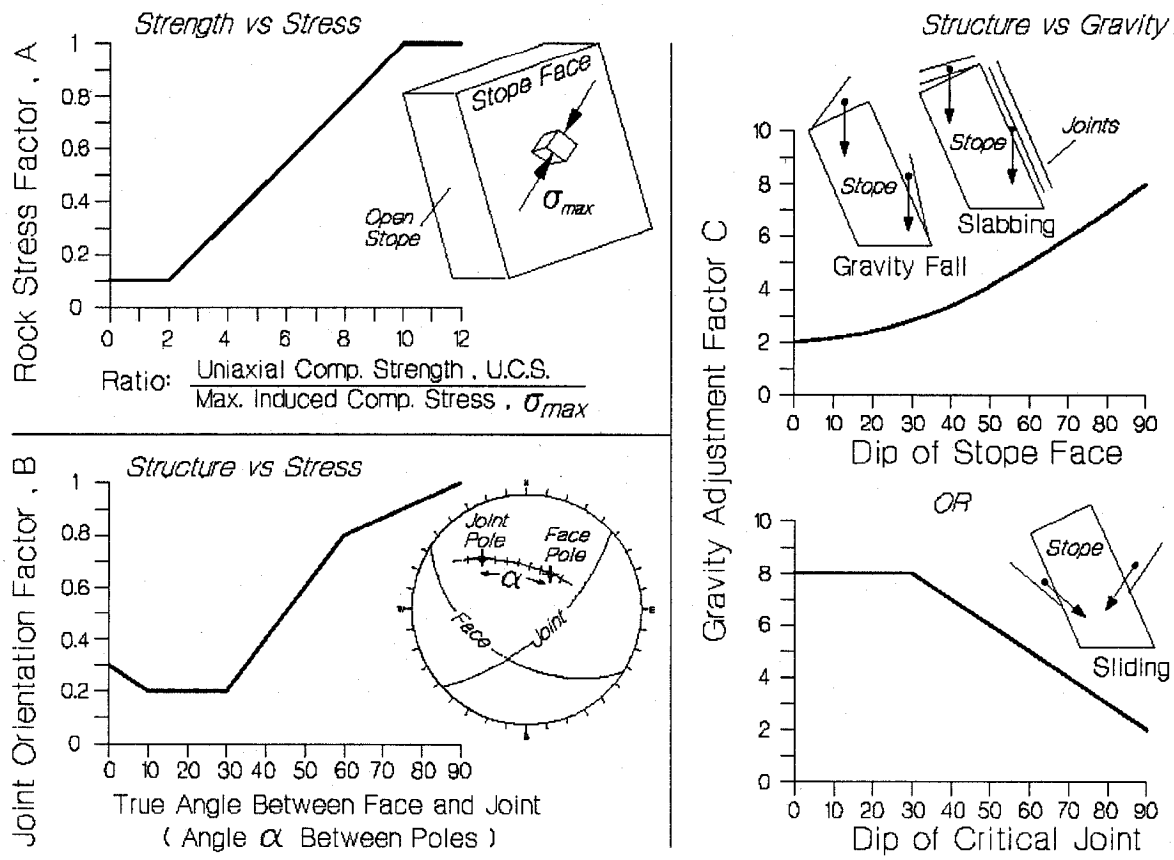

Figure 2.13 Stability parameters for the Modified Stability Graph, adopted from Hutchinson and Diederichs (1996)

2.7.2 Limitations of the Stability Graph method

The main limitations of the Stability Graph method are:

- Application of the Stability Graph method is limited to cases that are similar to those in the developmental database.
- Stability Graph method does not consider stope face abutment relaxation (Diederichs et al., 2000).
- Changes in stress magnitudes and orientation are not accounted for as mining progresses (Malek et al., 2001).

- The sensitivity of wall stability to undulations in the azimuth of the stope strike, with respect to field and induced stress, including "stress shadowing" is not accounted for.
- Stability Graph method is inappropriate for severe rockbursting conditions, in highly deformable or creeping rockmasses, and for entry methods (Potvin and Hadjigorgiou, 2001).
- Time of exposure of stope surfaces is not accounted for but should be considered since long exposure times lead to significant stress changes.
- Hydraulic radius is inadequate for partly filled stopes, undercut stopes, or stope surfaces with complex geometry (Suorineni, 1998). Another limitation of hydraulic radius is that a given value of *HR* can be associated with a variety of stope geometries. This is discussed further in Section 5.3.
- It does not account for blasting effects.
- Stress induced damage, as well as faults, shear zones and fissures are not specifically included in the factors. An approach for incorporating stress induced damage has been suggested by Sprott et al., 1999. A fault factor has been developed (Suorineni et al., 1999). Both factors have not yet been widely employed by practitioners.
- Differing operating practices as well as subtle but important differences in the pre-mining conditions that are not adequately accounted for (Calvert et al., 2000).
- Existing Stability Graph methods are not sufficient to assess differences between primary and secondary stope dilution. Mining sequence and type of stope, (such as primary and secondary) is not taken into account.
- Variations in stope design, construction, production blasting and mucking rate are not taken into account.

2.7.3 Empirical relationships incorporating factors influencing unplanned dilution

Pakalnis (1986) related the Bieniawski rockmass rating (*RMR*) to wall sloughage to develop a dilution-based open stope empirical design method. Details of the *RMR* classification system are described in Bieniawski (1989). Exposure rate and hydraulic radius are major factors in this design approach. They account for rockmass quality deterioration with time, and stope surface geometrical effects on stability. Figure 2.14 illustrates the method.

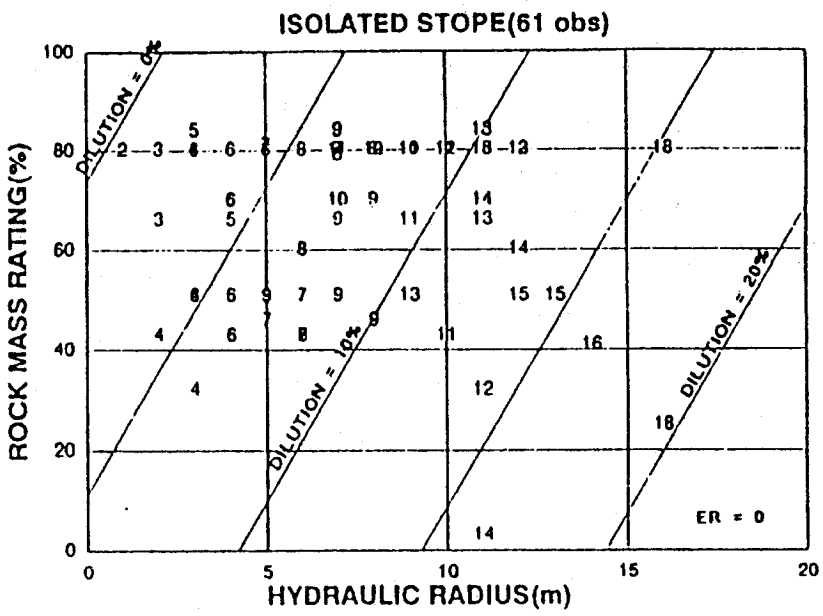

Figure 2.14 Dilution based empirical design for an isolated stope, Pakalnis and Vongpaisal (1993)

The instability and caving limits in the Stability Graph are based loosely on the apparent area of instability across the stope face. Based on local site experience, dilution severity versus *HR* relationship for any rock quality can be obtained and used in economic analyses to optimize stope dimensions (Elbrond, 1994; Planeta et al., 1990; Diederichs and Kaiser, 1996). Example plots of empirical estimates of unplanned dilution are provided in Figure 2.15.

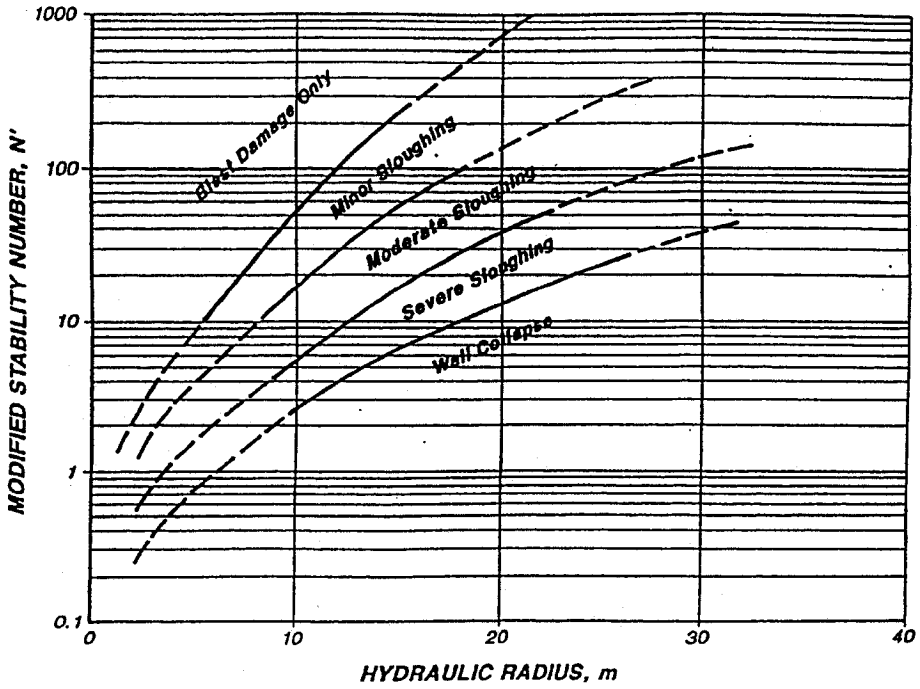

Scoble and Moss, 1994

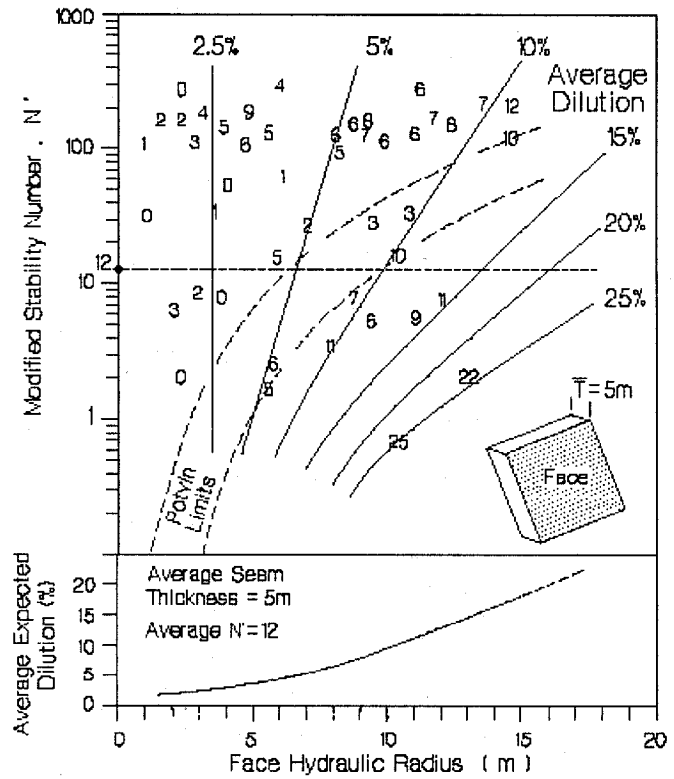

Hutchinson and Diederichs, 1996

Figure 2.15 Empirical estimation of unplanned dilution

If the volume of failure is considered and divided by the volume of the ore in the stope, a measure of the unplanned dilution for a particular stope surface (ELOS) is obtained. Clark and Pakalnis (1997) and Pakalnis and Vongpaisal (1998) describe an ELOS design chart, presented in Figure 2.16. Four design zones were identified; definitions are presented in Table 2.3.

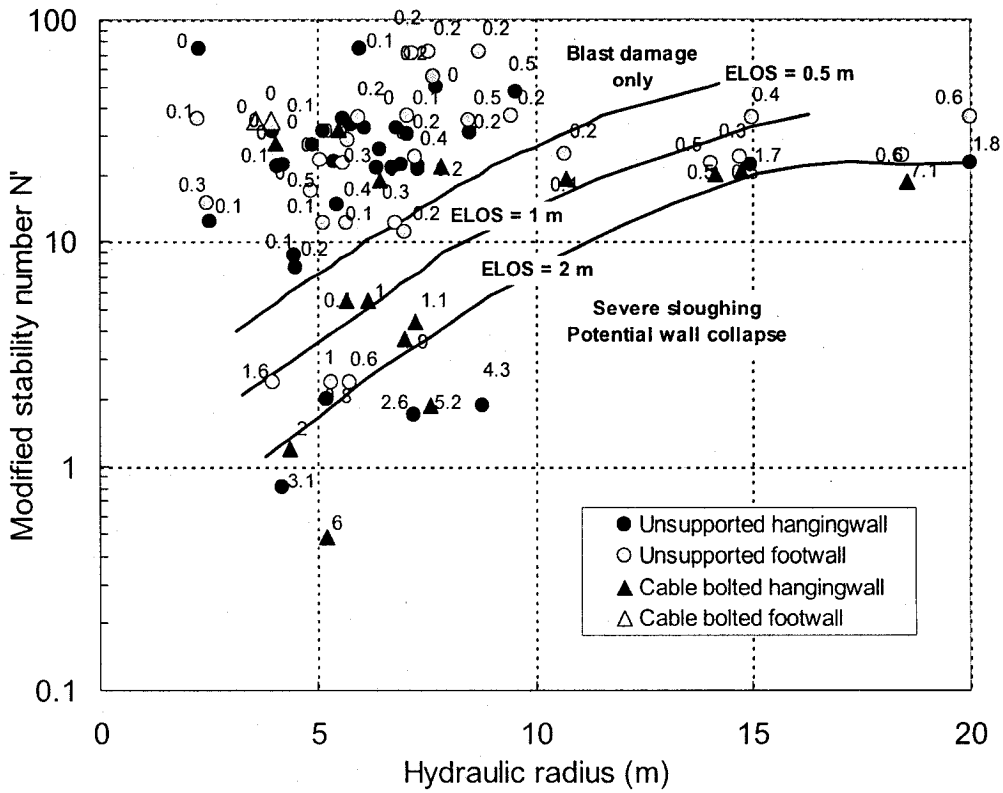

Figure 2.16 ELOS design chart. Values represent measured ELOS value for stope wall, Pakalnis and Vongpaisal (1998)

Table 2.3 ELOS design zones definitions (after Clark and Pakalnis, 1997)

ELOS Range	**ELOS design zones**
ELOS < 0.5m	Blast Damage only: surface is self supporting
ELOS = 0.5m - 1.0m	Minor Sloughing: some failure from unsupported stope wall should be anticipated before a stable configuration is reached.
ELOS = 1.0m - 2.0m	Moderate Sloughing: significant failure from unsupported stope wall is anticipated before reaching stable configuration.
ELOS > 2m	Severe Sloughing: large failures from unsupported stope wall should be anticipated. Wall collapse is possible.

An example of another ELOS design chart, developed uniquely from Campbell mine data, is shown in Figure 2.17. Although ELOS empirical plots are frequently used as a technique for evaluating unplanned dilution in long-hole stopes, this design approach has a major deficiency; they are site specific.

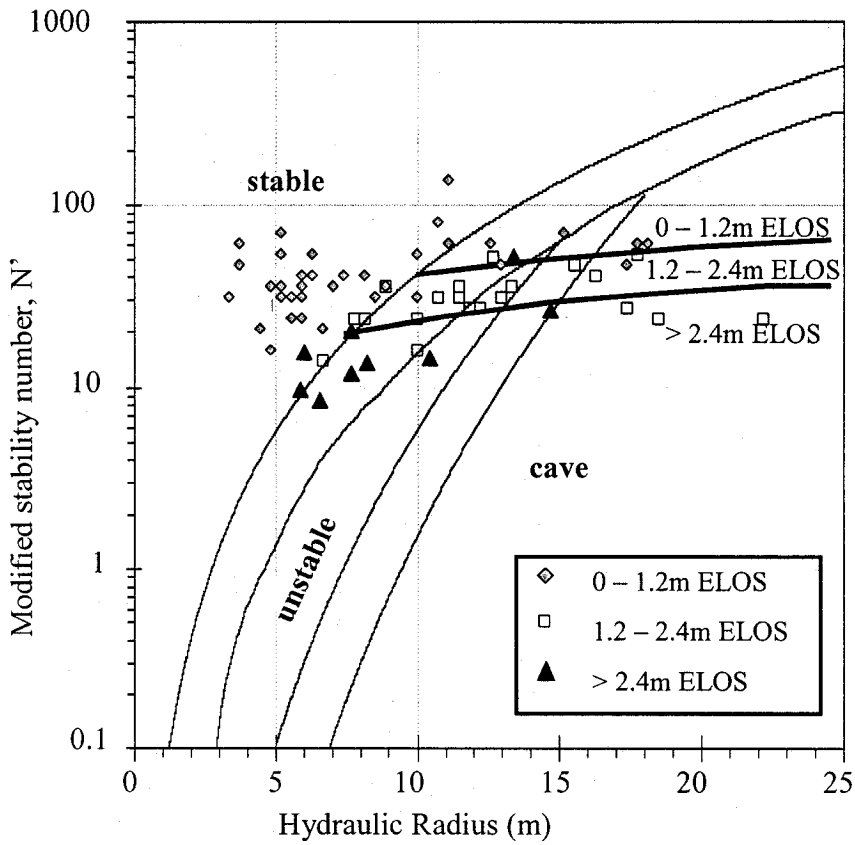

Figure 2.17 Empirical estimation of unplanned dilution at Campbell mine using ELOS values, modified from Alcott (2002)

An examination of factors influencing stope hanging-wall stability was undertaken at the Bousquet #2 mine, comparing neighbouring primary and secondary stope blocks (Henning and Mitri, 1999). Even though the stopes had similar hydraulic radius, significant differences in hanging-wall and footwall ELOS values suggest that factors other than rockmass quality may affect stope wall stability and unplanned dilution. These factors are examined in Chapter 3.

CHAPTER 3

PARAMETERS CONTROLLING ORE DILUTION IN A BLASTHOLE STOPING ENVIRONMENT

3.1 Introduction to the blasthole mining method

Blasthole mining, also referred to as long-hole mining, is a general term applied to mining methods that employ long hole drilling for the production of ore. It is a system of large-scale drilling and blasting in which large amounts of ore are broken in single blasts. Blasted slices of rock fall into an open void within the stope. The rock is extracted and the empty stope is backfilled (delayed backfilling). The method is used to mine ore where both the ore and wall rocks are relatively strong. The method may be applied to a variety of vertical or steeply dipping orebody shapes and sizes (Hamrin, 1980). Normally the vertical dimension is the largest, as illustrated in Figure 3.1.

The blasthole mining method provides limited selectivity. Since it is a bulk method, blasthole mining results in some overbreak. The orebody should preferably be regular, as changes in orebody geometry outlines are difficult to compensate for. Production holes, commonly in the range of 50mm to 110mm diameter, are drilled either in a fan-shaped pattern, or in a pattern parallel to the stope dip. Drilling can be done in advance of ore extraction. Stope dimensions are determined from local ground conditions. Mined stope width varies with orebody thickness.

The blasthole mining method originates from the Noranda Horne mine in the late 1930's (Hall, 1937), when, as a replacement to bench mining, a method of

sublevel mining with ring drilling of blastholes (sectional steel and diamond drilling) was developed. The adoption of the blasthole mining method was also accompanied by the introduction of cemented backfill utilizing granulated slag and pyrrhotite tailings, Patton (1952). This new and safer mining system enabled the mine to increase production while lowering costs and helped to extract almost 100% of the ore from the lower "H" orebody at the Horne mine. By 1948, the blasthole mining method was in use at the INCO Frood-Stobie mine (Boldt and Queneau, 1967). The blasthole method has since found worldwide acceptance.

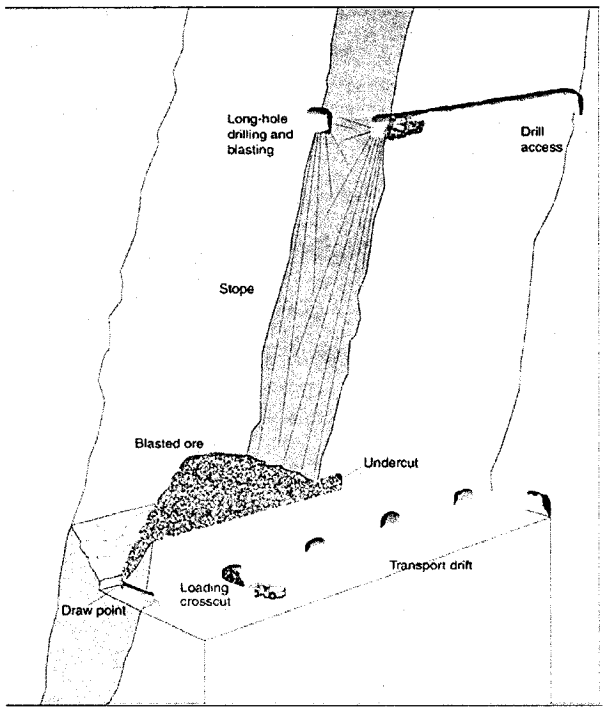

Figure 3.1 Blasthole mining method, Hamrin (2001)

3.2 Variations of blasthole mining method

Stope blocks are accessed in transverse or longitudinal directions. Transverse stoping is common to tabular orezones of widths exceeding 5 meters, where stope access is driven normal orezone strike. Narrower width orezones are mined longitudinally, with stope access driven parallel to, and within, the orezone strike. The two stoping directions are illustrated schematically in Figure 3.2.

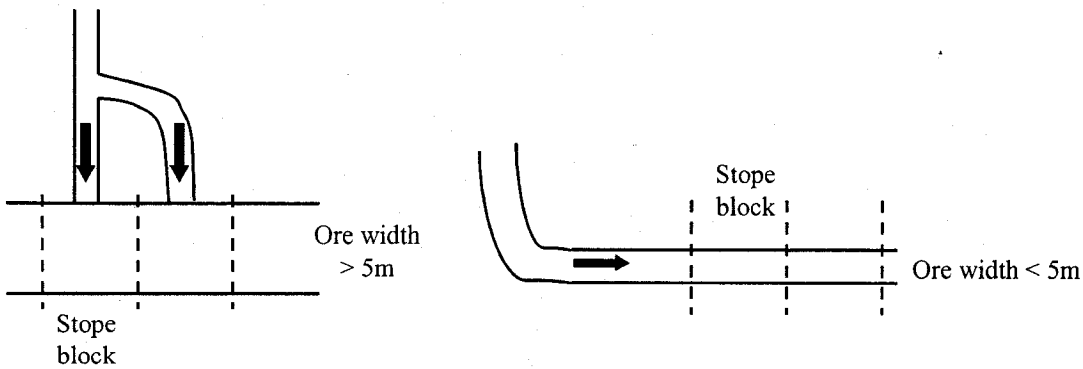

(a) Transverse mining direction (b) Longitudinal mining direction

Figure 3.2 Illustration of transverse and longitudinal mining directions. Arrow indicates direction of stope access

3.2.1 Transverse blasthole stoping

In transverse mining, a tabular orebody is subdivided into stopes and pillars. Typically, an expansion slot is developed by enlarging slot raise to the width of the stope, using parallel hole blasting (Henning et al., 2001a). Ore is fragmented in the stope using long parallel (primary stopes) or ring-drilled (secondary stopes), and mucked from a drift, orientated perpendicular to the stope strike, at the base of the stope. Stopes are backfilled with cemented backfill if the secondary pillars are to be recovered. For secondary stope mining, it is important that the pillar is not too highly stressed for practical extraction. Therefore primary stopes do not necessarily have the same dimensions or excavation design as secondary pillar stopes, as illustrated in Figures 3.3 and 3.4.

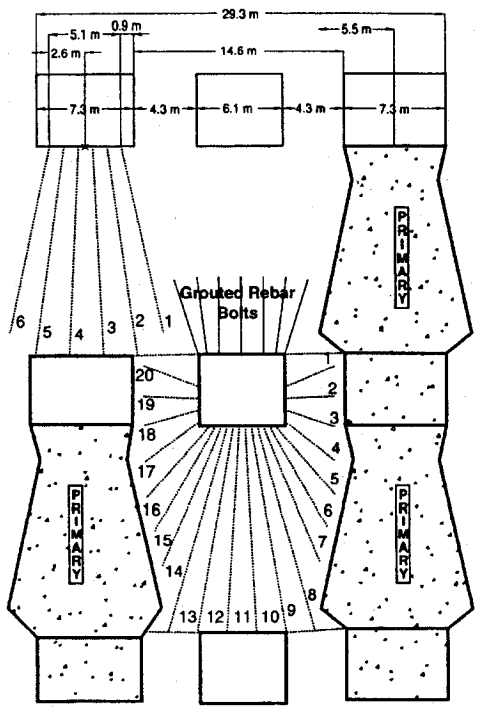

Figure 3.3 Transverse stope and pillar stope design at the Lamefoot mine, longitudinal view, Fellows (2001)

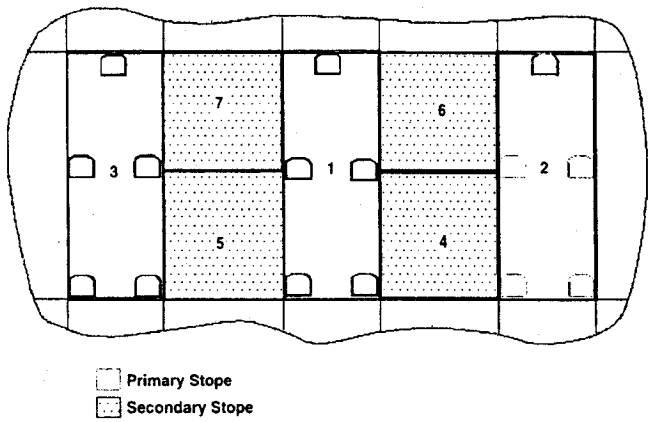

Figure 3.4 Transverse stope and pillar stope design at Pyhäsalmi mine, longitudinal view, Pera et al. (2001)

3.2.2 Longitudinal blasthole stoping

Longitudinal blasthole stoping is generally a pillarless mining method, commonly developed in narrow, steeply dipping deposits, as described by Gauthier (2001) and Makuch (2001). The top sills are excavated to the full stope strike width to permit drilling of parallel blastholes, typically at a staggered pattern, as illustrated in Figure 3.5.

Compared to transverse access stoping, longitudinal stoping has positive benefits. Improved wall stability and dilution control is possible, as the strike length can be reduced to compensate for low quality hanging-wall or footwall conditions. Secondly, selective blasthole mining is possible, as zones of subgrade material can be left in place by re-slotting. Disadvantages to longitudinal stoping include reduced stope productivity (due to long haulage distance and smaller stope volume), and reduced mining rate, since pillarless longitudinal stoping allows fewer active stope blocks than transverse open stoping.

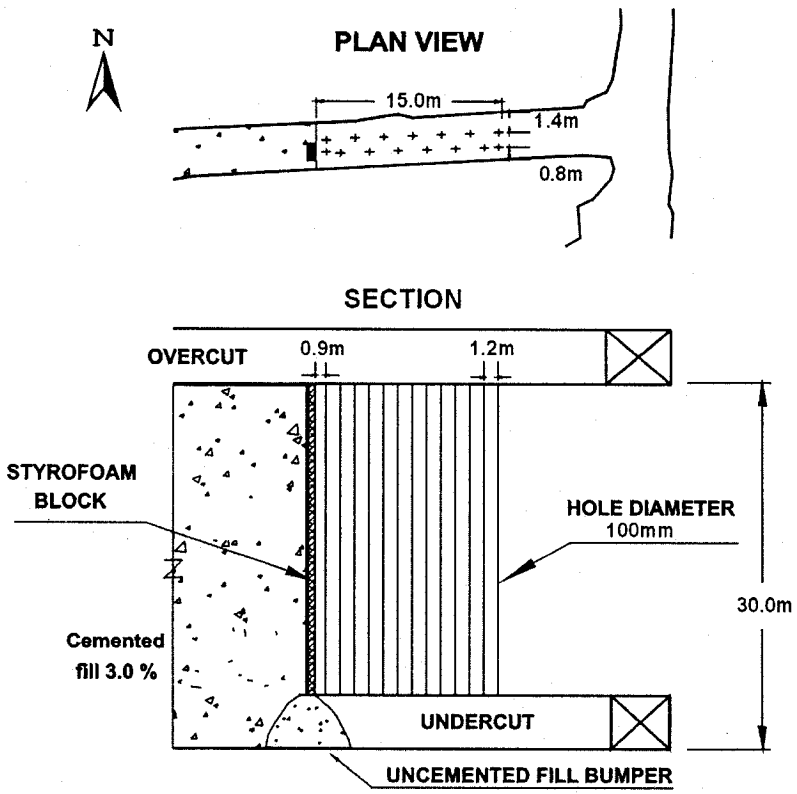

Figure 3.5 Longitudinal blasthole stoping at Bousquet mine, Gauthier (2001)

3.2.3 Sublevel blasthole stoping

The height of a blasthole stope is constrained by drill equipment limitations and accuracy of drilling: drill deviation increases with the length of the drill string. Sublevels designed at intervals in the range of 25m to 40m give access for longhole drilling in the stopes in order to permit the excavation of larger stopes, such as 91m-high stopes at Kidd Creek mine (Belford, 1981) and 300m-high stopes at Mount Isa Copper mine (Potvin, 1998). The method is more common to massive deposits, than to vein-type orebodies. An example of a typical sublevel stoping arrangements used at the Mount Isa mine is provided in Figure 3.6.

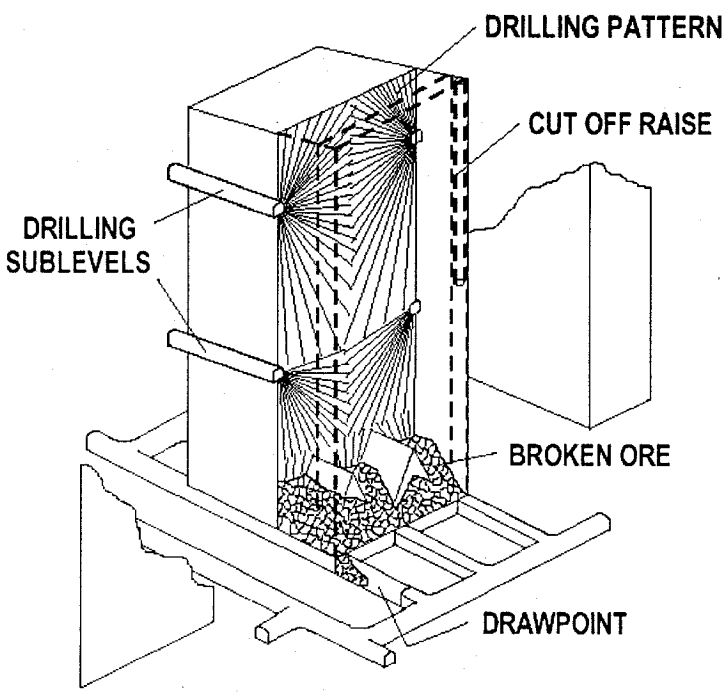

Figure 3.6 Idealized isometric drawing of a sub-level blasthole stope at Mount Isa Copper Mine, Grant and DeKruijff (2000)

3.2.4 VCR blasthole stoping

Vertical crater retreat (VCR) is a comparatively new method of blasthole mining in which horizontal slices of ore are blasted down into an opening below the block of ore being mined. As described by Villaescusa (2000) and Bastien (2001), large diameter holes are charged from the overcut and blasted by means of horizontal slices of ore progressing from the bottom level to the top level, see Figure 3.7. Following blasting, only a slight amount of broken ore is mucked, so that sufficient room is available for a subsequent blast to break into. This keeps the stope full of broken rock, thereby providing passive support to the exposed stope walls, until blasting to the stope overcut is complete, Lang (1998).

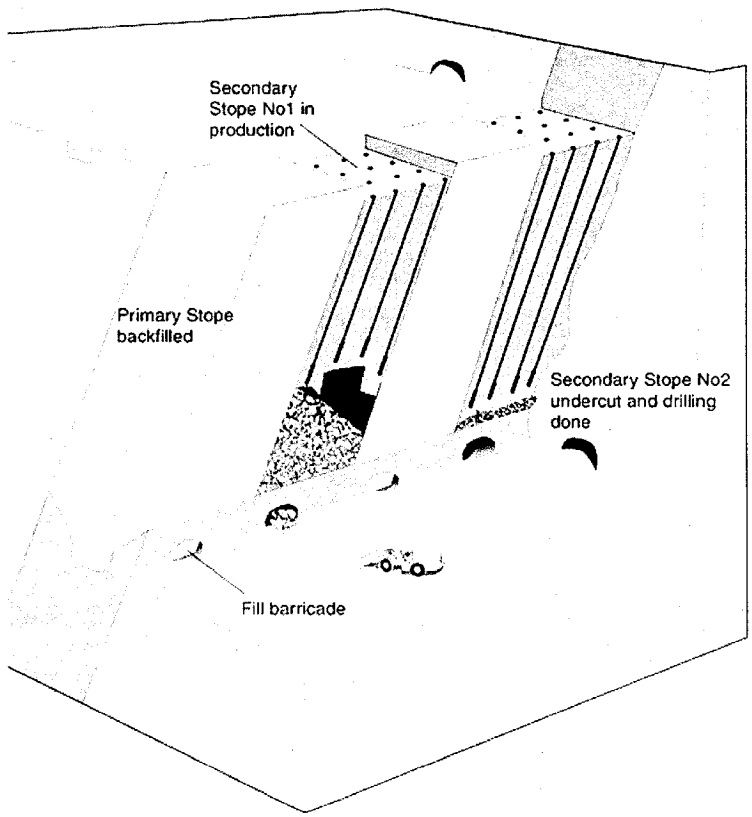

Figure 3.7 VCR blasthole stoping method, Hamrin (2001)

3.2.5 Blasthole stoping with rock pillars

With some orezones, backfill is not used. The broken rock is extracted and the resulting void is left unfilled. Between stopes, parts of the orezone are not mined to serve as supports as either vertical (rib or longitudinal) or horizontal (sill pillar) separations.

On occasion, pillars are subsequently recovered either partially or fully. Recovery normally takes place at the final stage of the mining operation, or mining of a stope panel, to ensure that a possible collapse of surrounding rock no longer poses a hazard to mining personnel and/or equipment and no longer affects normal mining activities.

3.2.6 Backfill for blasthole mining

Methods such as blasthole mining require that rock pillars be left in place in order to provide rock mechanical support by bearing tributary loads. In order to maximize ore recovery, it is very common to return and mine pillars following primary mining recovery. Primary stopes are filled with consolidated backfill to permit recovery of the secondary stopes, as illustrated in Figure 3.8. Common materials used with blasthole stopes are consolidated rockfill (Yu and Counter, 1983; Grice, 1989; Ley et al., 1998), and paste fill (Doucet and Harvey, 2001; Goulet and Blais; 2001; Melong and Naylor, 1997).

As pillars are extracted, large vertical heights of backfill are exposed. It is necessary that the backfill exhibit sufficient strength to remain free standing during and after pillar extraction. Example approaches for selecting appropriate fill characteristics are described in Barrett et al. (1978) and by Yu (1992).

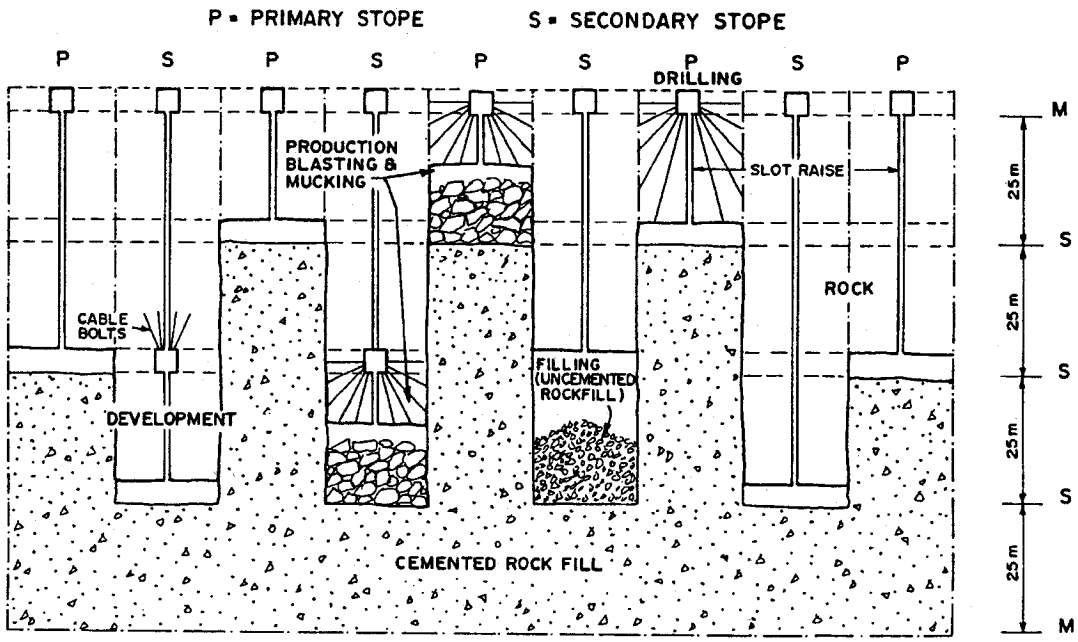

Figure 3.8 Blasthole mining at Williams mine, Bronkhorst et al. (1993)

3.3 Stope design influences on overbreak: physical and geometrical factors

To be realistic in assessing dilution, it is necessary to understand the way a stope operates (Clow, 1991). Empirical stope design techniques developed by Mathews et al. (1981) and refined by Potvin (1988) and others, have gained acceptance as a simple, 'first-pass' means of designing primary stopes. As discussed in Chapter 2, empirical stability graph methods have numerous deficiencies, and as a result, can only provide broad design guidelines.

In a general sense, a mine is a factory with standardized practices, equipment and materials for stope design and excavation. However, no two stopes are the same, as each has numerous potential variables that may impact recovery and unplanned dilution, as suggested in Figure 3.9. Clark and Pakalnis (1997) identified several development factors that ultimately may influence stope dilution, including:

- stope dimensioning,
- design of the production drill and slot patterns, and

- stope construction, such as accuracy of drilling and blasting.

These and other factors are discussed in the following sections.

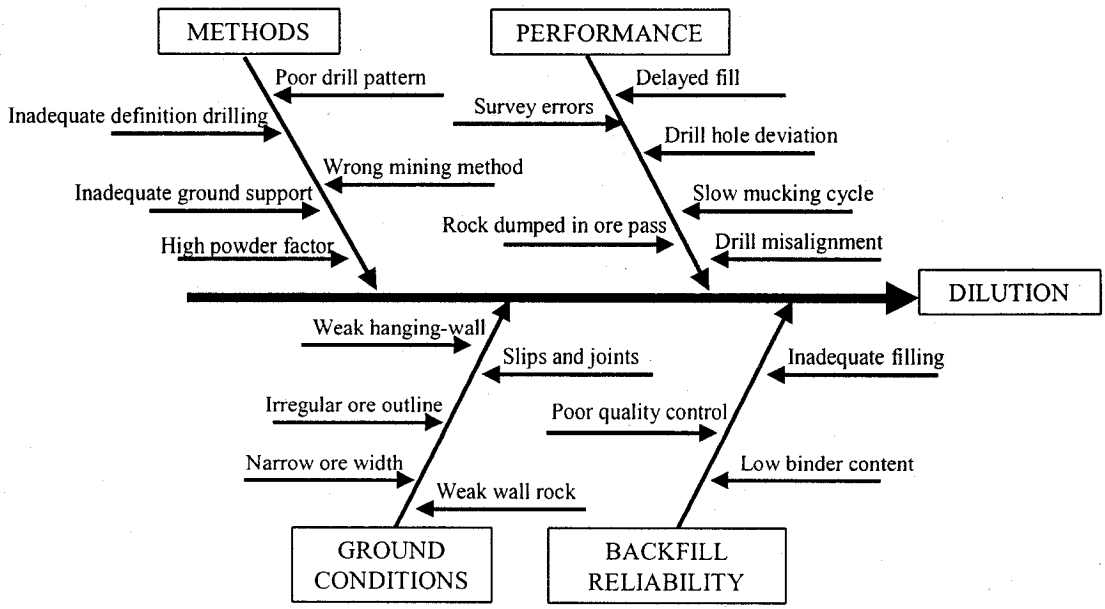

Figure 3.9 Fishbone chart illustrating potential factors causing dilution, De la Vergne, (2000)

3.3.1 Stope complexity

There is a tendency for overbreak to increase as the regularity of the wall geometry decreases, Clark and Pakalnis, (1997). A quantitative index of stope complexity proposed by Germain et al. (1996), and updated in Germain and Hadjigeorgiou (1998) compared the volume of a stope and its total surface area. This index of stope complexity, termed RVS, was used to determine the suitability of hydraulic radius and by extension the empirical stability graph design methods. The relationship between span, hydraulic radius and RVS is plotted in Figure 3.10. For two stopes with equal volume but differing level of geometrical complexity, the more geometrically complex stope will have a greater total surface area and a lower RVS.

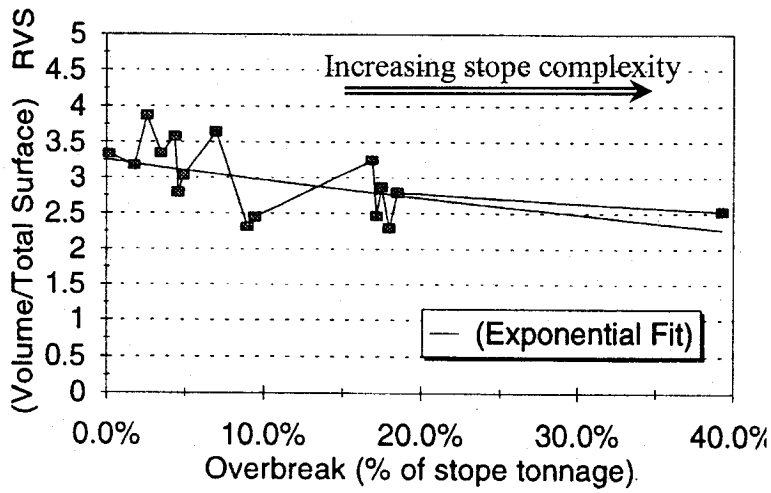

Figure 3.10 Relationship between RVS and observed overbreak, (Germain et al., 1996)

Under the classification system for stope complexity used by Germain et al. (1996), surfaces requiring careful blast pattern design, due to sharp edges of the stope profile, were considered as complex. Surfaces with some undulation were considered as irregular, while planar stope surfaces were considered as regular. Based on their comparisons between predicted and actual stope stability at the Louvicourt mine, it was shown that for stopes of complex geometry, the hydraulic radius was an inadequate tool.

The severity of stope complexity varies from stope-to-stope. For orebodies of uniform geometry, stope complexity could typically range from regular to irregular. Examples of irregular stope surface complexity include fluctuation in hanging-wall and footwall contacts along strike of orezone, and undulations along the dip of the orebody, creating a 'dogleg-type' stope profile, as illustrated in Figure 3.11.

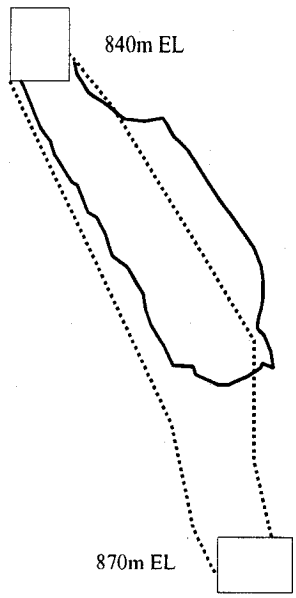

Figure 3.11 Overbreak in stope with irregular (dog-leg) geometry. Dashed line represents planned mining represented as dashed line, CMS profile shown as solid line. Modified from Yao et al. (1999)

3.3.2 Stope height

Published data suggests that unplanned dilution, particularly from the hanging-wall, is sensitive to the height and dip of the hanging-wall. Increased overbreak may be associated with equipment limitations, such as increased borehole deviation, or to rockmass stability.

Perron (1999) describes instabilities associated with high stopes at the Langlois mine that ultimately required a re-design of both the stope height and mining sequence to reduce dilution. 60m high x 20m wide stopes were originally designed for transverse (primary and secondary) mining. Wall instability was found to be greater than anticipated. To improve stability and to lower dilution, additional sub-levels were developed in ore, reducing stope dimensions to a more stable 30m high x 20m dimension. A consequence of this conversion was a change to pillarless (longitudinal) mining, with a lower rate of production.

At the Trout Lake mine (Yao et al., 1999), it was found that that the exposed hanging-wall height had a greater influence on overbreak than stope strike length. At a hanging-wall height (along dip) exceeding 40m, the risk of substantial hanging-wall overbreak was high, and was attributed to deviation of long production blastholes.

A study examining dilution influences from stope shape and dimensions at the Doyon mine (Friedrich and Charette, 1997) found that total unplanned dilution increased dramatically for parallel stope heights exceeding 30m, as illustrated in Figure 3.12. Below the 30m threshold, no direct relationship between overbreak and stope height was apparent. In both the Trout Lake and Doyon studies, it was suggested that the exposed hanging-wall height had a greater influence on hanging-wall overbreak than did stope strike length.

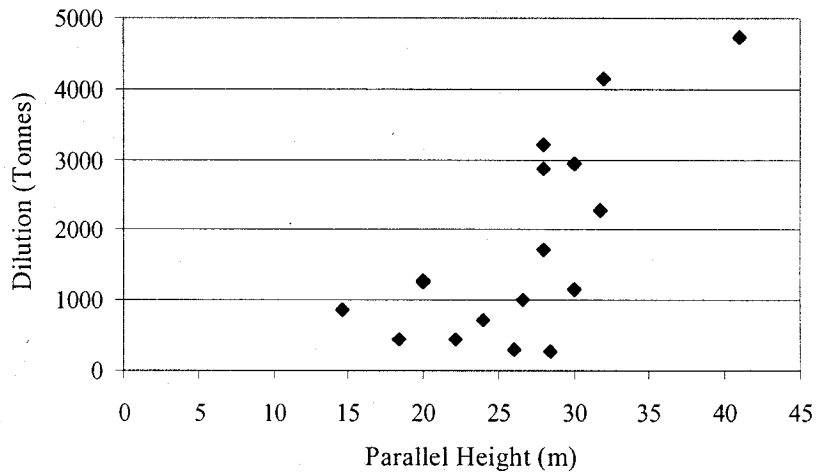

Figure 3.12 Total dilution compared to hanging-wall height, Friedrich and Charette (1997)

3.3.3 Hanging-wall dip angle

Hanging-wall dip is accounted for in the empirical stability graph as the factor *B*. However, its influence on overbreak can be significant. With steeply dipping orezones, vertical stresses are shed around the orebody. As the dip of the stope hanging-wall becomes shallower, vertical stresses are shed onto the orebody,

leading to larger displacements. An example of the influence of hanging-wall dip on stope overbreak is described in Yao et al. (1999), where depth of overbreak was observed to increase as the hanging-wall dip became shallower, see Figure 3.13. In many mines, such as the Agnico-Eagle mine (Bastien, 2001), it is common to display the orezone in a longitudinal section, showing the stopes in terms of parallel stope height. With this practice, the influence of actual hanging-wall dip fluctuations may be overlooked, resulting in a potential underestimation of the true exposed hanging-wall length, as illustrated in Figure 3.14.

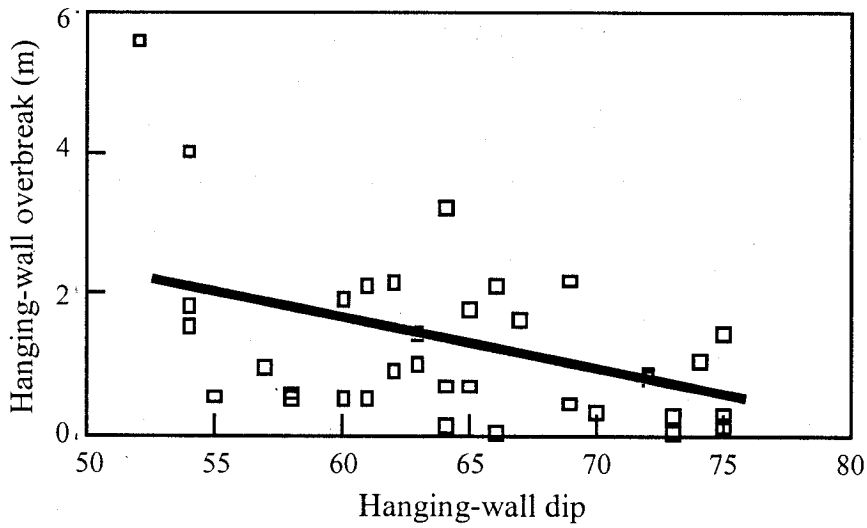

Figure 3.13 Hanging-wall overbreak as a function of hanging-wall dip angle. Solid line represents best-fit trend, Yao et al. (1999)

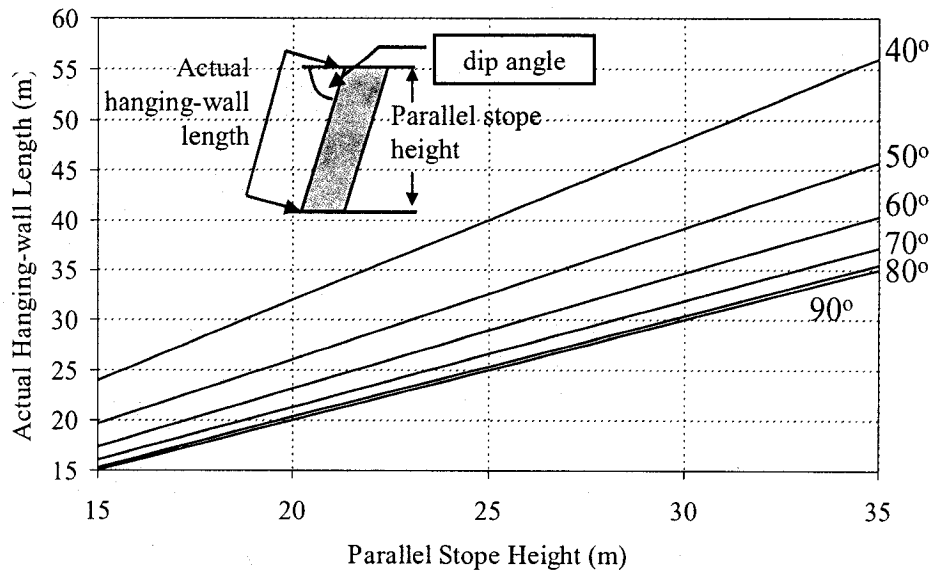

Figure 3.14 Relationship between actual hanging-wall length and parallel stope height across a range of stope wall dip angles

3.3.4 Undercutting of stope walls

Undercutting the stope hanging-wall is a well-recognized factor that contributes to hanging-wall instability and dilution. For many mines, undercutting the hanging-wall breaks the integrity of the rockmass that may form along continuous foliation or bedding planes parallel to the stope hanging-wall contact, reducing stability (Wang et al., 2002a). This is illustrated schematically in Figure 3.15.

Case histories have confirmed that undercutting the hanging-wall during development is one of the biggest contributing factors resulting in hanging-wall overbreak. When the hanging-wall is undercut, it tends to slough to the depth of the undercut, (Yao et al., 1999). In a study performed at the Detour Lake mine, (Dunne et al., 1996), dilution levels, due solely to the existence of the undercuts, were in excess of 5%.

The destabilizing effect of undercutting is dependent on the empirical stability graph stability number (N'). According to Clark and Pakalnis (1997), stope walls with low N' values appeared very sensitive to undercutting.

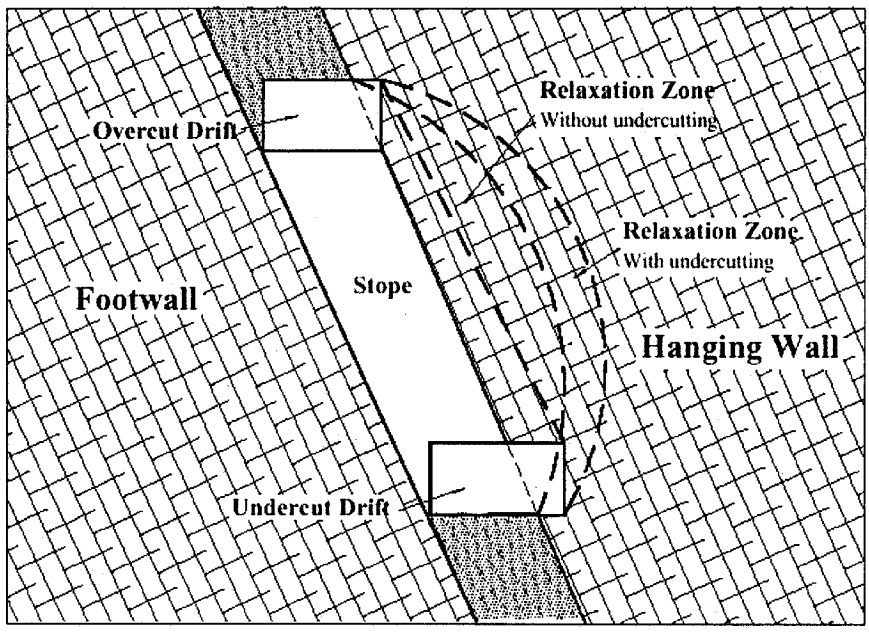

Figure 3.15 Schematic illustration of the influence of stope wall undermining on stope relaxation, Wang et al. (2002a)

3.2.5 Time effects

Stopes are normally designed to be open, from the initial blast to depletion, for a minimum of time. Delays in the stope blasting/mucking cycle or delays to the backfilling cycle may result in increased dilution from the exposed stope walls. An example from the Detour Lake mine, (Dunne et al., 1996) illustrates the effect that time has on excavation stability. Two surveys spaced a year apart were performed. The unplanned dilution in the area, immediately after mining, was calculated as 6%. When the void was resurveyed a year later, the severity of dilution had increased to 45%. A similar example of progressive stope unravelling encountered at the Ruttan mine is shown in Figure 3.16.

Time effects on rockmass stability, and the consequences on unplanned dilution are presented in Suorineni and Kaiser, 2002. In their study, open stope performance data was incorporated as stand-up time on the Stability Graph method, shown in Figure 3.17, illustrating that both rockmass quality and stope sizes show time-dependence.

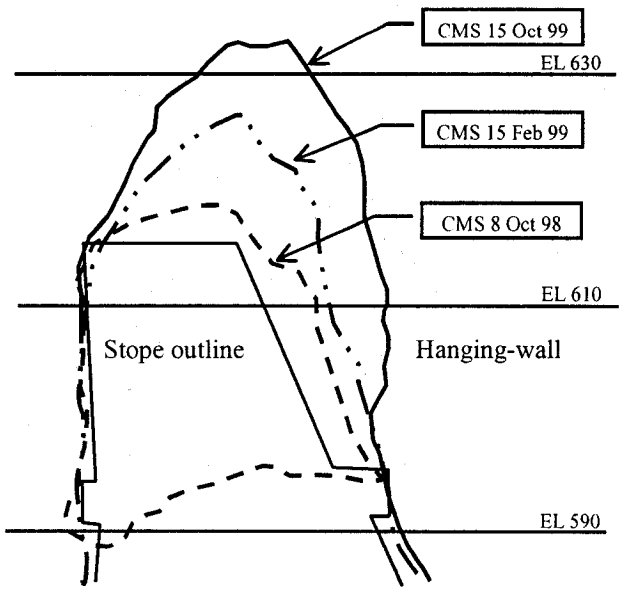

Figure 3.16 Progressive stope caving, modified from Ran (2002)

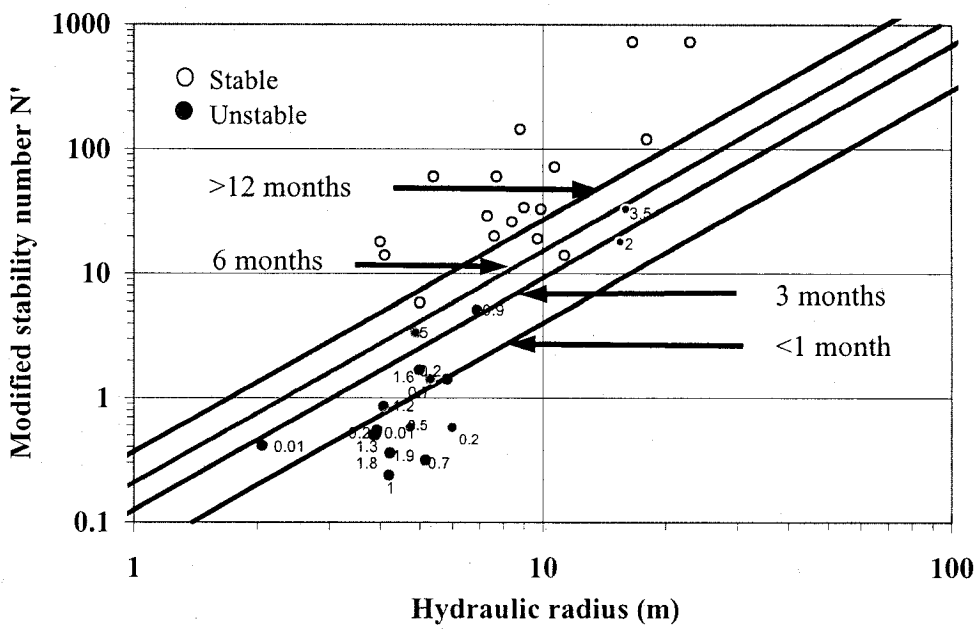

Figure 3.17 Stand-up time dependent stability graph for open stope design. Numbers on graph are stand-up times in months, Suorineni and Kaiser (2002)

3.4 Stress environment

When a drift, stope or other underground opening is excavated into a stressed rockmass, stresses near the new opening are disrupted and re-distributed.

As a blasthole stope is mined, a zone of low stress develops as stresses normal to the hanging-wall are shed to the abutments, see Figure 3.18. This envelope of elastic relaxation extends further into the hanging-wall as the distance to the supporting abutments increases. According to Kaiser et al., (1997) rockmass relaxation refers mostly to stress reduction parallel to the excavation wall and not to stress reductions in the radial direction or a reduction in confinement. Stresses in the tangential direction to the excavation wall (the major and/or intermediate principal stress) are reduced in the rockmass, often to values far below those predicted by linear elastic models, because the rockmass has been allowed to deform at some distance from the excavation.

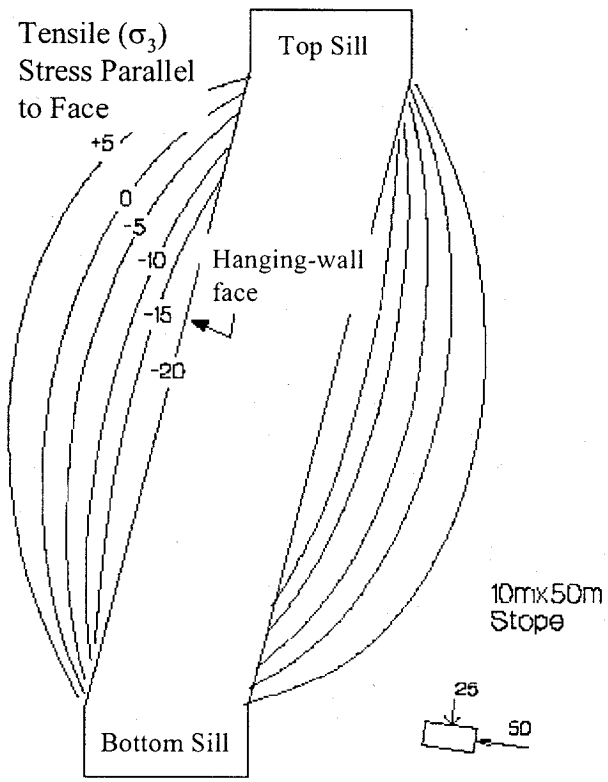

Figure 3.18 Envelope of induced hanging-wall relaxation, Diederichs (1999)

In the relaxation zone, the absence of significant clamping stresses is often cited as one of the main reasons for the instability of large hanging-walls, (Milne and Pakalnis, 1997). The depth or volume of this relaxation zone in a stope hanging-wall is dependent upon the pre-existing stress state and the size or hydraulic radius of the hanging-wall (Clark, 1998). The shape of the stope hanging-wall also influences the total volume, or average depth of the relaxation zone in the hanging-wall, (Tannant et al., 1998; Wang et al., 2002a). Diederichs and Kaiser (1999) have also shown that relaxation, causing near zero stress conditions tangential to excavation spans, reduces the self-supporting capacity of an excavation in fractured ground. This relaxation can also drastically reduce the performance of cablebolts, which are often used to support hanging-walls (Kaiser et al., 1992). Tannant et al. (1998) reported that tension can manifest itself as delamination of foliation planes and dilation of cross jointing, leading to unravelling failure in laminated rock.

The notion that a simple confining stress (tensile strength) criterion can be used to assess hanging-wall stability and dilution potential has been reported by Mitri et al. (1998), Martin et al. (1999), and Alcott et al. (1999). In the region of confinement loss ($\sigma_3 = 0$ MPa) a potential for sloughage exists. However, not all of this zone will fail if the rockmass has some self-supporting capacity. The occurrence and potential severity of this sloughage depends on the tensile strength of the rockmass. In turn, the tensile strength depends on the material properties of the rock and the structures present within it.

A common practice is to reconcile stope overbreak, measured from CMS survey, using numerical modelling. In a case example described by Martin et al. (2000), the distribution of three principal stresses within a hanging-wall, obtained from 3-D elastic modelling, were plotted against the surveyed stope profile. Results from this study, shown in Figure 3.19, suggested that the contours of minimum principal stress at $\sigma_3 = 0$ best reflected the observed geometry.

A case study from the Bousquet #2 mine (Henning et al., 2001b) found hanging-wall dilution, as represented by the CMS profile at the stope mid-strike, of a

secondary stope corresponded to the σ_3 = 0 MPa contour, while hanging-wall overbreak in a primary stope followed σ_3 = 5 MPa contour. Differences between the two stopes suggested that the extent of dilution was quantified by the loss of confinement within the hanging-wall. A possible explanation for the difference in confinement levels was that the secondary stope had been pre-conditioned due to adjacent mining activities. This is discussed further in Section 6.9.

A field study performed at the Campbell mine by Alcott and Kaiser (1999) evaluated sloughage potential within a mining zone as a function of loss of confinement ($\sigma_3 \leq 0$) and the exploitation of this confinement loss by structures or planes of preferential weakness within that zone. The sloughage potential criteria (tensile strengths relative to structures present) defined for the study are presented in Table 3.1. The volume of rock exceeding any one of these criteria was assumed to be a potential sloughage hazard and to be representative of the tonnage at risk.

Table 3.1 Sloughage hazard assessment criteria for Campbell mine, Alcott and Kaiser (1999)

Sloughage criteria	Description
σ_3 = 0 MPa	Loss of confinement, potential for failure along major structure, such as faults, contacts, and shear zones.
σ_3 = -5 MPa	Exceeds tensile strength of rockmass, potential for failure along critically oriented minor structure, such as parallel jointing.
σ_3 = -10 MPa	Exceeds tensile strength of intact rock, potential for failure regardless of structure.

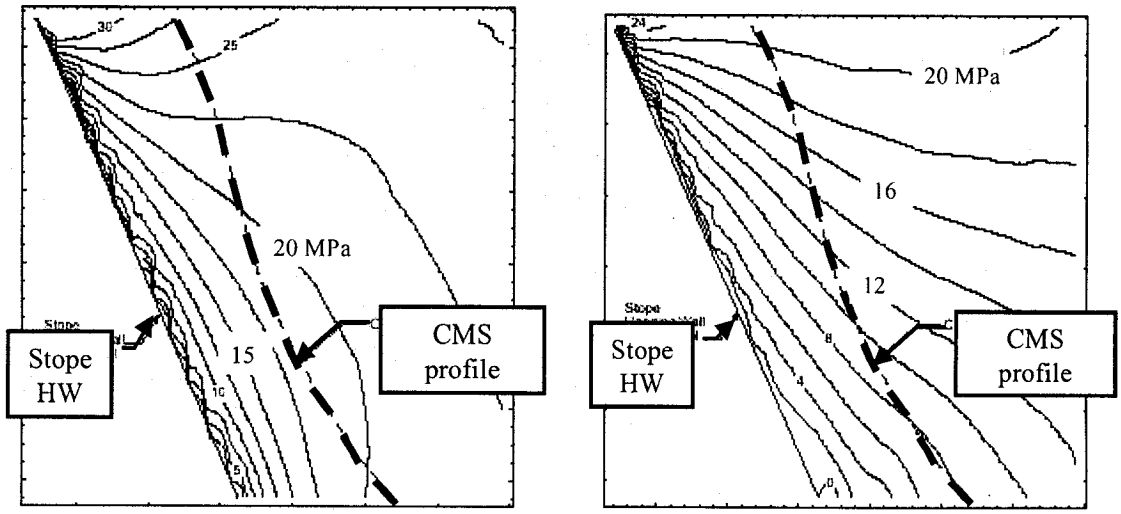

(a) σ_1 contours

(b) σ_2 contours

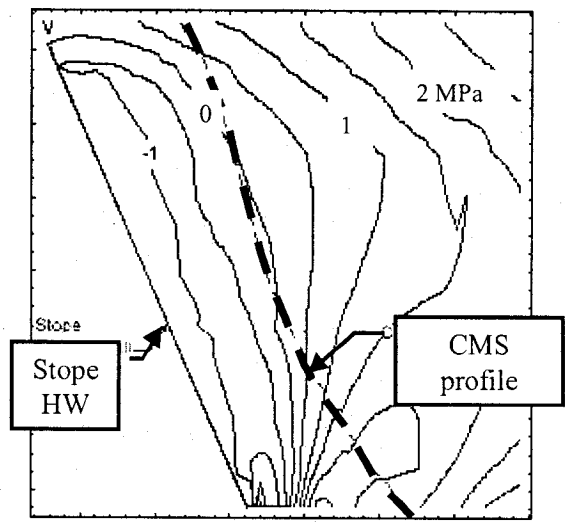

(c) σ_3 contours

Figure 3.19 Vertical section through stope showing σ_1, σ_2 and σ_3 contours. Hanging-wall overbreak, measured from CMS survey results, is indicated by a dashed line, Martin et al. (2000)

3.5 Identification of missing parameters

Two additional factors, referred to here as Stope Construction and Stope Category, are integral elements affecting stoping success. Stope construction refers to the techniques employed to prepare and extract a stope block. Stope category is the location a stope block within the actual mining sequence.

3.5.1 Stope construction

The various components involved with the design, drilling, and excavation of an individual stope play a critical role determining mining success. The role of stope construction is divided into two components: Drilling and Blasting.

Drilling components focus on those aspects that, prior to the blasting of the stope, may pre-determine the severity of stope overbreak. The factors include: hole diameter, designed blasthole drill pattern, drill set-up, and slot placement. Blasting components assess how the process of stope excavation influences stope overbreak. Blasting factors include: stope blasting sequence, blast size, selection of explosives, and slot excavation technique.

3.5.1.1 Drilling

3.5.1.1.1 Hole diameter

In most blasthole methods the ore is blasted into a vertical opening. The blastholes may be small diameter long hole carbide drill holes or larger diameter holes drilled with in-the-hole (ITH) drills, or they may be a combination of both. Drilling of small diameter (50mm to 60mm) production holes requires the use of longhole rock drills, equipped with extension steel in 1.2m to 1.8m sections. The hole length varies with the hole pattern but normally does not exceed 24m as longer holes may cause problems due to deflection from the intended direction. The burden (thickness) between drilling patterns is typically 1.2m or more.

Since drilling can be isolated from the rest of the mining cycle (muck and blast), large mechanized equipment can be used efficiently, and a more controlled and accurate hole alignment is possible. A common technique for blasthole mining uses ITH hammers, drilling production holes with diameters of 100mm or more, over lengths up to 60m. The burden (thickness) between drilling patterns is in the range of 2.4m to 3m or greater.

3.5.1.1.2 Drill pattern design

The distribution of the explosives within a stope influences stope recovery. The designed drill pattern and slot placement for an individual stope varies with the access available for drilling. In a typical primary / secondary transverse stope sequence, the drill pattern may vary with stope type. For example, at the Bousquet #2 mine, the top sill of primary transverse stopes is excavated to the full stope strike length to permit drilling of parallel blastholes, with an off-center 1.2 meter diameter raisebore slot. Secondary transverse stopes are drilled in a fan-pattern from a narrow, five meter-wide, top sill access, with a central 1.2 m diameter raisebore slot, (Henning, 1998). At other mines, such as the Williams mine (Bronkhorst and Brouwer, 2001); both primary and secondary transverse stopes have similar drill patterns. Examples of parallel and fan drill patterns are shown in Figure 3.20.

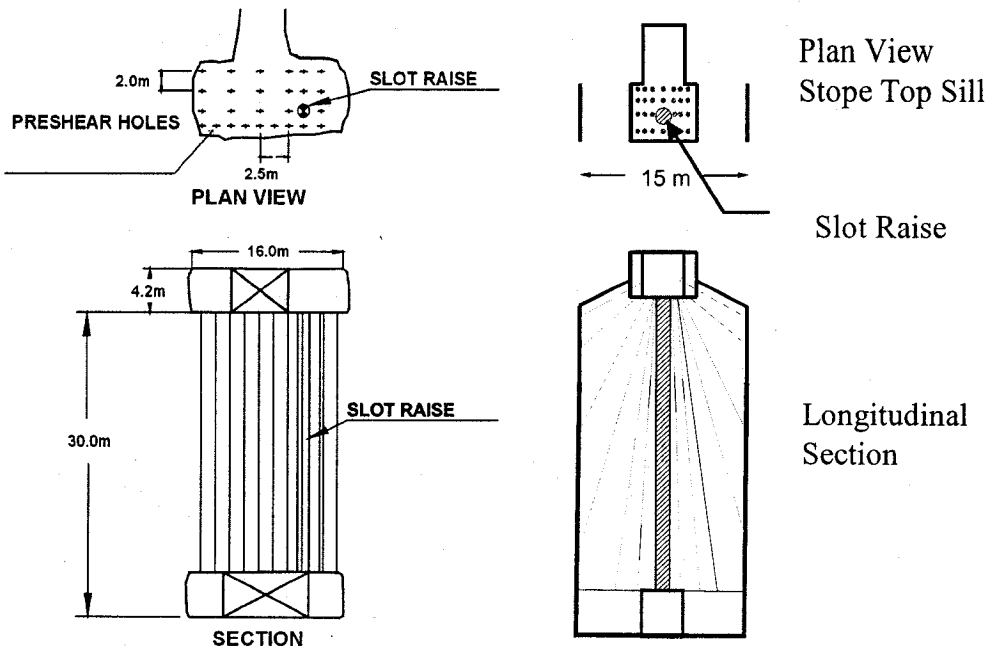

Parallel drill pattern Fan drill pattern

Figure 3.20 Schematic illustration of parallel and fan drill patterns, modified from Henning et al. (2001a)

3.5.1.1.3 Drilling inaccuracy

A Noranda study indicated that about 50% of unplanned dilution came from rock sloughing due to blast damage and weakened rock walls or exposed backfill, (Piché et al., 1998). Drillhole inaccuracy was identified as one of the major factors causing ore dilution, (Beauchamp and Cameron, 1999). Stope walls were significantly damaged when deviated perimeter holes were blasted. Within the stope block, drilling inaccuracy resulted in poor blasts with higher vibration levels and a wider spread of muck size distribution and induces, which translate into higher damage and dilution potential.

Drilling accuracy can be jeopardized by many factors, including:

- Inaccurate placement of drill reference marks,
- Incorrect drill set-up,
- Limitations of the drilling equipment,

- Condition of the drilling equipment,
- Inconsistent drill operation, and
- Geological structure.

Drill error is discussed further in Chapter 5.

Additional sources of dilution associated with stope drilling include:

- Increased charge per delay and the blasting damage associated with larger diameter blast holes, Butcher (2000).
- The setting of unrealistic drilling and blasting targets, Butcher (2000).
- Stope complexity, Germain and Hagjigeorgiou (1998). Stopes with complex geometry usually require a more complicated drilling pattern. The distribution of the explosives within the more complicated drilling pattern is a parameter affecting stope performance.

3.5.1.2 Blasting

3.5.1.2.1 Slot excavation technique

Blasthole methods require a slot raise to provide an opening into which subsequent slices of the ore can be thrown. As illustrated in Figure 3-20, slot location influences the stope drill pattern, and can range from the mid-span to the extremity of the stope panel. Yao et al. (1999) reported that slots located far away from hanging-wall contact produce less hanging-wall overbreak.

There are a wide variety of slot excavation techniques available. Selection of which depends upon stope geometry and extraction sequence. Common slotting methods through rock include: alimak raise, drop raise and raise bore. With other methods a void is created either against or through an adjacent backfilled stope, such as a Styrofoam slot (Trahan, 1995) illustrated in Figure 3.21, a slot reamed

through backfill (Perron, 1999; Bruce and Kord, 1992), or a drop raise blasted against backfill (Grenier and Gauthier, 2001).

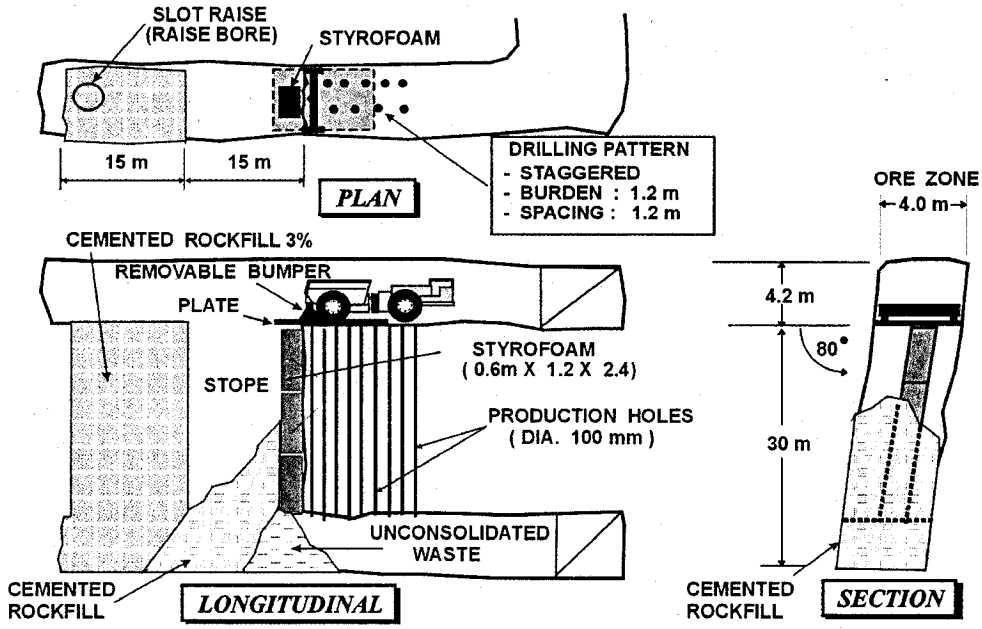

Figure 3.21 Styrofoam slot method, after Trahan (1995)

3.5.1.2.2 Blast sequence

A study performed by Pierce (1998) examined the sensitivity of hanging-wall failure to the direction of excavation of a primary transverse stope. The numerical modelling indicated that, with the principal major stress orientated at 45° to the orebody, the degree of stress-driven hanging-wall failure was potentially 25% greater when the stope sequence retreated from west to east. The modelling also suggested that excavating the stope with a greater number of smaller blasts reduced the severity of hanging-wall failure.

The sequence with which a stope block is excavated is influenced by the pattern of drilled blastholes, as illustrated in Figure 3.22. The type and volume of

explosive agent used may vary between individual blastholes and between stages of the blast sequence, potentially leading to differences in stope overbreak.

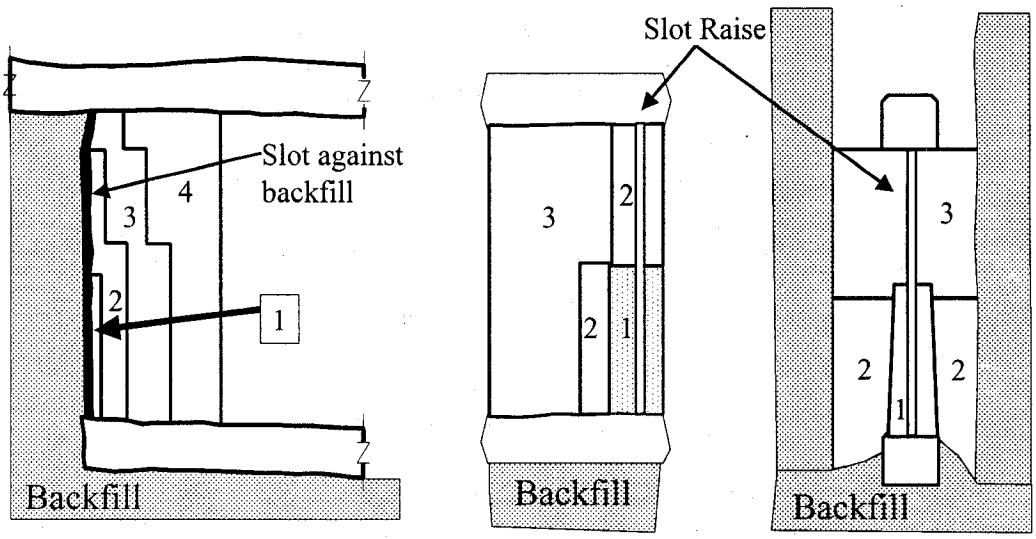

Figure 3.22 Examples of blast sequences, associated with (a) Longitudinal parallel drilling, (b) Transverse parallel drilling, and (c) Transverse fan drill pattern. Modified from Henning et al. (2001a)

3.5.1.2.3 Blast vibration

Blast induced damage is a result of the interaction of the rockmass and the explosive product. The damage inflicted on the boundary of the excavation is directly related to the type and amount of energy required to adequately fragment a volume of rock. The reduction in rockmass quality thus results from weakening or dilation of existing discontinuities and the creation of new fractures. Mackenzie (1987) defined blast-induced damage as the change in the in situ block size distribution due to blasting. His observations of blasting indicated that high-pressure explosive gas products penetrate along fractures in all directions around

a blasthole. The influence of the gas is strongly dependent on the state of fracture of the rock.

Scoble and Moss (1994) suggest that a one meter depth of overbreak is typical in blasthole stopes. They also state that blast damage at the slot tends to be greater due to effects of confinement and to higher powder factors required. Power factor is computed as the quantity of explosives used divided by the volume of rock to be blasted, (Atlas Powder Company, 1987). Higher power factors result in fine fragmentation.

Yu (1980) described the generation of elevated blast vibration levels, associated with large diameter (200mm) blastholes, caused excessive stope wall sloughage. According to Scoble et al. (1997), other mining-induced damage factors that can control the extent of the blast induced damage zone include:

- Explosive product
- Blasting pattern
- Powder factor (as a function of pattern and explosive)
- Charge concentration
- Delay timing

Blast damage criteria in common practice correlate damage to vibration level, measured as peak particle velocity (PPV). PPV values represent the peak vector sum velocities of individual blast holes, measured at a known distance from the centre of the blast hole column by triaxial geophones. According to Oriard (1982), most rockmasses suffer some damage, in the form of new tensile fractures and radial cracking, as PPV values exceed a threshold of 635 mm/sec. A damage criterion, based on observed damage in relation to measured PPV at the Kidd Creek mine (Yu, 1980) is provided in Table 3.2. A similar blast damage curve from the Williams mine is provided in Figure 3.23.

Table 3.2 Blast damage criteria for Kidd Creek mine, Yu (1980)

PPV (mm/sec)	Type of damage
250	No noticeable damage to underground workings.
500	Minor slabbing failure observed.
750	Development of cracks in weak ground.
1000	Potential formation of cracks to 15mm wide along weak plane of geologic structure.
1250	Major slabbing failure along drift, failure along strong geologic features.
> 1500	Formation of cracks to 15mm wide in competent rock.

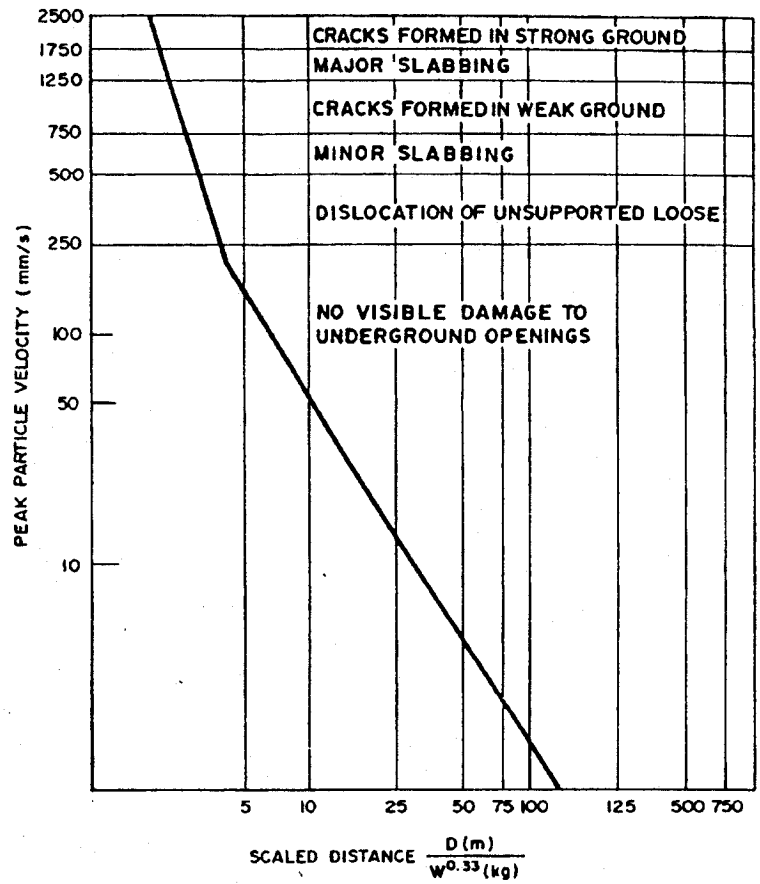

Figure 3.23 Blast damage curve from the Williams mine, Bronkhorst et al. (1993)

3.5.2 Stope category

An important, sometimes overlooked, parameter affecting unplanned dilution is the local stope setting within the mining sequence. Depending on its placement within a planned mining sequence, a stope may be bound by rock on both walls and above (a primary stope), or it may have backfill on one or both walls (a secondary stope). Potential stope categories are compiled in Table 3.3, and illustrated in Figures 3.24 to 3.26.

Each stope category may differ in terms of state of hanging-wall and footwall relaxation (Bawden et al., 1998; Tannant et al., 1998; Henning et al., 2001b; Wang et al., 2002b), and stope construction (Henning et al., 2001a).

Table 3.3 Potential stope categories, based on setting within mine sequence

Stope category	Code	Description
Primary 1	P1	Rock on both side walls. Stope located one lift above fill horizon.
Primary 2	P2	Rock on both side walls. Stope located two lifts above fill horizon.
Primary 3	P3	Rock on both side walls. Stope located three lifts above fill horizon.
Secondary 1	S1	Rock on one side. Other stope wall is against backfill. Also considered as Pillarless stope sequence extraction.
Secondary 2	S2	Both side walls of stope are against backfill.

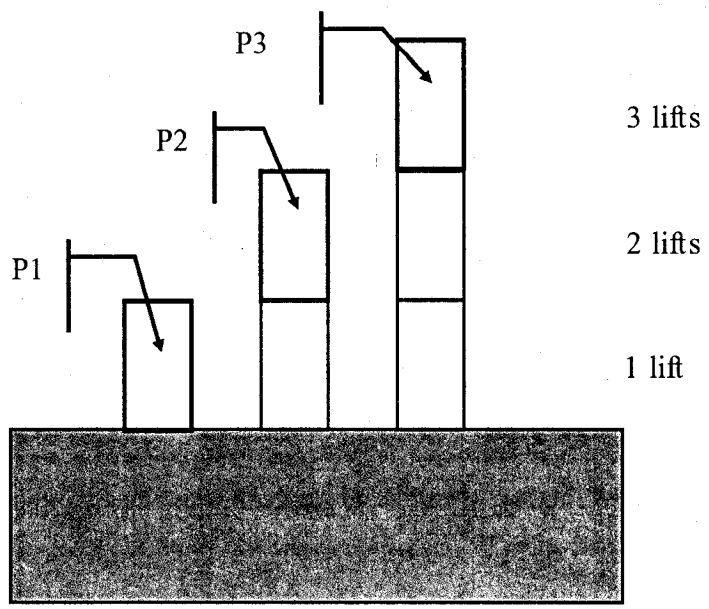

Figure 3.24 Primary stope sequence category. Shaded areas indicate mined and backfilled region

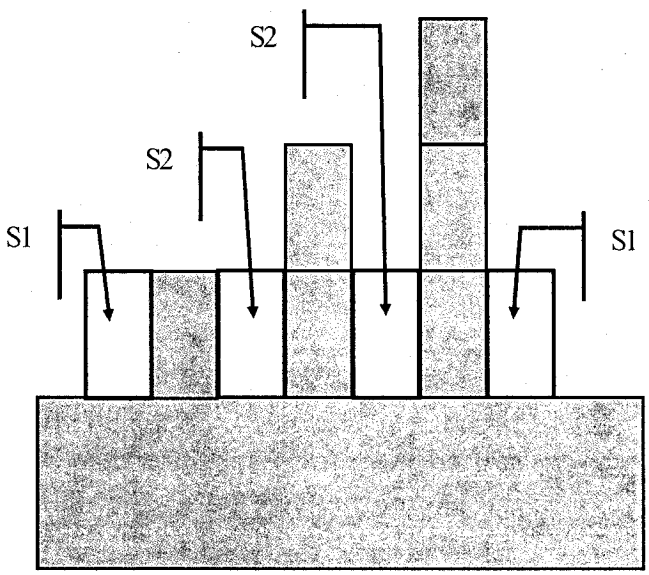

Figure 3.25 Secondary stope sequence category. Shaded areas indicate mined and backfilled region

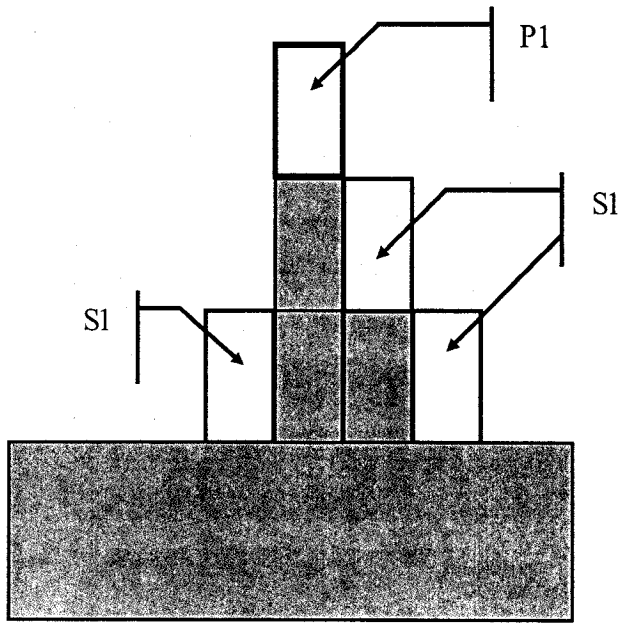

Figure 3.26 Pillarless stope sequence category. Shaded areas indicate mined and backfilled region

CHAPTER 4

NUMERICAL MODELLING FOR ORE DILUTION

Parameters influencing ore dilution in a blasthole stoping environment were introduced in Chapter 3. Examples of stope design and construction influences are presented in Figure 4.1. Numerical modelling is undertaken to examine the sensitivity of various factors influencing stope overbreak. Criteria applied for establishing a representative parametric study are outlined in this Chapter.

4.1 Modelling methods

Commercial computer programs are available for both two-dimensional (2-D) and three-dimensional (3-D) models. 2-D models are used for the analysis of stresses and displacements in the rock surrounding a tunnel, shaft or borehole, where the length of the opening is much larger than its cross-sectional dimensions. The stresses and displacements in a plane, normal to the axis of the opening, are not influenced by the ends of the opening, provided that these ends are far enough away.

Most underground excavations are complex three-dimensional shapes with irregular form. Complexity increases on a larger, mine-side, scale since these individual mine openings are frequently grouped close to other excavations. With advances in numerical modelling and computer technology, numerical modelling has become a powerful tool for underground opening design. Hoek et al. (1995) divide the numerical methods for the analysis of stress driven problems in rock mechanics into two classes: (1) Boundary methods and (2) Domain methods.

Other terminology, such as Integral and Differential is used to describe Boundary methods and Domain methods, respectively (Hoek et al., 1989). The approach taken by each of the methods involves breaking down the problem domain into smaller problem domains, or elements which are easier to understand and easier to describe mathematically. The way in which elements are used to solve the problems differentiate the two methods.

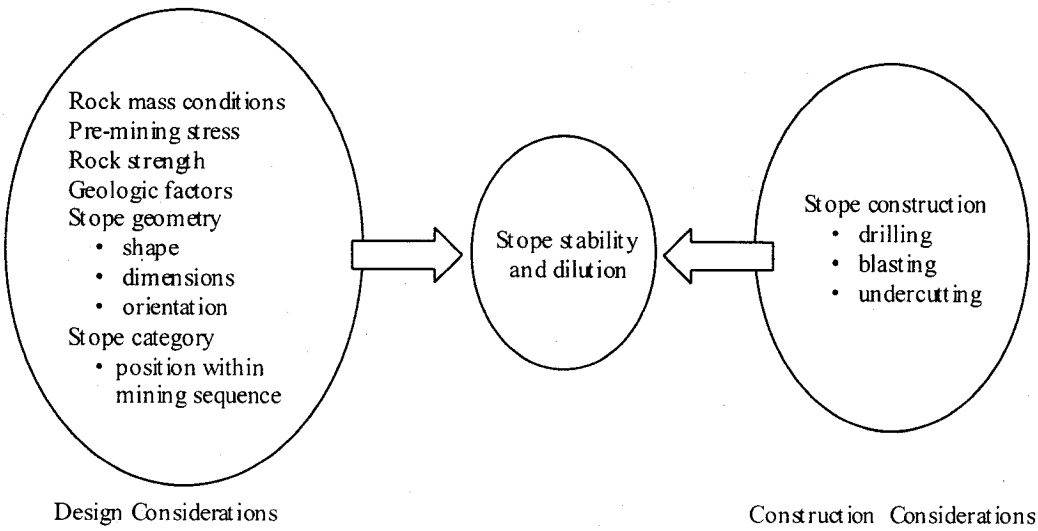

Figure 4.1 Factors influencing ore dilution

With the Boundary method, the boundary of an excavation is divided into elements, with the surrounding rockmass represented mathematically as an infinite continuum. Far field conditions need only be specified as stresses acting on the entire rockmass and no outer boundaries are required. Stresses are solved in terms of surface values of traction and displacement variables (Brady and Brown, 1985). The Boundary method is well suited for large scale models with complex geometries. The Boundary Element method (BEM) and Displacement Discontinuity method (DDM) are examples of techniques that employ the Boundary method.

In Domain methods, the interior of the rockmass is divided into geometrically simple elements each with assumed physical and mechanical properties. The complete problem domain is discretized. Finite element (FEM) and finite difference (FDM) methods are domain techniques which treat the rockmass as a continuum. The distinct element method (DEM) is also a domain method which models each individual block of rock as a unique element. The various types of modelling methods in use in the field of rock mechanics are described below.

Boundary Element Method (BEM)

With boundary element methods, rather than discretizing the entire problem domain (as in the case of finite difference and finite element methods) only the mining excavation is discretized. The boundary of an excavation is divided into elements, with the surrounding rockmass represented implicitly. Conditions on a surface are related to the state at all points throughout the remaining rock. Stresses acting inside the rockmass are extrapolated from the boundary solution.

The advantage of the BEM is that it models the far field boundary condition correctly, restricts discretization errors to the problem boundary, and ensures a fully continuous variation of stress and displacement throughout the whole medium (Brady and Brown, 1985). 3-D BEM software developed for mining rock mechanics applications such as Map3D (Wiles, 2005) and Examine3D (Rocscience, 1998) are well suited for large scale models with complex geometries. Compared to Domain methods, much fewer elements are required, with a result that there is less demand on computer memory.

Displacement Discontinuity (DDM)

The displacement discontinuity method is commonly used in the modelling of tabular orebodies, where the entire ore seam is simulated as a 'discontinuity'. The orebody is discretized into a grid of square two-dimensional elements, with the orebody thickness representing the third dimension. Mining is simulated by

reducing ore stiffness to zero in areas where mining has occurred, producing stress re-distribution to surrounding pillars, (Hoek et al., 1995). Each element within the model has the same thickness as that part of the orebody to be mined. Output stress values obtained at specified hanging-wall or footwall sites, or within the plane of the orebody, provide a three-dimensional modelling output.

NFOLD (Golder Associates, 1989) is similar to other tabular displacement discontinuity software, such as ExamineTAB (Rocscience, 2004), but possesses additional features, such as: (1) the option of non-linear material behaviour, (2) post-process options to generate off-seam stress and displacement values, (3) backfill placement into mined stopes, and (4) variable orezone thickness.

Finite Element Method (FEM)

The finite element method involves discretizing the problem domain into elements. The finite elements are also related to the field variables by means of a governing equation which completely describes how the field variables (usually displacement) vary across the element with respect to a given boundary condition. The relationship between the boundary conditions and field variables for each element are expressed in the form of a stiffness matrix determined from the minimizing process described above. Such a matrix is then combined into a large global stiffness matrix and solved for nodal displacements.

The advantage of FEM software, such as the commonly used 2-D Phase2 (Rocscience, 2002) is that non-linear and heterogeneous material properties may be readily accommodated. Each element can have different material properties. FEM is well suited for small scale or very detailed modelling.

The major disadvantage of the FEM is that the outer boundary of the problem domain is defined arbitrarily, and discretisation errors occur throughout the domain. Model solution time increases as mesh density increases. FEM is rarely used for large scale mine models, due to complexity of model/mesh construction, and to long computing time.

Finite Difference Method (FDM)

With the finite difference method, the rockmass is treated as a continuum. Interior of rockmass is explicitly divided into zones. Zones are described by the location of nodes, with adjacent zones sharing common nodes. The finite difference method assumes that, for a small time step, disturbances at points (nodes) within the rockmass influence only its immediate neighbors. The rockmass is discretized and nodal displacements are solved individually, with no matrices being formed. Disturbances propagate through the rockmass over many time-steps until numerical convergence is attained. This process is known as explicit FDM; it involves successive, small time steps to ensure solution stability. Materials are represented by elements within a grid, which behave according to prescribed linear or non-linear constitutive models, in response to applied forces or boundary constraints.

Features of FDM modelling software, such as Flac2D (Itasca, 2002) include: 'time-dependant' analysis ("time-stepping") rather than only seeing the final solution, and the incorporation of rock structures and ground support elements into the model. FDM is appropriate for modelling of large scale deformations. The use of FDM modelling software in the mining industry is limited by user expertise. Solutions from FDM modelling can be sensitive to assumptions of joint properties, joint persistence and joint distribution.

Discrete Element Method (DEM)

For the discrete element method, the interior of the rockmass is explicitly divided into zones. Each individual block of rock is treated as a unique element that may interact at contact locations with surrounding blocks. The individual pieces of rock may be free to rotate and translate. Contacts may be represented by the overlaps of adjacent blocks, thereby avoiding the necessity of unique joint elements.

DEM is well suited for modelling structurally controlled blocky rockmasses or wedge intersections. With commercially available software, such as UDEC (Itasca, 2000), ground support elements can be incorporated in the model.

DEM software is not commonly used in the mining industry, due to high capital cost and limited user expertise available. Other limitations include the significant computational time and effort required for large or complex models, and that model solution can be sensitive to assumptions of joint properties or distribution.

A sub-class of the distinct element method is the Particle Flow Code (PFC). PFC is a program for modelling the movement and interaction of assemblies of arbitrarily-sized circular (PFC-2D) or spherical (PFC-3D) particles, (Itasca, 1995) by allowing finite displacements and rotations of discrete bodies including complete detachment. The particles may represent individual grains in a granular material or they may be bonded together to represent a solid material, in which case, fracturing occurs via progressive bond breakage. The particles are rigid but deform locally at contact points using a soft contact approach, in which finite normal and shear stiffnesses are taken to represent measurable contact stiffnesses. PFC is not commonly used for mining simulations, however, it does have applications as a research tool for simulations of bulk flow (Hadjigeorgiou et al., 2002) or studies of micro-cracking in solid bodies (Diederichs, 1999).

4.2 Selection of modelling tools

Numerical modelling is an attempt to mathematically simulate the way the rockmass responds to mining. The user specifies the loading conditions, specifies the geometry, assumes that elasticity and/or non-linearity applies, and then solves the model to predict stresses, strains and displacements throughout the rockmass.

- Loading conditions - Prior to mining the rockmass is loaded by overburden and tectonic forces. These are commonly referred to as the far field or in situ pre-mining stresses.

- Geometry - When excavations are made, the pre-existing loads are redistributed around the excavations, concentrating in abutments and pillars.
- Elasticity - At locations where the stresses do not exceed the strength, the rock deforms in a more or less elastic manner. This simply means that the deformations are relatively small in magnitude and are mostly recoverable. Unless it is of low quality, a rockmass will respond more or less elastically (Kaiser et al., 2002). Yielding zones tend to be confined to locations in the immediate vicinity of mining excavations. At these locations, stresses are concentrated to the point where they exceed the strength of the rockmass, leading to yield and deformation. Such deformations can be relatively large in magnitude and are mostly non-recoverable.

All numerical models provide predictions of stresses, strains and displacements. While modelling by itself is reasonably straight forward, it is the interpretation of the modelling results that is the real challenge. Model predictions of stress, strain or displacement must be related to the response onserved in situ. For example, by examining modelling results from the stress analysis, locations and magnitudes of over-stressed (or potential yielding) of stress-relief (or relaxation) can be determined for a given mine geometry.

In Canadian hard rock mines, the boundary element method (BEM) and finite element method (FEM) approaches are commonly employed for underground excavation design, Two modelling packages, Map3D (Wiles, 2005) and Phase2 (Rocscience, 2002) have been selected for the model parametric study.

4.2.1 Map3D software

Map3D (Wiles, 2005) is a comprehensive three-dimensional rock stability analysis package, based on BEM. The program is capable of constructing 3-D geometries, analysing induced stress and displaying displacements, strains and

stresses. For this study, the Standard Version (SV) program was used for its ability to model up to 300,000 elements. The program can accommodate multi-step mining sequences and multiple material zones with different material properties and stress states.

The standard linear elastic version of Map3D features a built-in CAD interface, the ability to analyze very large problem sizes, multiple elastic zones with different moduli. Shapes ranging from simple tabular shapes to detailed 3-D excavation shapes and large scale mine wide problems can be simulated. Users build models using a series of three-dimensional building blocks to define excavations, accesses and geologic features. A model comprises one or more connected or unconnected blocks and/or planes that can be mined and filled in a specified sequence. Surfaces of blocks and planes are subsequently discretized into a number of boundary elements by the program.

Analysis results can be contoured on element surfaces or on a series of used defined field point grid planes. These later planes can be positioned at any desired location and allow contouring of stresses, strains, displacements, strength factors or any desired combination of these components.

4.2.2 Phase2 software

While boundary elements are an efficient means to determine the elastic stress distribution, finite element programs offer the added functionality of being able to determine stress redistribution during pillar failure provided that the post-peak behaviour of the rock is known. Phase2 (Rocscience, 2002) is a windows-based two-dimensional rock stability analysis package, using a FEM solution, with automatic finite element mesh generation capabilities.

With Phase2, stresses and displacements around underground or surface excavations are calculated to assess elastic or non-linear progressive failure. The software is applicable to a wide range of engineering applications, including

complex tunneling problems in weak rock, underground powerhouse caverns, surface excavations such as open pit mines, and slopes in rock or soil.

Excavation, material and stage boundaries can be defined using drawing tools, or by entering the coordinates. Materials and excavation sequences are assigned with the click of a mouse. The analysis interface allows contouring of stresses, strains, displacements, strength factors or any desired combination of these components.

4.3 Characterization of input data for ore dilution models

The sensitivity of controlling stope geometry and stope setting on potential overbreak is examined in this section. Trends identified from numerical modelling, along with discussions on construction considerations are presented in Chapter 5.

4.3.1 Stope geometry

Stope geometry common to Canadian long-hole mining operations were selected for the model. Examples of reported long-hole stope geometries from Canadian mines are listed in Table 4.1. Terminology used to describe stope geometry is shown schematically in Figure 4.2.

For this parametric study, stope dimensions varying from 10m to 40m in both strike length and vertical stope height were assessed. Modelled stopes were assigned a width of 10m. Two values of hanging-wall dip were assessed: 80^{o} and 60^{o}. Footwall dip was kept parallel to the modelled hanging-wall dip angle to maintain the tabular nature of the orebody.

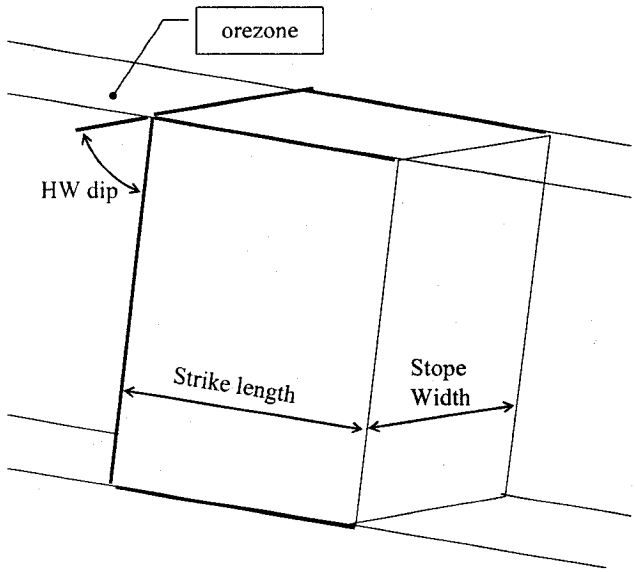

Oblique view

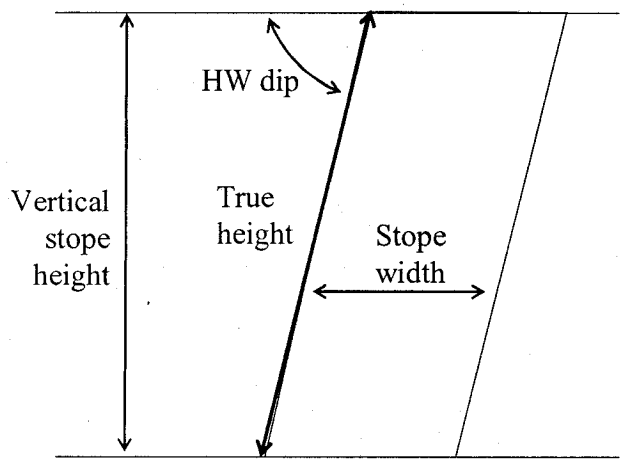

Section view

Figure 4.2 Modelled stope geometry terminology

Table 4.1 Example long-hole stope geometries, typical Canadian mine environment

Company, Mine	Location	Vertical height, m	Strike Length, m	Stope width, m	Hanging wall dip	Depth, m	Source
Barrick Gold, Bousquet 2 mine	Preissac, Quebec	30	10 to 15	3 to 15	80° - 85°	1240	(1), (2)
Agnico Eagle, Laronde mine	Preissac, Quebec	30	15	8	80°	970	(3)
Cambior, Doyon mine	Rouyn-Noranda, Quebec	13 to 30	10 to 15	8 to 20	65°	1000	(1)
Falconbridge, Kidd Creek mine	Timmins, Ontario	30 to 40	25	15 to 20	75° - 90°	1555	(1)
Inco, Garson mine	Sudbury, Ontario	30	10	12	70°	1293	(1)
Falconbridge, Thayer Lindsley mine	Sudbury, Ontario	20	4 to 10	30	55° - 85°	1628	(1)
Newmont, Golden Giant mine	Marathon, Ontario	30	15	20	60° - 70°	1145	(1)
Barrick Gold, Williams mine	Marathon, Ontario	25	20	20	60° - 70°	1205	(1), (4)
Inco, T-3 and 1-D mine	Thompson, Manitoba	30	15	15	60° - 90°	805	(1)
Hudson Bay, Trout Lake mine	Flin Flon, Manitoba	30	25	8	55° - 60°	1100	(1)

Note: (1) Canadian Mining Journal (2003); (2) Henning et al. (2001a); (3) Gauthier, 1992; (4) Bronkhorst and Brouwer (2001)

4.3.2 Stope type

A stoping sequence common to many Canadian mines employing longhole methods uses a pyramidal or chevron mining front. An example, adopted from Heal et al. (2005) is shown in Figure 4.3. Stopes are sequenced to maintain a triangular shape to the mined-out area by mining vertically with a lead stope, then outward along the rill of the triangle towards its base.

The lead primary stope, subjected to elevated stresses as a result of the high level of confinement, creates a 'bow wave' effect that tends to distress adjacent primary stopes and shed stresses to the abutments. This 'halo' of failed ground in the bow wave of the lead stope should allow improved ground conditions in subsequent panels (Board et al., 2001). With careful scheduling, adjacent primary stopes are mined and filled for two vertical lifts before mining of the secondary stope between them is started (Bronkhorst and Brouwer, 2001; Potvin and Hudyma, 2000).

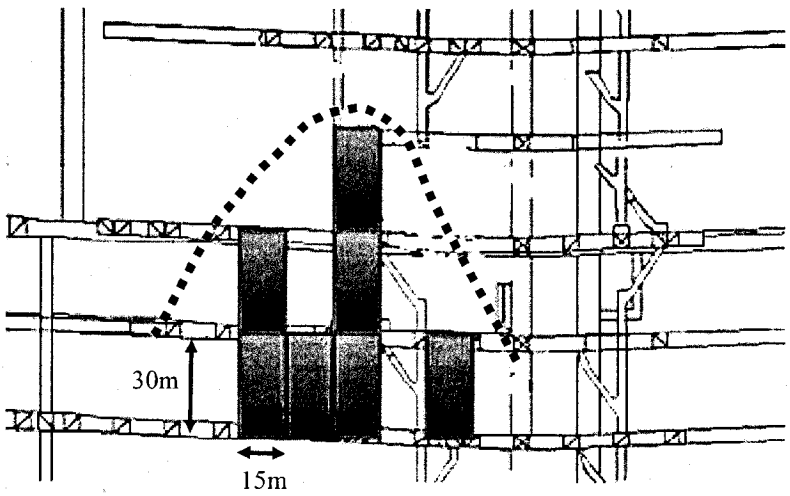

Figure 4.3 Illustration of stope categories at Laronde mine. Dashed line represents advancing chevron mining front (modified from Heal et al., 2005)

As discussed in Section 3.5.2, an important, sometimes overlooked, parameter affecting unplanned dilution is the local stope setting within the mining sequence. Depending on its placement within a planned mining sequence, a stope may be

bound by rock on both walls and above (a primary stope), or it may have backfill on one or both walls (a secondary stope). The hanging-wall stress setting differs between primary and secondary stopes, (Wang, 2004; Henning et al., 2001b; Hyett et al., 1997).

For this parametric study, a block of equally dimensioned stopes measuring three stopes high by three stopes wide were generated in Map3D. Potential stope categories are compiled in Table 4.2 and illustrated in Figure 4.4. Modelled stope geometries for primary and secondary stopes are illustrated in Figure 4.5 and 4.6.

Table 4.2 Stope categories, based on setting within mine sequence; Figure 4.4

Stope category	Code	Description
Primary 1	P1	Rock on both side
Primary 2	P2	Rock on both side walls. Stope located above backfilled stope.
Primary 3	P3	Rock on both side walls. Stope located above two backfilled stopes.
Secondary 1	S1	Rock on one side. Other stope wall is against backfill.
Secondary 2	S2	Both side walls of stope are against backfill

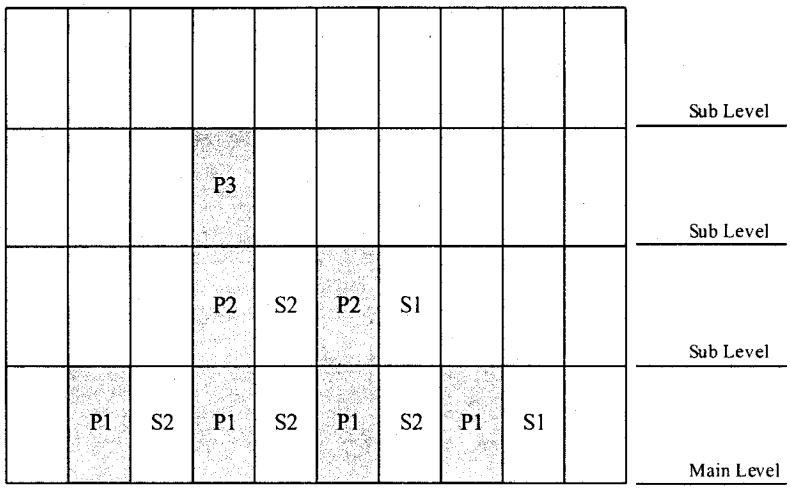

Figure 4.4 Stope categories within mining block

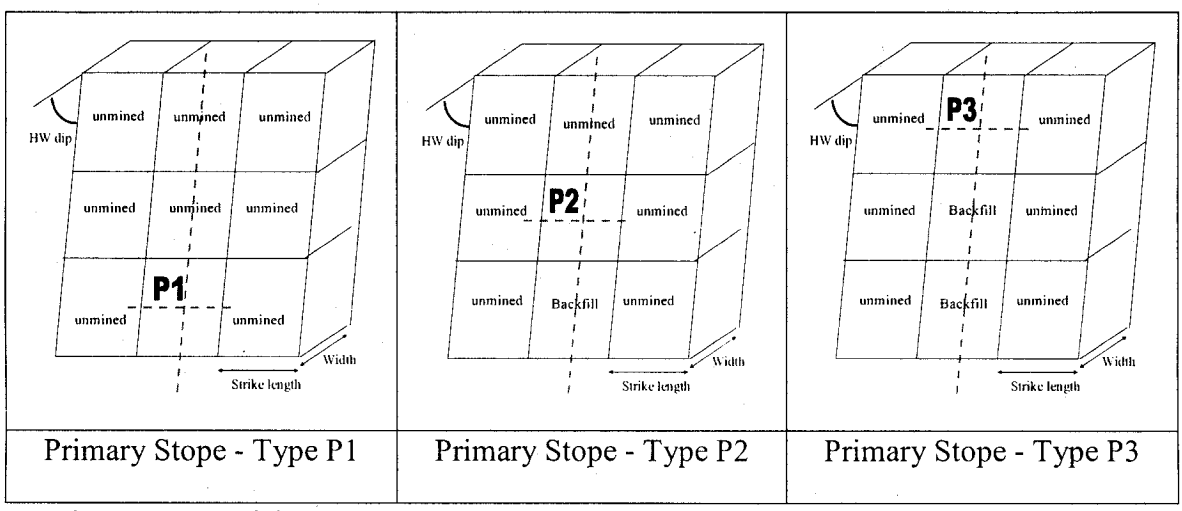

Primary Stope - Type P1 | Primary Stope - Type P2 | Primary Stope - Type P3

Figure 4.5 Model geometry - Primary Stope types

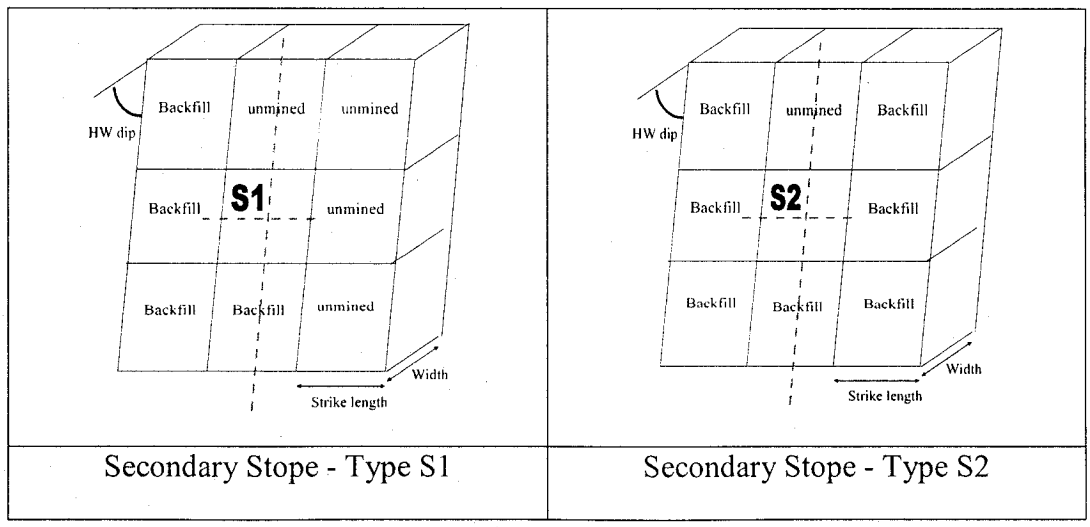

Secondary Stope - Type S1 | Secondary Stope - Type S2

Figure 4.6 Model geometry - Secondary Stope types

4.3.3 In situ stress

When an excavation is made in a rockmass, the initial in situ stresses are disturbed and redistributed in the vicinity of the excavation. In situ stresses can therefore be categorized into pre-mining (natural, far field) stresses and induced (due to excavation) stresses.

4.3.3.1 Pre-mining stress

Pre-mining stresses are those found in rock at depth prior to man-made excavations. These natural stresses result from the weight of the overlying strata (gravitational stress) and from locked in stresses of tectonic origin (tectonic stress). Gravitational stress is due to the effect of gravity on the overburden rock. Tectonic processes have been responsible for faulting, shearing, folding and variations in surface elevations over geologic time. In the Canadian Shield, these tectonic stresses tend to be lateral.

Pre-mining or in situ stresses are usually reported in terms of principal stresses σ_1, σ_2 and σ_3 and their associated orientations in terms of trend and plunge. In the Canadian Shield the major and intermediate principal stresses σ_1 and σ_2 tend to be near horizontal with plunges between zero and about 10°, and the minor principal stress σ_3 is approximately vertical, (Arjang and Herget, 1997). Consequently, the maximum and minimum horizontal stresses σ_H and σ_h and the vertical stress σ_v are used synonymously with σ_1, σ_2 and σ_3 respectively. The ratio of the average horizontal stress to the vertical stress is denoted by the letter k such that:

$$\sigma_h = k \cdot \sigma_v \qquad (4\text{-}1)$$

Measurements of horizontal stresses show that the ratio k tends to be high at shallow depth and that it decreases at depth (Hoek and Brown, 1980; Herget, 1988), as illustrated in Figure 4.7.

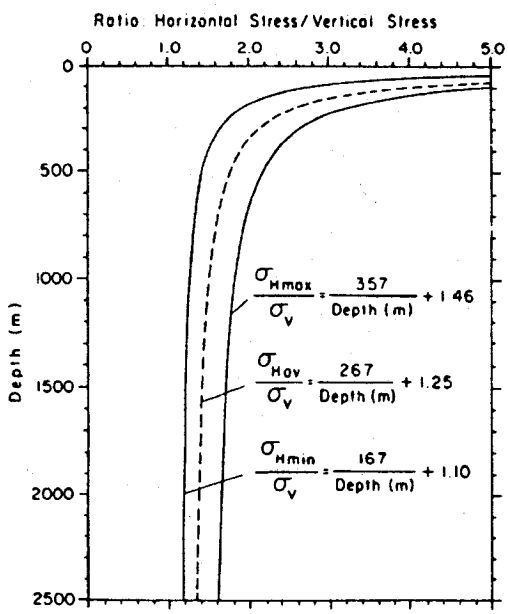

Figure 4.7 Variation of horizontal in situ stress-to-vertical stress ratio with depth, Herget (1988)

The gravitational vertical stress σ_v at a depth H is the product of the depth and the unit weight of the overlying rockmass, γ, implying that the overburden stress should increase linearly with depth. While measurements of the vertical stress at various mining and civil engineering sites support this linear relationship, the vertical stress can vary significantly as a result of tectonic activities. Horizontal stresses at depth in the Canadian Shield have a non-linear trend with depth for horizontal stresses, as indicated in Figure 4.8. Re-evaluation of documented stress data by Diederichs (1999) recommended that only the vertical stress be estimated by a linear depth relationship (Equation 4-2). Maximum and minimum horizontal stresses are estimated from non-linear depth functions (Equations 4-3 and 4-4).

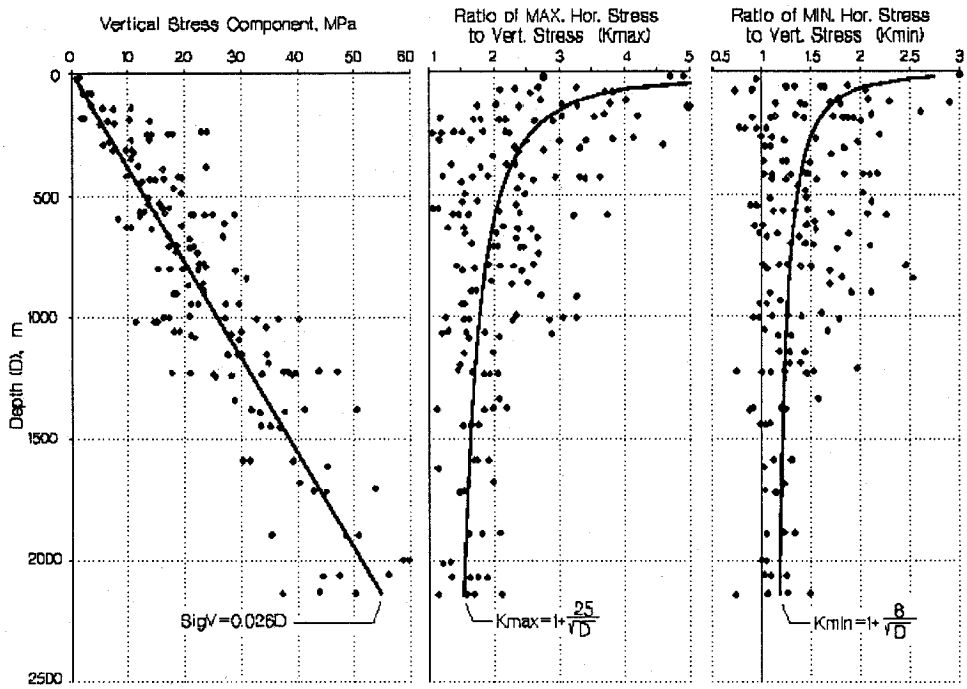

Figure 4.8 Stress data (after Arjang and Herget, 1997) reinterpreted by non-linear depth functions (Diederichs, 1999)

σ_v = 0.026 D (MPa), where D is the depth in metres below surface (4-2)

$\sigma H_{max} = K_{max} \cdot \sigma_v$ (MPa), where (4-3)

$$K_{max} = 1 + \frac{25}{\sqrt{D}}$$

$\sigma h_{min} = K_{min} \cdot \sigma_v$ (MPa), where (4-4)

$$K_{min} = 1 + \frac{8}{\sqrt{D}}$$

For the parametric study, stress regimes at three depths were considered, separated in 750m intervals of depth. Shallow depth corresponds to a 750m depth. A depth of 1500m was considered moderate, while deep mining was

represented by stopes at a depth of 2250m; see Table 4.3. Horizontal-to-vertical stress ratio decreases from 1.9 to 1.5 with depth.

Table 4.3 Pre-mining stress magnitudes associated with shallow, moderate and deep mining

Depth category	Depth below surface	σ_H	σ_h	σ_v	k
Shallow	750m	37.3 MPa	25.2 MPa	19.5 MPa	1.9
Moderate	1500m	64.2 MPa	47.1 MPa	39.0 MPa	1.6
Deep	2250m	89.3 MPa	68.4 MPa	58.5 MPa	1.5

4.3.3.2 Induced stress

Induced stresses are the result of excavation activity. Because of its natural, virgin stresses, all rock is subjected to compression. When an excavation is made, the rock left standing has to take more load since the original confinement provided by the rock within the excavation has been removed. The stresses and displacements induced in the rock surrounding an excavation depend on:

- The initial, pre-mining state of stress (which may, itself, have been influenced by other nearby openings),
- the geometry of the excavation, and
- the constitutive (stress-strain) behaviour of the rockmass.

These induced stresses and displacements influence the stability of the excavation and possible extent of hanging-wall dilution.

4.3.4 Rockmass quality

Numerous rockmass classification systems have been proposed and used in engineering practice, such as the RQD (Deere, 1968), Rock Mass Rating (RMR) (Bieniawski, 1976), Q (Barton et al., 1974), and RMi system (Palmstrøm, 1996). Some systems are based on the modification of the existing ones to suit specific application. For example, the RMR system was modified by Laubscher (1990) for mine design. The Q-system was modified by Potvin (1988) for stope design.

For the parametric study, three categories of rockmass quality were considered, ranging across the spectrum of rockmass qualities common to Canadian mines employing long-hole mining (Potvin and Hudyma, 2000; Choquet, 1988). They are: Very good quality rock, good quality, and fair quality rock.

Rockmass conditions were classified using the Geological Strength Index (GSI) system, developed for Canadian mining by Hoek et al. (1995). See Figure 4.9. The GSI system, like the RMR and Q classification systems, relies on the visible structure of the rockmass as represented by joint spacing and surface characteristics. However, unlike the RMR and Q-systems, the GSI approach considers the qualitative characteristics of the rockmass as a whole, rather than assessing the quantitative characteristics of discrete joint sets. With the GSI approach, the rockmass is assessed by the visual geological description its block size and joint surface condition or by its typical block size (Cai et al., 2004). Rockmass quality decreases as the structure of the exposed rock face becomes less interlocked. Rockmass quality is further diminished as quality of the joint surfaces is reduced. Terminology used by Hoek et al. (1995) to define the structural and surface conditions is summarized in Table 4.4. GSI classification of the three ranges of rockmass quality used in this study is described in Table 4.5.

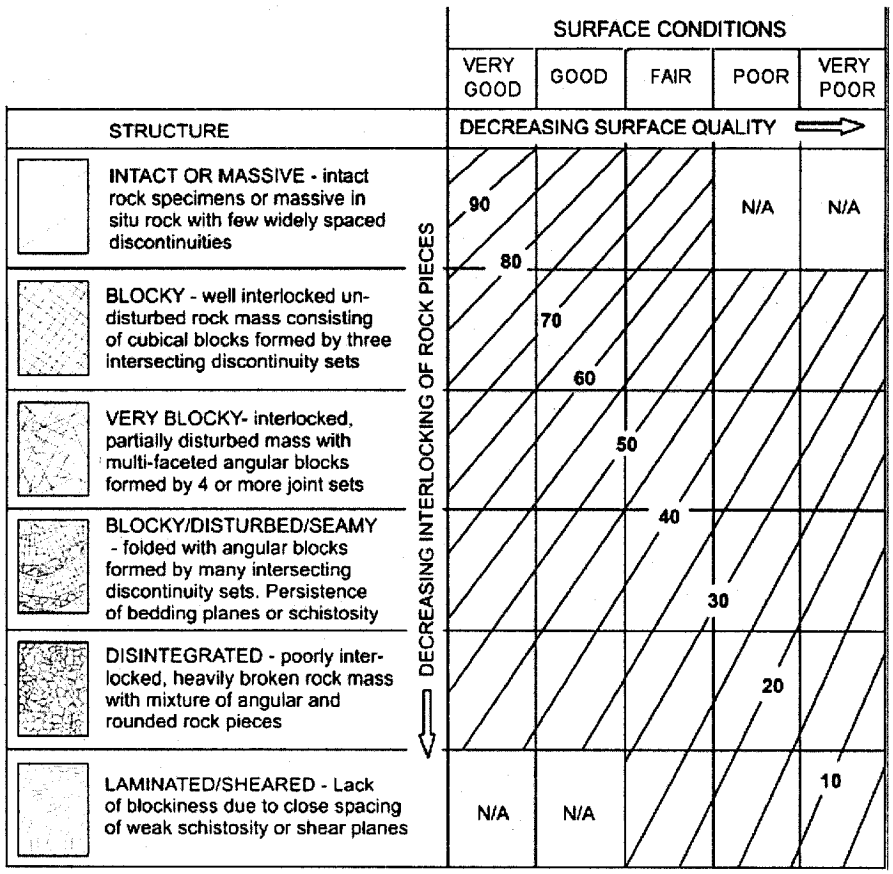

Figure 4.9 Geological Strength Index (GSI) classification, Hoek et al. (1995)

Table 4.4 GSI classification categories (Hoek at al., 1995)

1.0 Structural conditions		
	Category	**Description**
Decreasing condition ⇩	Intact or Massive	Intact rock specimens or massive in situ rock with few widely spaced discontinuities.
	Blocky	Very well interlocked undisturbed rockmass consisting of cubical blocks formed by three orthogonal discontinuity sets.
	Very Blocky	Interlocked, partially disturbed rockmass with multifaceted angular blocks formed by four or more discontinuity sets.
	Blocky / Disturbed	Folded and faulted with many intersecting discontinuities forming angular blocks.
	Disintegrated	Poorly interlocked, heavily broken rockmass with a mixture of angular and rounded blocks.
2.0 Surface conditions		
	Category	**Description**
Decreasing condition ⇩	Very Good	Very rough, unweathered surfaces.
	Good	Rough, slightly weathered, iron stained surfaces.
	Fair	Smooth, moderately weathered or altered surfaces.
	Poor	Slickensided, highly weathered surfaces with compact coatings or fillings containing angular rock fragments.
	Very Poor	Slickensided, highly weathered surfaces with soft clay coatings or fillings.

Table 4.5 Physical description of rockmass quality ranges

Rockmass quality category	GSI value	Relative quality	Typical description	Typical block size (Cai et al., 2004)	Equivalent rockmass classification (Equations 4-5 to 4-7)
Very good	80	Very good	Massive to blocky rock, good surface conditions	$125cm^3$	RMR ~ 80 Q ~ 50
Good	65	Good	Blocky rock, good surface conditions	$50cm^3$	RMR ~ 65 Q ~ 10
Fair	50	Fair	Blocky to very blocky rock, good to fair surface conditions	$15cm^3$	RMR ~ 50 Q ~ 2

GSI can also be related to other classification methods, such as RMR and Q, for use with existing empirical design approaches, as shown in Equations (4-5) and (4-7), (Hoek et al., 1995; Kaiser et al., 1986; Milne et al., 1998).

$$GSI = RMR_{76} \quad (4\text{-}5)$$

$$GSI = RMR_{89} - 5 \quad (4\text{-}6)$$

$$GSI = 9\ln Q + 44 \quad (4\text{-}7)$$

Hoek–Brown strength parameters m_b and s; as well as elastic modulus E can be determined from GSI values for design purposes. Equations for obtaining

generalized Hoek-Brown criterion for jointed rockmasses, described in (Hoek et al., 2002) are provided in Table 4.6. The uniaxial compressive strength of the rock considers detailed failure propagation process. Global "rock mass strength" considers the overall behaviour of a rockmass. For example, when considering the strength of a pillar, it is useful to have an estimate of the overall strength of the pillar rather than a detailed knowledge of the extent of fracture propagation in the pillar.

Table 4.6 Mechanical rockmass properties as determined from the GSI classification (Hoek et al., 1995)

Hoek-Brown (H-B) 'm'	$m_b = m_i \exp\left(\frac{GSI-100}{28-14D}\right)$
Hoek-Brown (H-B) 's'	$s = \exp\left(\frac{GSI-100}{9-3D}\right)$
Hoek-Brown (H-B) 'a'	$a = \frac{1}{2} + \frac{1}{6}\left(e^{-GSI/15} - e^{-20/3}\right)$
Elastic Modulus (σ_c > 100 MPa)	$E_{rm}(GPa) = \left(1 - \frac{D}{2}\right) \cdot 10^{((GSI-10)/40)}$
uniaxial rockmass compressive strength	$\sigma_c = \sigma_{ci} . s^a$
global "rock mass strength"	$\sigma'_{cm} = \sigma_{ci} \cdot \frac{(m_b + 4s - a(m_b - 8s))(m_b/4 + s)^{a-1}}{2(1+a)(2+a)}$
rockmass tensile strength	$\sigma_t = -\frac{s\sigma_{ci}}{m_b}$

Note: D is a factor which depends on the degree of disturbance to which the rockmass has been subjected by blast damage and stress relaxation. For undisturbed in situ rockmasses: D=0, for very disturbed rockmasses: D=1. Factor D is discussed in Chapter 5.

4.3.5 Rock strength property

Canadian mineral deposits are typically associated with the crystalline rock forming the Precambrian age Canadian Shield physiographic region. Lithic assemblages associated with mineral deposits are igneous rock, such as basalt, andesite, rhyolite and granite, or metamorphically altered rock, such as greywacke, conglomerate and breccia, (Lang et al., 1968). For the parametric study a uniaxial compressive strength value of σ_c = 175 MPa was used, which corresponds to a mid-range strong rock, as shown in Table 4.7. The data in Table 4.7 is extracted from Adler and Thompson (1992), Mitri et al. (2005), Mitri and Bétournay (2005), and Morrison (1976).

Table 4.7 Rocks classified by strength

Class	Uniaxial Compressive Strength (σ_c), intact rock	Examples
Weak	< 40 MPa	coal, potash, weathered rock, alluvium
Moderate	40 MPa – 140 MPa	shale, sandstone, limestone, schist
Strong	140 MPa – 200 MPa	granite, andesite, rhyolite breccia, tuff, porphyry, marble, slate
Very Strong	> 200 MPa	quartzite, basalt, diabase, gabbro, norite, tuff, porphyry

4.3.6 Other influences

The study assumes homogenous rockmass conditions. In reality, local factors such as the occurrence of faulting near the stope boundary and laminar/foliated structure parallel to the exposed hanging-wall will influence severity of overbreak.

4.3.6.1 Faulting influence on dilution

Behaviour at the stope walls is largely controlled by the strength of the rockmass surrounding a stope, which in turn depends on the geometrical nature and strength of the geological discontinuities as well as the physical properties of the intact rock bridges (Diederichs and Kaiser, 1999). Major discontinuities (usually continuous on the scale of a stoping block) such as faults, shears and dykes usually have very low shear strength and, if oriented unfavorably, provide a failure surface when exposed by, or are in close proximity (see Figure 4.10) to the stope walls. Such geological discontinuities largely control overbreak and stability around exposed stope walls. The location of these main geological discontinuities is well defined and most mines have a three-dimensional model of the local fault/shear network

According to Suorineni et al. (1999b), the most important factors influencing the severity of fault-related sloughage are; (1) the angle between a fault and a stope, and (2) the position of the fault relative to the stope. Sloughage increases as the angle between the stope surface and the fault increases from 0° toward a critical range of 20° to 45°, then decreases, as the fault becomes perpendicular to the stope wall. Sloughage is worst when the intersection occurs near the bottom of the stope for faults dipping toward a stope and intersecting the stope wall. When faults are near a stope but do not intersect it, the distance to the fault controls the amount of fault-related sloughage. Fault-related sloughage is greatest when the fault is located closer than 0.2 times the stope height from the stope wall (Suorineni, 1998). When a fault is further than 0.3 times the stope height from the wall, it has little effect on sloughage.

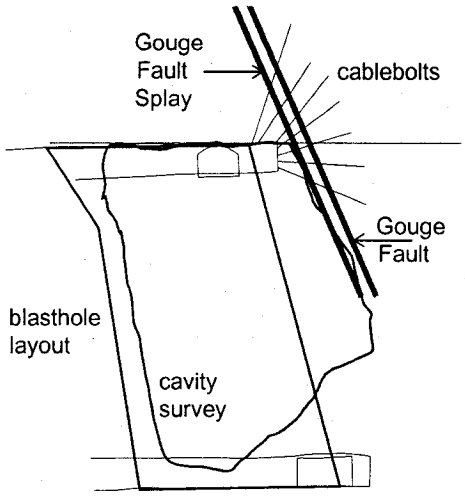

Figure 4.10 Stope section showing hanging-wall sloughage and geologic structure. Modified from Tannant et al., 1998

4.3.6.2 Foliation influence on dilution

Stope wall behaviour is also a function of the number, size, frequency and orientation of the minor scale geological discontinuities. The geometrical discontinuity set characteristics (size, frequency, orientation, etc) relative to the stope walls can influence the nature and amount of dilution experienced. A rockmass comprised of discontinuous joint sets has a greater self-support capacity than when joint sets are continuous, Diederichs and Kaiser (1999).

Foliated rock consists of individual strata with little or no resistance against separation along the boundaries between the strata. When exposed in the stope hanging-wall, relaxation-induced hanging-wall delamination can occur (Kaiser et al., 2001).

Foliation that is orientated parallel to the stope wall causes less problems than foliation that is at a shallow (< 20°) angle to the wall. See Figures 4.11(a) and 4.11(b). When the foliation cuts across the wall of a stope, as shown in Figure 4.11(a), the rock is allowed to unravel and cave more easily. Foliation orientated perpendicular to the stope wall (Figure 4.11c) represents the most stable condition

for a stope within a foliated rockmass. Undercutting of the hanging-wall further promotes overbreak (discussed in Section 5.8.3).

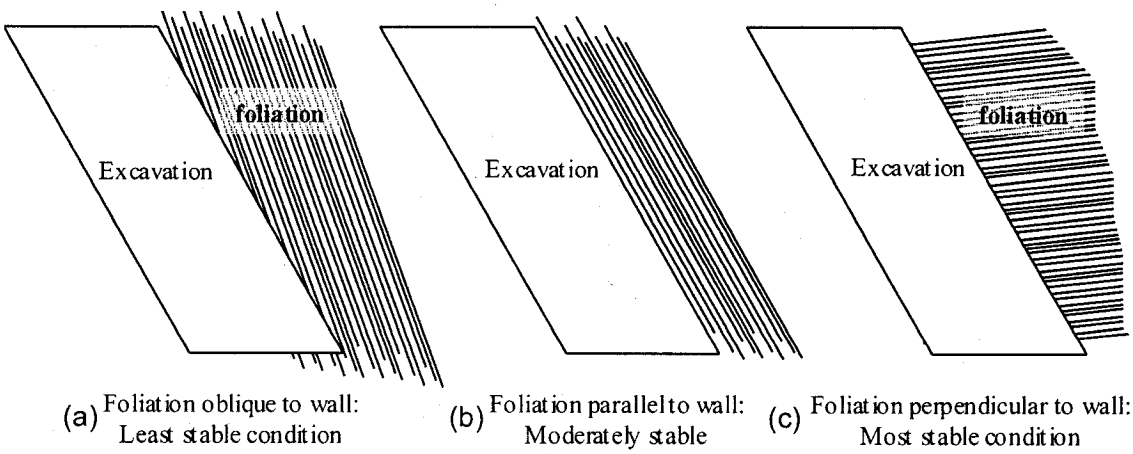

Figure 4.11 Effect of rockmass foliation on stope wall stability

Buckling failure of large thin slabs of rock is possible in stopes that have their walls oriented parallel to the rockmass foliation (Figure 4.12). The severity of buckling failure is dependant on the tangential stress around the opening, wall height, and the thickness of the slabs created by the foliation (Quesnel and Ley, 1991). Buckling failures can be controlled or prevented by using rockbolts or cablebolts installed across the foliation planes in order to tie a number of thin slabs into thicker, more stable, slabs.

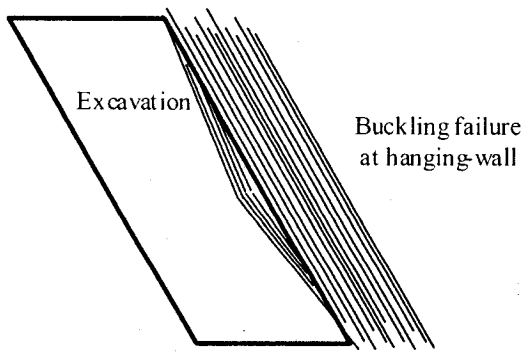

Figure 4.12 Possible buckling failure mode when the rockmass structure contains thin slabs parallel to the hanging-wall

4.4 "Typical" stope description for the model parametric study

A primary (type-P1) stope with an 80 degree hanging-wall and footwall dip, and dimensions measuring 30m high x 10m thick, with a strike range of 10m to 40m was selected as a base case. See Figure 4.13. The setting of the base-case stope was at moderate depth (Z = 1500m), in moderately strong rock, with mid-range rockmass quality (GSI = 65) for both the orezone and hostrock. Stopes of these dimensions area not uncommon to Canadian blasthole mines, as indicated by Table 4.1.

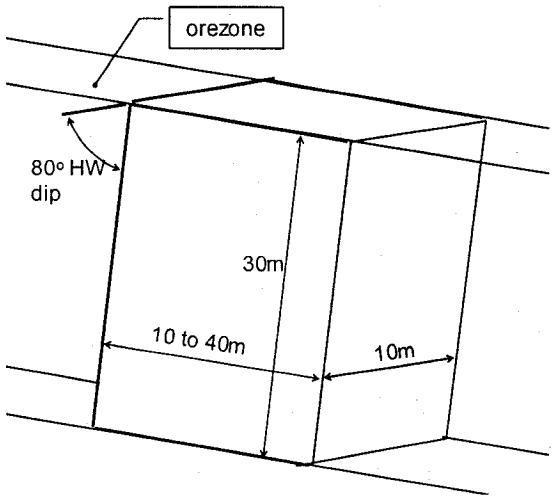

Figure 4.13 "Typical" stope geometry used for the model parametric study

4.5 Model parameters

Input parameters for the modelling, summarized in Table 4.8 were obtained from relationships described in Section 4.3. In the model, as in common practice, backfill provides a measure of surface confinement to the walls of the mined stope, hence reducing the magnitude of unfavelling over time. With longhole mining, in order to maximize ore recovery, it is common to return and mine pillars following primary mining recovery. As this is done, large surface areas of backfill may be exposed as a free standing wall. Cemented fill is used as an artificial support. Results of practical studies show that cement content in a fill and its slurry density are essential factors affecting fill stability and the economy

of backfilling (Hassani and Archibald, 1998). Primary stopes are commonly backfilled with materials such as consolidated or cemented rockfill (CRF), cemented tailings and pastefill. Stopes not requiring consolidated backfill, such as secondary stopes, may be filled with waste rock. For the parametric study, mined stopes were backfilled with CRF material, using parameters listed in Table 4.9.

Table 4.8 Model parameters for host and orezone rock

	Very good rockmass quality	Good rockmass quality	Fair rockmass quality
Material values			
GSI	80	65	50
Uniaxial compressive strength, (σ_c)	175 MPa	175 MPa	175 MPa
Hoek-Brown constant for intact rock, (m_i)	25	25	25
Poisson Ratio	0.25	0.25	0.25
Rockmass values calculated with GSI value			
Rockmass elastic modulus, (E_{rm})	56234 MPa	23713 MPa	10000 MPa
Hoek-Brown 'm'	12.24	7.16	4.19
Hoek-Brown 's'	0.108	0.021	0.004
Hoek-Brown 'a'	0.501	0.502	0.506
Rockmass tensile strength, (σ_t)	1.55 MPa	0.50 MPa	0.16 MPa
Global rockmass compressive strength, (σ_{cm})	91.5 MPa	64.6 MPa	47.5 MPa

Table 4.9 Model parameters for consolidated rockfill, Hassani and Archibald (1998)

Parameter	**Material Value**
Uniaxial compressive strength, σ_c	3 MPa
Elastic modulus, E	2500 MPa
Poisson Ratio, υ	0.35
Mohr-coulomb parameters	
Cohesive strength	0.1 MPa
Internal angle of friction	35 degrees

4.6 Design criteria for stope overbreak evaluation

When an excavation is made in a prestressed rock, the magnitude and orientation of stresses in the vicinity of the excavation will be changed. Following the creation of the excavation, the surface of the excavation may become de-stressed. Within the de-stressed area, a zone of tensile stress (zone of relaxation) may develop. Instability in an underground excavation is closely related to the zone of relaxation (Diederichs and Kaiser, 1999; Kaiser et al., 1997, Martin et al., 2000, Stewart and Trueman, 2004). Milne et al. (1996) divide the mechanisms that drive hanging-wall deformation into three general stages:

(1) With initial exposure, elastic relaxation and stress redistribution around the hanging-wall contributes to rapid stress redistribution. Results of the response of an instrumented hanging-wall, reported by Hyett et al. (1997), show a near-instantaneous response. Event 'A' in Figure 4.14 shows immediate response after blast. Event B illustrates time-dependant hanging-wall deterioration.

(2) With increased time of hanging-wall exposure, the rockmass modulus decreases as fractures in the rockmass dilate towards the stope. See event 'B' in Figure 4.14. This degradation of the rockmass was described in Kaiser et al. (1997) as a condition where the rockmass quality has been reduced relative to its virgin state. Rockmass degradation, described as a loss of strength to the rockmass, can be induced artificially by poor blasting practices. In moderately jointed, hard rocks, rockmass degradation is mostly caused by high stresses.

(3) With longer exposure time the rockmass further deteriorates and an arching or discontinuum mechanism may control deformation.

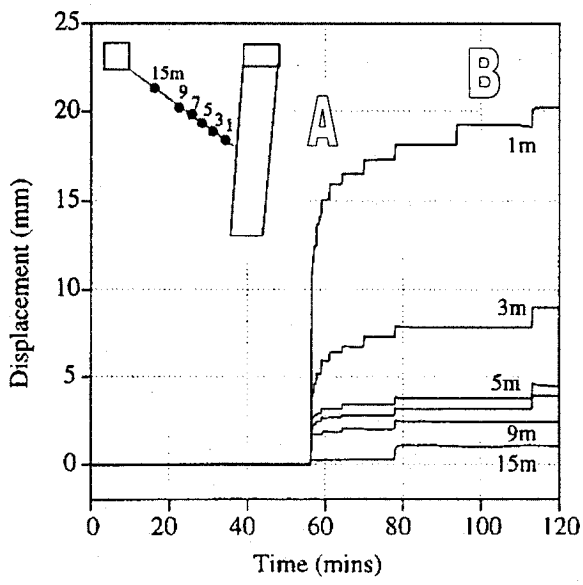

Figure 4.14 Time dependant hanging-wall response to a blast. Modified from Hyett et al., 1997

4.6.1 Criteria for sloughage potential

With stope excavation, principal in situ stresses rotate such that the major (σ_1) and intermediate (σ_2) principal stress are aligned parallel to the excavation hanging-wall. Minor principal stress (σ_3) tends to align perpendicular to the excavation boundary, as shown in Figure 4.15 (Kaiser et al., 2001). The stress field on excavation wall always has no shear and no normal stress, hence, the excavation

wall is always a principal stress plane and two stress components must be parallel to the wall. Overbreak occurs due to the loss of confinement in the radial direction to the stope wall and a drop in σ_1 and σ_2 The tangential stresses σ_1 and σ_2 may decrease in addition to the decrease of σ_3 causing a larger area of caving or this may bring stable hanging-walls to failure.

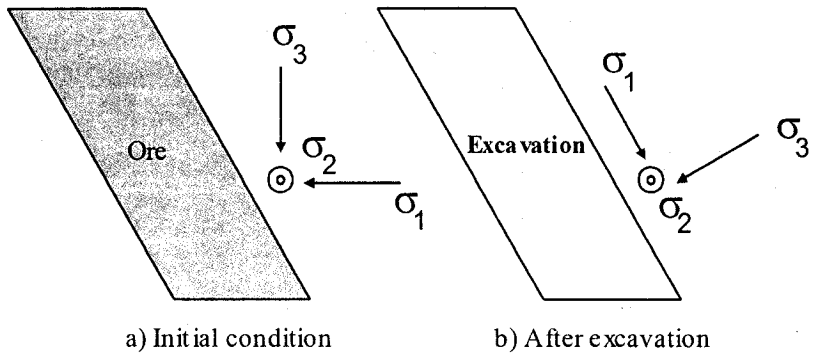

Figure 4.15 Principal stress orientation before and after stope excavation

The zone of relaxation defines an envelope within which gravity driven block failures may occur. It can be assumed that the volume of hanging-wall relaxation represents a potential volume of unplanned dilution. The notion that a simple confining stress (tensile strength) criterion can be used to assess hanging-wall stability and dilution potential has been reported by Mitri et al. (1998), Martin et al. (1999), Martin et al. (2000), and Alcott et al. (1999). A potential for sloughage exists in this region with confinement loss ($\sigma_3 \leq 0$ MPa). However, not all of this zone will fail if the rockmass has some self-supporting capacity.

Sloughage potential is assumed to be a function of loss of confinement, which results in the creation of zones of relaxation, and the exploitation of this confinement loss by structures or planes of preferential weakness within that zone. The nature of the structures determines the tensile strength of the rockmass in question. In massive to moderately jointed rock, residual tensile load bearing strength arising from incomplete fracturing or from rock bridges separating non-

persistent jointing is a key factor in the control of ultimate gravity driven failure of jointed or stress damaged ground (Diederichs, 1999).

The occurrence and potential severity of overbreak is influenced by the tensile strength of the rockmass. In turn, the tensile strength depends on the material properties of the rock and the structures present within it. For good rockmass conditions (GSI = 65), the corresponding rockmass tensile strength is σ_t = 0.5 MPa, as calculated from the equation provided in Table 4.6.

4.6.2 Estimation of overbreak volume

Relaxation depth was determined from iso-contours of minimum principal stress (σ_3), located on a vertical plane located at the stope mid-spans. For the parametric study, hanging-wall relaxation depth was defined as the maximum depth of the σ_3 = 0 contour relative to the excavation boundary, measured from the center of the stope wall.

With the Map3D models, hanging-wall stresses were plotted onto grids placed at the mid-span and mid-height of the stope, as illustrated in Figure 4.16. Grid planes were orientated normal to the hanging-wall dip, and extend a distance of 15m away from the stope boundary. The extent of the potential relaxation zone associated with a given stope geometry of setting was determined from contours of minimum stress.

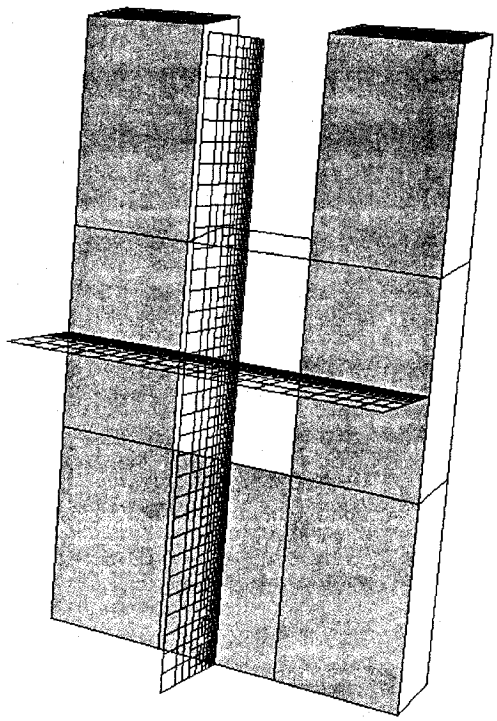

Figure 4.16 Grid plane position at stope mid-height and mid-span. Secondary (S2) stope model shown

The volume of potential hanging-wall relaxation for a given 3-D stope geometry was estimated using an approach described in Pakalnis et al. (1998) in which the overbreak volume was represented as the volume of half a prolate ellipsoid, illustrated in Figure 4.17. The volume (V) of hanging-wall relaxation is calculated as:

$$V = 2/3\pi \cdot r_1 \cdot r_2 \cdot r_3 \ (m^3) \qquad (4\text{-}8)$$

where r_1, r_2 and r_3 correspond to the perpendicular, vertical and horizontal radius distances from center (mid-span and mid-height) of stope hanging-wall contact.

When using a 2-D numerical model, such as Phase2, the third dimension is infinitely long. Overbreak is defined in terms of depth of hanging-wall relaxation

(r_1) and height of relaxation zone ($2 \cdot r_2$), as illustrated in Figure 4.18. For a 2-dimensional case, the area (A) of hanging-wall relaxation is calculated as:

$$A = \frac{1}{2} \pi \cdot r_1 \cdot r_2 \ (m^2) \qquad (4\text{-}9)$$

where r_1 and r_2 correspond to the perpendicular and vertical radius distances from center (mid-span and mid-height) of stope hanging-wall contact.

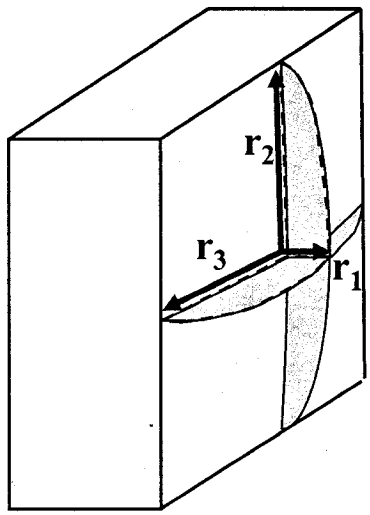

Figure 4.17 Schematic illustration of zone of hanging-wall overbreak represented as half of a prolate ellipsoid

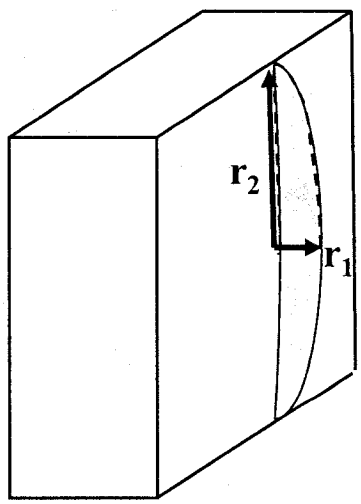

Figure 4.18 Schematic illustration of zone of hanging-wall relaxation represented in 2-D model

CHAPTER 5

NUMERICAL MODEL PARAMETRIC STUDY

In this chapter, the results of parametric modelling study are described. Numerical modelling was used as a tool to assess the influence that the following factors have on ore dilution:

- Mine depth
- Hanging-wall dimensions: stope height and strike length
- Hanging-wall dip angle
- Stress orientation
- Stope type
- Rockmass quality
- Construction factors

Numerical models were developed using the approach described in Chapter 4. The results, summarized in this chapter, are provided in Appendix A.

5.1 Quantifying ore dilution

As stated previously, a potential for overbreak exists within the envelope of confinement loss, defined by $\sigma_3 \leq 0$ MPa. The height of such envelope was determined from iso-contours of minimum principal stress (σ_3), located on a vertical and horizontal planes located at the stope mid-span and mid-height respectively, as illustrated in Figure 5.1.

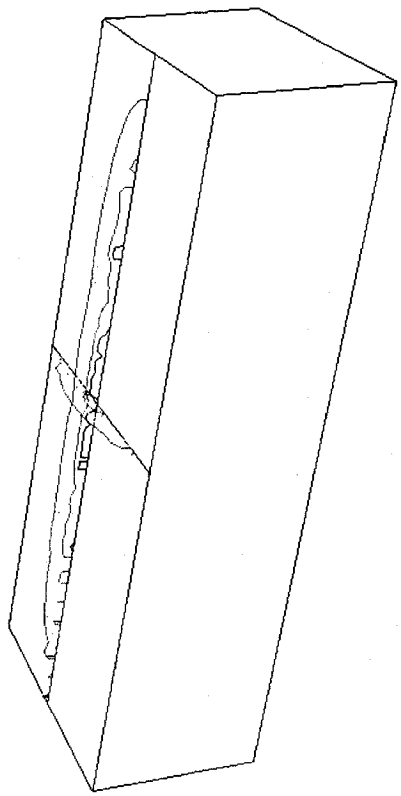

Figure 5.1 Illustration of overbreak envelope, indicated by σ_3 iso-contours

To quantify modelled and observed ore dilution, the following terminologies are introduced:

(1) For three-dimensional simulations, the ore Dilution Density (*DD*) is a term introduced in this study to denote potential hanging-wall overbreak. *DD* represents the volume of potential relaxation, bound by a specified stress contour, typically the zero stress contour (σ_3 = 0 MPa) or the rockmass tensile strength contour ($\sigma_3 = \sigma_t$)

$$DD = \frac{\text{Volume of half of a prolate ellipsoid } (m^3)}{\text{Surface area exposed } (m^2)} \qquad (5\text{-}1)$$

(2) For overbreak data measured by cavity survey (CMS) from mined stopes, measured Dilution Density (DD_{cms}) is a term introduced in this study. It is the volume of overbreak on an exposed surface, and is expressed as:

$$DD_{cms} = \frac{\text{Overbreak Volume } (m^3)}{\text{Surface area exposed } (m^2)} \qquad (5\text{-}2)$$

The DD and DD_{cms} terms suggest similar terminology, in that both express a measure of overbreak. However, they are calculated from differing sources: DD_{cms} is derived from observed overbreak volume, measured via a cavity survey of the excavated stope (CMS). DD represents overbreak simulated by the distribution of σ_3 stresses around stope blocks created in a 3-D elastic stress model. Computations for DD and DD_{cms} are compared in Table 5.1.

Table 5.1 Comparison of *DD* and DD_{cms} parameters

	DD	DD_{cms}
Data source	3-D numerical model	CMS
Known parameters	Radial distances from centre of stope to σ_3 stress iso-contour, (r_1, r_2, and r_3); where r_1 = perpendicular radius distance, r_2 = vertical radius distance, r_3 = horizontal radius distance	Measured overbreak volume from CMS, V
	Modelled hanging-wall dimensions: • Modelled strike length, l' • Modelled stope height, h'	Measured hanging-wall dimensions: • Strike length, l • Stope height, h
Computed parameters	Calculate volume of half a prolate ellipsoid, V_{pe} $V_{pe} = 2/3\pi \cdot r_1 \cdot r_2 \cdot r_3$	Calculate equivalent depth of sloughage, DD_{cms} $DD_{cms} = V / (l \cdot h)$
	Calculate depth of modelled overbreak, *DD* $DD = V_{pe} / (l' \cdot h')$	

5.1.1 Phase2 versus Map3D

To illustrate the differences between elastic 2-D and elastic 3-D numerical modelling approaches, distances between the hanging-wall depth from the stope boundary to σ_3 contour were determined. Maximum depth of hanging-wall relaxation will be defined as the furthest distance from the excavation boundary the σ_3 remains tensile ($\sigma_3 \leq 0$).

For both 2-D and 3-D models, the 'typical' stope (described in Section 4.4) was used. Stope strike lengths ranging from 10m to 40m were simulated with Map3D; the Phase2 model represented a cross-section. Aspect ratio is used to describe the geometrical shape of the hanging-wall, and is calculated as follows:

$$\text{Aspect Ratio} = \frac{\text{Strike length of exposed wall}}{\text{True height of exposed wall}} \qquad (5\text{-}3)$$

Numerical model results are compared in Figure 5.2 for a base case 30m high stope of type P1, located at a depth of 1500m and in good quality (GSI = 65) rockmass. With Map3D, it can be seen that the depth of relaxation increases with stope strike until an aspect ratio of 1: 1 is attained. For strike lengths exceeding stope height, the maximum depth of relaxation becomes constant, similar to that of the 2-D model.

For the example used, the maximum relaxation depth calculated with Phase2 intersects the Map3D results at a strike length of 27m. Map3D is more sensitive to varying strike lengths. Phase2 over estimates depth of relaxation for stopes of strike less than 27m, and under estimates depth of relaxation for strike lengths exceeding 27m.

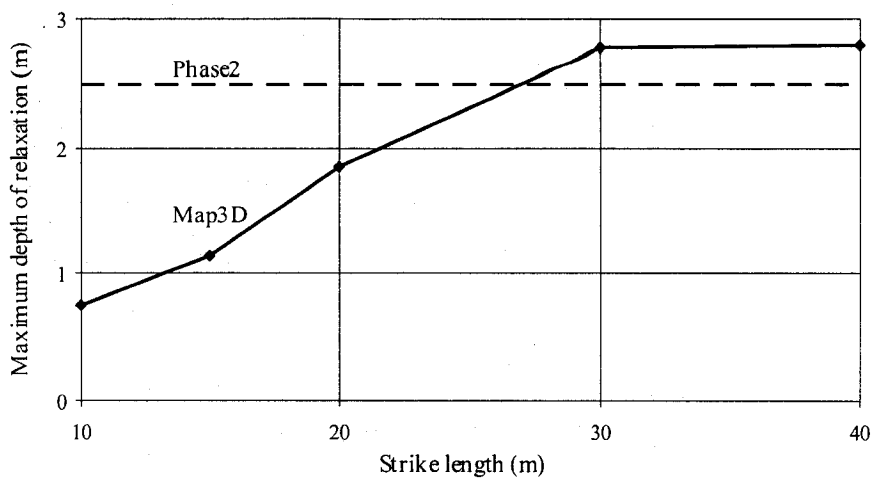

Figure 5.2 Maximum depth of relaxation, Phase2 versus Map3D

5.2 Effect of mining depth

The influence of mining depth (or stress setting) on the envelope of potential overbreak was assessed using Map3D. The base-case stope (30m vertical height, 80° dip, GSI = 65, σ_1° perpendicular to hanging-wall, P1 type primary stope), with strike lengths ranging from 10m to 40m, was modelled across the shallow, moderate and deep mining range of stope settings described in Section 4.3.3. Results were expressed as modelled Dilution Density (*DD*). Two *DD* values were calculated: (i) The σ_3 = 0 MPa, represents the volume of relaxed ground available for overbreak, assuming the rockmass has no tensile strength; (ii) *DD* values were also determined for the $\sigma_3 = \sigma_t$ contour, which accounts for rockmass tensile strength. For GSI = 65, rockmass tensile strength was calculated to be σ_t = 0.5 MPa (Table 4.8).

Trends associated with Dilution Density for the σ_3 = 0 MPa contour are presented in Figure 5.3. For a given stope dimension, the stress model suggests that the Dilution Density (*DD*) remains relatively uniform. Trend lines between the data points show only marginal increase, in the range of 0.02m *DD* per 500m increase in depth. Of greater impact on *DD* increase is the influence of strike length. This relationship is examined further in Section 5.3.

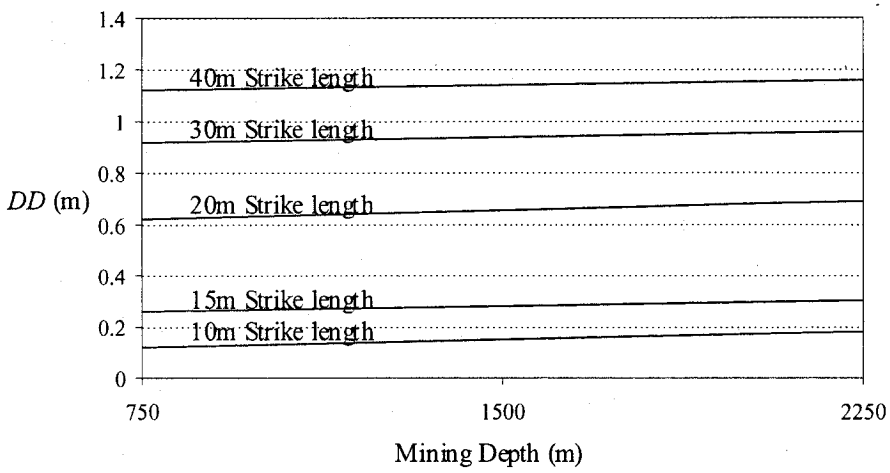

Figure 5.3 Modelled Dilution Density trend lines as a function of mining depth, (σ_3 = 0 MPa contour)

Trends associated with Dilution Density for the σ_3 = -0.5 MPa contour, shown in Figure 5.4 show a relationship influenced by depth. The envelope defined by the σ_3 = -0.5 MPa contour, representing the rockmass tensile strength of a good quality (GSI = 65) rockmass, increases with depth. At shallow depth, this contour generates minimal (near-zero) *DD* values. However, with depth the density of *DD* increases. The σ_3 = -0.5 MPa contour varies with strike length. At stope strike lengths $\leq$ 15m, minimal (near-zero) *DD* occurs. Increased strike length leads to increased *DD* values

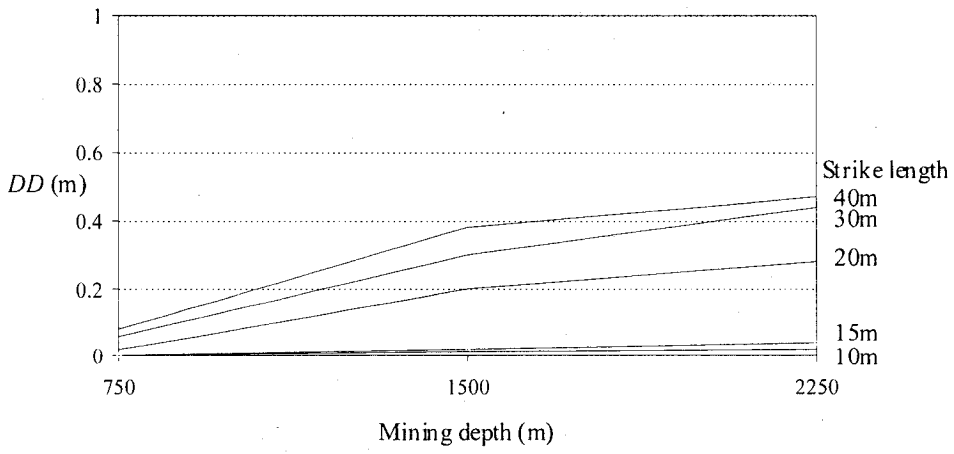

Figure 5.4 Modelled Dilution Density trend lines as a function of mining depth (σ_3 = -0.5 MPa contour)

Dilution Density trends associated with a stope located at moderate depth (1500m) are shown in Figure 5.5. *DD* values associated with the σ_3 = 0 MPa and σ_3 = -0.5 MPa show a linear trend, increasing with strike length between 20m and 40m. A stepped increase (jump) occurs between strike lengths of 15m and 20m. As expected, *DD* is significantly higher for the case of σ_3 = 0 MPa.

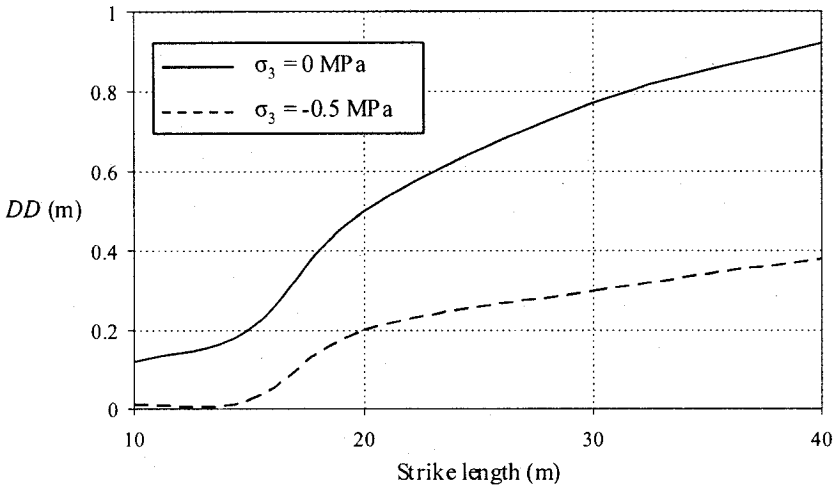

Figure 5.5 Dilution Density values associated with σ_3 = 0 MPa and -0.5 MPa contours

5.3 Dilution density relationship with varying stope height and strike length

Unlike factors such as mine depth and hanging-wall dip angle, which are outside of the control of the mine operator, stope dimensions are a variable factor that influences overbreak, which can be established during the initial mine design. Selection of stope dimensions, and in particular stope height, represents a compromise between 'acceptable' overbreak and the cost and time required to establish additional lateral infrastructure in order to mine smaller, more stable blocks. For example, mining of a 120m high orezone in 30m vertical increments would require four lateral mine horizons. Mining of the same block in 20m vertical increments may generate less overbreak, but would require six mine levels, or approximately 50% more lateral development.

When unacceptable severity of overbreak occurs, the mine operator must consider available options for modifying stope dimensions, or changing mining sequence or mining method. The Gonzague Langlois mine, located in northern Quebec, provides an illustration of a mine that readjusted its stope dimensions. The Gonzague Langlois mine officially opened in June 1996. Initial stope dimensions of 60m high x 20m along strike, designed using the Stability Graph method led to excessive overbreak. Operations were shut down in December 1996, and work began on re-engineering the mining method to incorporate sub-levels in an effort to assure lower dilution and higher grades, (Cambior, 1997). When the mine re-opened in July, 1997 stope dimensions had been revised to 30m high x 20m along strike, with a reported dilution of 15.6%, Perron (1999).

The influence of stope hanging-wall dimensions (height and strike length) on potential overbreak was assessed using Map3D. The base-case stope setting (80^{o} dip, GSI = 65, $\sigma_1{}^{o}$ perpendicular to hanging-wall, P1 type primary stope) was applied across the range of dimensions described in Section 4.4. Results for the $\sigma_3 = 0$ MPa contour were expressed in terms of Dilution Density (*DD*) values.

The results from the study into the effect of mine depth on dilution density (Section 5.2) suggest that mining depth does not play a significant role in the extent of $\sigma_3 = 0$ MPa contour within the hanging-wall. When investigating trends associated with varying stope dimensions, data from stopes in a shallow, moderate and deep mine setting was collected. As there was little scatter in the data points, analysis is based on averaged values.

Trends associated with Dilution Density for the $\sigma_3 = 0$ MPa contour as a function of strike length and vertical stope height are presented in Figures 5.6 and 5.7. From Figure 5.6, it can be seen that the 10m high stopes are relatively stable, with low (less than 0.2m) levels of *DD* generated across the full range of strike lengths. The taller stopes also exhibit low *DD* values at strike lengths $\leq$ 15m. For 20m, 30, and 40m high stopes, *DD* increases as strike lengths exceeds 15m. With all stope heights, the increase in dilution density is not linear. Typically, there was a

sharp increase between the 15m and 20m strike lengths. Beyond the 20m strike length, there was a more gradual increase in *DD*.

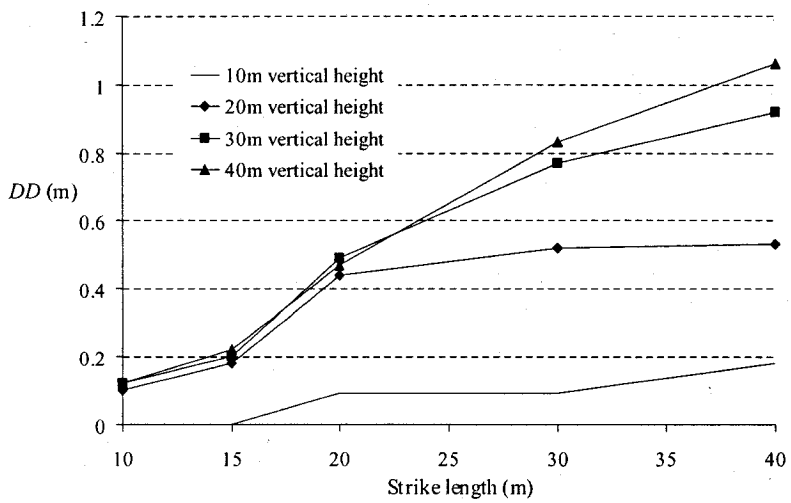

Figure 5.6 Dilution Density associated with varying hanging-wall dimensions, σ_3 = 0 MPa contour

Figure 5.7 represents a design tool, plotting contours of anticipated dilution density against stope dimension for the base case stope. Villaescusa (2000) qualitatively described a similar hyperbolic curve defining stable / unstable region (see Figure 5.8). He suggested that it was possible to achieve stope wall stability (with minimal dilution) by either excavating openings having long vertical and short horizontal dimensions, or openings having long horizontal and short vertical dimensions.

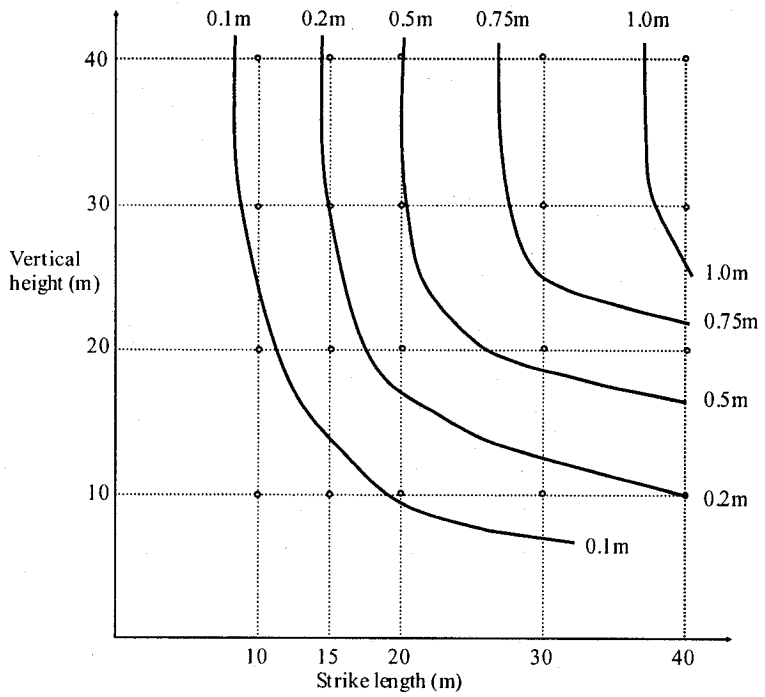

Figure 5.7 Dilution Density (*DD*) as a function of stope hanging-wall dimension for the base-case stope, $\sigma_3 = 0$ MPa contour

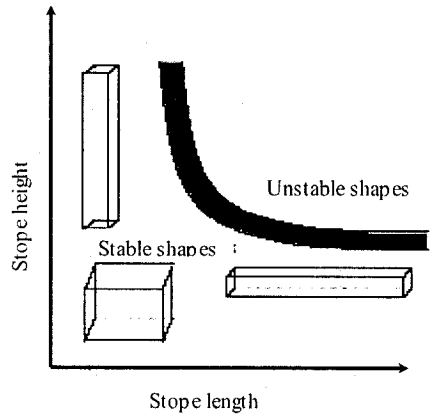

Figure 5.8 Stable stope shapes, after Villaescusa (2000)

As indicated by Figure 5.6, the shape of the exposed hanging-wall influences overbreak. Figure 5.9 plots dilution density values for the range of stopes modelled against stope geometry. Here, stope geometry is described by its Aspect Ratio (see Equation 5-3) and vertical height. From this plot, it can be seen that

stopes with a small vertical height or tall stopes with a short strike length generate the lowest *DD*. Severity of dilution density increases as the strike length of the hanging-wall expands.

Aspect ratio is used to describe the strike length to height relationship that defines hanging-wall geometry. Hydraulic Radius (*HR*), described in Section 2.7.1 is another commonly used approach for assessing stope dimensions. However, a limitation of expressing stopes in terms of *HR* is that unique stope geometry is not specified. An example of this limitation is provided in Table 5.2, where it is shown that a single *HR* value can be used to describe a variety of stope geometries.

Table 5.2 Comparison of Hydraulic Radius and Aspect Ratio

Stope Strike	Stope Height	Hydraulic Radius (Equation 2-15)	Aspect Ratio (Equation 5-3)
20 m	20 m	5 m	1:1
15 m	30 m	5 m	1:2
30 m	15 m	5 m	2:1

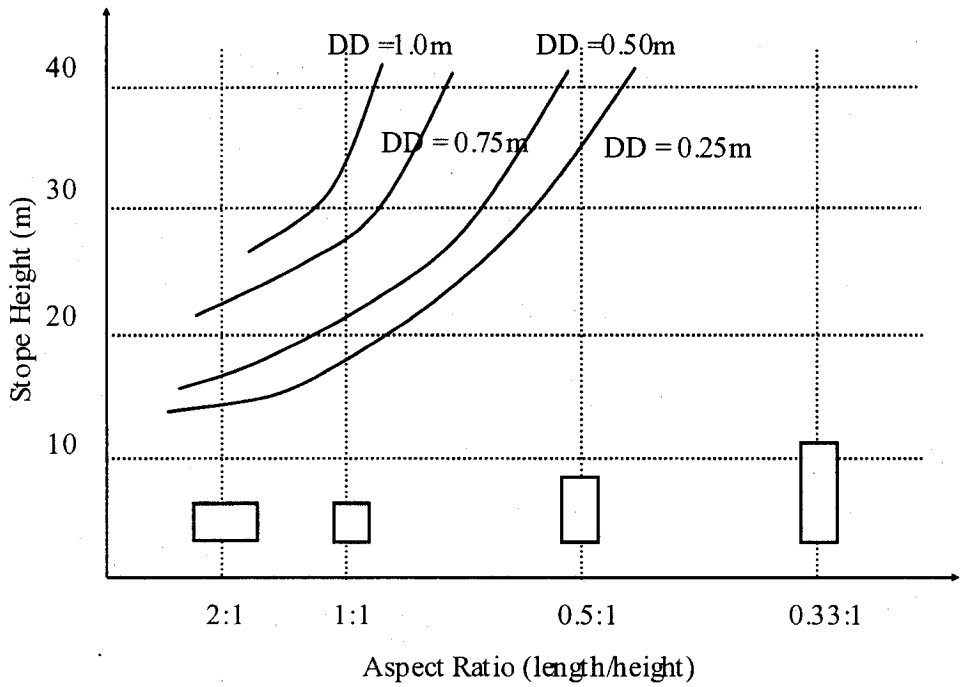

Figure 5.9 Dilution Density associated with stope height and aspect ratio for the base case stope, σ_3 = 0 MPa contour

5.4 Effect of hanging-wall dip angle on dilution density

The influence of the hanging-wall dip angle on overbreak has been discussed by others, including O'Hara (1980) and Yao et al. (1999). With a shallower hanging-wall dip, the distribution of low σ_3 stress contours becomes increasingly asymmetric, as illustrated in Figure 5.10, leading to a favourable orientation for release of unstable wedge intersections from the exposed hanging-wall. Another factor to consider is the true height of exposed hanging-wall, which, as presented in Section 3.3.3, increases as the hanging-wall dip angle decreases. True height can be calculated from dip angle and vertical height using Equation 5-4.

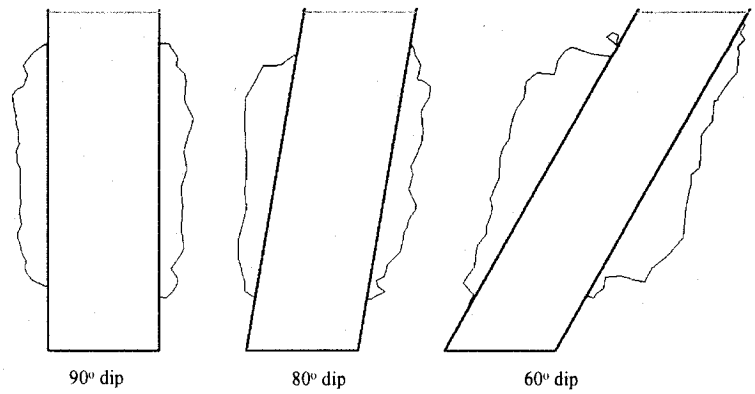

Figure 5.10 Distribution of relaxation zone (σ_3 = 0 MPa contour) under varying hanging-wall dip angles

$$\text{True height} = \text{Vertical Height} / \sin \varnothing \qquad (5\text{-}4)$$

where: $\varnothing$ = hanging-wall dip angle (measured from horizontal)

The influence of hanging-wall dip angle on the envelope of potential overbreak was assessed using Map3D. Stopes with height of 20m, 30m and 40m were examined in the base-case model setting: z =1500m, GSI = 65, σ_1° perpendicular to hanging-wall, P1 primary stope. Hanging-wall dip angles of 80° and 60° were considered. *DD* results, defined by the σ_3 = 0 MPa contour, were determined.

Trends associated with Dilution Density for varying hanging-wall dip angles are presented in Figure 5.11. *DD* values cluster together for strike lengths $\leq$ 20m. As shown in Section 5.2, smaller stopes have more stable geometry. Hanging-wall dip influences stope overbreak as strike length increases beyond 20m. At a 30m strike length, the *DD* associated with three stope heights increased by a least 38% with the shallower hanging-wall dip. At a 40m strike length, the *DD* increased by more than 52% with the shallower hanging-wall dip of 60°.

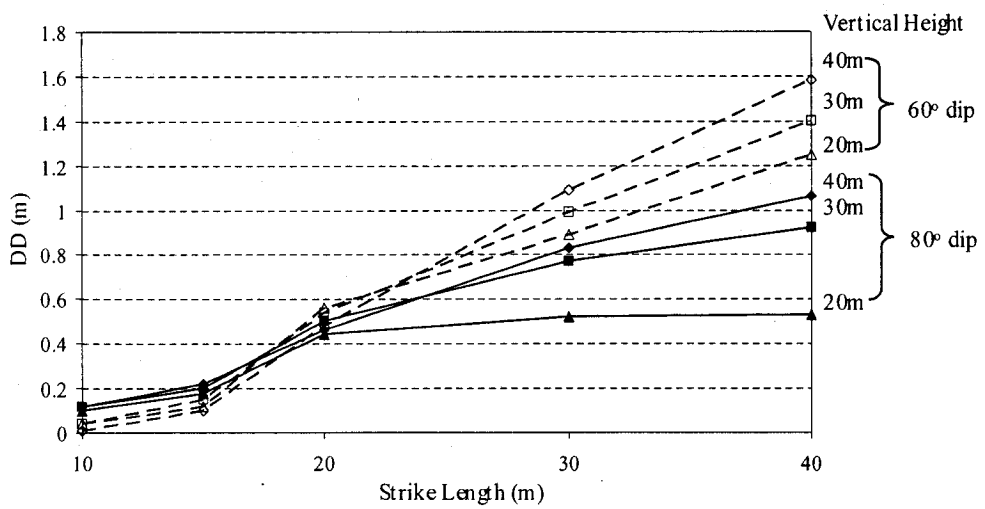

Figure 5.11 Influence of hanging-wall dip on overbreak. Base-case stope, $\sigma_3 = 0$ MPa contour

5.5 Effect of stress orientation on dilution density

The influence of major principal stress orientation with respect to the stope hanging-wall was assessed using Map3D. Base case stopes (30m vertical height, z =1500m, GSI = 65, P1 primary stope) were examined. Hanging-wall dip angles of 80° and 60° were considered. Two major principal stress orientations were considered: (i) σ_1° perpendicular to stope strike, and (ii) σ_1° parallel to stope strike.

Dilution Density trends, defined by the $\sigma_3 = 0$ MPa contour, associated with varying σ_1 orientations are found in Figure 5.12. *DD* values cluster together for strike lengths $\leq$ 20m. Major principal stress orientation influences stope overbreak as strike length increases beyond 20m. *DD* is reduced when σ_1 is parallel to the strike of the stope. The amount of *DD* reduction ranged from 14% for a stope with a 80° hanging-wall dip angle, to 17% for a stope with a 60° hanging-wall dip angle.

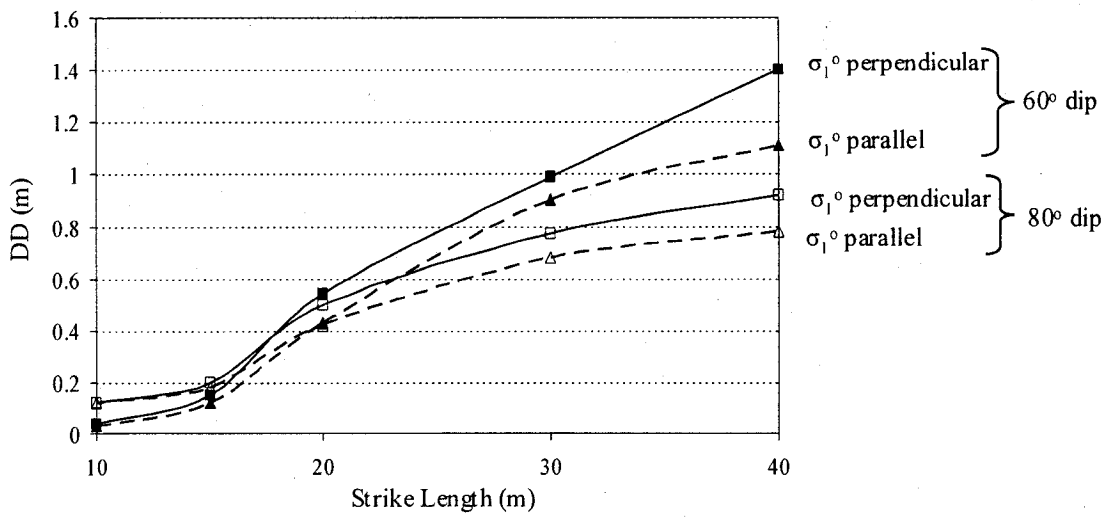

Figure 5.12 Influence of major principal stress orientation on overbreak. Base-case stope, σ_3 = 0 MPa contour

5.6 Effect of stope type on dilution density

As discussed in Section 4.3.2, a parameter affecting unplanned ore dilution is the local stope setting within the mining sequence. Depending on its placement within a planned mining sequence, a stope may be bound by rock on both walls (a primary stope), or it may have backfill on one or both walls (a secondary stope). Modelled stope geometries for primary and secondary stopes are illustrated in Figures 4.5 and 4.6. The base-case stope setting (30m vertical height, z=1500m, 80° dip, GSI = 65, σ_1° perpendicular to the hanging-wall), with studied strike lengths ranging from 10m to 40m. A P1 stope is an isolated mine block, and is the basis for other parametric modelling described in this chapter. With the P2, P3, S1 and S2 stope types, previously mined stopes were backfilled; refer to Table 4.2 for definition of stope types.

Two *DD* values were calculated: (i) defined by the σ_3 = 0 MPa, represents the volume of relaxed ground available for overbreak, assuming the rockmass has no tensile strength; (ii) *DD* values were also determined for the $\sigma_3 = \sigma_t$ = -0.5 MPa contour, which accounts for rockmass tensile strength.

Trends associated with Dilution Density for the σ_3 = 0 MPa contour are presented in Figure 5.13. Compared against the P1 stope, extraction of the P2 and P3 stopes is associated with greater values of *DD*. *DD* increases of 32% to 65% occurred between P1 and P2 mining. Extraction of the P3 stope resulted in only minor *DD* increases (typically, in the range of 5%) over the P2 stope. Trends associated with Dilution Density for the $\sigma_3 = \sigma_t$ = -0.5 MPa contour, shown in Figure 5.14 show a similar pattern. The envelope defined by the σ_3 = -0.5 MPa contour, representing rockmass tensile strength for GSI 65, increases as stope sequence progresses beyond the P1 stope.

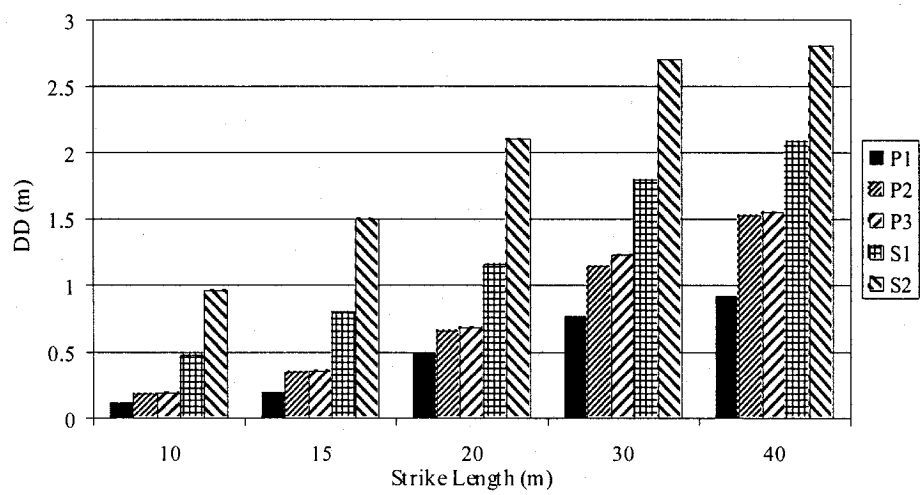

Figure 5.13 Influence of stope type on Dilution Density. Base-case stope at σ_3 = 0 MPa contour

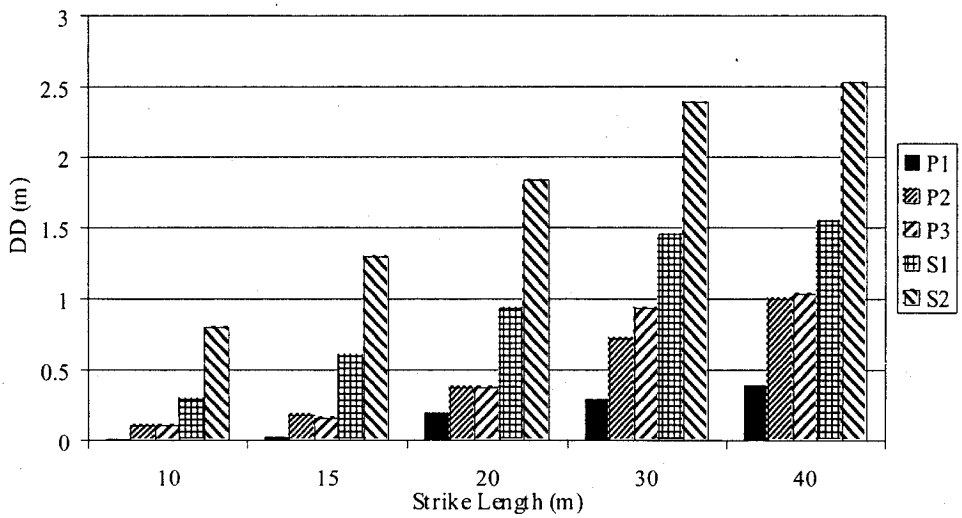

Figure 5.14 Influence of stope type on Dilution Density. Base-case stope at σ_3 = -0.5 MPa contour

5.7 Effect of rockmass quality on dilution density

The influence of rockmass quality on the envelope of potential overbreak was assessed using Map3D. The base-case stope (30m vertical height, 80° dip, σ_1° perpendicular to hanging-wall, P1 primary stope), with strike lengths ranging from 10m to 40m, was modelled across a range of host and orezone rockmass qualities. The high-, mid-, and low range rockmass qualities assigned and corresponding rockmass tensile strengths are summarized in Table 5.3. Rockmass ranges are detailed in Section 4.3.4.

As before, the results were expressed as modelled Dilution Density (*DD*). Two *DD* values were calculated: (1) defined by the σ_3 = 0 MPa, represents the volume of relaxed ground available for overbreak, assuming the rockmass has no tensile strength; (2) *DD* values were also determined for the $\sigma_3 = \sigma_t$ contour, which accounts for rockmass tensile strength. The tensile strength contour used varies with the quality of host rock encasing the orezone and excavated stope, as illustrated in Figure 5.15.

Table 5.3 Ranges of rockmass quality examined

Rockmass quality	**GSI**	**Rockmass tensile strength (Table 4.8)**
High range (Very good quality)	80	σ_t = 1.55 MPa
Mid range (Good quality)	65	σ_t = 0.50 MPa
Low range (Fair quality)	50	σ_t = 0.16 MPa

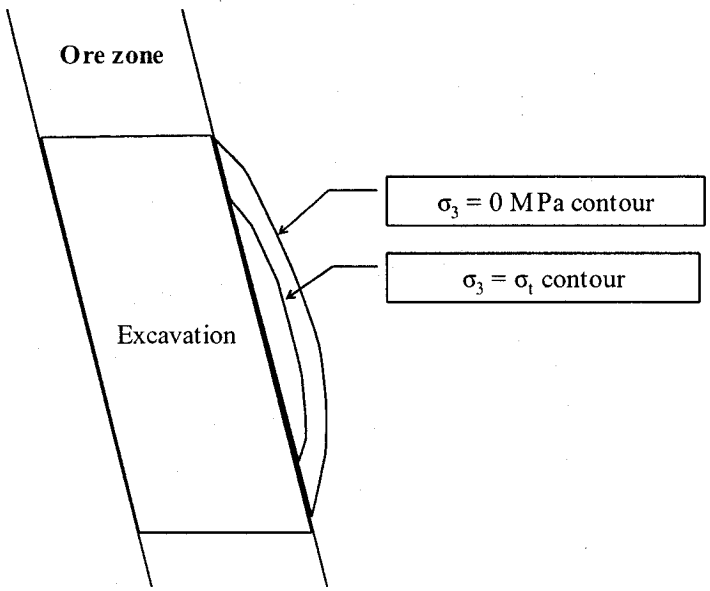

Figure 5.15 Schematic illustration of terminology used

Contours of σ_3 = 0 MPa were similar for the three rockmass quality ranges. This trend was anticipated since a rockmass with no tensile strength (σ_3 = 0) is equivalent to low quality rock (GSI << 50). The σ_3 = σ_t contours varied across the three quality ranges, as shown in Figure 5.16. A high quality rockmass (GSI=80) has a more competent structure and will have greater tensile capacity. As a result, the severity of anticipated overbreak diminishes as the rockmass quality of the host rock increases.

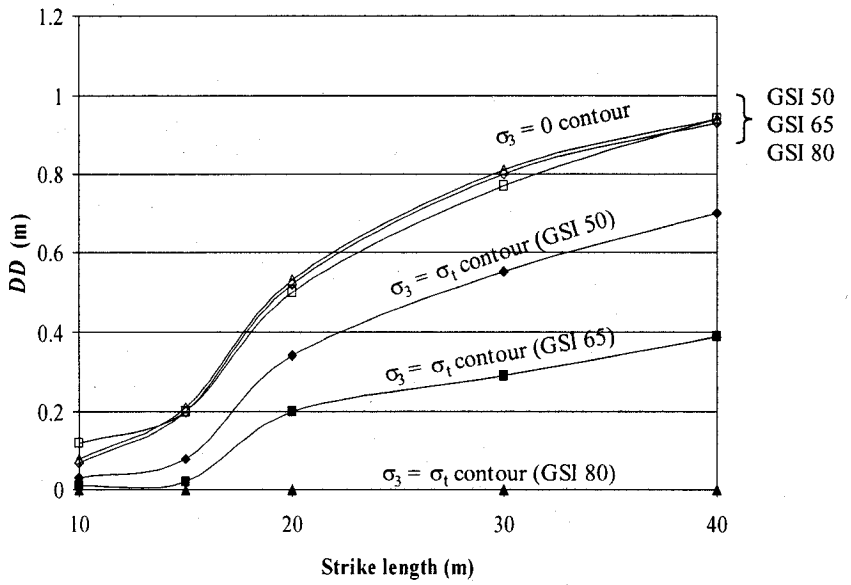

Figure 5.16 Influence of rockmass quality on Dilution Density at $\sigma_3 = 0$ and $\sigma_3 = \sigma_t$ contour.

5.8 Effect of Construction factors on dilution density

Stope construction refers to the techniques employed to prepare and extract a stope block. The various components involved with the design, drilling, and excavation of an individual stope play a critical role determining mining success. Construction factors include:

- Factors that generate local damage to the hanging-wall rockmass, such as blast vibration damage
- Factors that physically damage the designed hanging-wall span, such as deviation of production blastholes and undercutting

5.8.1 Blasting influence on overbreak

Blast damage refers to any strength deterioration of the remaining rock due to the presence of blast induced cracks and to the opening, shearing and extension of pre-existing or newly generated planes of weakness. Villaescusa et al. (2004) defines blast damage as the creation, extension and/or opening of pre-existing

geological discontinuities in the rockmass. Blast induced damage weakens a rockmass, potentially leading to stability problems.

Mackenzie (1987) defines blast-induced damage as the change of in situ block size distribution due to blasting. Blast induced damage is a result of the interaction of the rockmass and the explosive product, resulting in a reduction in quality or integrity of rockmass. The damage inflicted on the boundary of the excavation is directly related to the type and amount of energy required to adequately fragment a volume of rock. The reduction in rockmass quality thus results from weakening or dilation of existing discontinuities and the creation of new fractures.

5.8.1.1 Blast damage factors

There are essentially two sets of factors that can control the extent of the blast induced damage zone in an underground mining operation (Scoble et al., 1997). Geological factors, such as rockmass quality, in situ stress and intact rock strength influence inherent damage. Mining factors, such as induced stress damage and blast induced damage, further impact wall stability.

It is generally accepted that the damage is caused by expanding gases through the geological discontinuities (see Figure 5.17) and to the vibrations experienced from the blasting process. Potential damage mechanisms resulting from blast gas penetrating in to the rockmass, identified by Connors et al. (1996) include: (i) physical dislodgement of in situ blocks, (ii) a significant reduction in strength of block interfaces that increases the potential for immediate or long-term failure due to gravity, stress or blast vibration. Repetitive blasting also imposes a dynamic loading to the exposed stope walls away from a blasted volume, and may trigger structurally controlled fall-off and ultimately overbreak (Villaescusa et al., 2004).

In a drill and blast mining operation, the energy of the explosive, blast pattern, time delays, number of blast holes, their burden and spacing are key factors (Cameron et al., 1995). These factors in addition to other related factors have a

bearing on the amount of damage inflicted on the remaining rockmass, and the ground support used as part of the underground excavation infrastructure. Traditionally, blast design factors are considered globally, using such parameters as powder factor, only from the view point of their influence over fragmentation, rather than rockmass damage. The powder factor is the expression of average kilograms of explosive used to break one cubic metre of ore in a stope.

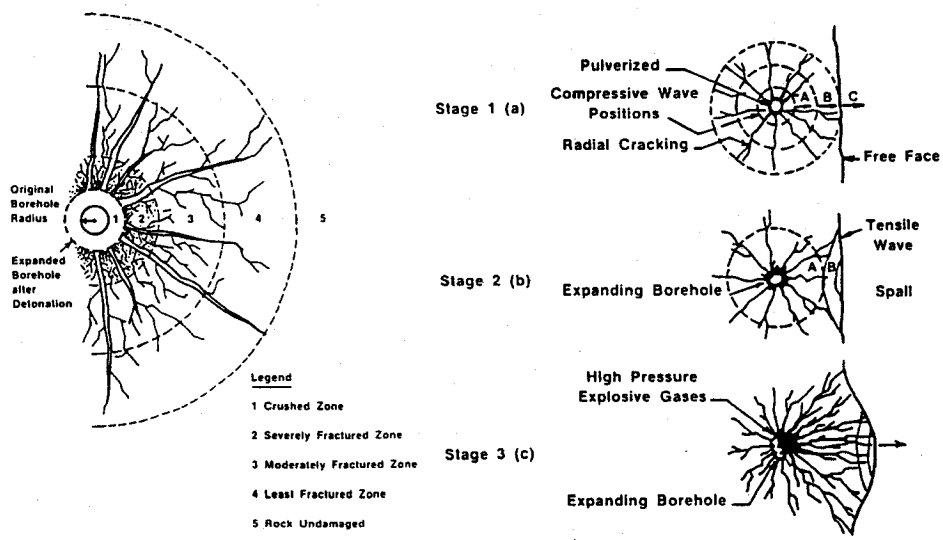

Figure 5.17 Physical phenomena in rock blasting (after Lizotte and Scoble, 1994)

The type of explosive used forms an important part of blast design. The selection of explosive type is usually based on the analysis of factors that include rockmass characteristics, volume of rock to be blasted, presence of water, safety conditions, supply problems as well as the cost of rock breakage. For underground open stope mining, a commonly used explosive is ANFO (Ammonium Nitrate and Fuel Oil) due to its low cost and safety. High energy explosives produce good fragmentation but may cause damage to the stope hanging-wall. To avoid this, a common practice is to utilize low density explosives, such as *AMEX K40*[*] or low energy cartridge explosives, such as *Powersplit*[*] in blastholes drilled in close

[*] *AMEX K40* and *Powersplit* are products of Orica Canada Inc.

proximity to the hanging-wall (Andrieux and Rodgers, 1997; Henning et al., 1997).

5.8.1.2 Assessment of blast damage

Blast-induced damage results from the interaction of the rockmass, stress, and the explosive product. The extent of blast-induced damage is important from the point of view of safety, ground control, support, and dilution.

For lateral development, a large amount of work has been performed on quantifying blast vibration damage associated with drift blasting. Studies such as those performed by Forsyth and Moss (1990), Paventi (1995), and Cotesta et al. (1999) assess the blast damage quality in terms of:

- The integrity of the rock along the back, typically using a scaling bar
- The percent of half barrels visible along the drift surface
- The amount of blast overbreak or underbreak (blasted shape versus designed shape)
- Drilling quality, such deviations of hole spacing and hole orientation from design.

Blast induced damage to hanging-walls of primary stopes is examined in Villaesusa et al. (2004), Connors et al. (1996) and Liu et al. (1995). These studies incorporate measured blast vibrations, with surveys of the mined stope geometry to assess hanging-wall stability. Instability may be an indicator of blast damage. Henning and Mitri (1999) used a similar approach in comparing primary and secondary stopes.

For stope blasting, vibration damage is quantified in terms of physical damage to the integrity of adjacent rockmass exposures. Damage by the shock energy from an explosive charge close to a blast can be related to the level of vibrations

measured around the blasted volume. As described in Chapter 3, severity of damage to mine workings increases with the magnitude of blast vibration.

Blast vibration is measured as peak particle velocity (PPV). Langefors and Kihlstrom (1978) proposed the following criteria for tunnels: PPV's of 305 mm/sec result in the fall of rock in unlined tunnels, and PPVs of 610 mm/sec result in the formation of new cracks. Bauer and Calder (1978) observed that no fracturing of intact rock will occur with a PPV of less than 254 mm/sec. However, PPVs of 254 to 635 mm/sec result in minor tensile slabbing, and PPVs of 635 to 2540 mm/sec would cause strong tensile and some radial cracking. The break up of a rockmass occurs at PPV exceeding 2540 mm/sec. Oriard (1982) proposed that most rockmasses suffer some damage at PPV above 635 mm/sec.

A damage criteria incorporating blast vibration and rockmass quality was suggested by Yu (1993). The Blast Damage Index (BDI), a dimensionless indicator, is defined by dividing the induced stress with a quantitative value of damage resistance, as shown for common rock types in Equation 5-5.

$$BDI = 0.64\ V / K_r \qquad (5\text{-}5)$$

where: V = peak particle velocity (m/second)

K_r = site quality constant

The site quality constant (K_r) is determined by either (i) dividing the rockmass rating (RMR) at the site by 100, or (ii) by sounding the ground with a scaling bar to evaluate ground conditions. The relationship between BDI and severity of damage is provided in Table 5.4.

Table 5.4 Blast damage index (BDI) and severity of blast damage to tunnel walls (after Yu and Vongpaisal, 1996)

BDI	Type of damage
≤ 0.125	No damage to underground excavations
0.25	No noticeable damage
0.5	Minor and discrete slabbing
0.75	Moderate and discontinuous slabbing
1.0	Major and continuous slabbing failure, requiring rehabilitation
1.5	Severe damage to an entire opening. Rehabilitation work is difficult or impossible
≥ 2.0	Major caving, normally resulting in abandoned accesses

Blast vibration data is commonly obtained using a multi-channel blast vibration monitor and triaxial geophones. Reusable, surface mount triaxial geophones are installed onto a solid, competent wall surface using anchor bolts in combination with resin bonding. Ideally, the geophones are located in a hanging-wall access drift at a distance of 0.75 to 1.50 charge length away from the blastholes, within the geophone limit for near-field blast monitoring suggested by Andrieux and Heilig (1994).

Hanging-wall vibration data is compiled using the peak vector sum velocities of individual blast holes. Non-distinct or overlapping waveforms were omitted from the database, as were blast vibration values likely influenced by air gaps between the blasthole and the geophone. Blast vibration data is statistically analyzed using scaled distance relationships (Atlas, 1987), to determine the Site Factors "K" and "a", used in the following equation:

$$PPV = K (R/W^{1/2})^{-a} \qquad (5\text{-}6)$$

where PPV = peak particle velocity (mm / second); R = radial distance from blast center (meters); and W = explosive charge per delay (kg). Site Factors ''K'' and ''a'' are functions of the effect of local rock characteristics on ground motion. Factor ''K'' applies to amplitude whereas "a" indicates vibration attenuation. Site Factors are obtained from a plot of PPV against Scaled Distance blast data, see Figure 5.18. The slope of the linear regression best-fit through the data line represents Factor "a"; Factor "K" corresponds to the intercept of the regression line with the PPV axis. From the data shown in Figure 5.18, Site Factors "K" and "a" were found to be 498 mm/sec and 1.19, respectively (Henning et al., 1997)

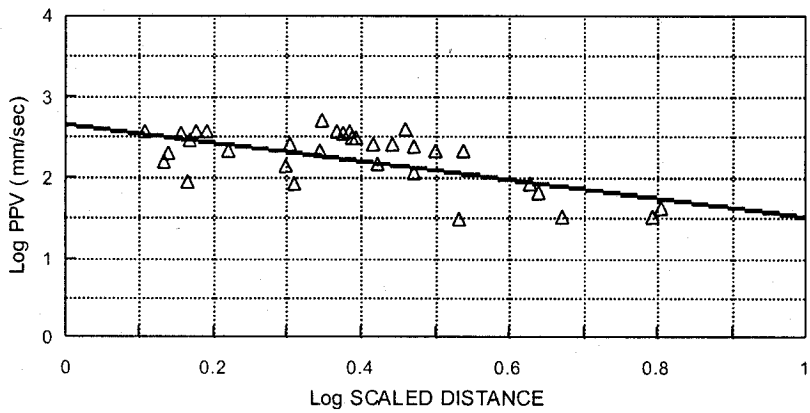

Figure 5.18 Blast vibration versus scaled distance plots, Henning et al. (1997)

The level of blast vibration attenuates with distance away from the blasthole. Yang et al. (1994) measured the near field (< 10m from the explosive charges) peak particle velocity around a borehole. Figure 5.19 displays measured PPV values, along predictions using the conventional charge-weight scaling law (Holmberg and Persson, 1979). Figure 5.19 suggests that vibration attenuates in an exponential manner away from the blasthole. Using a common blast damage threshold of crack formation at PPV values in the range of 600mm/sec, blast damage would be anticipated within 8m of the blasthole. A blasthole loaded with high energy explosives, such as ANFO, located within 8m of the hanging-wall may induce blast vibration damage within the hanging-wall.

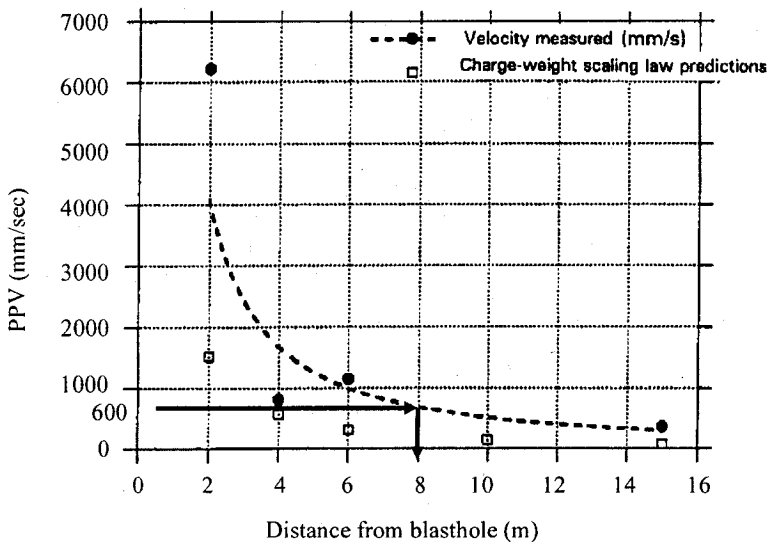

Figure 5.19 Peak particle velocity (PPV) as a function of distance from blasthole, after Yang et al. (1993).

5.8.1.3 Influence of stope type on blast vibration

Blast vibration monitoring was employed for back-analysis of hanging-wall behaviour of adjacent primary and secondary long-hole stopes within a highly stressed, foliated rockmass (Henning and Mitri, 1999). The severity of production blast vibrations within the stope hanging-wall region was monitored on both stopes using triaxial geophones installed onto a solid, competent wall surface, Henning et al. (1997). Calculated Site Factors are listed in Table 5.5. The lower Site Factors for the secondary stope indicate that a lower amplitude vibration is reaching the geophones, due to increased hanging-wall vibration attenuation from the blast source. Lower vibration levels were associated with observed de-lamination of schistocity parallel to the stope wall.

To predict the impact of individual blastholes on the hanging-wall, explosive-specific Site Factors were calculated from the vibrations generated by individual explosive types. ANFO loaded 100 mm diameter blastholes, representing 48% and 40% of the total blast populations for the 9-0-15 and 9-0-11 stopes respectively, were compared. Vibration attenuation plots for a typical blasthole,

located at 2.5 m from the stope / hanging-wall boundary, and loaded with 100 kg ANFO, provided in Figure 5.20, show estimated hanging-wall vibration levels within five meters of the stope boundary.

The plots in Figure 5.20 indicate:

- Using a common blast damage threshold of crack formation at PPV values exceeding 600 mm/second, blast damage may persist into the hanging-wall to a depth of 1.0 meter. The severity of blast vibration damage diminishes away from the stope boundary.
- Mid-stope blastholes, located at a distance of 2.0 to 2.5 meters from the hanging-wall contact, generate significant peak vibrations into the hanging-wall.
- A greater rate of blast vibration attenuation in the hanging-wall of the secondary stope.

Table 5.5 Calculated blast vibration Site Factors

	Primary stope		Secondary stope	
	K	a	K	a
Total Blast Population	498	1.19	126	0.70
ANFO Blast Population	283	0.58	141	1.20

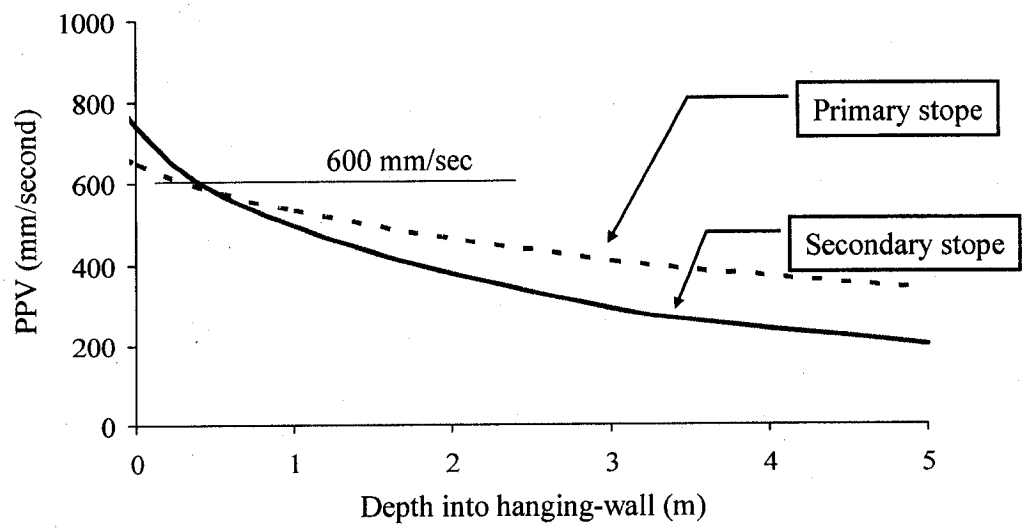

Figure 5.20 Hanging-wall blast vibration attenuation, (Henning et al., 1997)

5.8.1.2 Accounting for blast damage in the model parametric study

In the proceeding section, it was shown that blast damage may persist to a depth of several metres into a stope hanging-wall. Procedures have been developed to adjust rockmass quality classification to arrive at a more realistic value that reflects the quality of rockmass. Kaiser et al. (2003) introduced a construction factor for lateral development that was used to adjust the NGI-Q classification, arriving at a value that reflects the quality of rockmass to be supported (Suorineni et al., 2005).

Hoek et al. (2002) introduced a damage parameter D that accounts for the degree of disturbance to which the rockmass has been subjected by blast damage and stress relaxation. Damage parameter D varies from 0 for undisturbed in situ rockmasses to 1 for very disturbed rockmasses, see Table 5.6. For very poor quality blasting in a hard rock tunnel, resulting in severe local damage extending 2 or 3m in the surrounding rockmass, a value of $D = 0.8$ is suggested. Factor D is incorporated into the generalized Hoek-Brown criterion according to the equations provided in Table 5.7.

Table 5.6. Guidelines for estimating disturbance factor D, (Hoek et al., 2002)

Description of rockmass	**Suggested value of *D***
Excellent quality controlled blasting or excavation by Tunnel Boring Machine results in minimal disturbance to the confined rockmass surrounding a tunnel.	$D = 0$
Mechanical or hand excavation in poor quality rockmasses (no blasting) results in minimal disturbance to surrounding rockmass.	$D = 0$
Very poor quality blasting in a hard rock tunnel results in severe local damage, extending 2 or 3 m into the surrounding rockmass.	$D = 0.8$
Small scale blasting in civil engineering slopes results in modest rockmass damage, particularly if controlled blasting is used.	Good blasting; $D = 0.7$ Poor blasting; $D = 1.0$
Very large open pit mine slopes suffer significant disturbance due to heavy production blasting and also due to stress relief from overburden removal. In some softer rocks excavation can be carried out by ripping and dozing; the degree of damage to the slopes is less.	Production blasting; $D = 1.0$ Mechanical excavation; $D = 0.7$

Table 5.7 Incorporation of damage parameter D into generalized Hoek-Brown criterion

Hoek-Brown (H-B) 'm'	$m_b = m_i \exp\left(\frac{GSI-100}{28-14D}\right)$
Hoek-Brown (H-B) 's'	$s = \exp\left(\frac{GSI-100}{9-3D}\right)$
Elastic Modulus (σ_c > 100 MPa)	$E_m(GPa) = \left(1-\frac{D}{2}\right)\cdot 10^{((GSI-10)/40)}$

5.8.1.5 Parametric evaluation

The potential influence of a blast damaged hanging-wall on overbreak was assessed parametrically. Rockmass quality within a 2m wide envelope, located immediately adjacent to the stope hanging-wall contact was downgraded, using the Hoek et al., (2002) damage parameter, to simulate an envelope of damaged rock. See Figure 5.21. Initially developed for tunneling and slope stability applications, the Hoek damage parameter D = 0.8 was applied to reflect severe local damage associated with very poor quality blasting in the stope wall. The 2m envelope of damaged ground is consistent with vibration attenuation trends shown in Figures 5.19 and 5.20.

Input parameters for the modelling, summarized in Table 5.8 were obtained from relationships described in Section 4.3.3 and Table 5.7. Two rockmass conditions were considered: (i) no blast damage (D = 0), and (ii) very poor quality blasting, resulting in severe blast damage (D = 0.8).

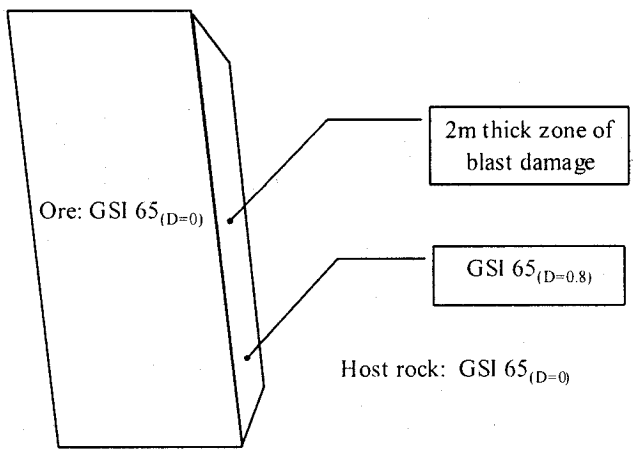

Figure 5.21 Schematic section through stope showing modelled blast damage envelope

The influence of a 2m thick envelope of blast damaged rockmass on the envelope of potential overbreak was assessed using Map3D. The base-case stope (GSI = 65, 30m vertical height, 80° dip, σ_1° perpendicular to hanging-wall, P1 primary stope), with strike lengths ranging from 10m to 40m, was modelled under two

conditions: (i) no blast damage (D = 0), and (ii) with a 2m thick envelope of blast damaged rockmass (D = 0.8). Results were expressed as modelled Dilution Density (*DD*). Two *DD* values were calculated: (i) defined by the σ_3 = 0 MPa, represents the volume of relaxed ground available for overbreak, assuming the rockmass has no tensile strength; (ii) *DD* values were also determined for the $\sigma_3 = \sigma_t$ contour, which accounts for rockmass tensile strength. The tensile strength contour used varies with the quality of host rock adjacent to the excavated stope.

Modelling results are presented in Figure 5-22. Beyond a strike length of 15m, contours of σ_3 = 0 MPa suggest a *DD* increase of 15% to 22% when a 2m thick blast damage envelope is modelled. Increased *DD* associated with the damaged envelope reflects the influence of the lower rockmass quality. Similar trends were noted in Section 5-7. The $\sigma_3 = \sigma_t$ contours vary for the two conditions. The rockmass within the blast damaged envelope is of lower quality, and hence, has less tensile strength than the remaining host rock. Beyond a strike length of 15m, contours of $\sigma_3 = \sigma_t$ suggest a *DD* increase of 40% to 100% when a 2m thick blast damage zone is modelled.

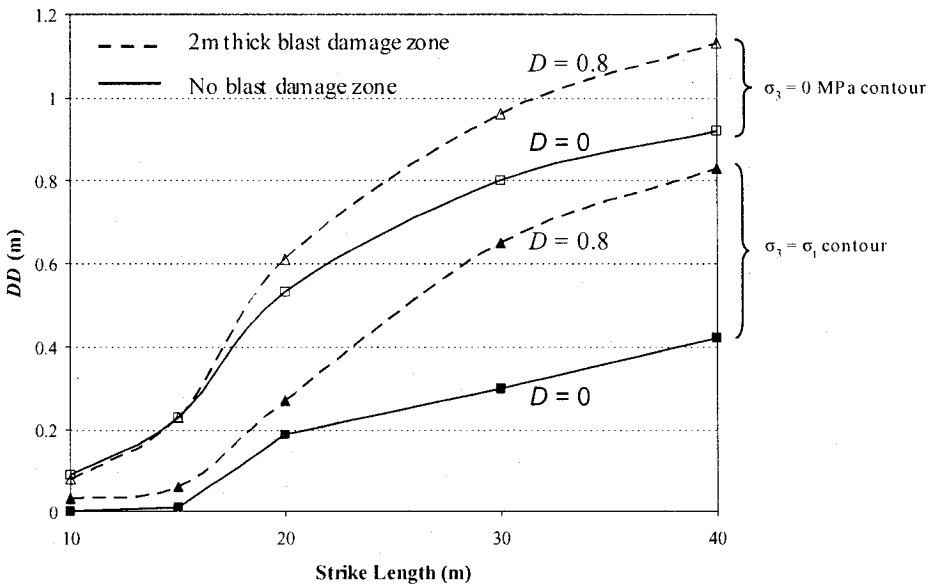

Figure 5.22 Influence of rockmass quality degradation due to blast damage on Dilution Density at σ_3 = 0 MPa and $\sigma_3 = \sigma_t$ contours, base-case stope

Table 5.8 Model parameters for undamaged and blast damaged rock

	Mid range rockmass quality with no blast damage	Mid range rockmass quality with severe blast damage
Material values		
GSI	65	
Uniaxial compressive strength, (σ_c)	175 MPa	
Hoek-Brown constant for intact rock, (m_i)	25	
Disturbance factor, *D*	0	0.8
Poisson Ratio	0.25	
Rockmass values calculated with GSI value		
Rockmass elastic modulus, (E_{rm})	23700 MPa	14200 MPa
Hoek-Brown 'm'	7.16	3.11
Hoek-Brown 's'	0.021	0.005
Hoek-Brown 'a'	0.502	0.502
Rockmass tensile strength, (σ_t)	0.50 MPa	0.25 MPa
Global rockmass compressive strength, (σ_{cm})	64.6 MPa	41.8 MPa

5.8.2 Drill hole deviation

Drill hole deviation refers to the improper orientation of the holes closest to the hanging-wall / ore contact relative to the stope hanging-wall. Incorrect setting of drill angles (set-up error), borehole wander and drilling to incorrect depths can significantly influence stoping success. Examples of common drill errors are shown in Figure 5.23.

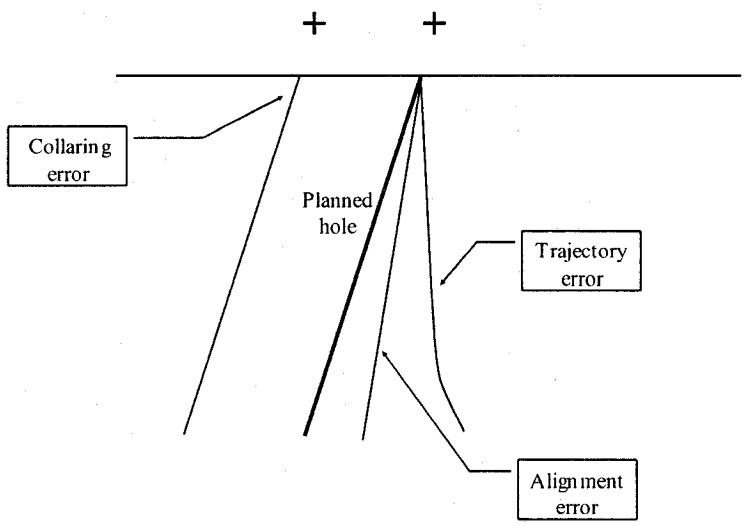

Figure 5.23 Examples of drill error sources

Blasthole location is an important feature of blast design. It largely controls the distribution of explosive energy in the rockmass. If holes are not drilled accurately there will be variable and often unmeasured burdens on the explosive charge. Excessively large burdens lead to over confinement, which increased the amount of gas penetration induced damage, Cameron et al. (1995). If holes are too close together there is a potential for sympathetic detonation or damage to adjacent charge.

Deviation, or drill error, can be influenced by operator skill, diameter of the drill rods, and type of drill. For example, with a top hammer drill (such as Data-Solo), the hammering mechanism is located on the drill itself. The hammering action is sent to the bit via the drill string. With an in-the-hole (ITH) drill, the hammering

mechanism is located between the drill string and the bit. ITH drill rods do not have to withstand percussion pressure.

Connors et al. (1996) describe sources of error in drilling accuracy in terms of external and internal factors. The sum total of all errors is the final measure of drilling accuracy. External factors include: incorrect surveying of collar location and drill orientation, incorrect drill set up, incorrect boom alignment, poor collaring practice. An improperly aligned drill results in large toe location error. Vertical holes have less collaring error than inclined holes. Excessive feed pressure is used by the drill operator to increase footage (and bonus) at the expense of hole accuracy. Angle indicators used by the drill operators may be less accurate than the detail of design. Internal factors are drill errors within the hole, such as physical limitations of drilling equipment, poor drill operation (thrust, rpm), equipment physical state (worn rods, dull bits) and geologic conditions.

Consequences of drilled blasthole deviation include:

- Dilution directly caused by blastholes inadvertently deviating into the footwall or hanging-wall of the stope.
- Poor fragmentation, resulting in oversize and/or excessive fines. Oversize muck causes hang-ups within the stope, increased secondary blasting, low bucket fill factors of hauling equipment, and mucking delays. Excessive fines can cause buildups that reduce ore flow within the stope, increased oxidation rates, and ore loss during transport.
- Ground control problems. Excessively deviated holes with large burden and spacing lead to increased ground vibrations when blasted.
- Ore losses, caused by the drill pattern not adequately covering the stope. This results in some ore not being blasted and consequently left behind.
- Re-drilling or drilling of additional holes to avoid ore losses.

Drill deviation can be measured by instrumentation such as Boretrak®, which uses inclinometers and rigid hinged rods to survey boreholes. A study of Boretrac borehole surveys by Tannant et al. (1998b), reported an average deviation of 0.5m for 15 to 20m long, 64mm diameter drill holes. Assuming that the drill hole deviation occurs on both sides of a 20m high, 3m wide section of a stope, the measured deviation could generate approximately 16% dilution; see Figure 5.24. For the stope dimensions used, 16% dilution corresponds to dilution density (*DD*) of 0.5m.

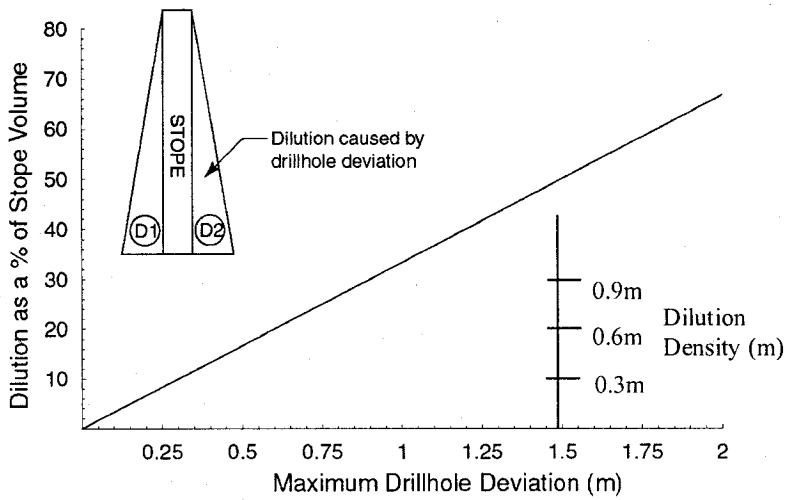

Figure 5.24 Effect of drill hole deviation on dilution, after Tannant et al. (1998b)

5.8.3 Undercutting

Undercutting of the hanging-wall occurs when the drift does not accurately follow the ore / waste contact and moves into the waste hanging-wall rock. Cutting into the hanging-wall waste rock, breaks the integrity of the rock beam that often makes up the immediate hanging-wall rock. Data compiled by Wang (2004) of undercutting associated with 150 blasthole stopes at Hudson Bay Mining and Smelting Co. Ltd. operations found that 36% of the stopes were undercut in excess of one meter. See Figure 5.25.

A stope will tend to slough to the width of the development unless ground conditions are extremely favourable or the undercut is supported. In less

favourable ground conditions, this may lead to unravelling and excessive dilution. Diederichs and Kaiser (1999) showed that even a few millimeters of hanging-wall or abutment relaxation can lead to the failure of previously stable spans or may bring stable hanging-walls to failure.

As discussed in Chapter 4, dilution occurs due to the loss of confinement in the radial direction to the stope wall and a drop in σ_1 and σ_2, Figure 5.26(a). Displacements occur parallel to the hanging-wall due to the undercutting, Figure 5.26(b). Undercutting the stope decreases σ_3 even further, and reduces both σ_1 and σ_2 and hence promotes the potential for dilution, Figure 5.26(c).

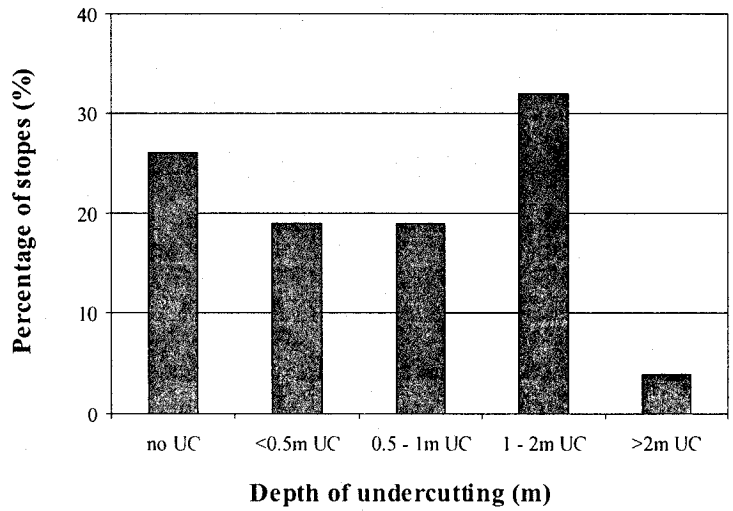

Figure 5.25 Extent of undercutting in stopes at Hudson Bay Mining and Smelting Co. Ltd. operations, (after Wang, 2004)

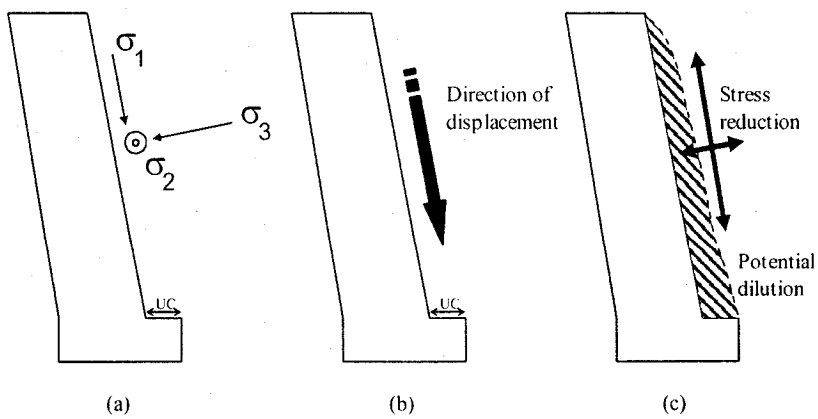

Figure 5.26 Stress reductions caused by displacements into an undercut stope

To account for the influence of undercutting, Wang et al. (2002a) proposed the Undercutting Factor (UF). The Undercutting Factor considers (i) dimensions of the stope hanging-wall, (ii) undercutting on both the overcut and undercut drifts, as well as (iii) the length of undercutting parallel to the stope hanging-wall on both overcut and undercut drifts. Stress setting of the stope prior to mining is not considered. UF is analogous to Dilution Density in that both factors express overbreak as depth over the entire stope surface. UF (Figure 5.27) is expressed as:

$$UF = \frac{l_o + l_u}{2\,(L+H)} \cdot \frac{d_o + d_u}{2} \qquad (5\text{-}7)$$

where:

UF = Undercutting Factor (m)

l_o = Drift length where undercutting occurs on the overcut drift (top sill)

l_u = Drift length where undercutting occurs on the undercut drift (bottom sill)

L = Stope strike length

H = Stope height (up dip)

d_o = average depth of undercutting along the length of overcut drift (top sill)

d_u = average depth of undercutting along the length of undercut drift (bottom sill)

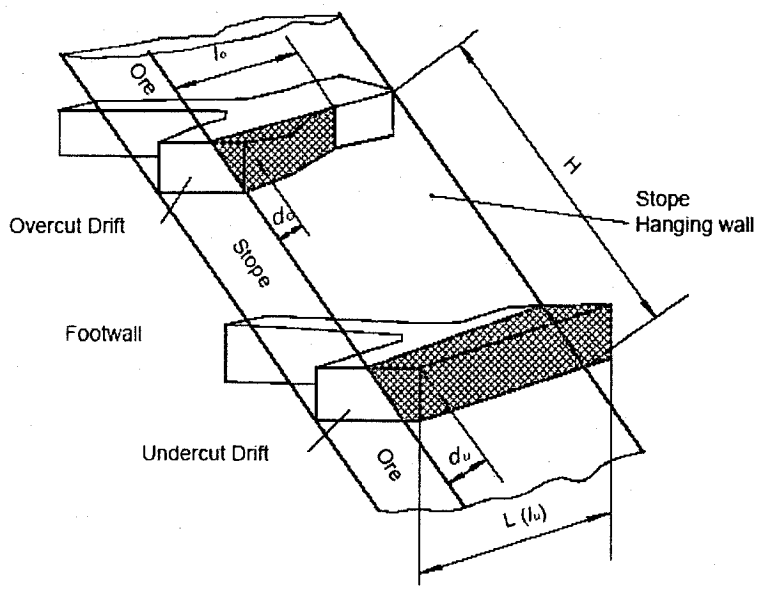

Figure 5.27 Undercutting parameters, Wang (2004)

Dilution Density associated with undercutting of the stope hanging-wall was evaluated across the base-case 30m height stope with 80° hanging-wall dip using Equation 5-7. Potential overbreak generated by undercutting the top and bottom sills of the stope by depths of 1m and 2m is provided in Figure 5.28. For example, undercutting to a depth of one meter may contribute up to 0.33m overbreak to a 30m high stope with a 15m strike length. If 50% of the top and bottom sills of that same stope are undercut to a depth of one meter, overbreak to a depth of 0.17m is suggested.

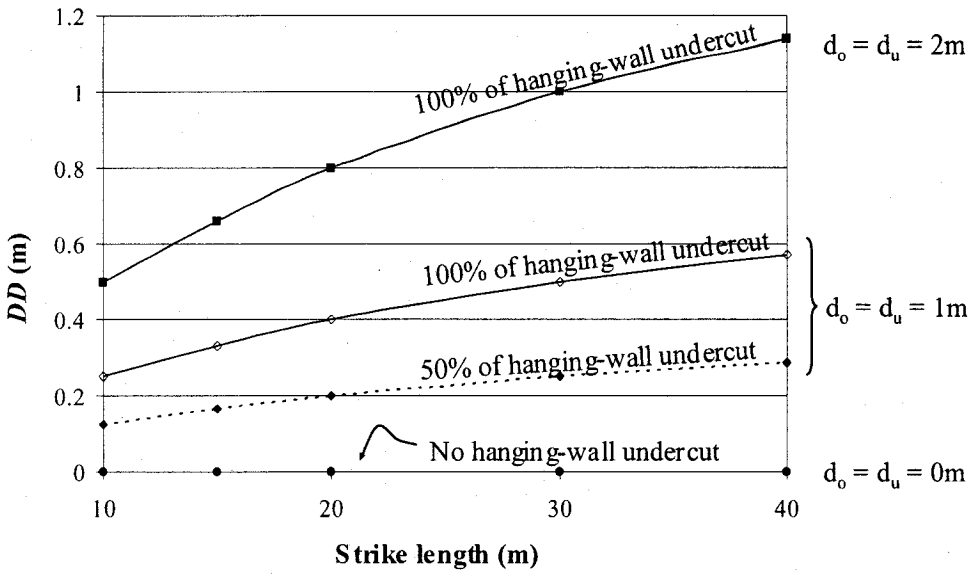

Figure 5.28 Influence of undercutting on Dilution Density, 30m height stope with 80° hanging-wall dip

5.9 Summary of parametric results

Parametric numerical modelling studies were undertaken to examine the impact of a variety of factors on hanging-wall ore dilution. The key observations of the sensitivity of individual factors on potential overbreak include:

- Mine depth does not play a significant role in the extent of σ_3 = 0 MPa contour within the hanging-wall as overbreak associated with σ_3=0 contour does not increase significantly with depth. For example, as the mining depth increases from 750m to 2250m, the increase in *DD* is only 0.05m or 8.6% for a 20m long stope. However, for stopes with strike lengths exceeding 15 meters, overbreak associated with rockmass tensile strength (σ_t) contour increased with depth. With a 20m long stope, the severity of potential dilution associated with the $\sigma_3 = \sigma_t$ contour increased from 0.02m to 0.2m between shallow and moderate depth. As mining depth increased from 1500m to 2250m depth, *DD* associated with the $\sigma_3 = \sigma_t$ contour increased from 0.2m to 0.28m.

- Stopes with large vertical and short horizontal dimensions or stopes having long horizontal and short vertical dimensions are more stable than large rectangular stopes. Rectangular stopes with vertical height and strike lengths of 15m or less are more stable than large rectangular stopes. *DD* is reduced for stopes with Aspect Ratios of 0.5 or less, or rectangular stopes with vertical height and strike lengths less than 15m. Increased overbreak is associated with Aspect Ratios of 1.

- Modelled overbreak increased as the hanging-wall dip angle becomes increasingly shallow. The influence on hanging-wall dip angle on overbreak is more pronounced as strike length increases. For a 30m high × 30 long stope, overbreak increases by 0.22m or 29% when the dip angle changes from 80^{o} to 60^{o}.

- Modelled overbreak is reduced when the orientation of pre-mining principal stress (σ_1) is parallel to the strike of the stope. A decrease in *DD* by 0.08m or 16% occurs when premining stresses are parallel rather than perpendicular on a 20m long stope. Major principal stress orientation influences stope overbreak as strike length increases beyond 20m for a 30m high stope.

- The influence of rockmass quality did not impact Dilution Density values associated with the $\sigma_3 = 0$ contour. With the elastic numerical modelling, the shape of the $\sigma_3 = 0$ contour varied with stope shape and was not influenced by rockmass quality. However, Dilution Density values associated with the $\sigma_3 = \sigma_t$ contours varied across the three quality ranges. A high quality rockmass has a more competent structure and will have greater tensile capacity prior to failure. As a result, the severity of anticipated overbreak diminishes as the rockmass quality of the host rock increases.

Five stope types were identified, based on their position within a tabular blasthole mining sequence. Three stope types are classified as primary (P1, P2 and P3) and two are secondary stopes (S1 and S2). The type of stope influences the severity of modelled overbreak. Overbreak potential increased slightly between the three primary stope types, and increased significantly when comparing the primary and secondary stope types. In a general sense, this can be expressed as:

$$DD_P < DD_{S1} < DD_{S2} \quad (5\text{-}8)$$

where: $DD_P = DD$ generated by primary (P1, P2 and P3) type stopes

$DD_{S1} = DD$ generated by S1-type stopes

$DD_{S2} = DD$ generated by S2-type stopes

Stope type influences severity of modelled overbreak. Compared against the P1 stope, extraction of the P2 and P3 stopes is associated with greater values of overbreak. Compared against the P2 stope, extraction of the P3 stopes resulted in a slight increase (in the range of 5%) in overbreak. Overbreak values for the secondary S1 and S2 stopes are significantly greater than that associated with P1 stopes. The greatest potential overbreak was associated with S2 stopes, which are bound on three sides by mined stopes.

Three construction factors (DD_{Cf}) were identified: Blasting, drillhole deviation and undercutting. With blasting, the severity of overbreak was reduced by limiting blast vibrations to less than 600 mm/second within hanging-wall rock. A good quality host rockmass is less susceptible to blast vibration damage. Overbreak damages associated with drill hole deviation are reduced by good operator practices, such as avoiding set-up errors, and using good, well maintained, equipment. The extent of hanging-wall undercutting on both the top and bottom sill exposures directly influence overbreak. Factors involved in stope construction influence the severity of modelled overbreak.

- Blast damage may generate a zone of decreased rockmass quality at the stope boundary, to a depth exceeding one meter within the hanging-wall.

The severity of blast vibration damage diminishes away from the stope boundary.

- Overbreak increases as the depth and lateral extent of undercutting increases. A stope will tend to slough to the width of the development.
- Dilution associated with drill hole deviation is largely governed by human error and operator skill.

The parametric study considered two criteria for overbreak: (i) the volume of relaxed ground available for overbreak, assuming the rockmass has no tensile strength, represented by the $\sigma_3 = 0$ MPa; and (ii) the $\sigma_3 = \sigma_t$ contour, which accounts for rockmass tensile strength. Modelling results found that these two criteria did not parallel each other. When comparing overbreak associated with the $\sigma_3 = 0$ MPa and $\sigma_3 = \sigma_t$ contours against depth (Figure 5.29), it was found that the $\sigma_3 = 0$ MPa contour remained near-constant with depth for a given stope geometry or hanging-wall dip. Conversely, potential overbreak associated with the contour of rockmass tensile strength increased with depth for a given stope geometry or hanging-wall dip.

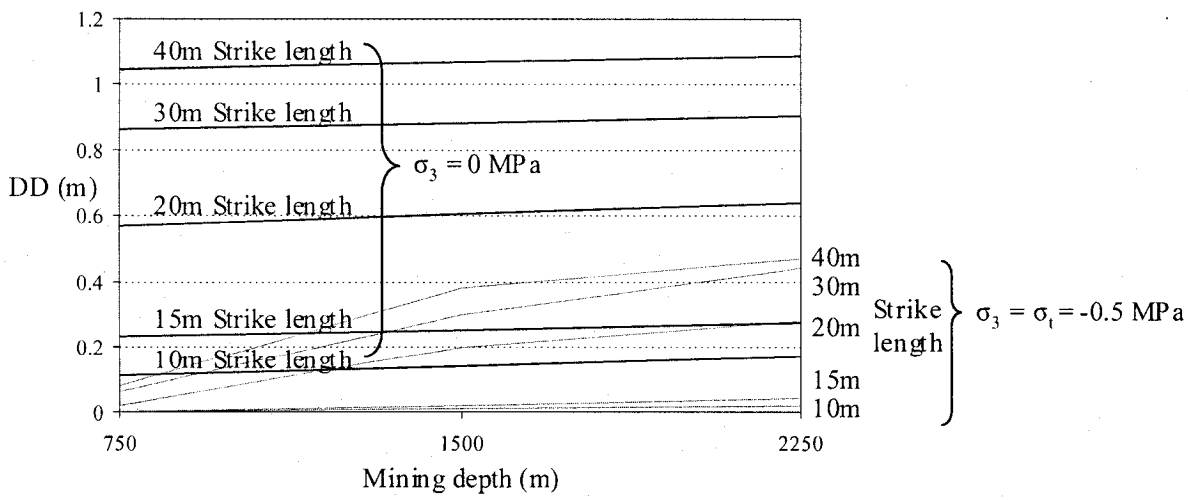

Figure 5.29 Modelled *DD* for stope of 30m vertical height. Values associated with $\sigma_3 = 0$ and $\sigma_3 = \sigma_t = -0.5$ MPa contours plotted

To quantify modelled overbreak, the following terminologies, illustrated in Figure 5.30, are introduced:

- No-tension overbreak (DD_0), corresponding to the σ_3 = 0 MPa contour represents overbreak that may happen, assuming that the rockmass has no inherent strength. The σ_3=0 indicates transition from tension to compression state. The No-tension overbreak contour varies with stope geometry and hanging-wall dip, and is roughly independent of depth. The influence of stope shape on the zone of relaxation, defined as σ_3=0 (Hutchinson and Diederichs, 1996), is illustrated in Figure 5.31.
- Confinement overbreak (DD_T), corresponding with the $\sigma_3 = \sigma_t$ contour represents slough that will happen. The extent of Confinement overbreak increases with depth for a given stope geometry or hanging-wall dip angle. The relationship between No-tension and Confinement overbreak as a function of depth is illustrated in Figure 5.32. DD_T is a less conservative estimate of ore dilution density than DD_0; $DD_T < DD_0$

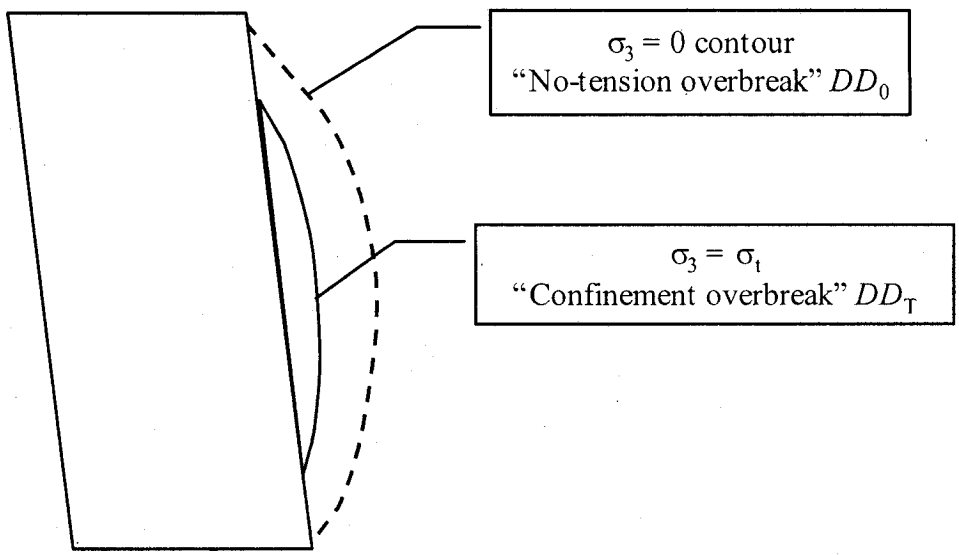

Figure 5.30 Two overbreak regimes: (i) Geometric overbreak (DD_0) and (ii) Confinement overbreak (DD_T)

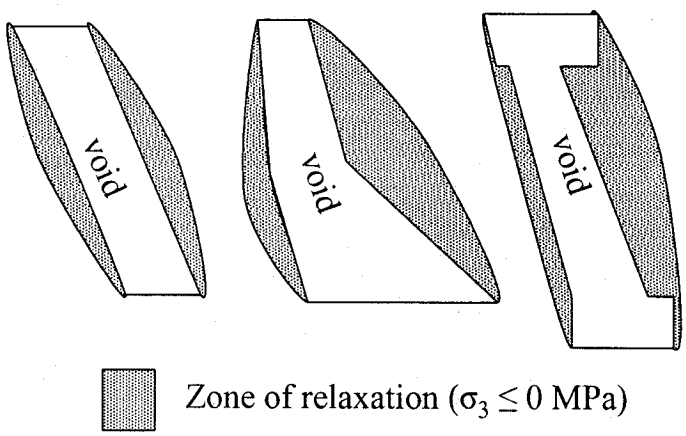

Figure 5.31 Influence of geometry on the zone of relaxation, after Hutchinson and Diederichs (1996)

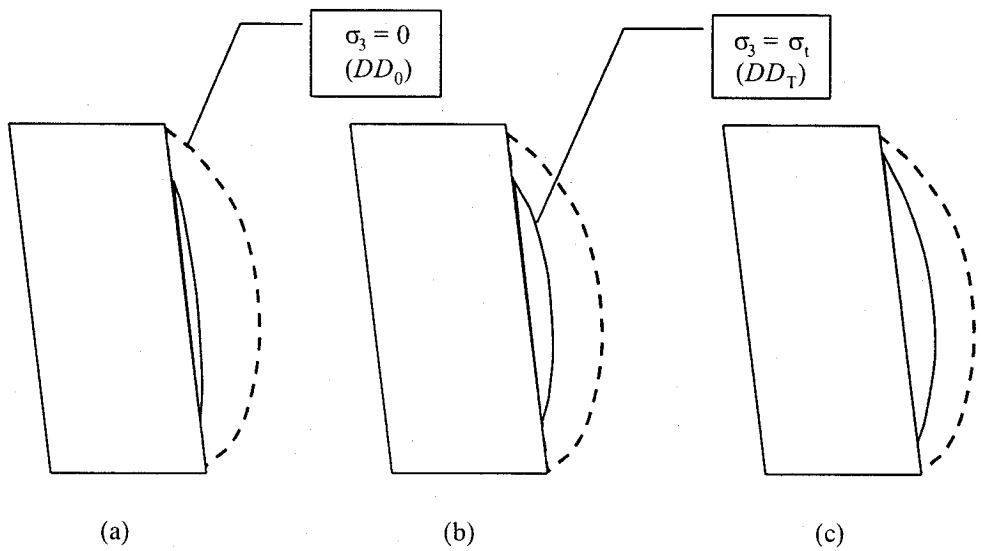

Figure 5.32 Influence of mining depth on overbreak regimes: (a) shallow depth, (b) moderate depth, (c) deep

Two other factors influence the likelihood of dilution occurring within (and beyond) the envelope of No-tension overbreak.

- External Factors (DD_E) represent physical conditions of the stope setting that influence hanging-wall stability. These conditions include rockmass quality, orientation of principal stress, and stope type.
- Construction Factors (DD_{Cf}) are human influences impacting overbreak. Construction Factors include blasting, drillhole deviation, and undercutting.

No-tension overbreak (DD_0) represents overbreak that may happen, depending largely on the severity of Construction Factors (DD_{Cf}) in damaging the tensile capacity of the rockmass. Confinement overbreak (DD_T), which increases with depth, represents dilution that will occur as a result of tensile failure of the hanging-wall rock into the mined stope. The magnitude of overbreak may be further increased by External Factors (DD_E).

CHAPTER 6

ORE DILUTION AT BOUSQUET #2 MINE – CASE STUDY

6.1 Historical background

The Bousquet property is situated in the Abitibi region of northwest Quebec, 50 kilometers west of the city of Val d'Or, as shown in Figure 6.1. The property is composed of former mining claims held by Thompson-Bousquet Gold Mines and Bijou Gold Mines. The mining rights were acquired by Long Lac Minerals, (later to become LAC Minerals Limited), in 1974. In 1986, exploration conducted by LAC Minerals at its Bousquet property resulted in the discovery of a gold bearing massive sulphide deposit located 1.2 km east of the existing Bousquet #1 shaft. See Figure 6.2.

Construction of the surface facilities, including the hoist building, headframe and service buildings were completed in 1988. Excavation of a 5.8 meter diameter circular concrete-lined shaft was completed to a depth of 1245 meters by March 1990. Commercial production began from the 6th Mine Level (805m depth) in October 1990. In 1991, construction work included the installation of the shaft bottom load-out station and a crusher on the 9th Mine Level, (1176 m depth). An additional expansion phase completed in 1994 provided ramp, sublevel, and infrastructure development to access mineralized zones existing below the crusher, to a depth of 1326 meters.

By the end of 1994, 750,000 gold ounces had been produced at the Bousquet #2 mine from 2,550,000 tonnes. During the third quarter of 1994, Barrick Gold Corporation acquired LAC Minerals Ltd., which included the Bousquet #2 mine.

With depletion of reserves, the mine ceased production in 2002, having produced 2,129,600 ounces of gold from 8,143,000 tonnes of mined rock. In 2003, the Bousquet property was purchased by Agnico-Eagle Mines Limited.

Figure 6.1 Bousquet property location

6.2 Geologic setting

The Bousquet #2 deposit is a lens of massive sulphide and associated disseminated breccia and stringer sulphides, occurring in a pyritic horizon within a series of volcanic rocks, primarily schists of varying quality, striking east-west and dipping steeply to the south. The horizon extends approximately 400 meters from the eastern boundary of the property at a depth of 180 meters, and is open at depth. Gold mineralization is associated with the pyritic horizon and shows a strong relationship to pyrite and copper content which varies from massive, to stringers, to disseminated, going from east to west. Massive sulphide mineralization is composed of 30% to almost 100% pyrite bands, up to several meters thick, with minor amounts of copper.

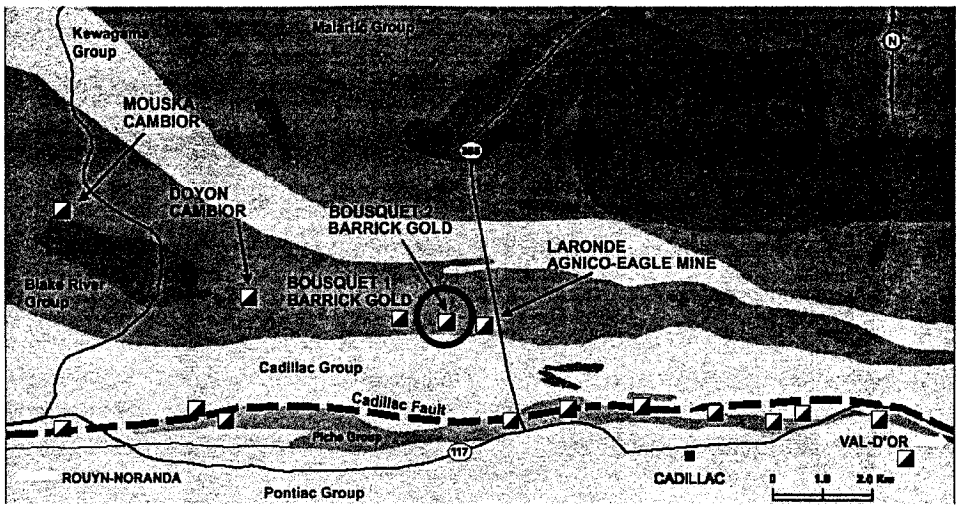

Figure 6.2 Surface plan showing mine properties and geologic setting

6.2.1 Regional geologic setting

The Bousquet #2 deposit, described by Tourigny et al. (1993), occurs in the southern part of the Abitibi Greenstone Belt in the Superior Province of the Canadian Shield. The supracrustal rocks of the district consists of a typical Archean volcano-sedimentary assemblage of mafic to felsic rocks (Blake River Group) flanked by clastic sedimentary rock units to the north and the south. This volcano-sedimentary assemblage strikes east-west, dips steeply to the south, and exhibits a strong east-west regional tactonic fabric.

The southern portion of the Blake River Group corresponds to a 500 m wide tectonic belt including anastomosing zones of volcanic derived schist such as chlorite-carbonate schist, quartz-muscovite schist and andalusite-kyanite schist. This structural domain is characterized by several smaller scale shear zones which can be observed throughout Bousquet #2 and which often act against the stability of mine openings. The foliation trend which dominates the structure in the hanging-wall is a characteristic of this zone.

6.2.1.1 Economic geology

Mineralization at Bousquet #2 mine is hosted by faulted andalusite-kyanite schist. The principal gold-bearing lens of the mine contained 6,737,000 tonnes grading 0.22 ounces per ton Au and 0.57% Cu. The zone strikes east-west, dips N80° south and plunges westward at 70°. This orebody is lenticutar shaped, ranging in thickness from 4 to 19 meters, with lateral and vertical dimensions of 300 m and 1500 m respectively.

Recrystallized pyrite (35% to 95%) is the dominant sulphide mineral in the orezone and is generally accompanied by minor amounts (less than 5%) of chalcopytite, boronite, chalcocite and gold. A feature of the principal lens is the presence of two distinct morphofacies: (1) massive pyrite lenses composed of up to 95% pyrite; and (2) sulphide matrix breccia containing 35 to 55% sulphides.

6.2.2 Description of orezones

The Bousquet #2 mine was subdivided into six mining blocks labeled Block 1 through Block 5 and Zone 3-1 which is located between the Bousquet #1 shaft and the Bousquet #2 shaft. Figure 6.3 provides a longitudinal section of the Bousquet property.

At the Bousquet #2 mine, sills were established on Level 8 at 1045m depth (Block 4) and Level 6, 805m depth (Block 3). Block 5 located at 1045m to 1195m depth, underlying Block 4, was advanced upwards at the mined sill on Level 8. Block 6 located at 1195m to 1315m depth, underlying Block 5, was advanced upwards to the mined sill at the base of Block 5 on Level 10-3. The eastern border of the Bousquet mine is bound by the Laronde mine of Agnico-Eagle Mines Ltd.

Zone 3-1, located approximately 1000m west of the Bousquet #2 orebody was mined at depths of 1340 to 1580 meters below surface. Zone 3-1 was accessed by a haulage drift from the base of the Bousquet #2 development, as shown in Figure 6.4.

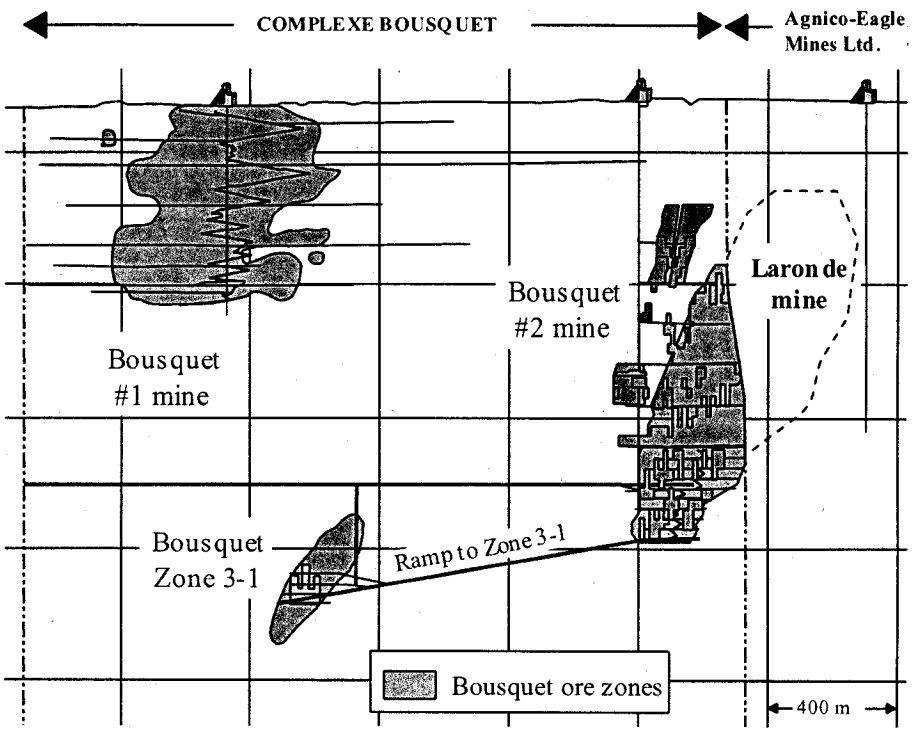

Figure 6.3 Longitudinal section of Bousquet mine property

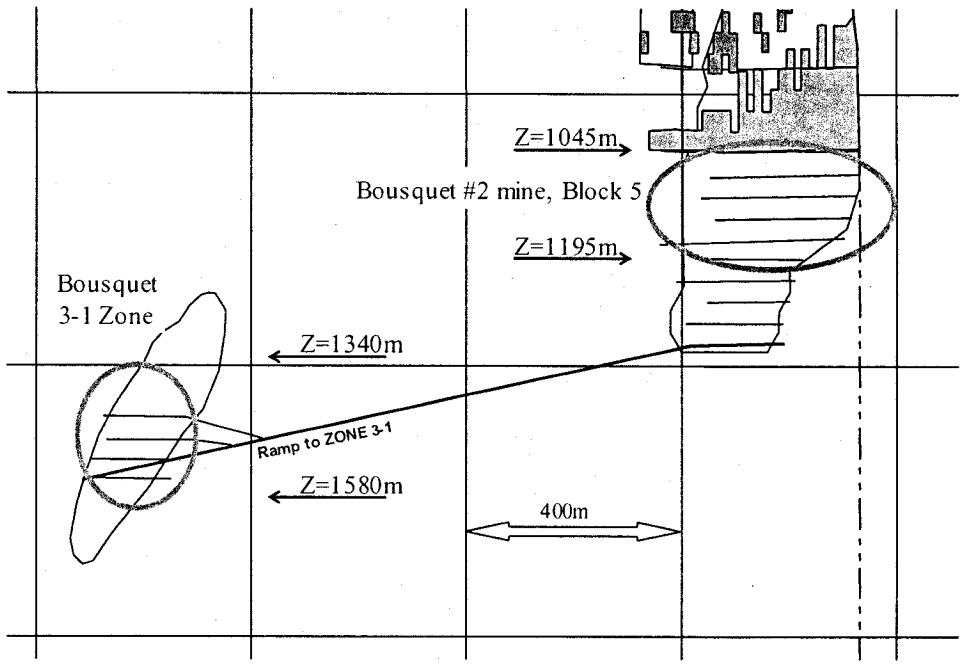

Figure 6.4 Detail showing locations of Block 5 and Zone 3-1, longitudinal view

6.3 Mine description

The mineralized zone at the Bousquet #2 mine follows the regional structural trend, dipping steeply south in a tabular form. The orebody is accessed by a single 5.8 m diameter concrete lined circular shaft, driven to a depth of 1245 meters on the footwall side of the orebody. Shaft stations located at 122 meter intervals access the main levels of the mine. An internal ramp connects the main production levels with three sublevels which are developed at 30 meter intervals between the main levels. Footwall haulage drifts, running parallel to the orebody, with 50 meter long drawpoint crosscuts provide direct access for removing the ore bearing rock from the stopes. Mined rock is hauled to ore and waste pass dumps, located in the footwall of each sublevel at a distance of approximately 60 to 80 meters from the orezone, with 6-yard scooptrams. The backfill, ore and waste rock passes were driven with Alimak raise climbers to dimensions up to 3 m diameter. Ventilation raises, located in the footwall at a distance of 80 meters from the orebody, were driven to a diameter of 2.1 meters.

The mineralized zone extends towards the east beyond the Bousquet #2 property limit, where it is mined by Agnico-Eagle Mines Limited, as the Laronde Mine. There is no barrier pillar between the two mines. Stope sequencing along the boundary of the two mines is integrated into the mine design of the two mines according to pre-determined guidelines.

Bousquet #2 mine is a trackless bulk-mining operation. Production from below the 9-1 sublevel, (1135 m depth), is hauled by a 40-ton capacity truck up from the 11-3 level (1315 m depth), to be dumped in ore and waste bins located above the 9-0 level crusher, located at a depth of 1165m. When active, production rates were approximately 1800 tonnes per day.

Mining methods, equipment, manpower and design used for mining the main Bousquet #2 orebody (including Block 5) were also employed for mining of Zone 3-1. Broken ore from Zone 3-1 was hauled by 40-ton capacity truck up to the 11-3 level (1315 m depth), where it was transferred and transported to the ore bin located above the 9-0 level crusher.

The Block 5 and Zone 3-1 orezones were divided into transverse primary and secondary stopes with sublevels located at 30 meter vertical intervals. Typical design dimensions of Block 5 and Zone 3-1 stopes are provided in Table 6.1. The open stope mining with delayed backfill method is used to take advantage of steeply dipping tabular orebody geometry, and to optimize production rates and recovery. Block 5, shown longitudinally in Figure 6.5, consisted of ninety seven stopes, distributed over five stoping horizons. The strike length of the Block 5 orezone was up to 330m. Figure 6.6 showing lateral development on Level 9-3 infrastructure, including hanging-wall cablebolt drift and Main zone stopes.

Zone 3-1, shown longitudinally in Figure 6.7 consisted of seventy five stopes, distributed over eight stoping horizons. The strike length of the 3-1 zone was up to 110m. Figure 6.8 showing lateral development on Level 3470 infrastructure, geologic units and Main zone stopes.

Table 6.1 Typical transverse stope dimensions

	Block 5		Zone 3-1	
	Primary	Secondary	Primary	Secondary
Vertical height	30m	30m	30m	30m
Strike length	15m	15m	10m	10m
Stope tonnage	11000 to 14000 tonnes		4000 to 5000 tonnes	

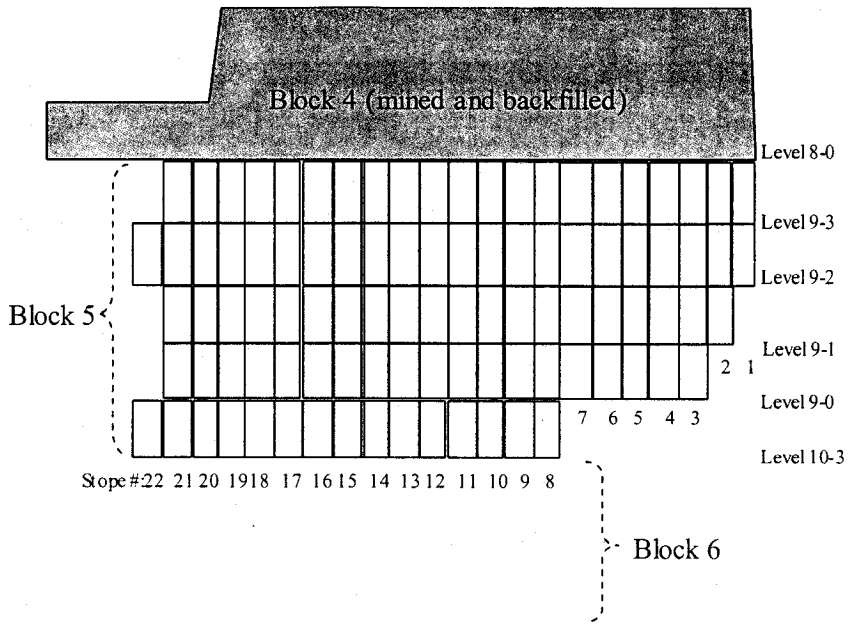

Figure 6.5 Detail of Block 5, showing stope numbering and levels

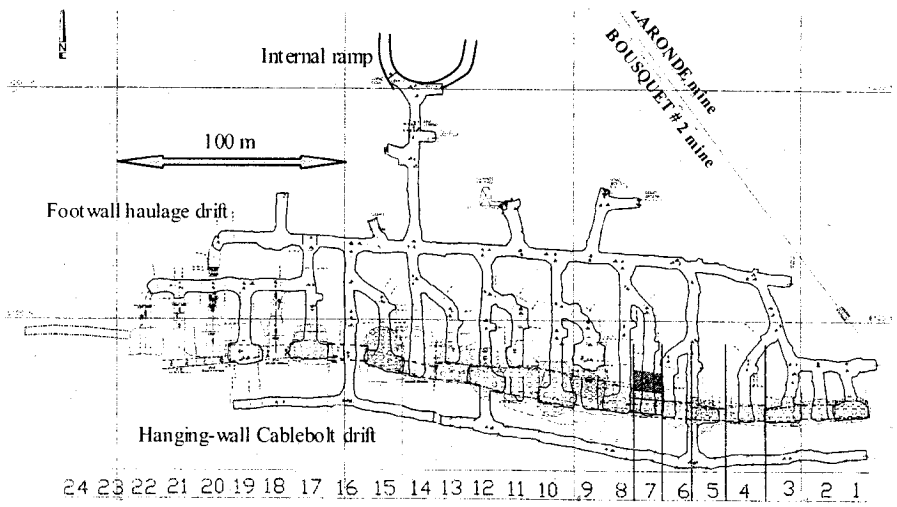

Figure 6.6 Bousquet Block 5, level 9-3

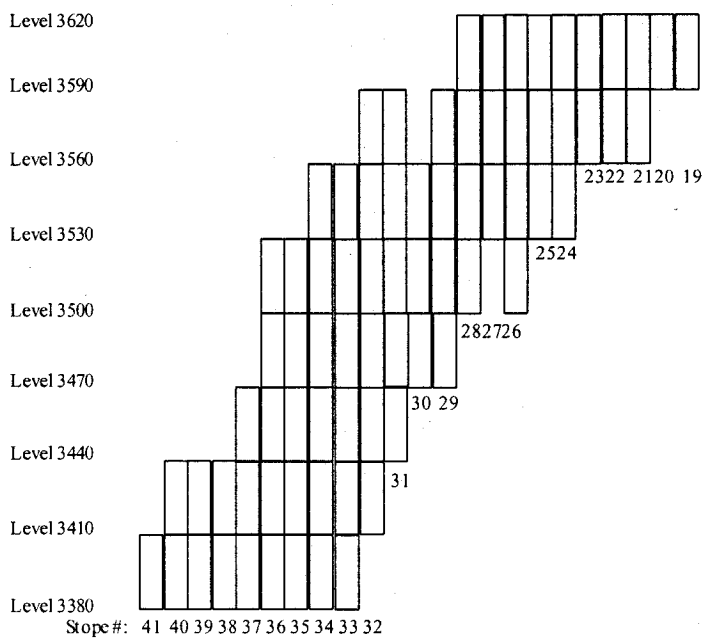

Figure 6.7 Detail of Zone 3-1, showing stope numbering and levels

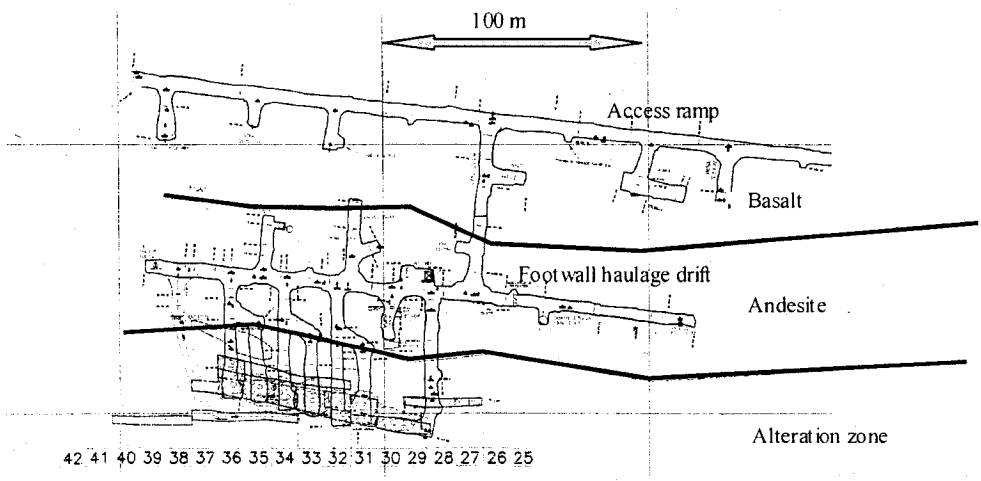

Figure 6.8 Bousquet Zone 3-1, Level 3470

6.3.1 Mining method description

In the massive ore, with widths exceeding four meters, stopes are mined transversely. In the transverse open stope mining method, an expansion slot is developed by enlarging slot raise to the width of the stope, using parallel hole blasting. Ore is fragmented in the stope using ring-drilled or long parallel blast holes, and mucked from a drift, orientated perpendicular to the stope strike, at the base of the stope. Following the completion of stope mucking, cement rockfill backfill (CRF) is placed into the stope, either into the top of the stope, or via an overhead slot / backfill raise. Typical Block 5 and Zone 3-1 open stope mining pattern and sequence is illustrated in Figure 6.9.

Primary stopes are mined one lift at a time and backfilled with cemented rockfill. Secondary stopes are mined between two primary stopes when the latter stopes have been mined over two lifts. Secondary stopes are backfilled with non-cemented rockfill.

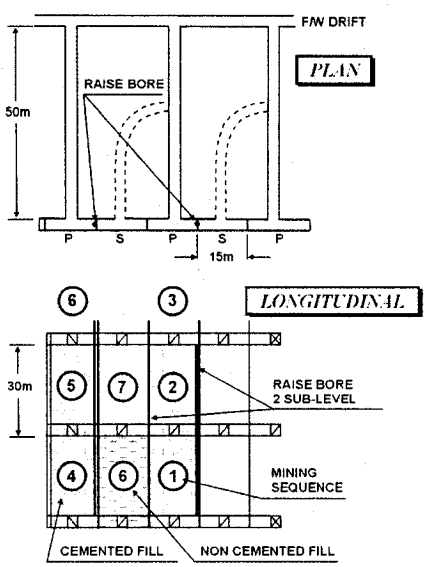

Figure 6.9 Transverse primary and secondary stoping sequence

A variation of open stope mining used in the narrower regions of the orebody found at the lateral fringes of the orezone, is the Eureka mining method (Trahan, 1995). This mining method is applied to longitudinal access stope blocks, in ore

widths of four meters or less. With the Eureka method, shown in Figure 6.10, normally only the first stope in the longitudinal zone requires a drilled slot. Subsequent stope slots are generated from slot blasting against a styrofoam core suspended against the previous stope end wall prior to backfilling. With this technique, the styrofoam provides the void for slot blasting.

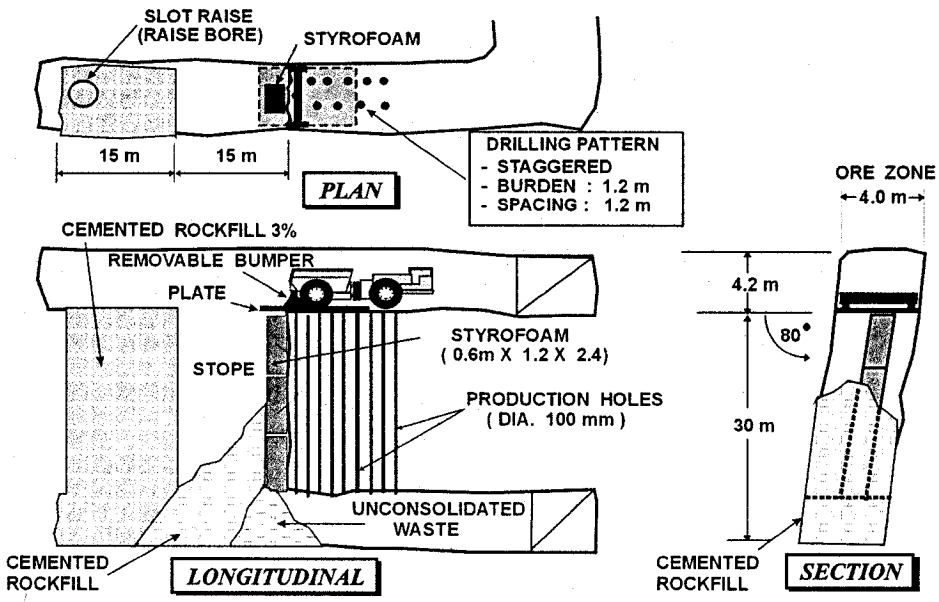

Figure 6.10 Eureka Mining Method, after Trahan (1995)

6.3.2 Stope drilling and blasting methods

Stope production drilling pattern varies between the primary and the secondary stope blocks. The top sill of primary transverse stopes is excavated to the full stope strike length to permit drilling of parallel 100 mm diameter blastholes, typically at a 2.5 meter burden and 2.0 meter spacing, with an off-center 1.07 meter diameter raisebore slot. Secondary transverse stopes are located between previously mined and backfilled primary stopes. In these secondary stopes, 100 mm diameter blastholes are usually drilled in a fan-pattern from a narrow, (5 m wide), top sill access, with a central 1.07m diameter raisebore slot.

In Block 5 and Zone 3-1, both types of drill pattern were employed. Figure 6.11 provides a summary of the number of stopes drilled in parallel, fan and longitudinal pattern for each orezone. Details are provided in Appendix B. Both sites were drilled by the same equipment and operators. Drilling trends for the two zones were similar, with the Fan drilling pattern being most commonly used, followed by parallel drilling. As stated above, the use of longitudinal drilling is site-specific, restricted only to narrow orezone widths.

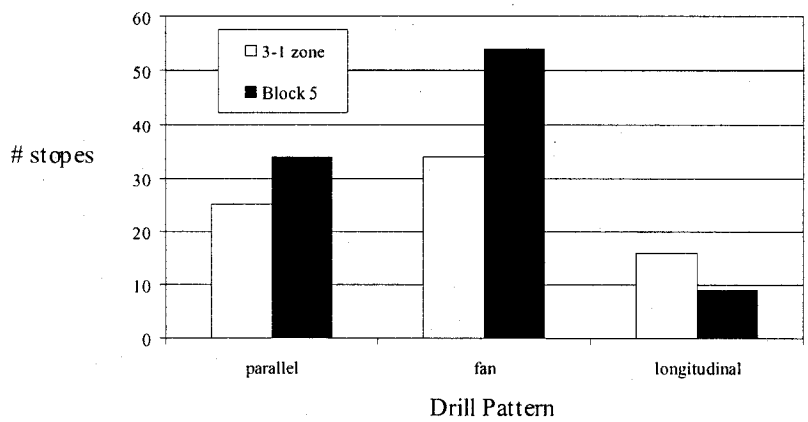

Figure 6.11 Drill patterns used in Block 5 and Zone 3-1

6.3.2.1 Transverse stopes

Production blasting of the transverse and longitudinal stopes is performed with ANFO explosives in mid-stope blastholes. Lower density ANFO explosives are used in the footwall blastholes. Low energy cartridge explosives are used in the blastholes located closest to the hanging-wall to minimize hanging-wall blast vibration damage, (Henning et al., 1997). See Figure 6.12.

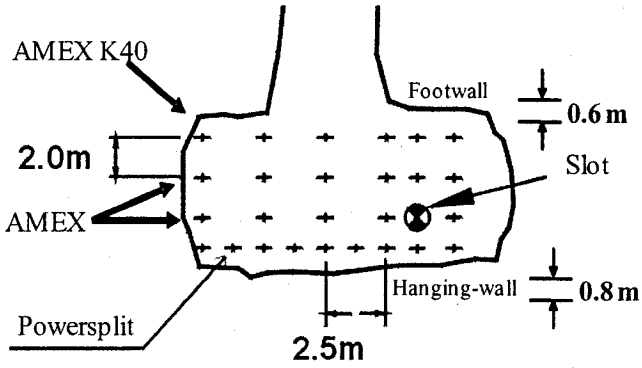

Figure 6.12 Stope drilling and loading practice, transverse stope

Transverse stopes are normally mined in three blasts. In primary stopes, the first two blasts widen the slot area to the full stope thickness in 10 to 14 meter lifts. For the stope final blast, the remaining blastholes are loaded full column, to a maximum charge per delay of 175 kg, and fired into the open slot. For a typical Block 5 stope, the first two 'slot' blasts represent approximately 15% and 20%, respectively, of the total stope volume. The remaining 65% is broken in the third and final blast. Typical schematic primary stope drilling pattern and blast sequence is shown in Figure 6.13.

With transverse secondary stopes, the lower half in the stope excavated by the first two blasts. For the final blast, the remaining blasthole rings are fired inwards, towards the central slot. The combination of a fan-drilling pattern with a lower stress environment, permit the blasting of larger volumes at the initial stages of secondary stope extraction. Usually, the first two 'slot' blasts of a Block 5 stope represent approximately 15% and 35%, respectively, of the total stope volume. The remaining 50% is broken in the third and final blast. Typical secondary stope drilling pattern and blast sequence is shown in Figure 6.14. Blast details from Block 5 are provided in Appendix B.

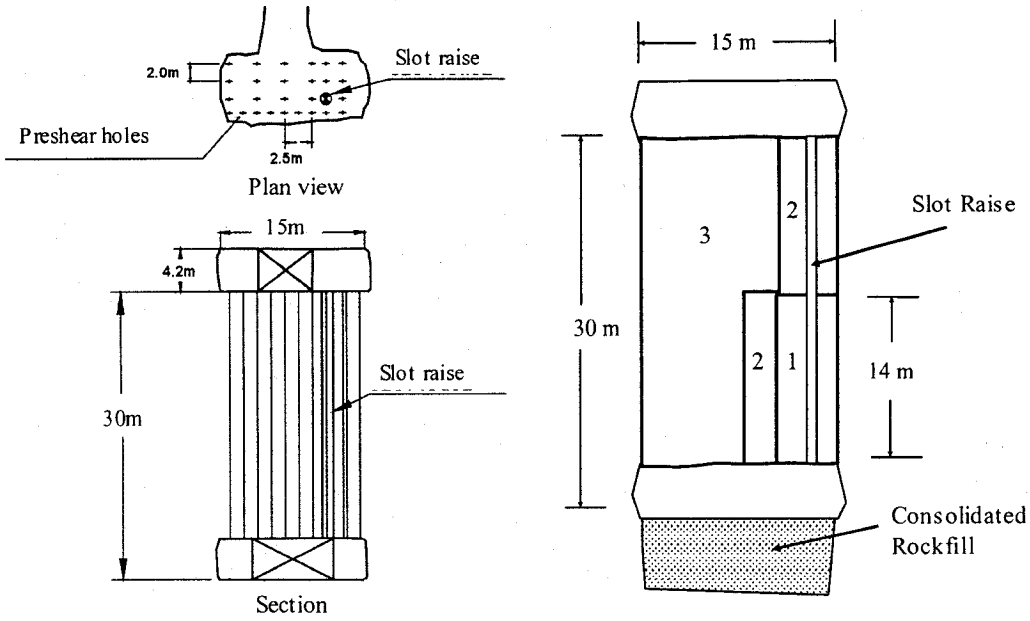

Figure 6.13 Primary stope schematic drilling pattern and blast sequence

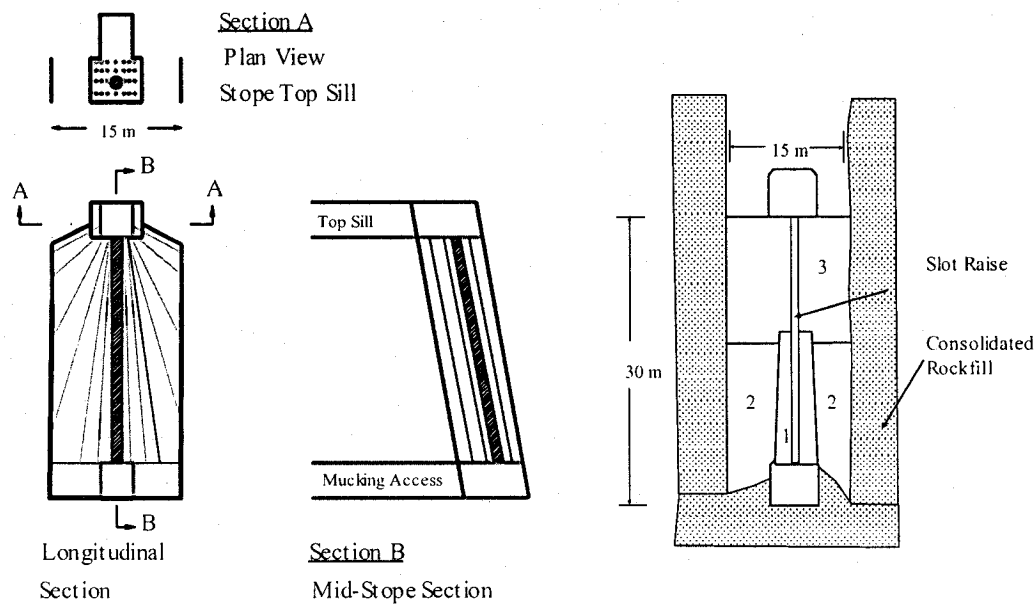

Figure 6.14 Secondary stope schematic drilling pattern and blast sequence

6.3.2.2 Longitudinal stopes

In ore widths of 4 meters or less, stope blocks are accessed longitudinally. The top sills of the longitudinal stopes are excavated to the full stope strike width to permit drilling of parallel 100 mm diameter blastholes, typically at a staggered 1.8

meter burden and 2 meter spacing pattern, as illustrated in Figure 6.15. As with the transverse stopes, low energy explosives were used in blast holes located closest to the hanging-wall and footwall. See Figure 6.16.

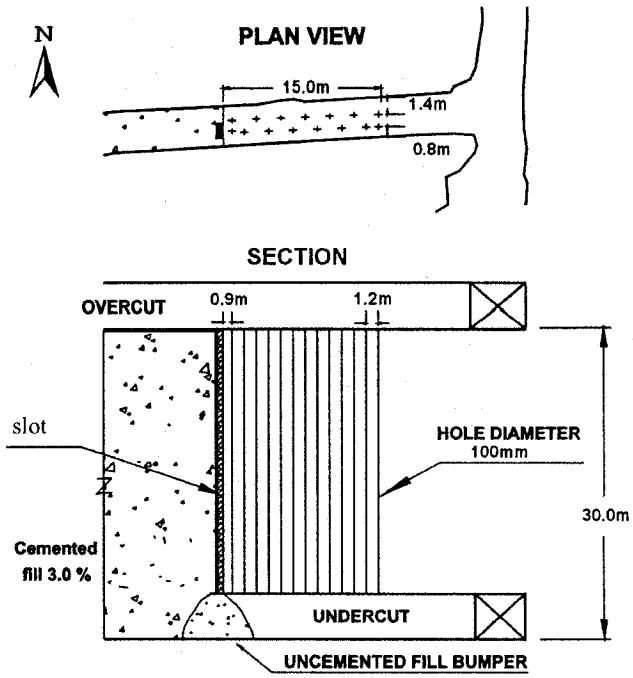

Figure 6.15 Longitudinal stope schematic drilling pattern

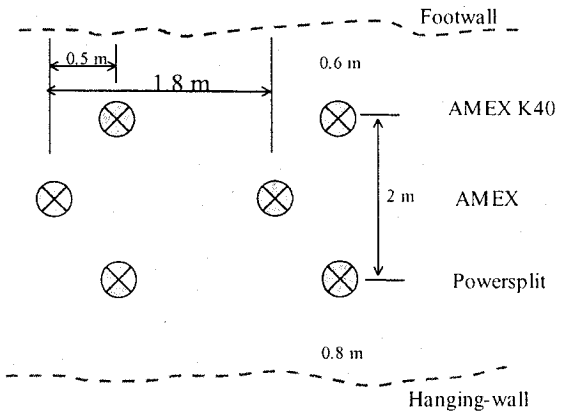

Figure 6.16 Stope drilling and loading practice, longitudinal stope (Gauthier, 2001)

Longitudinal stopes are mined in three or four blasts, depending on the type of slot used. A stope with a drilled slot is mined in three blasts, in a manner similar to the primary transverse stopes. See Figure 6.17(a). The first two blasts widen the slot area to the full stope thickness in 14 meter lifts. For the stope final blast, the remaining blastholes are loaded full column, to a maximum charge per delay of 160 kg, and fired into the open slot. Typically, the first two 'slot' blasts represent approximately 15% and 20%, respectively, of the total stope volume. The remaining 65% is broken in the third and final blast.

Longitudinal stopes utilizing the 'Eureka' mining method (Styrofoam slot) are mined in four blasts, as illustrated in Figure 6.17(b). A small initial blast, representing roughly 4% of the stope volume creates a narrow, 10 meter-high excavation along the cavity against consolidated backfill of the previous stope. The second and third blasts, representing approximately 12% and 24%, respectively, of the stope volume, complete the 'slot' blasting. The remaining 60% of the stope volume is broken in the fourth blast (Gauthier, 2001).

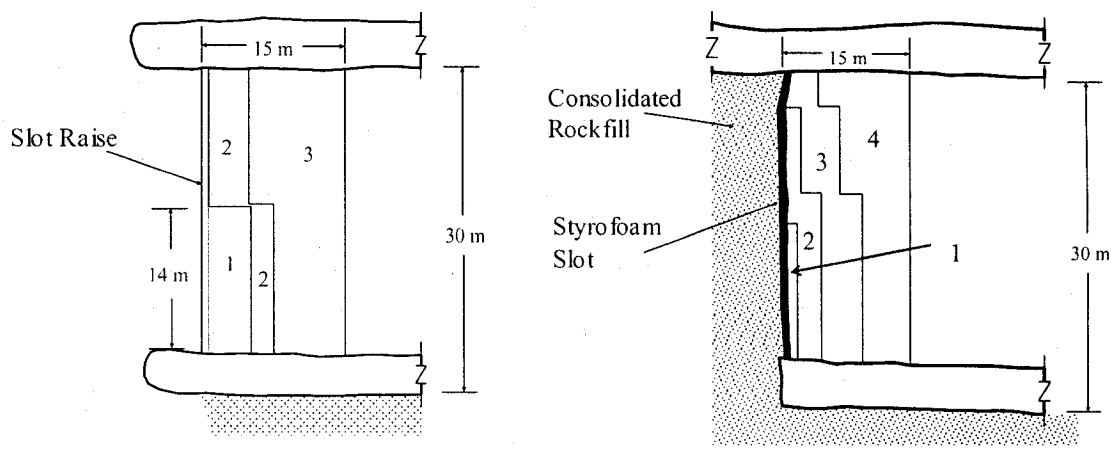

(a) Blast sequence with slot raise (b) Blast sequence with Styrofoam raise

Figure 6.17 Longitudinal stope schematic blast sequence

6.4 Rockmass conditions

Underground geotechnical mapping, first performed by Golder (1988), has been undertaken at Bousquet #2 on a regular basis. Four main joint sets, summarized in Table 6.2, are encountered.

Table 6.2 Summary of rock discontinuity sets

Discontinuity Set	Dip	Dip Direction	Description
J1	57° to 88°	162° to 190°	Sub-vertical set parallels the orebody, striking east-west and dipping steeply south. The joints are typically smooth, planar and tight. Joint spacing ranges from 5 mm to 800 mm, but is typically 200 mm in the hanging-wall.
J2	45° to 85°	85° to 102°	Joint Set #2 is orientated perpendicular to the orebody. Spacing of this joint set ranges from 60 mm to 450 mm and averages 200 mm. The joints are typically smooth to slightly rough and planar.
J3	20° to 60°	260° to 287°	Joint Set #3 is a prominent joint set in the hanging-wall. Spacing ranges from 200 mm to 1300 mm. The set is generally smooth to slightly rough, planar and tight.
J4	5° to 25°	322° to 022°	Joint Set #4 is a sub-horizontal joint set with a spacing of 300 mm to 1000 mm, average 500mm. The joints are slightly rough, planar and tight with quartz infilling.

Bousquet rockmass conditions are controlled extensively by the geological setting, with the dominant schistose fabric controlling the behaviour of wall rocks in all underground excavations. The rockmass can be described as: fresh to slightly weathered, strongly schistose, quartz-mica schist. The schistocity contains sericite and acts as a dominant low friction angle weakness plane in the rockmass. Schistocity planes form platy blocks between a few millimeters to approximately 50 mm in thickness. The rockmass is dry but of poor quality.

The behaviour of the rockmass during mining is controlled to a large extent by the effects of load re-distribution on the dominant parallel schistocity planes, especially those which are closely-spaced and infilled with weak sericite. Loading is transferred to the sidewalls of openings and there is a strong tendency for ''pack of cards'' buckling, as illustrated in Figure 6.18, to take place, especially on the hanging-wall side of drifts parallel to the orebody.

Figure 6.18 Buckling-type failure, Bousquet #2 mine

6.4.1 Block 5

The main orezone of Bousquet #2 (Block 5) deposit is a lens of massive sulphide and associated disseminated breccia and stringer sulphides, hosted within schistose volcanic rock. Rockmass classification for the hanging-wall, main

orezone and footwall are summarized in Table 6.3. Hanging-wall and footwall have similar characteristics (Henning, 1998). For this study, the host rock encasing the orezone rock was assigned values equivalent to the hanging-wall rockmass. The elastic parameters of Block 5 host and orezone rock were evaluated from uniaxial compressive testing of core samples by Prasad (1996). Results from the rock tested are summarized in Table 6.4.

Table 6.3 Summary of average rockmass classification values (Henning, 1998)

Domain	**RQD**	**RMR**	**GSI ***	**Q**	**Q'**
Hanging-wall	35	50	50	0.47	1.17
Orezone	85	75	75	7.0	7.0
Stope Footwall	45	55	55	0.50	1.25

* new values calculated based on Hoek et al. (2002)

Table 6.4 Uniaxial compressive test results (Prasad, 1996)

Domain	**Rock Type**	**Uniaxial Compressive Strength (σ_c)**	**Young's Modulus (E)**	**Poisson Ratio (υ)**
Host rock	Rhyolite Tuff	112 to 160 MPa	53 to 76 GPa	0.21
Orezone	Massive Sulphide	211 MPa	127 GPa	0.10

6.4.2 Zone 3-1

The Zone 3-1 deposit occurs as disseminated stringer sulphides within an equally schistose volcanic rock. Hanging-wall, orezone and footwall are located within the Alteration zone rock unit have similar characteristics (Henning, 1996).

Rockmass classification for the host rock and orezone are summarized in Table 6.5. Uniaxial compressive strength testing of 3-1 Zone core samples were performed at Queen's University (Hyett, 1996). Test results are summarized in Table 6.6. The ore-bearing alteration zone has properties similar to moderately foliated Bousquet #2 host rock.

Table 6.5 Summary of average rockmass classification values (Henning, 1996)

Domain	**Rock Type**	**RQD**	**RMR**	**GSI ***	**Q**	**Q'**
Host rock	Alteration Zone	50	48	48	1.4	2.8
Orezone	Alteration Zone	50	48	48	1.4	2.8

* new values calculated based on Hoek et al. (2002)

Table 6.6 Uniaxial Core Test Results, Zone 3-1 (Hyett, 1996)

Domain	**Rock Type**	**Uniaxial Compressive Strength (σ_c)**	**Young's Modulus (E)**	**Poisson Ratio (υ)**
Host rock	Alteration Zone	59 MPa	37 GPa	0.14
Orezone	Alteration Zone	59 MPa	37 GPa	0.14

6.4.3 Bousquet rockmass parameters

Bousquet Block 5 and Zone 3-1 rock parameters are summarized in Table 6.7. Rockmass parameters were obtained using relationships described in Section 4.3 (Table 4.6).

Table 6.7 Block 5 and Zone 3-1 rockmass conditions

Parameter	**Block 5**		**Zone 3-1**
	Host rock	Ore	Host rock and Orezone
Rock type	foliated rhyolite tuff	massive sulphide	foliated rhyolite tuff "alteration zone"
Orezone dip	80° to 85°	80° to 85°	75° to 80°
RQD	35%	85%	50%
RMR_{79} / GSI	50	75	48
Q	0.47	7	1.4
Q'	1.17	7	2.8
UCS (σ_c)	112 MPa	211 MPa	59 MPa
Poisson ratio (υ)	0.21	0.1	0.14
m_i	10 (schistose rock)	17 (fine grain igneous rock)	10 (schistose rock)
Density	2.8 tonnes/m^3	4.0 tonnes/m^3	3.2 tonnes/m^3
Rockmass Parameters			
Hoek-Brown 'm'	1.677	6.961	1.561
Hoek-Brown 's'	0.0039	0.0622	0.0031
Rockmass elastic modulus, (E_{rm})	10000 MPa	42170 MPa	6846 MPa
Rockmass tensile strength, (σ_t)	0.258 MPa	1.885 MPa	0.177 MPa
Global rockmass compressive strength, (σ_{cm})	19.5 MPa	83.5 MPa	9.844 MPa

6.4.4 Stress environment

Overcore stress monitoring was conducted at the Bousquet #2 mine in 1988 (Arjang, 1988) at a depth 900 meters using a CSIR triaxial strain cell in a 150 mm diameter horizontal borehole, drilled perpendicular to the structural plane and schistocity.

Results of pre-mining ground stresses indicated that the maximum and the intermediate principal compressive stresses were horizontal. The minimum principal compressive stresses were orientated vertically. Test results and orientations were comparable with other regional stress data, (Arjang, 1996).

The average horizontal compressive stress gradient was 0.0505 MPa/m, with a ratio of maximum and minimum horizontal compressive stresses (σ_H^o/σ_h^o) in the range of 1.5. In relation to the orezones, (striking approximately N105E, dipping 80° to 85° South), σ_H^o acts perpendicular while σ_h^o is orientated on-strike to the orezones and main structural features. On the basis of the testing, the following pre-mining in-situ stress relationships were established:

$$\sigma_V = 0.027\ Z \qquad (6\text{-}1)$$

$$\sigma_H^o = 2.24 \cdot \sigma_V = 0.061\ Z \qquad (6\text{-}2)$$

$$\sigma_h^o = 1.50 \cdot \sigma_V = 0.041\ Z \qquad (6\text{-}3)$$

where σ_V = Vertical stress, MPa

σ_H^o = Maximum lateral stress, MPa (perpendicular to orebody)

σ_h^o = Minimum lateral stress, MPa (parallel to orebody strike)

Z = Depth below surface, m

6.4.5 Stability Graph analysis of stope geometry

The Stability Graph method for open stope design, described previously in Section 2.7, combines information about rockmass strength and structure, the stresses around the opening and the size, shape and orientation of the opening to predict stope stability. Two parameters are needed: the Stability Index number (*N'*), which is a measure of the rockmass ability to stand up under a given stress condition, and the Hydraulic Radius (*HR*), which represents the dimensions of the stope face. Parameters used for assessing *N'* for the hanging-walls of Bousquet Block 5 and Zone 3-1 are summarized in Table 6.8. Details for determining Hydraulic Radius for the two zones are provided in Table 6.9.

The stability of hanging-walls of Block 5 and Zone 3-1 stopes were assessed using the Stability Graph. Results, plotted on Figure 6.19 indicate the following trends:

- Block 5: The hanging-wall of typical stopes within Block 5 are potentially unstable. Hanging-wall stability decreases with rockmass quality. Hanging-walls within low-range rockmasses are strongly unstable
- Zone 3-1: Compared to Block 5, Zone 3-1 stopes benefit from both a slightly more competent rockmass, and reduced hanging-wall dimensions. According to the Stability graph approach, the hanging-wall of typical stopes within Zone 3-1 is potentially stable. Hanging-wall stability decreases with rockmass quality. Hanging-walls within low-range rockmasses are potentially unstable.

Table 6.8 Hanging-wall stability index values (N') for Block 5 and Zone 3-1

	Q'	A	B	C	N'
Block 5 (Henning, 1998)	Typical value: 1.2 (range: 0.21 to 2.08)	1	0.3	Typical value: 6.8 (range: 6.1 to 7.7)	Typical value: 2.4 (range: 0.4 to 4.8)
Zone 3-1 (Ruest 1998, Henning 1996)	Typical value: 2.8 (range: 0.3 to 3.6)	1	0.3	Typical value: 7.3 (range: 6.1 to 8)	Typical value: 6.1 (range: 0.5 to 8.6)

Table 6.9 Comparison of mined hanging-wall dimensions, Block 5 and Zone 3-1

Parameter	**Block 5**	**Zone 3-1**
Stope Depth	1045 – 1195m	1340 – 1580m
Mathews Stability Parameter (N')	Typical value: 2.4 (range: 0.4 to 4.8)	Typical value: 6.1 (range: 0.5 to 8.6)
Common stope dimensions		
Vertical height	30m	30m
Average hanging-wall dip angle	78°	83°
Exposed hanging-wall height (see Eq. 5-4)	30.7m	30.2m
Strike length	15m	10m
Hydraulic Radius	5m	3.8m

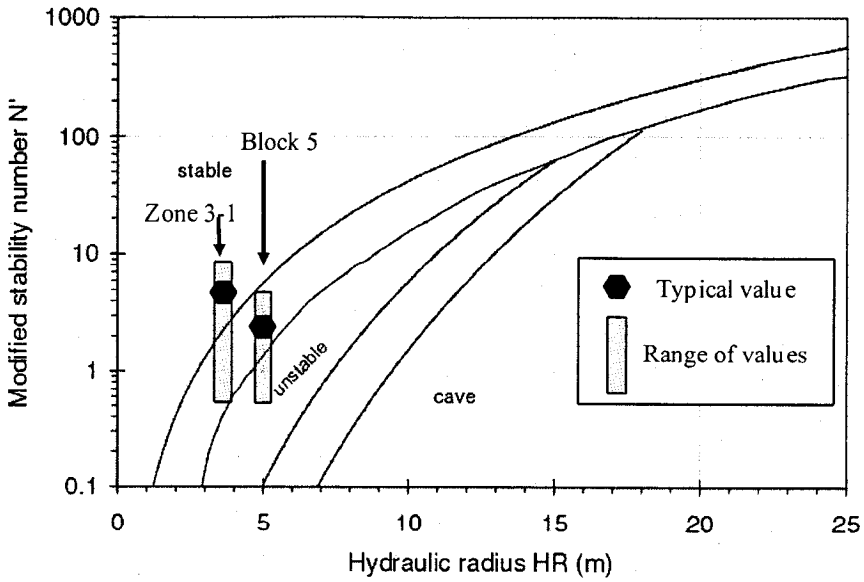

Figure 6.19 Stability Graph plot of Block 5 and Zone 3-1 stopes

6.5 Stope hanging-wall reinforcement

Cablebolting is a method of reinforcing loose rock or fractured in-situ rock to prevent caving or spalling, and to assist the rockmass to form its own load bearing structure, (Hutchinson and Diederichs, 1996). Cablebolts were used in Block 5 to provide hanging-wall support for dilution control. Stope hanging-walls are supported with modified geometry cablebolts installed on two meter centers, in a fanned pattern, from a hanging-wall cable drift. Hanging-wall cablebolt access drifts were driven at 60 meter vertical intervals, on every second sub-level. Hanging-wall cablebolt rings, shown in Figure 6.20, provide cablebolt reinforcement to stope blocks positioned above and below the cable drift elevation. Cablebolt orientation with respect to the stope hanging-wall ranges from approximately 85 degrees (near-perpendicular to the hanging-wall), to 40 degrees.

Cablebolts, ranging in length from 18 to 28 meters long, are grouted into 63 mm diameter holes. Grout tubes are fixed to the cablebolts installed into upholes. In downholes, the grout tube is slowly extracted from the bottom of the hole as

grouting progresses, while ensuring that the withdrawal rate does not exceed the rate at which the hole is filled.

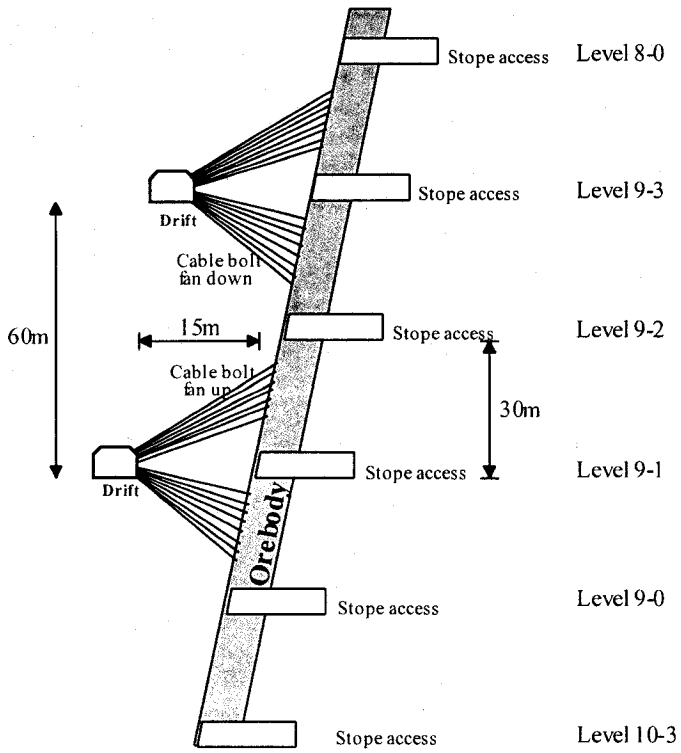

Figure 6.20 Hanging-wall cablebolt installation pattern, Block 5

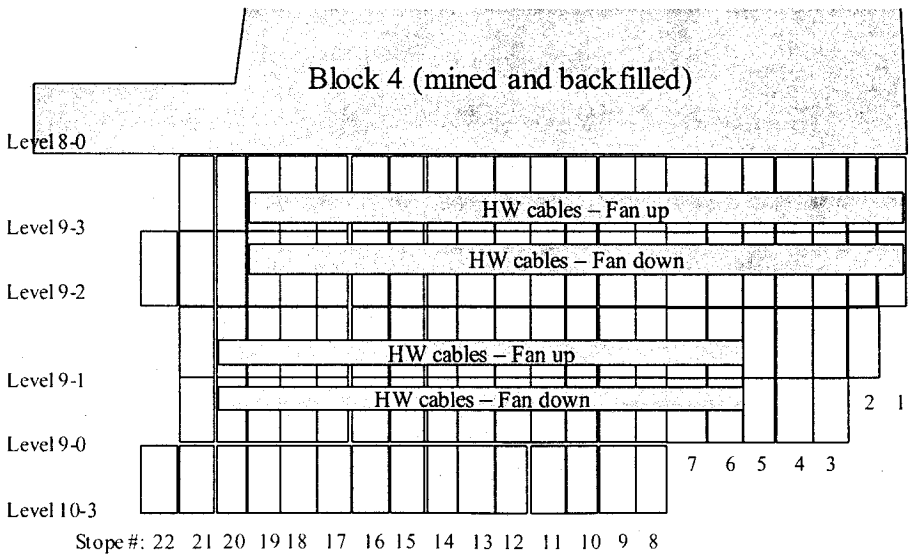

Figure 6.21 Longitudinal plot showing hanging-wall cablebolt coverage, Block 5

Figure 6.21 illustrates the regions of hanging-wall presupport with cablebolts installed from the hanging-wall cable drift. The hanging-wall cablebolt drifts were not developed at the lower-most levels of the Bousquet #2 mine (including Level 10-3 and Zone 3-1) for economic reasons due to the anticipated narrow orezone width. To minimize the initiation of unravelling from the base of the stope hanging-wall, cablebolts are installed from the sill of these narrow-span stopes in a fanning pattern upwards into the hanging-wall, as illustrated in Figure 6.22. The cablebolt rings are installed on two meter spacing. Table 6.10 presents a summary of the variety of hanging-wall reinforcement patterns employed in Block 5 and Zone 3-1.

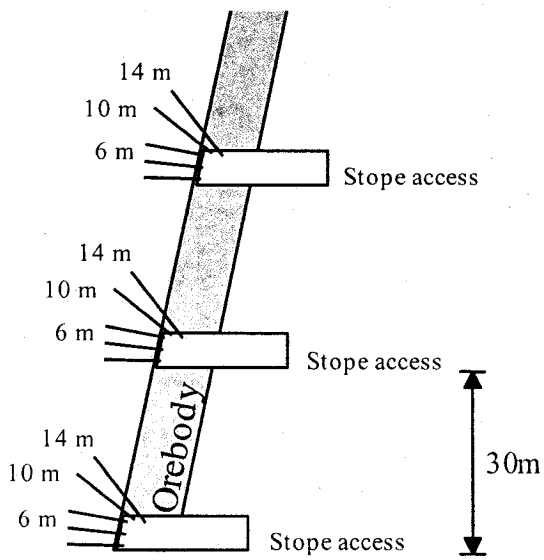

Figure 6.22 Stope sill cablebolt installation via stope sill, Zone 3-1

Table 6.10 Distribution of stope hanging-wall cablebolt installation pattern

	Hanging-wall cablebolt pattern		
	Upward fanning cablebolts	Downward fanning cablebolts	Cablebolts installed via stope sill
Block 5	34	34	29
Zone 3-1	nil	nil	76

6.6 Comparison of Block 5 and Zone 3-1 stope geometry, setting and construction

Differences and commonalities between Zone 3-1 and Block 5, in terms of stopes setting, construction and geometry are summarized in Tables 6.11, 6.12 and 6.13. Similarities occur in terms of stope construction and orezone orientation. Prominent differences include stope dimensions, depth of mining, hanging-wall reinforcement orezone rock strength and orezone rockmass quality.

Table 6.11 Comparison of Block 5 and Zone 3-1 stope setting factors

Factor	Block 5	Zone 3-1	Comment
Orezone depth	1045 – 1195m	1340 – 1580m	Zone 3-1 is at greater depth
Rockmass characteristics, host rock	Rhyolite Tuff, GSI = 50, Q = 0.47, σ_c = 112 MPa	Foliated rhyolite tuff, GSI = 48, Q = 1.4, σ_c = 59 MPa	Zone 3-1 occurs within a weaker rockmass
Rockmass characteristics, orezone	Massive Sulphide , GSI = 75, Q = 7, σ_c = 210 MPa	Foliated rhyolite tuff, GSI = 48, Q = 1.4, σ_c = 59 MPa	Block 5 ore occurs as a lens of competent rock, distinctly different from the host rock. There is no rockmass distinction between Zone 3-1 orezone and host rock.
Hanging-wall reinforcement	70% of Block 5 stope hanging-walls were reinforced by cablebolts, installed in a fan pattern from an access drift located in the hanging-wall, behind the stope. The remaining stope hanging-walls were with cablebolts installed from the stope sills.	All reinforcement was installed from the stope sills. No hanging-wall access drift was developed.	Density and areal coverage of hanging-wall reinforcement was greater for Block 5 stopes.
Stoping stress environment	Abutment stress: Block 5 advances up towards previously mined and backfilled stopes	No sills in Zone 3-1. Mining advances out from center of zone	
Stability graph (Figure 6.19)	Potentially unstable	Potentially stable	

Table 6.12 Comparison of Block 5 and Zone 3-1 stope construction factors

Factor	Block 5	Zone 3-1	Comment
Workforce skill, equipment			Construction Factors were common to the two zones. The same surveyors, drillers, design, blasting blast products, and equipment maintenance, were used
Stoping method	Transverse primary and secondary stopes	Transverse primary and secondary stopes	Similar stoping methods were used for the two zones
Drill pattern	35% parallel 56% fan 9% longitudinal	33% parallel 45% fan 21% longitudinal	Similar drilling patterns were used for the two zones

Table 6.13 Comparison of Block 5 and Zone 3-1 stope geometry factors

Factor	Block 5	Zone 3-1	Comment
Typical dimensions	15m x 30m	10m x 30m	Zone 3-1 stopes are smaller
Hydraulic radius	5m	3.8m	Zone 3-1 stopes are smaller
Dip of stope hanging-wall	80° to 85°	75° to 80°	The two zones had similar hanging-wall dips. Zone 3-1 stopes were slightly shallower

6.7 Empirical database description

A comprehensive database was established for this research, incorporating information related to the design, construction, excavation and CMS cavity surveys of 172 sequentially mined long-hole stope case histories from Block 5 and Zone 3-1 of the Bousquet #2 mine.

The following information was included in the database:

- Stope setting
- Stope geometry
- Stope category
- Stope construction
- Stope recovery

Rockmass properties, stope drilling patterns, and stope blasting methodology applied to stopes in Block 5 and Zone 3-1 were common to the individual stope blocks within each orezone. Descriptions are provided in Sections 6.3 to 6.5 of this Chapter.

Figure 6.23 shows the overall database structure. The information shown in the database structure was collected for each stope case history from a variety of sources in the Production, Geology and Engineering departments of the mine. The compiled database for Block 5 and Zone 3-1 stopes is provided in Appendix B.

Stope setting refers to the location and terminology used to describe a specific stope within the mining block. Details of stope setting within Block 5 and Zone 3-1 were provided previously in Figure 6.5 and 6.7, respectively. Stope category defines the local stope setting within the mining sequence. Stope geometry provides specific descriptions of excavated dimensions of individual stopes. Stope construction refers to mostly man-made influences on stope mining and recovery, excluding designed stope dimensions. Stope construction factors

associated with the design of hanging-wall reinforcement, drilling and blasting are discussed in Sections 6.3 and 6.5. Stope recovery refers to measured overbreak.

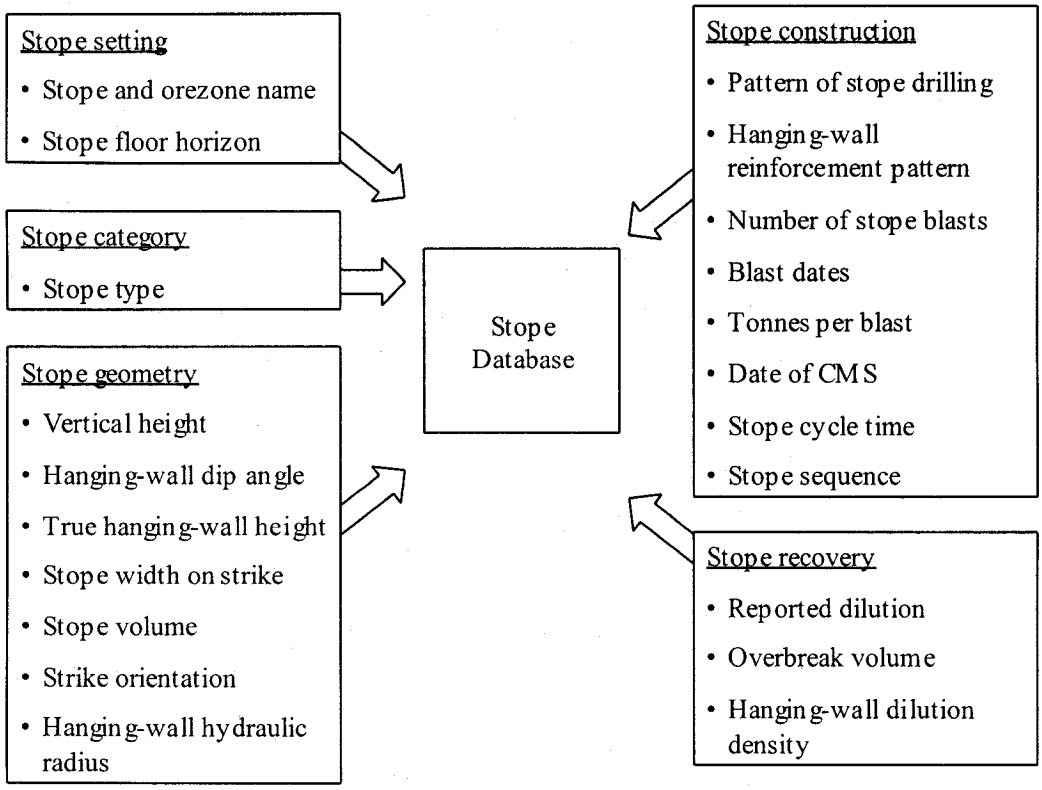

Figure 6.23 Database structure

Descriptions of the distribution of data from Block 5 and Zone 3-1 case histories are provided in the following sections.

6.7.1 Stope geometry

The stope geometry has a significant influence on the stability and the dilution that can be expected from a stope hanging-wall. As discussed in Section 5.3, stope dimensions are a variable factor, which can be established during initial mine design, that influences overbreak.

Geometry parameters collected from each of Block 5 and Zone 3-1 include: (1) hanging-wall dip angle, which influences (2) true stope height, (3) strike length,

(4) hydraulic radius of the stope hanging-wall, (5) designed stope size (tonnes blasted), and (6) the azimuth of the hanging-wall strike.

6.7.1.1 Block 5 stope geometry

The histograms in Figure 6.24 show distributions defining the stope geometry for all stopes considered for the Block 5 case histories. A statistical summary is given in Table 6.14.

In general, using calculated mean values, a typical hanging-wall of a Block 5 stope had a dip angle of 78°, a 31m true height, a 14m strike length, resulting in a hydraulic radius of 4.9m. Typical designed stope size was in the range of 12300 tonnes. The strike of the hanging-wall was orientated on azimuth 095°, or approximately normal to the orientation of major principal stress.

6.7.1.2 Zone 3-1 stope geometry

The histograms in Figure 6.25 show distributions defining the stope geometry for all stopes considered for the Zone 3-1 case histories. A statistical summary is given in Table 6.14.

In general, using calculated mean values, a typical hanging-wall of a Zone 3-1 stope had a dip angle of 83°, a 31m true height, a 10m strike length, resulting in a hydraulic radius of 3.9m. Typical designed stope size was in the range of 4800 tonnes. The strike of the hanging-wall was orientated on azimuth 097°, or approximately normal to the orientation of major principal stress.

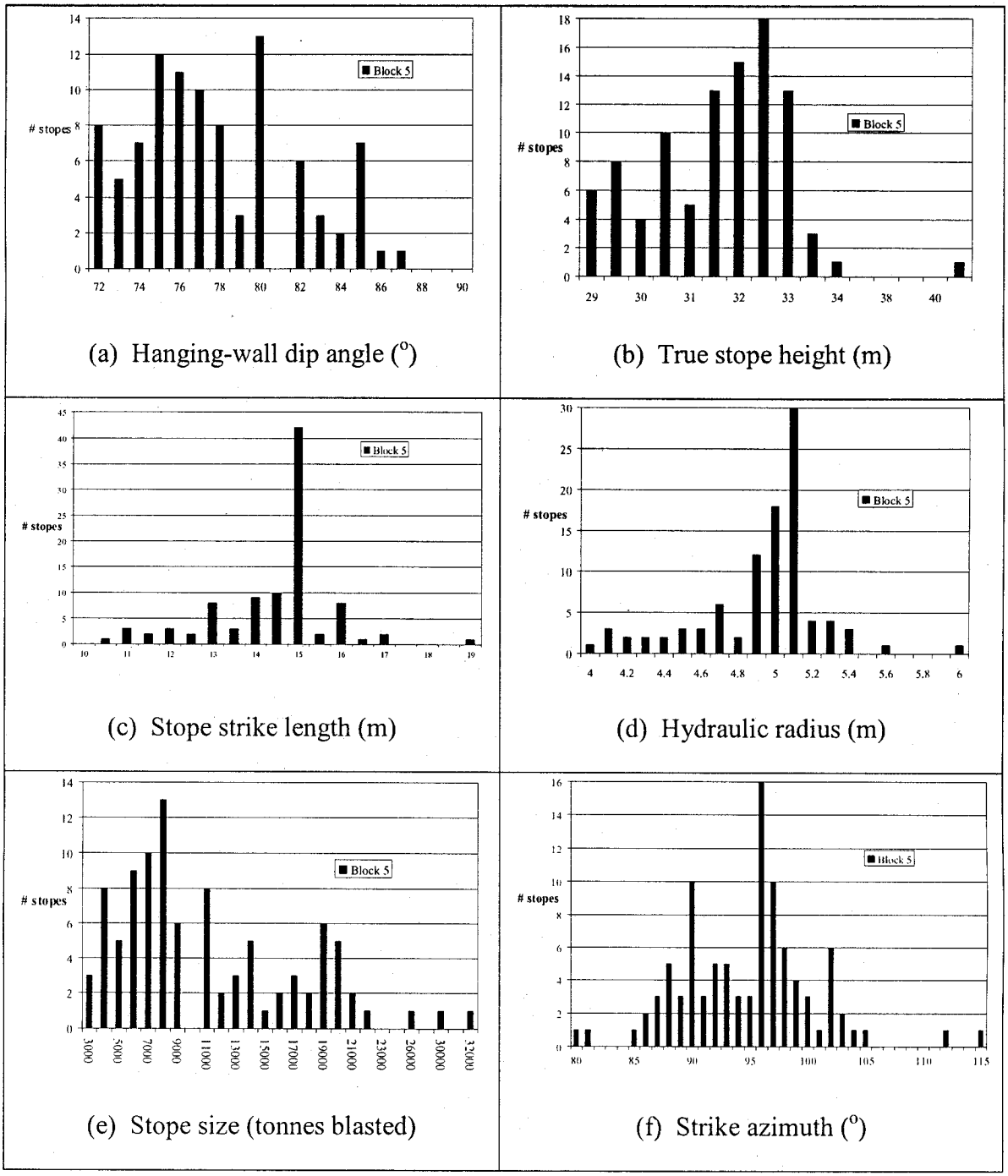

Figure 6.24 Geometry distributions, Block 5 stopes

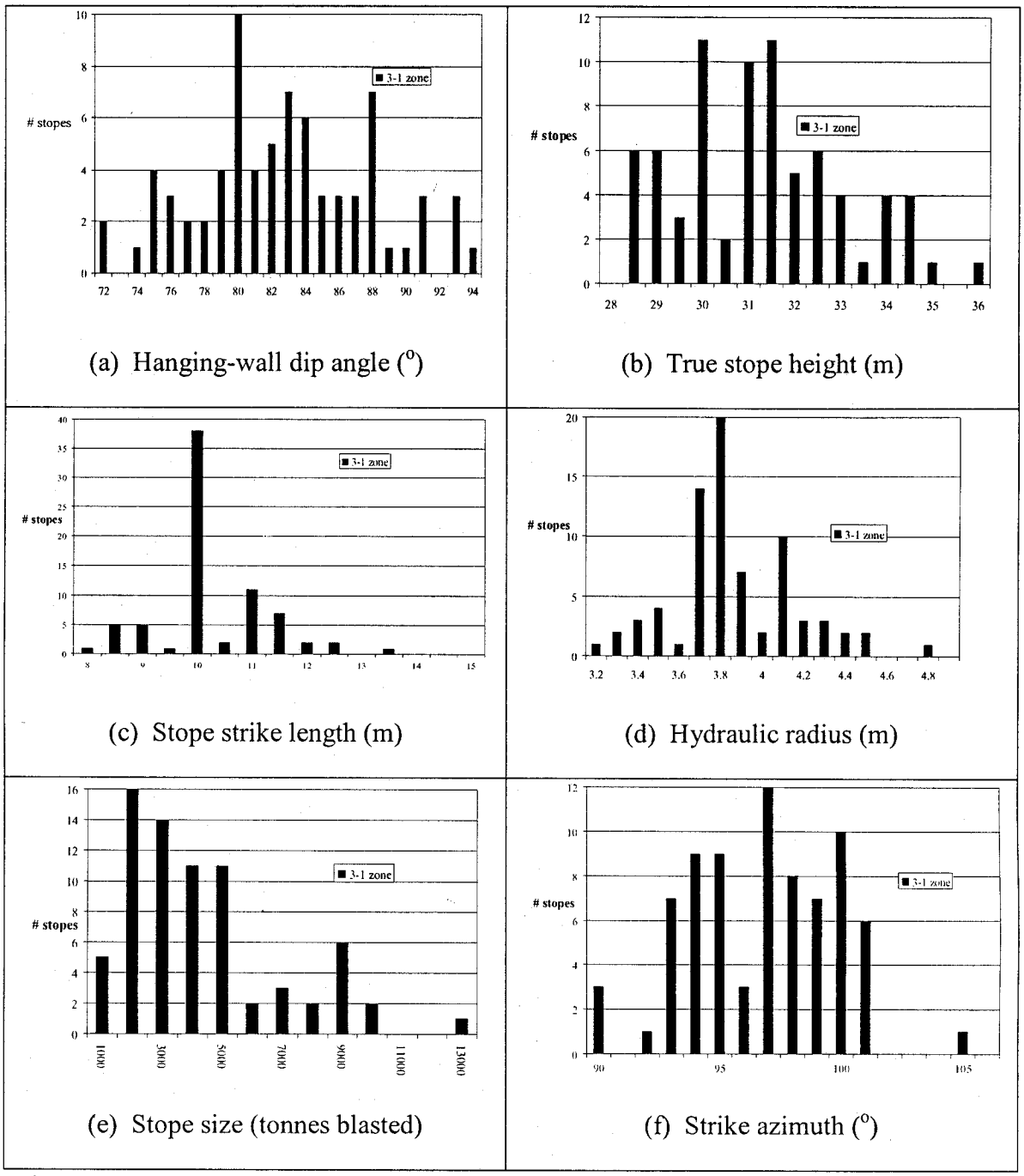

Figure 6.25 Geometry distributions, Zone 3-1 stopes

6.7.1.3 Summary of stope geometry comparison

Stope geometry statistics from the Block 5 and Zone 3-1 databases are summarized in Table 6.14. When comparing the geometries of the two zones, the following patterns were observed:

- Block 5 and Zone 3-1 have similar hanging-wall dip angles (78° versus 83°, respectively), and true stope height (31.4m versus 31.1m)
- Block 5 has greater strike length (15m) than Zone 3-1 (10m), which affects hydraulic radius values (5m verses 3.9m) of the stope hanging-wall
- Similar orientation of the hanging-wall strike of the two stopes (strike azimuth) suggests that the orientation of in situ principal stress (95° versus 97°) is approximately perpendicular for both Block 5 and Zone 3-1.
- Block 5 has greater stope volume, reflecting its greater thickness. An average stope of 12310 tonnes at Density 4.0 (tonnes/m3) corresponds to average thickness of 7m. For Zone 3-1, an average stope of 4837 tonnes at Density 3.2 (tonnes/m3) corresponds to average thickness of 4.7m
- The Aspect Ratio (AR) of Zone 3-1 stopes (AR = 0.33) is slightly lower that that of Block 5 stopes (AR = 0.45). According to the trends identified in Section 5.5, Zone 3-1 stopes, with a lower AR value, are more stable than Block 5 stopes. Aspect Ratio is described in Equation 5-3.

Table 6.14 Summary of stope geometry statistics

	Block 5				Zone 3-1			
	Mean value	**Median value**	**Standard deviation**	***CoV***	**Mean value**	**Median value**	**Standard deviation**	***CoV***
Hanging-wall dip angle (°)	77.8	77	3.9	5%	82.7	82.5	5.2	6%
True stope height (m)	31.4	31.7	1.6	5%	31.1	31	1.8	6%
Stope strike length (m)	14	15	1.4	10%	10.3	10	1	10%
Hydraulic radius (m)	4.9	5	0.3	7%	3.9	3.8	0.3	8%
Stope size (tonnes blasted)	12310	9693	6405	52%	4837	5500	2578	53%
Strike azimuth (°)	94.8	96	5.7	6%	96.7	97	3	3%

Similarities in mean values and median values, and correspondingly low *CoV* values indicate that data associated with Block 5 and Zone 3-1 stope geometries is reasonably symmetric and bell shaped data. The exception to this observation is the values of stope size. Greater variability in stope size reflects a range of stope thickness.

The mean ($\overline{x}$) is the center of gravity of the probability density distribution. The mean or expected value of a sample is defined as shown in Equation 6-4.

$$\overline{x} = \frac{1}{n}\sum_{i=1}^{n} x_i \tag{6-4}$$

where n refers to the number of events or items, and x_i is the value of an individual item in the sample under consideration

The median refers to the middle value in a distribution. It is equal to the mean in a normal distribution but very different in skewed distributions. In skewed distributions the median is more representative of the central value than the mean.

Standard deviation (s) is a measure of the spread or variability of values. Standard deviation is defined as shown in Equation 6-5.

$$s = \sqrt{\frac{1}{n-1}\sum_{i=1}^{n} (x_i - \overline{x})^2} \tag{6-5}$$

For a reasonably symmetric and bell shaped data set:

- Mean value ± standard deviation contains roughly 68% of the data (6-6)
- Mean value ± 2 × standard deviation contains roughly 95% of the data (6-7)

A relative measure of the scatter of a random variable is its coefficient of variation (*CoV*). *CoV* is the ratio of the standard deviation to the mean value of the sample as shown in Equation 6-8. *CoV* is a measure of uncertainty in the

central tendency. A large CoV, implies high uncertainty in the data and results, and a low CoV designates less dispersion and high certainty.

$$CoV\,(\%) = \frac{\text{Standard deviation}}{\text{Mean value}} \cdot 100 \qquad (6\text{-}8)$$

6.7.2 Stope type and extraction sequence

The Block 5 and Zone 3-1 orezones were subdivided into 97 and 75 stopes, respectively. Within each orezone, stopes were mined in a sequence that resulted in the creation of a variety of primary (P1, P2, and P3) and secondary (S1, S2) stope types. The five stope types were described previously in Section 4.3.2.

The Block 5 mining sequence and positions of the five stope types within the zone are shown in Figure 6.26 and Figure 6.27. Zone 3-1 mining sequence and stope type positions within Zone 3-1 are shown in Figure 6.28 and Figure 6.29. Stope details are provided in Appendix B.

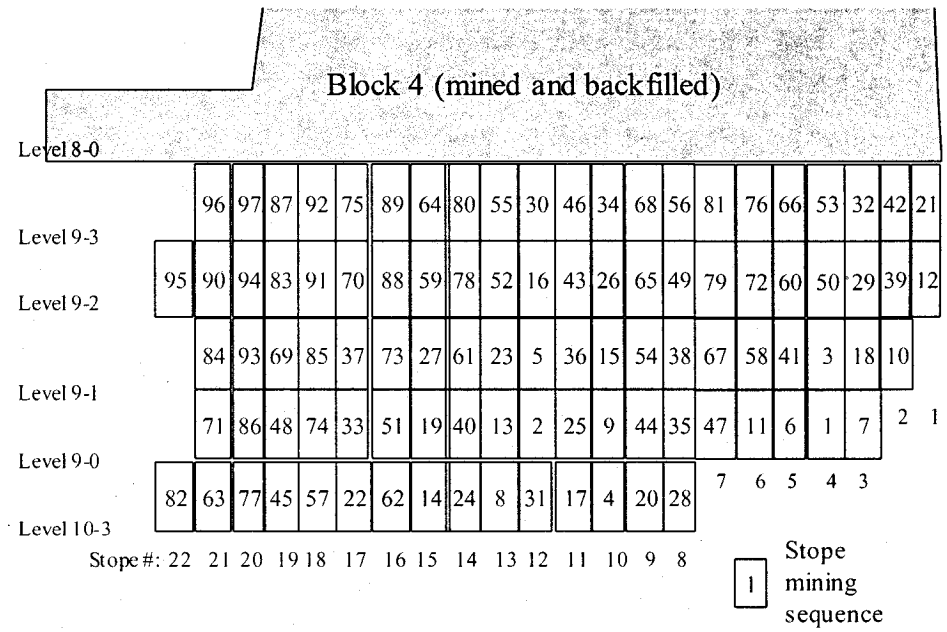

Figure 6.26 Block 5 mining sequence

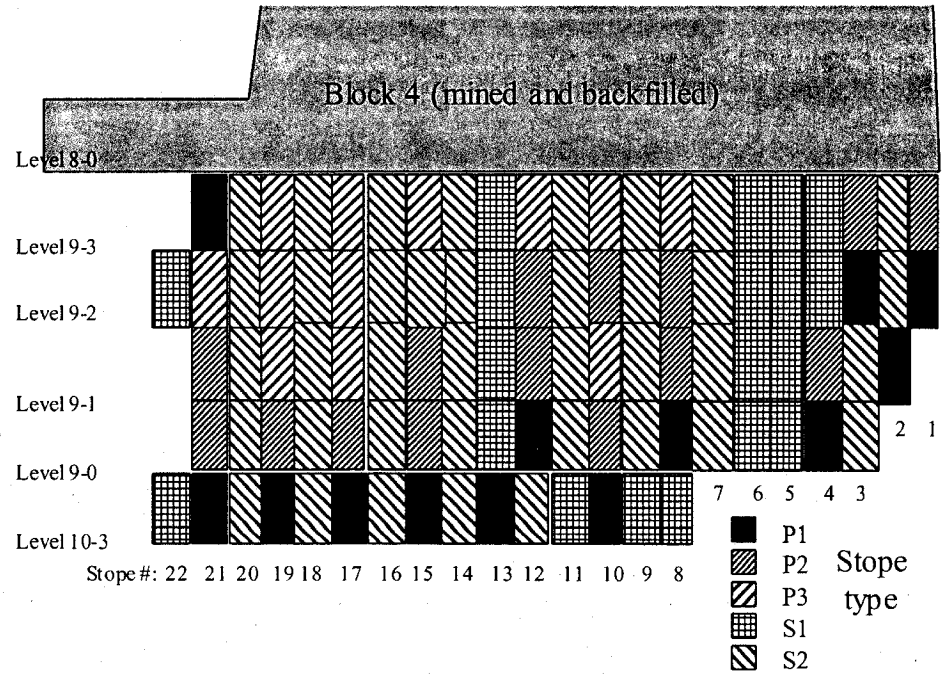

Figure 6.27 Longitudinal plan of Block 5 showing stope types

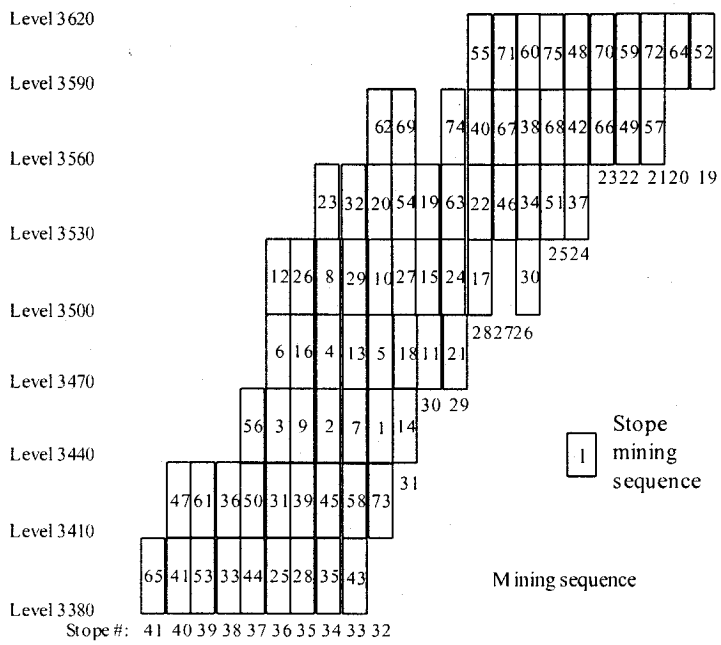

Figure 6.28 Zone 3-1 mining sequence

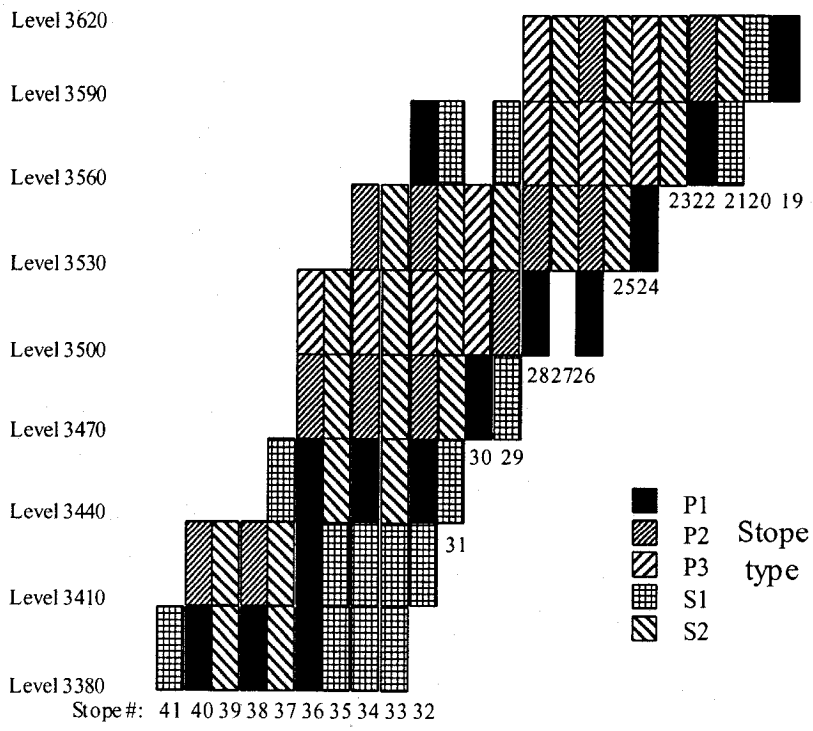

Figure 6.29 Longitudinal plan of Zone 3-1 showing stope types

The total number of stope types found in each of the two orezones is summarized in Table 6.15 and expressed as a percentage of total number of stopes in Figure 6.30. Similarities occur in both orezones with respect to the percentage of total stopes of each stope type. In terms of total primary and secondary stopes, Zone 3-1 consisted of 45% primary and 55% secondary stopes, including 35% true secondary (S2-type) stopes. With Block 5, 42% of the stopes mined were primary, while 58% were secondary stopes, including 37% true secondary (S2-type) stopes.

Table 6.15 Number of stope types

	P1	**P2**	**P3**	**S1**	**S2**
Zone 3-1	14	11	11	14	25
Block 5	13	15	13	20	36

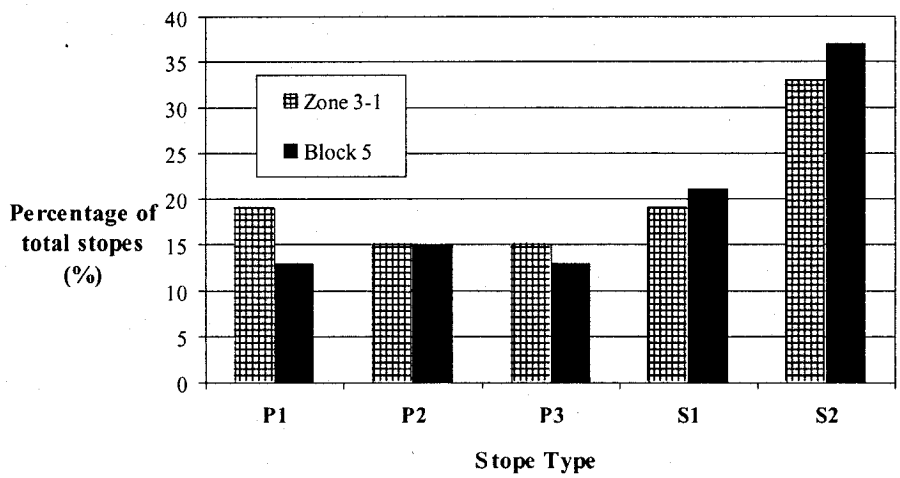

Figure 6.30 Stope types in Block 5 and Zone 3-1

Orezone sequencing, showing 25%, 50%, 75% and 100% extraction of Block 5 and Zone 3-1 is illustrated in Figures 6.31 and 6.32. Block 5 was mined in a pyramidal sequence over five mining horizons, advancing up towards previously mined and backfilled Block 4 stopes. With later stage extraction, mining advanced westward towards the abutment. Zone 3-1 was mined in a pyramidal sequence over eight mining horizons, advancing from a centre core towards the abutments. A narrow sill pillar, measuring approximately 60m along strike was created by mid-stage (50% and 75%) extraction below previously mined and backfilled first stage (25%) stopes.

Relationships between stope type and orezone sequencing, summarized in Figure 6.33, shows that the majority of stopes mined in both Zone 3-1 and Block 5, up to 50% orezone extraction, were primary-type stopes. Between 50% and 75% extraction (at approximately 57% extraction), the primary – secondary trend lines cross for both orezones. Beyond approximately 57% extraction, the percentage of secondary stopes mined is increasingly greater than that of the primary stopes.

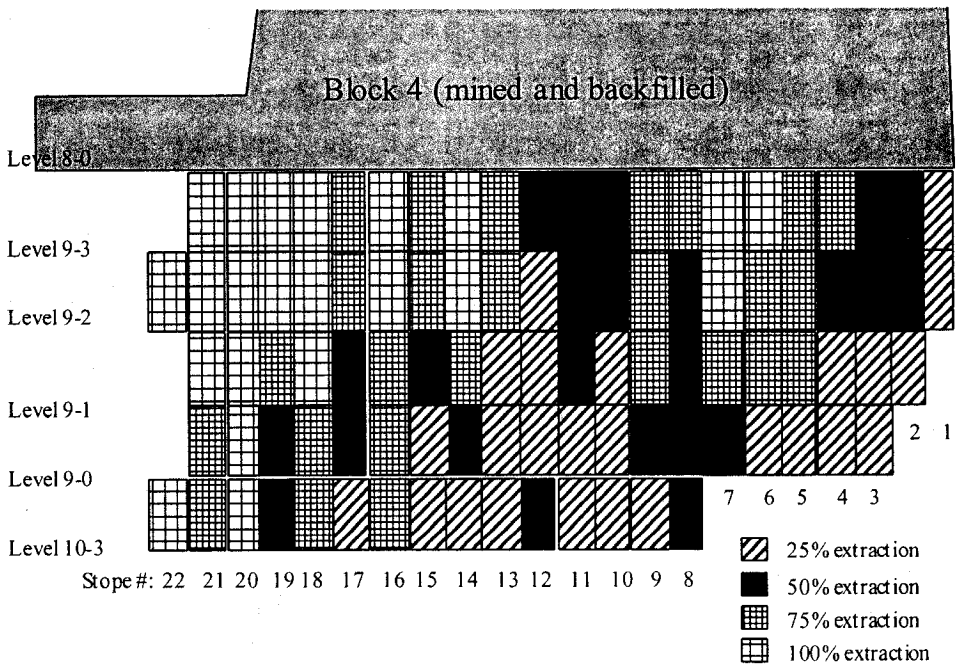

Figure 6.31 Longitudinal plan of Block 5 extraction sequence, view looking north

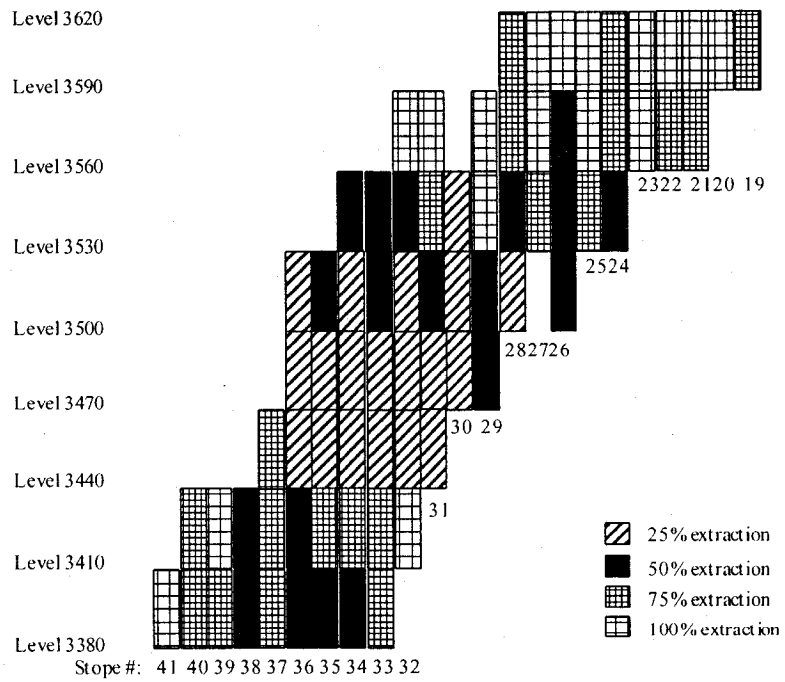

Figure 6.32 Longitudinal plan of Zone 3-1 extraction sequence, view looking north

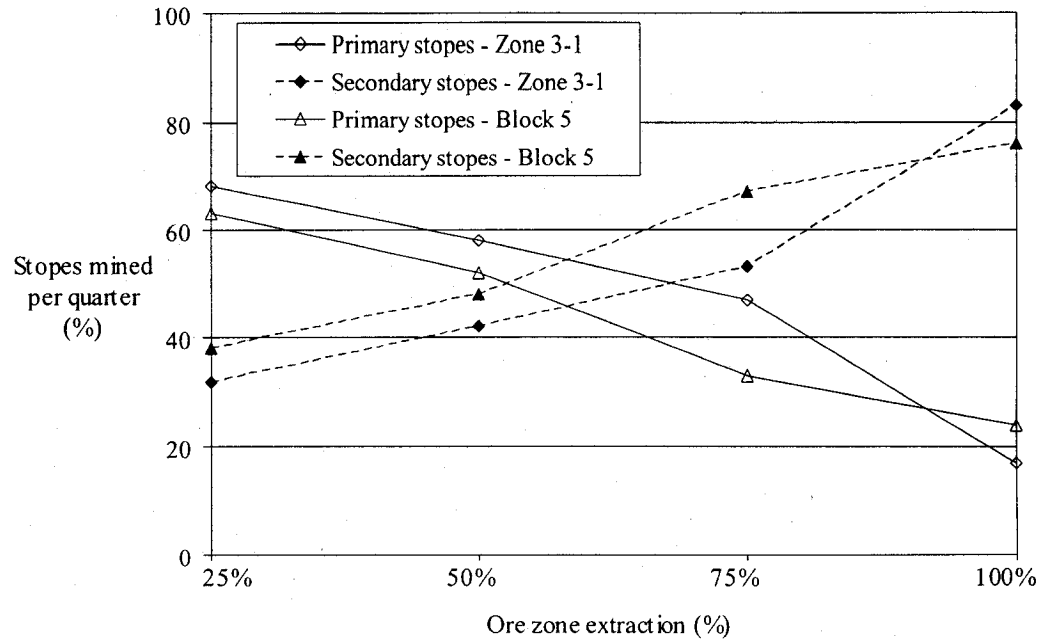

Figure 6.33 Stope type mined as a function of orezone extraction

6.7.3 Dilution

As discussed in Chapter 2, dilution has a direct and large influence on the cost of a stope, and ultimately on the profitability of a mining operation. A review of techniques to quantify the cost of dilution by Pakalnis et al. (1995) has shown that there are several definitions of dilution. At Bousquet #2 mine, dilution was calculated according to the following definition:

$$\% \text{ Dilution} = \frac{\text{Tonnes waste rock mined}}{\text{Tonnes ore mined}} \qquad (6\text{-}9)$$

where: Waste = Wall rock outside of the planned stope boundary;

Ore = Rock planned, drilled and blasted within the stope boundary.

The measurement of mined stope profile has traditionally been difficult due to the non-entry nature of the open stope mining method. A Cavity Monitoring System, (CMS), described in Section 2.6.1, has been employed at Bousquet on a systematic basis since 1995. Surveys conducted on each mined stope provide a

detailed picture of the stope boundary, from which dilution values are determined. CMS surveys were conducted on the majority (98%) of stopes mined in Block 5 and Zone 3-1 (97%). Results from CMS scans were processed by mine geologists who compared CMS and planned stope sections to determine overbreak volumes and to identify the source of the dilution, an example of which is provided in Figure 6.34.

For overbreak data measured by cavity survey (CMS) from mined stopes, measured Dilution Density (DD_{cms}) is a term introduced in this study. It is the volume of overbreak on an exposed surface, and is expressed as:

$$DD_{cms} = \frac{\text{Overbreak Volume } (m^3)}{\text{Surface area exposed } (m^2)} \qquad (6\text{-}10)$$

Where: Overbreak Volume = the volume of unplanned dilution from the hanging-wall of individual stopes, as measured by the CMS scan.

Surface area exposed = designed hanging-wall surface area, represented as true stope height multiplied by stope strike length.

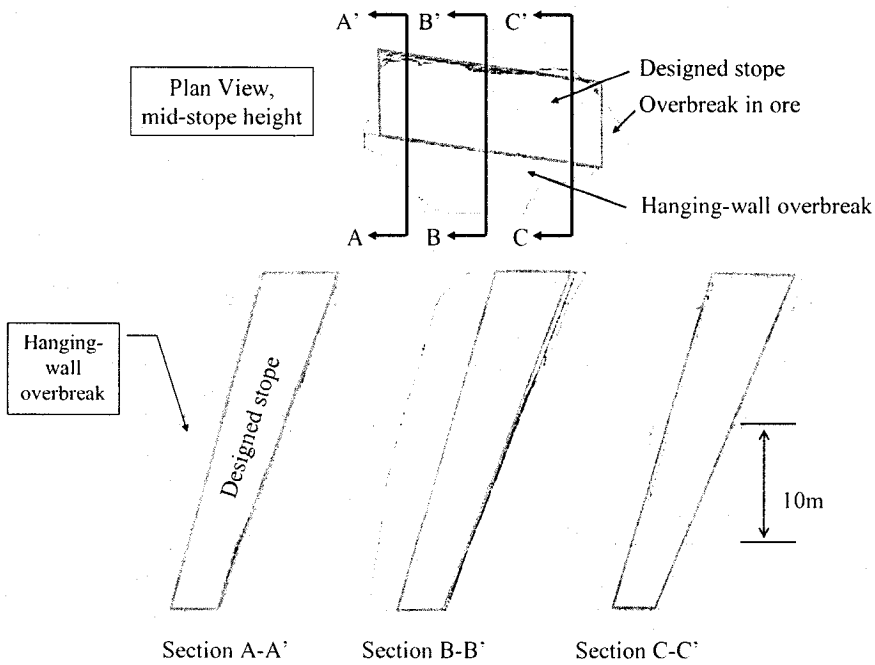

Figure 6.34 Example of measured overbreak plotted against designed stope

Summaries of overbreak measured from CMS scans of stopes within Block 5 and Zone 3-1 are compiled in Table 6.16. Dilution statistics incorporate overbreak measured from both the hanging-wall and footwall. Dilution percentages vary with stope type, but average at 29.6% and 37.7% for Block 5 and Zone 3-1, respectively.

Table 6.16 Summary of dilution statistics from CMS scans

Block 5			Zone 3-1	
Stope Type	Total Dilution, mean value		Stope Type	Total Dilution, mean value
P1	40.7%		P1	45.2%
P2	33.1%		P2	31.2%
P3	19.7%		P3	32.7%
S1	33.5%		S1	45.8%
S2	27.1%		S2	32.4%

As discussed previously in Chapter 2, a negative aspect of reporting dilution as a percentage is that the value is heavily influenced by the orezone width, and therefore, stope volume. The application of Dilution Density is used to quantify total overbreak as well as hanging-wall specific unplanned dilution. This is illustrated for all Block 5 and Zone 3-1 stopes, regardless of mining method, in Table 6.17, and for only stopes mined by transverse methods in Table 6.18. Average DD_{cms} values for (i) total stope overbreak from both the hanging-wall and footwall, and (ii) hanging-wall specific overbreak are presented for each stope type. Data trends from Tables 6.17 and 6.18 include:

- For each stope type, combined hanging-wall and footwall overbreak is greater in Block 5
- For each stope type, hanging-wall specific overbreak is greater in Block 5
- Much of the Block 5 overbreak is associated with the hanging-wall. This trend is less pronounced in Zone 3-1

Table 6.17 Summary of total surveyed stope dilution

	Stope Type	Total Dilution, mean value	Total Hanging-wall and Footwall DD_{cms}, mean value	Hanging-wall DD_{cms}, mean value
Block 5	P1	40.7%	1.75 m	1.53 m
	P2	33.1%	2.92 m	2.44 m
	P3	19.7%	2.54 m	1.83 m
	S1	33.5%	2.08 m	1.82 m
	S2	27.1%	2.72 m	2.05 m
Zone 3-1	P1	45.2%	1.55 m	0.86 m
	P2	31.2%	1.60 m	0.86 m
	P3	32.7%	1.61 m	0.68 m
	S1	45.8%	1.62 m	0.90 m
	S2	32.4%	1.92 m	1.17 m

Table 6.18 Summary of surveyed stope dilution from transverse-mined stopes

	Stope Type	Total Dilution, mean value	Total measured Hanging-wall and Footwall DD_{cms}	Hanging-wall DD_{cms}
Block 5	P1	34.0%	1.73 m	1.67 m
	P2	33.1%	2.92 m	2.44 m
	P3	19.7%	2.54 m	1.83 m
	S1	30.9%	2.20 m	1.89 m
	S2	29.0%	2.86 m	2.18 m
Zone 3-1	P1	33.0%	1.27 m	0.66 m
	P2	24.3%	1.33 m	0.57 m
	P3	34.3%	1.63 m	0.81 m
	S1	46.7%	1.71 m	0.81 m
	S2	30.9%	1.89 m	1.14 m

The distribution of measured Block 5 and Zone 3-1 hanging-wall overbreak is examined further in the following section.

6.7.3.1 Comparison of Zone 3-1 and Block 5 hanging-wall overbreak

The severity of hanging-wall overbreak, associated with Zone 3-1 and Block 5 stopes is summarized in Figure 6.35. Overbreak was calculated as equivalent Dilution Density (DD_{cms}) for each stope. Zone 3-1 experienced significantly less hanging-wall overbreak than did Block. The majority of Zone 3-1 stopes (61%) had generated hanging-wall DD_{cms} of 1m or less. Relatively few (7%) Zone 3-1 stopes experienced hanging-wall DD_{cms} exceeding 2m. Conversely, only 29% of

the Block 5 stopes generated hanging-wall DD_{cms} of 1m or less, while a significant number of Block 5 stopes (46%) experienced hanging-wall DD_{cms} exceeding 2m.

Differences between the two zones can be attributed, in part, to differences in hanging-wall dimension. On the basis of empirical (Stability Graph) and parametric trends, the smaller Zone 3-1 stopes were anticipated to be more stable, and as a result, generate less overbreak.

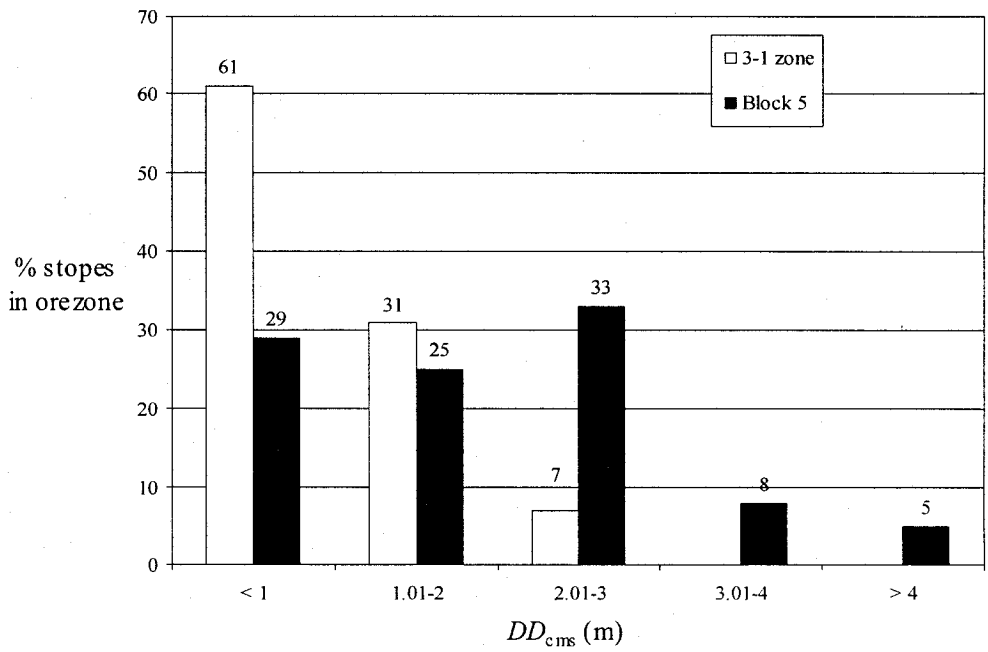

Figure 6.35 Hanging-wall DD_{cms}, Block 5 and Zone 3-1 stopes

The distribution of overbreak severity, using Dilution Density calculations, associated with the five stope types within Zone 3-1 and Block 5 is presented in Figure 6.36 and 6.37, respectively. With Zone 3-1, the majority of stopes of all types were associated with overbreak values of one meter or less. Only one primary stope, representing 3% of the total primary stope population had a Dilution Density exceeding two meters. Four secondary stopes, or 11% of the total secondary stope population, had Dilution Density exceeding two meters.

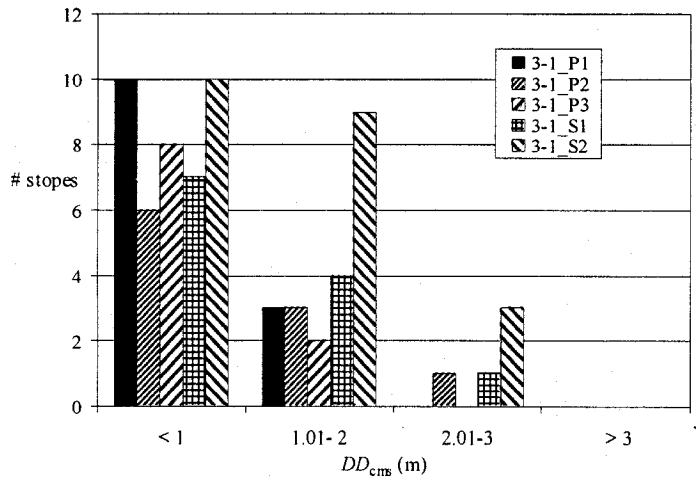

(a) Number of stopes per stope-type

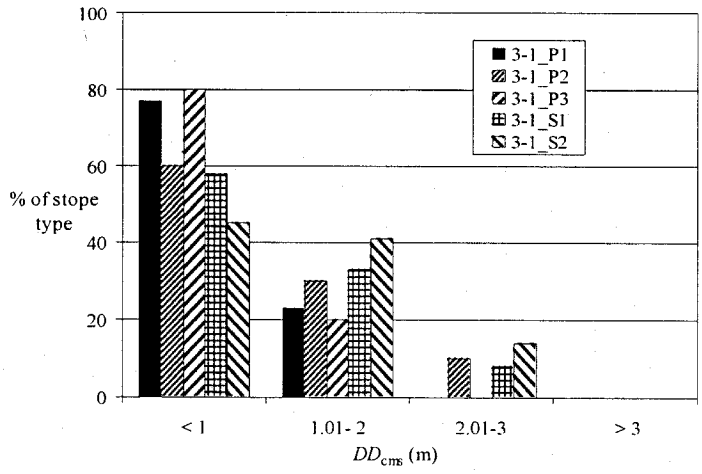

(b) Percentage of stopes per stope-type

Figure 6.36 Hanging-wall DD_{cms}, Zone 3-1 stopes

With Block 5 stopes, a minority of primary and secondary stopes, 29% and 30% respectively, had hanging-wall Dilution Density of one meter or less. 55% of primary stopes experienced hanging-wall Dilution Densities exceeding two meters, of which 11% exceeded three meters. Similarly, 44% of secondary stopes generated hanging-wall Dilution Densities exceeding two meters, including 16% of stopes which exceeded three meters.

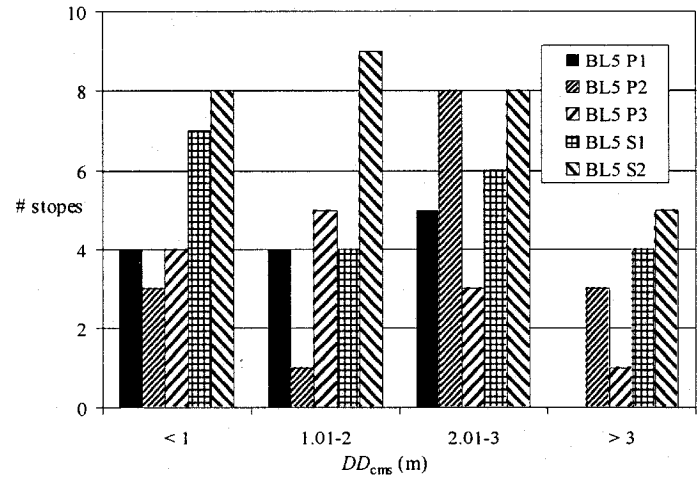

(a) Number of stopes per stope-type

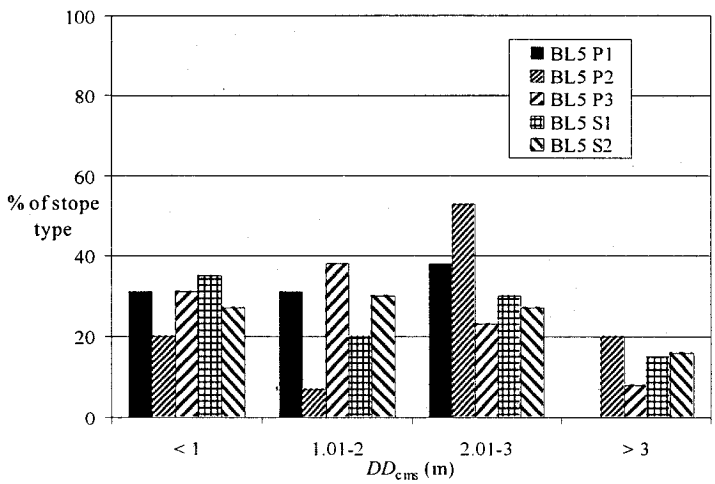

(b) Percentage of stopes per stope-type

Figure 6.37 Hanging-wall DD_{cms}, Block 5 stopes

Average depth of Dilution Density for a specific stope type is presented in Figure 6.38. With Zone 3-1, hanging-wall overbreak associated with each of the primary stope types (P1, P2 and P3) is less than that of the secondary stopes. S2-type stopes, representing a 'true' secondary stope with mined and backfilled stopes at both side walls, had the most severe overbreak. Hanging-wall Dilution Density of secondary stopes exceeded that of the average primary stope by 62%.

With Block 5, the distinction between primary and secondary stopes is less apparent. The DD_{cms} of the average primary stope was less than that of the S2-types secondary stopes (DD_{cms} = 2.02m verses DD_{cms} = 2.18m).

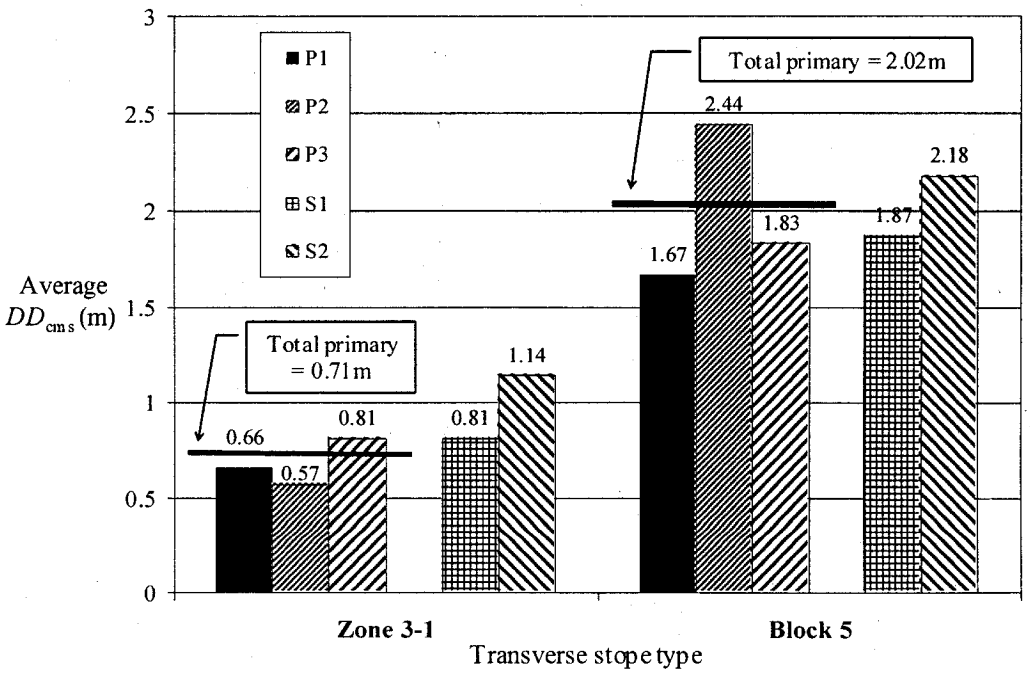

Figure 6.38 Average hanging-wall DD_{cms} versus stope type, transverse stopes

Relationships between the individual Zone 3-1 stope types are analogous to those identified in Chapter 5 (Section 5.6) although the actual DD_{cms} values for the 10m wide stopes were greater than the parametric estimates. Parametric modelling suggested that primary stopes would experience less hanging-wall overbreak than secondary stopes, with S2-type stopes experiencing the greatest dilution, as illustrated in Figure 6.39. Differences in the magnitude between actual and parametric values can be attributed to contributions from a variety of factors in addition to geometry, such as stope setting and construction.

Block 5 stope hanging-wall dilution values did not generate a distinctly similar trend, as average values for primary and secondary stopes tended to be similar. As with Zone 3-1, differences between the magnitude of actual and parametric values can be attributed to contributions from a variety of factors in addition to geometry, such as stope setting and construction.

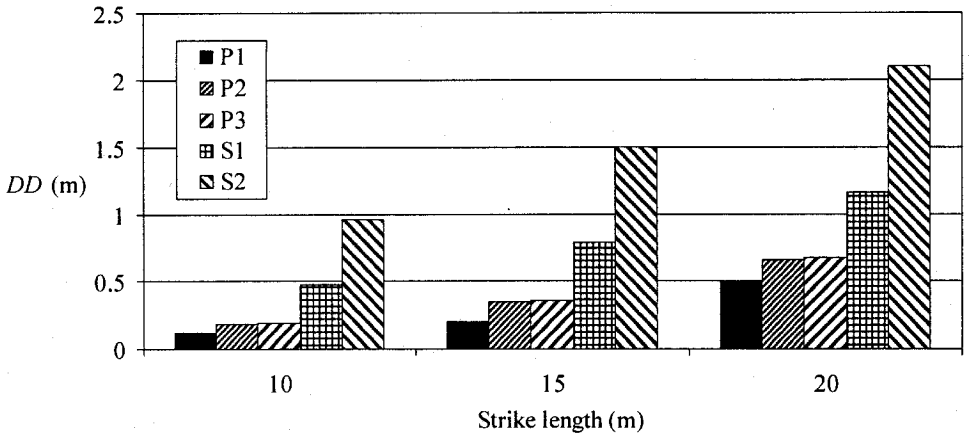

Figure 6.39 Parametric modelling – influence of stope type on Dilution Density

Differences of overbreak associated between the differing stope types of Zone 3-1 and Block 5 can be found in examining the presence and apparent effectiveness of hanging-wall cablebolt reinforcement. Unlike the hanging-wall of Zone 3-1, which was only reinforced by sill cablebolting (see Figure 6.22), the hanging-wall of the majority of Block 5 stopes were reinforced with cablebolts installed from a hanging-wall cable drift (see Figures 6.20 and 6.21). Block 5 hanging-wall cablebolts are discussed further in the following Section.

6.7.3.2 Influence of hanging-wall cablebolting on overbreak

To examine relationships between Dilution Density and Block 5 hanging-wall cablebolting, average DD_{cms} values from all primary stopes were compared against that of S2-type secondary stopes. As mentioned previously, S2-type stopes represent 'true' secondary stopes, with mined and backfilled primary stopes on both side walls. The data was further processed to isolate DD_{cms} values according to the orientation of the hanging-wall cablebolting; cable fan-up and cable fan-down. See Figure 6.40.

These values, plotted in Figure 6.41, show differences in Dilution Density severity associated with the orientation of the cablebolts. There was minimal difference (DD_{cms}= 0.1m) between primary stopes reinforced by either upward or

downward fanning cablebolts. For stopes reinforced by downward fanning cablebolts, overbreak was greater (by DD_{cms}= 0.55m) for primary stopes. For stopes reinforced by upward fanning cablebolts, overbreak was reduced (by DD = 0.4m) for primary stopes. However, overbreak in secondary stopes, reinforced by upward fanning cablebolts exceeded that of secondary stopes reinforced by downward fanning cablebolts by (DD_{cms}= 0.8m).

The orientation of the cablebolts with respect to the anticipated direction of hanging-wall sloughage plays a role in the effectiveness of the reinforcement. Cablebolt capacity is mobilized under tensile load (Hyett et al., 1992; Kaiser et al., 1992; Maloney et al., 1992). As discussed in Section 6.5.1, the development of tensile load is possible for cablebolts orientated in a downward fan, as illustrated in Figure 6.42(a). Under shear loading conditions, the cablebolt functions passively, providing localized reinforcement between unravelling blocks. Cablebolts orientated in an upward fan, illustrated in Figure 6.42(b), are subjected to more downward shear than tensile loading.

Taking the relative effectiveness of cablebolt reinforcement into account, the DD_{cms} values from stopes supported by upward fanning cablebolts are more representative of actual overbreak severity that would be generated with non-reinforced Block 5 stopes.

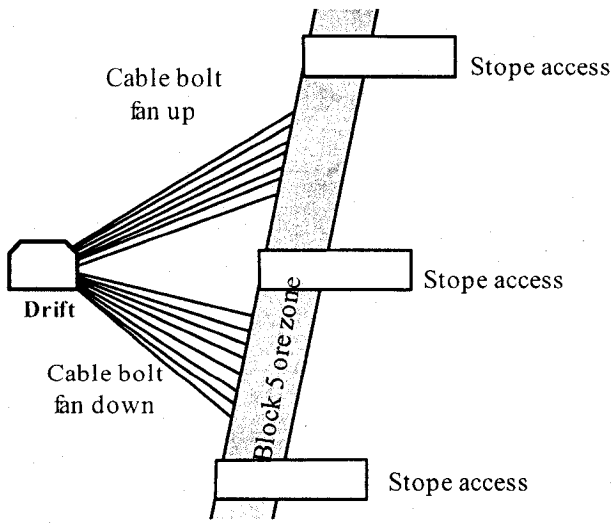

Figure 6.40 Hanging-wall cablebolt orientation

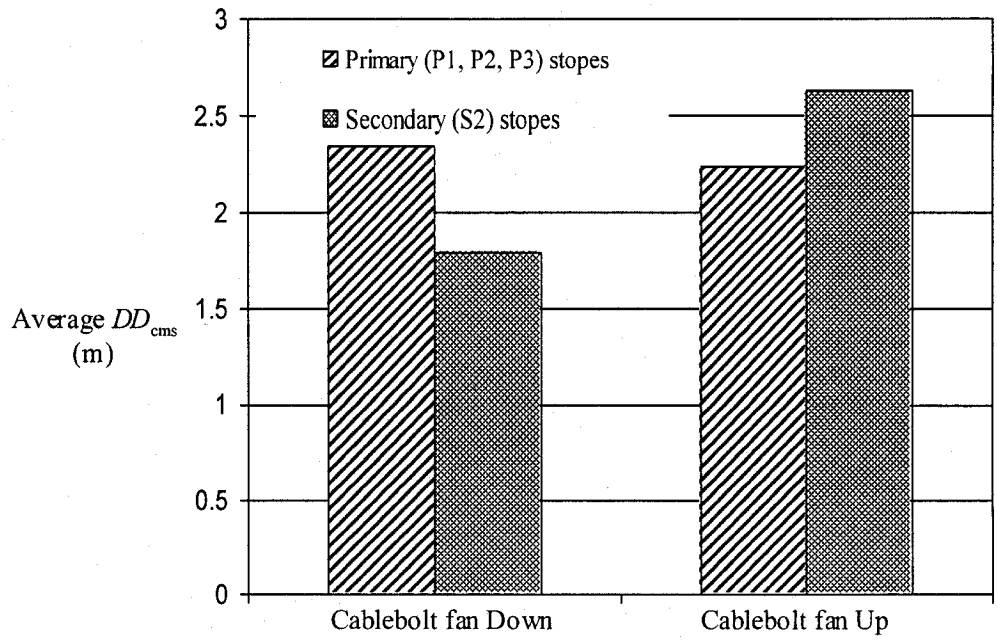

Figure 6.41 DD_{cms} versus hanging-wall cablebolt reinforcement, Block 5 stopes

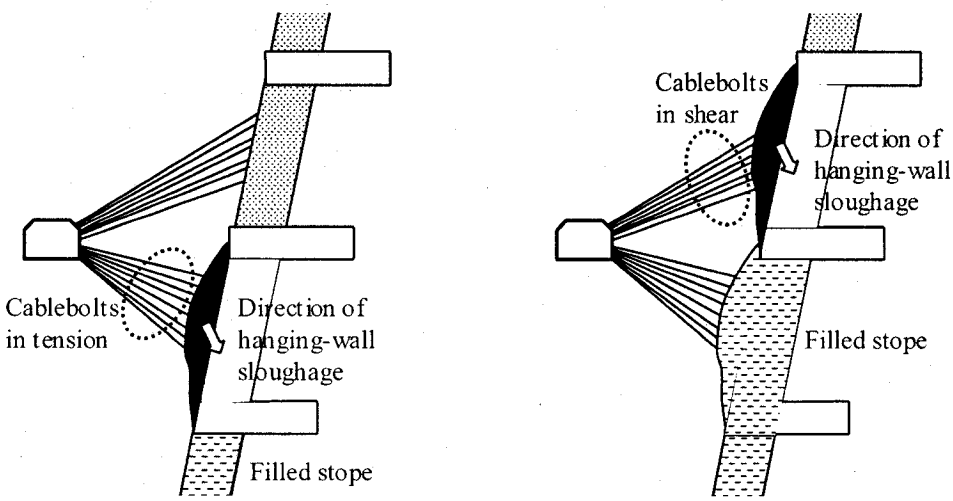

(a) Tension in down-fanning cablebolts (b) Shear in up-fanning cablebolts

Figure 6.42 Hanging-wall cablebolt orientation with respect to stope sequence

6.7.3.3 Relationship between hanging-wall overbreak and degree of orezone extraction

Relationships between the average hanging-wall overbreak and orezone sequencing 25%, 50%, 75% and 100% extraction are presented in Figure 6.43. Commonly, with each mining stage, average DD_{cms} associated with secondary stopes exceeds that of primary stopes.

As reported in Section 6.7.2, Block 5 was mined in a pyramidal sequence over five mining horizons, advancing up towards previously mined and backfilled Block 4 stopes. Average DD_{cms} values are similar for both primary and secondary stopes at early (25%) extraction of Block 5. Overbreak values increase with mid-stage (50%) extraction, as the sill pillar stopes directly underlying the previously mined Block 4 are mined. Late stage mining (75% and 100%) advances towards the abutments, effectively shedding stress away from the active mining front.

Zone 3-1 was mined in a pyramidal sequence over eight mining horizons, advancing from a centre core towards the abutments. A narrow sill pillar, measuring approximately 60m along strike was created by mid-stage (50% to 75%) extraction below previously mined and backfilled first stage (25%) stopes. Average DD_{cms} values for all combined stopes during all stages of orezone extraction stay relatively consistent.

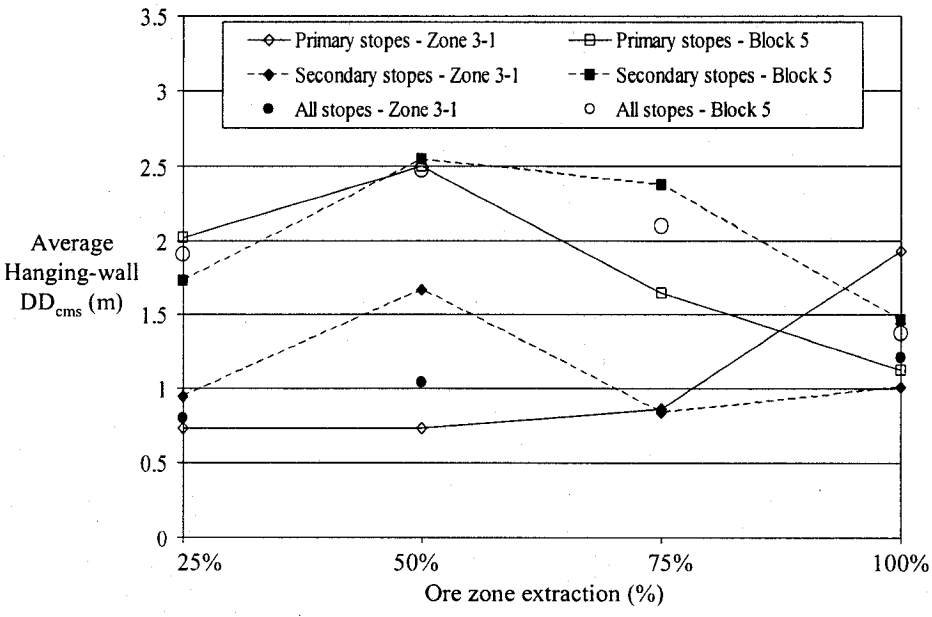

Figure 6.43 Average hanging-wall DD_{cms} as a function of orezone extraction

6.7.3.4 Relationship between hanging-wall overbreak and hydraulic radius

The relationship between the hanging-wall hydraulic radius (HR) and the measured hanging-wall overbreak (DD_{cms}) of stopes from both Zone 3-1 and Block 5 is plotted in Figure 6.44. Stopes are plotted according to the type of stope within the mining sequence. Clustering of data occurs, suggesting linear relationship between the two factors. Plotting the upper bound of the primary and secondary stopes, conservative design estimates of DD_{cms}, based on the hydraulic radius of stopes from both Block 5 and Zone 3-1, can be obtained. These design estimates are represented by the following relationships:

$$\text{Primary stopes: } DD_{cms} = (2.1 \cdot HR) - 5.2 \qquad (6\text{-}11)$$

$$\text{Secondary stopes: } DD_{cms} = (2.1 \cdot HR) - 4.5 \qquad (6\text{-}12)$$

where: HR = Hydraulic Radius (m), represented as true stope height multiplied by stope strike length.

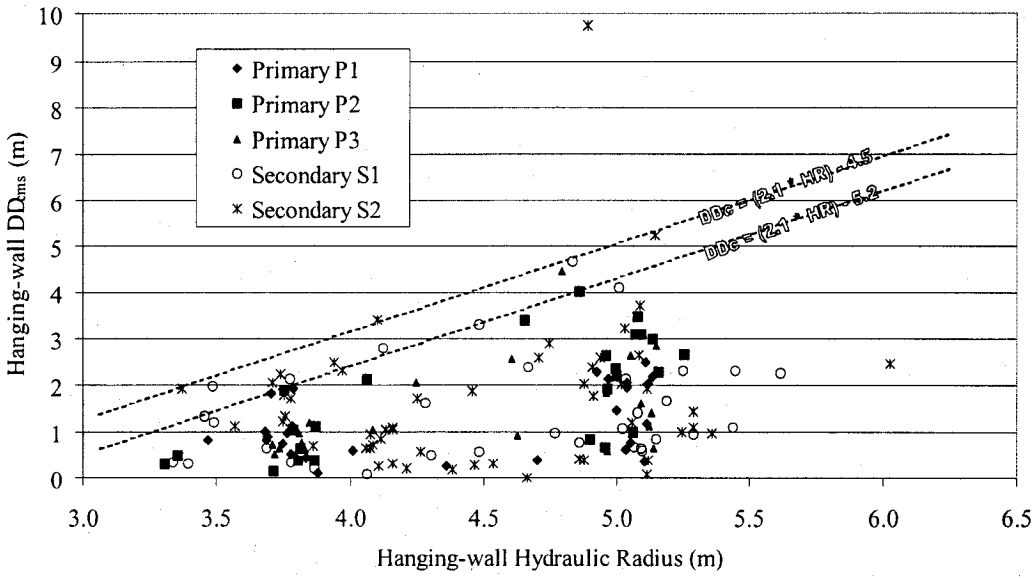

Figure 6.44 Average hanging-wall DD_{cms} as a function of hydraulic radius

6.7.3.5 Relationship between hanging-wall overbreak and stope cycle time

The open stope cycle time exposure time is defined as the number of days between the first blast and the data at which the CMS scan was conducted. At Bousquet #2 mine, CMS scans were performed immediately upon the completion of mucking, and prior to the start of backfilling.

For Block 5 stopes, the stope exposure time ranged from as little as 17 days to as many as 127 days. Fifty percent of Block 5 stopes had a hanging-wall exposure time less than 37 days. As anticipated, the smaller Zone 3-1 stopes typically had a shorter stope exposure time ranged from as little as 12 days to as many as 127 days. Fifty percent of Zone 3-1 stopes had a hanging-wall exposure time less than 24 days.

Comparison of stope cycle time against stope volume, shown in Figure 6.45, suggests a linear relationship for the rates at which the stopes were mucked, with a typical rate in the range of 370 tonnes per day. Upper and lower bounds correspond to 625 tonnes per day and 115 tonnes per day, respectively. No distinct difference between the mucking rates for Block 5 and Zone 3-1 stopes are apparent.

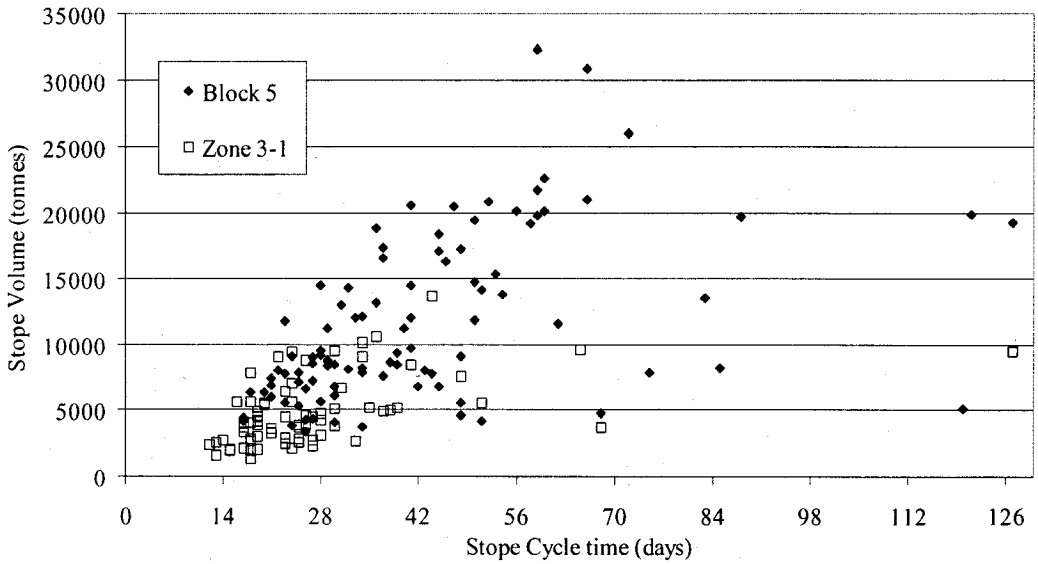

Figure 6.45 Comparison of rate of stope mucking against stope volume

Conversely, a comparison of stope cycle time against the measured hanging-wall Dilution Density, shown in Figure 6.46, does not show a direct relationship. In order to maintain the overall mine sequencing, stopes were promptly mucked and backfilled, thus hindering the potential for progressive, time-dependant degradation of the exposed stope walls (described previously in Chapter 3).

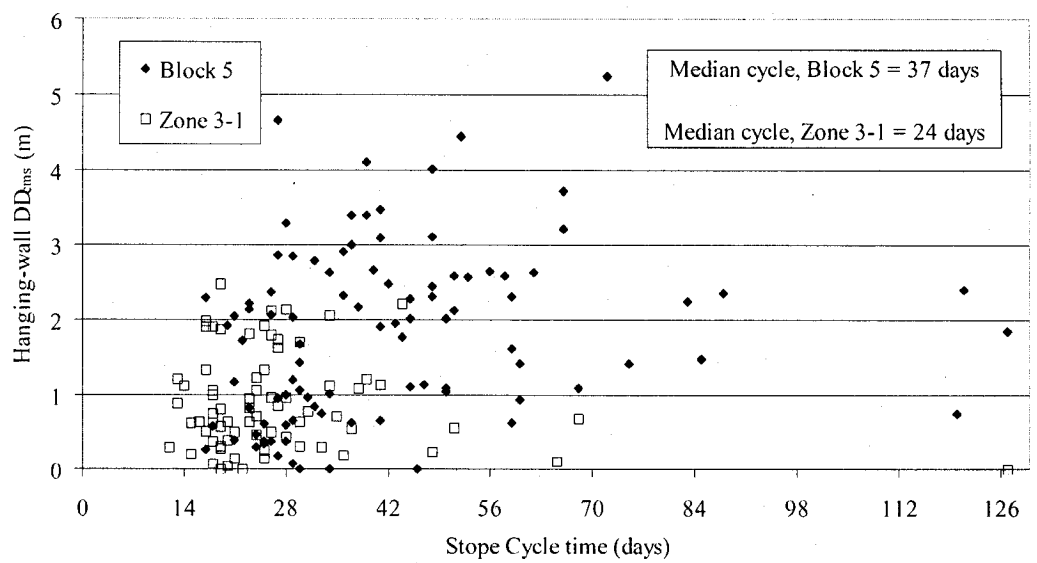

Figure 6.46 Comparison of rate of stope mucking against hanging-wall overbreak

6.7.3.6 Summary of hanging-wall dilution database

In Section 7.3.1, the severity of hanging-wall overbreak, as measured by CMS scans, was assessed for two discrete Bousquet orezone blocks: Zone 3-1 and Block 5. To aid in the comparisons, measured Dilution Density (DD_{cms}) was a term introduced.

Trends identified from the data, and summarized in Table 6.19, included:

- Overbreak associated between the differing stope types of Zone 3-1 and Block 5 was examined. With Zone 3-1, average hanging-wall overbreak associated with secondary stopes was found to exceed that of primary stope types by 69%.
- In Block 5, hanging-wall overbreak associated with secondary stopes was found to exceed that of primary stope types by 9%. However, it was shown that the magnitude of Block 5 hanging-wall dilution was influenced by the presence of cablebolt reinforcement. When considering only those stopes supported by cablebolts installed in an unfavourable orientation (cablebolts fanning upwards), average hanging-wall overbreak associated with secondary stopes was found to exceed that of primary stope types by 16%.
- Although at greater depth, Zone 3-1 stopes, with smaller hanging-wall dimensions, generated significantly less hanging-wall overbreak that did Block 5 stopes. Mean DD_{cms} values for Zone 3-1 stopes were 0.94m, values for Block 5 were DD_{cms} = 1.96m
- The Zone 3-1 stopes generated less total overbreak (hanging-wall and footwall overbreak combined) that did Block 5 stopes. Mean total DD_{cms} values for Zone 3-1 stopes were 1.69m, values for Block 5 were DD_{cms} = 2.45m
- The distribution of overbreak varied between the two orezones. In Block 5, 80% of the total overbreak was associated with the hanging-wall, while 60% of the total Zone 3-1 overbreak was associated with the hanging-wall.

- The stopes of Zone 3-1 and Block 5 had numerous comparable features, such as hanging-wall dip, mining method, stope construction, mucking rate and workforce.

Table 6.19 Summary of stope hanging-wall dilution

	Block 5				**Zone 3-1**			
	Mean value	Median value	Standard deviation	*CoV*	Mean value	Median value	Standard deviation	*CoV*
Dilution reported (%)	29.6%	24.2%	20.9%	71%	37.7%	32.2%	25%	66%
Total DD_{cms} from hanging-wall and footwall combined	2.45 m	2.26 m	1.57 m	64%	1.69 m	1.54 m	0.83 m	49%
Hanging-wall DD_{cms}	1.96 m	1.95 m	1.39 m	71%	0.94 m	0.80 m	0.63 m	66%
% DD_{cms} from hanging-wall source	80%	89%	22%	28%	57%	61%	26%	46%
Stope Cycle time (days)	42	37	21	50%	27	24	16	59%

6.8 Comparison of measured (DD_{cms}) and modelled (DD) overbreak

The interaction of overbreak with empirical design charts commonly plots measured hanging-wall dilution (in this case DD_{cms}) with respect to stope dimension, such as that found in Alcott (2002) and Mah (1997). Using this approach, data from Bousquet Block 5 and Zone 3-1 stopes, when plotted exhibits tight clustering due to their common hanging-wall dimensions. See Figure 6.19. Other approaches, such as that of Martin et al., (2000) and Henning et al., (2001b), have taken the stress setting into account in visually comparing the measured CMS contour at the mid-strike of a stope against the modelled distribution of σ_3.

In this Section, the DD_{cms} values obtained for the five stope-types are compared against DD values generated by 3-D elastic numerical modelling of individual stopes within the Block 5 and Zone 3-1 orebodies. The numerical modelling techniques used employed the same approach adopted for the parametric study, as described in Chapters 4 and 5.

6.8.1 Numerical model description

Detailed numerical models of the designed stopes of Block 5 and Zone 3-1 were constructed in Map3D. The Map3D model is based on the initial planned stope design and geometries. Individual stopes were constructed from the floor elevations at the base and top sill of each mining block from three-dimensional mine design CAD drawings. Stope setting, stope sequencing, hanging-wall dip angle, and orientation with respect to σ_1° are incorporated into the model. Individual stopes were modelled according to the actual stope sequencing for the two zones. See Figures 6.47 and 6.48. Only one stope was mined per modelled step. That same stope was backfilled in the subsequent modelling stage.

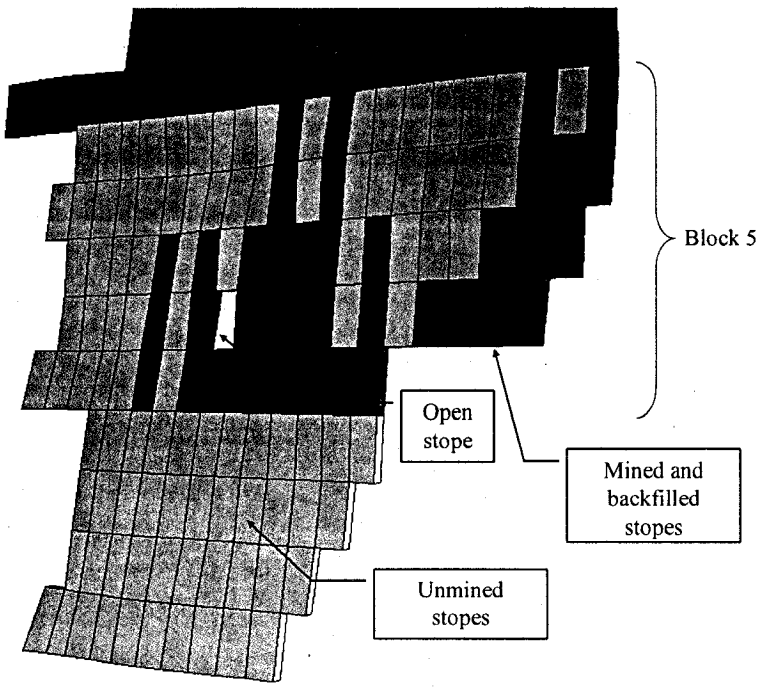

Figure 6.47 Block 5 perspective view showing unmined, open, and backfilled stopes

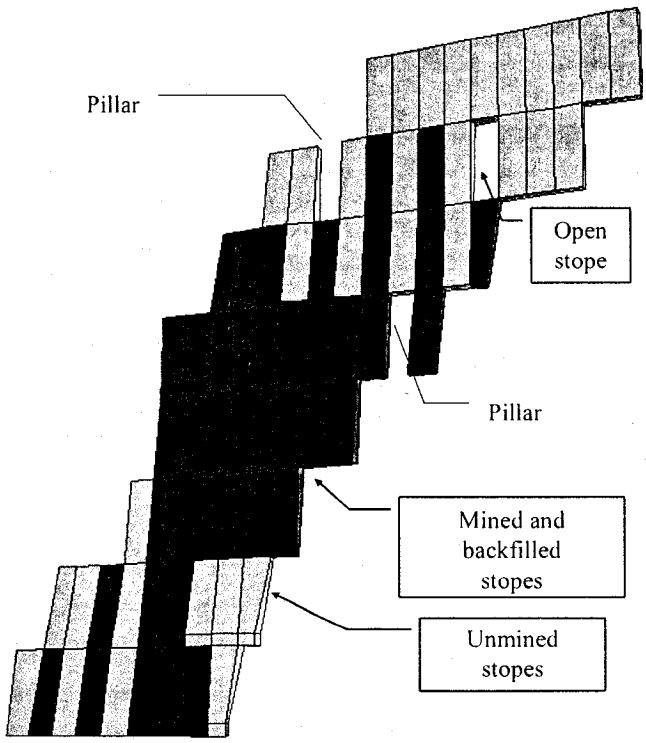

Figure 6.48 Zone 3-1 perspective view showing unmined, open, and backfilled stopes

Material properties for the host and orezone rock of Block 5 and Zone 3-1 were described previously in Section 6.4. As with the parametric modelling, rockmass input modelling parameters were obtained using Hoek-Brown relationships described in Section 4.3 (Table 4.6). Material and rockmass modelling input modelling parameters, assigned to the Block 5 and Zone 3-1 host and orezones are summarized in Table 6.20. Backfill modelling properties are provided in Table 6.21. Stress setting was obtained from relationships provided in Section 6.4.4 (Equations 6-1, 6-2, and 6-3).

For each stope, modelled stresses within the hanging-wall were plotted on vertical and horizontal grids located at mid-span and mid-height, respectively. See Figure 6.49. As with the parametric study, the grids extended to a depth of 10m from the stope. With the approach previously adopted for the parametric study, the volume of hanging-wall relaxation is calculated as the volume of one-half of a prolate ellipsoid. Measurement of *DD* is obtained using this volume and the surface area of each individual stope.

Table 6.20 Modelling input parameters, rockmass

Parameter	**Bousquet #2 mine, Block 5**		**Bousquet #2 mine, Zone 3-1**
	Host rock	Orezone	Host rock and Orezone
Rock type	foliated rhyolite tuff	massive sulphide	foliated rhyolite tuff "alteration zone"
RMR_{79} / GSI	50	75	48
UCS (σ_c)	112 MPa	211 MPa	59 MPa
Hoek-Brown 'm_i'	10	17	10
Disturbance Factor, *D*	0	0	0
Rockmass Parameters			
Hoek-Brown 'm'	1.677	6.961	1.56
Hoek-Brown 's'	0.004	0.062	0.003
Rockmass elastic modulus, (E_{rm})	10000 MPa	42200 MPa	6850 MPa
Rockmass tensile strength, (σ_t)	0.26 MPa	1.88 MPa	0.18 MPa
Global rockmass compressive strength, (σ_{cm})	19.5 MPa	83.5 MPa	9.8 MPa

Table 6.21 Modelling input parameters, backfill

Parameter	**Material Value**
Uniaxial compressive strength, σ_c	3 MPa
Elastic modulus, E	2500 MPa
Poisson Ratio, υ	0.35
Mohr-coulomb parameters	
Cohesive strength	0.1 MPa
Internal angle of friction	35 degrees

6.8.2 Model results

At each successive mining step, the extent of a given iso-contour of σ_3 was determined using the approach adopted for the parametric study, as described in Chapter 4 (section 4.6.2). See Figure 6.50. A database was constructed for the two orezones, in which values of modelled stope hanging-wall dimensions, stope type, radius distances of the three axes of the prolate ellipsoid, and calculated Dilution Densities are compiled for individual stopes.

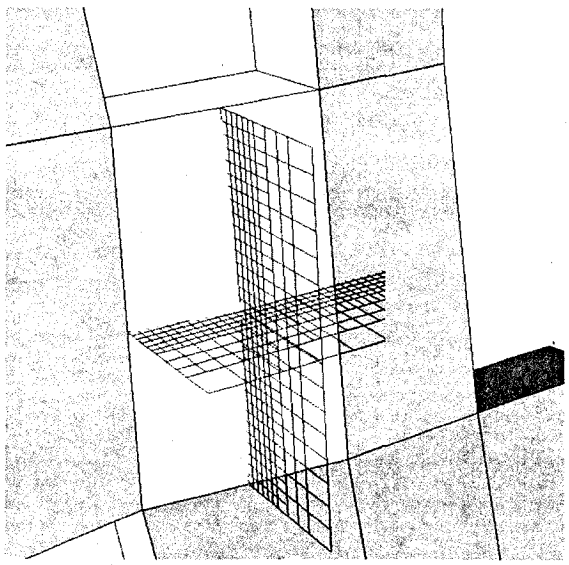

Figure 6.49 Grid positioning

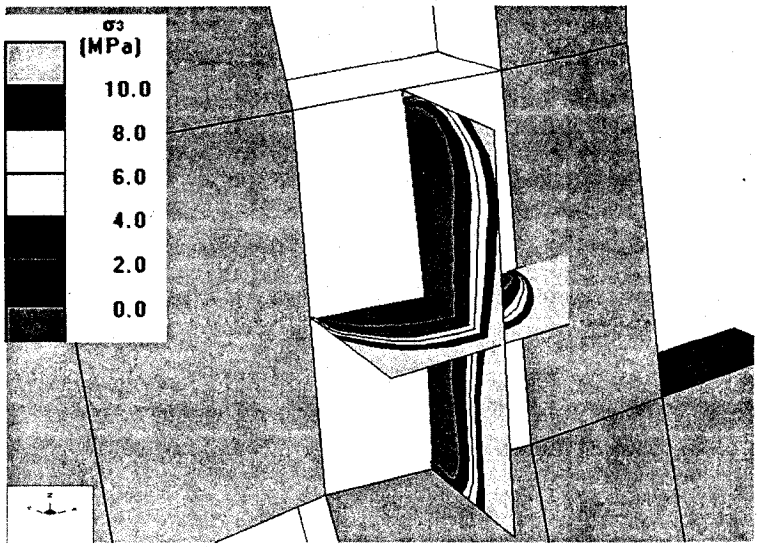

Figure 6.50 σ_3 iso-contours, secondary S2-type stope

Visually, the 3D elastic modelling results showed that the depth at which a given contour of σ_3 occurred in the hanging-wall varied with stope type. An example, provided in Figure 6.51, illustrates differences between a primary P-type and secondary S2-type stope. Two contours: $\sigma_3 = 0$ and $\sigma_3 = 2$MPa are shown. Note that for a given value, such as the $\sigma_3 = 0$ MPa contour, the extent of the contour is greater in the secondary stope.

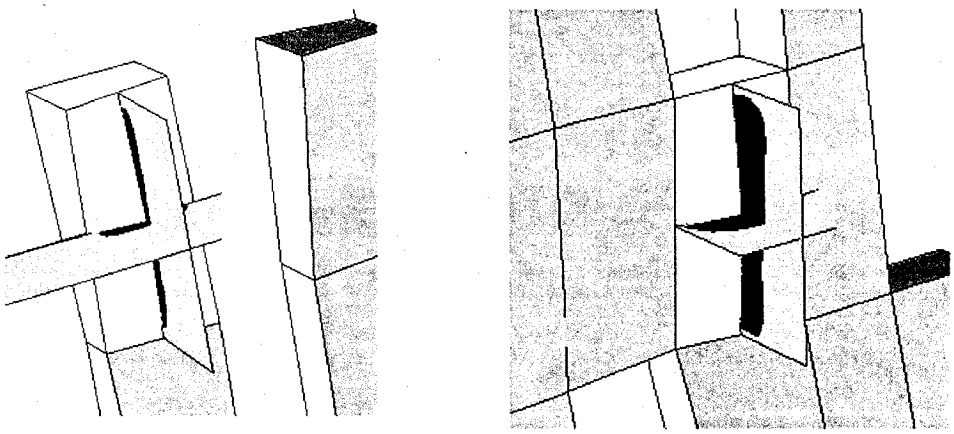

(a) primary stope, $\sigma_3 \leq 2$MPa shown (b) secondary stope, $\sigma_3 \leq 2$MPa shown

Figure 6.51 Comparison of σ_3 contours associated with primary and secondary stope hanging-wall

To quantify observed differences, values of *DD* associated with σ_3 contours, ranging from $\sigma_3 = \sigma_t$ (tensile conditions) to $\sigma_3 = +10$ MPa (low range compression conditions), were calculated for each individual stope. For each orezone, data was grouped according to stope type. Average values for stope type, for a given σ_3 contour, were compiled. These values are summarised and plotted in Figures 6.52 and 6.53. Plotted values of σ_3 greater than $\sigma_3 = 0$ MPa correspond to compression conditions. Model details are summarized in Appendix C.

The trends of Figures 6.52 and 6.53 show similarities between Block 5 and Zone 3-1 stopes. For both orezones, primary stope types cluster closely together, typically within a range of *DD* = 0.15m +/-. *DD* values increase slightly from P1 to P2 to P3-type stopes. For Block 5 stopes, S2-type stopes exhibit the greatest modelled overbreak, typically in the range of 1.06m *DD* greater than an averaged primary stope for a given σ_3 contour. S1-type stopes occur between the S2 and P-type stopes. Typically, potential modelled overbreak values in the range of 0.75m *DD* greater than an averaged primary stope were generated.

With the smaller Zone 3-1 stopes, a similar trend was evident. Lower values of *DD* are due, in part, to the smaller stope dimensions. S2-type stopes exhibit the greatest modelled overbreak, typically in the range of 0.62m *DD* greater than an averaged primary stope for a given σ_3 contour. As with Block 5 observations, S1-type stopes occur between the S2 and P-type stopes, with potential modelled overbreak values in the range of 0.31m *DD* greater than an averaged primary stope.

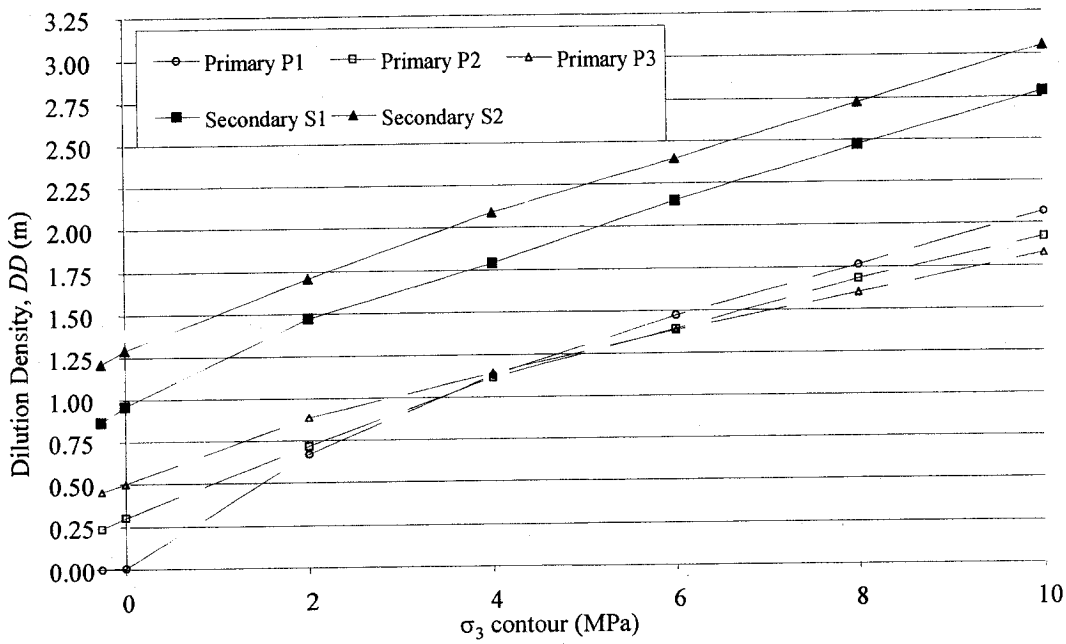

Figure 6.52 Average *DD* versus σ_3 contours, all Block 5 stopes

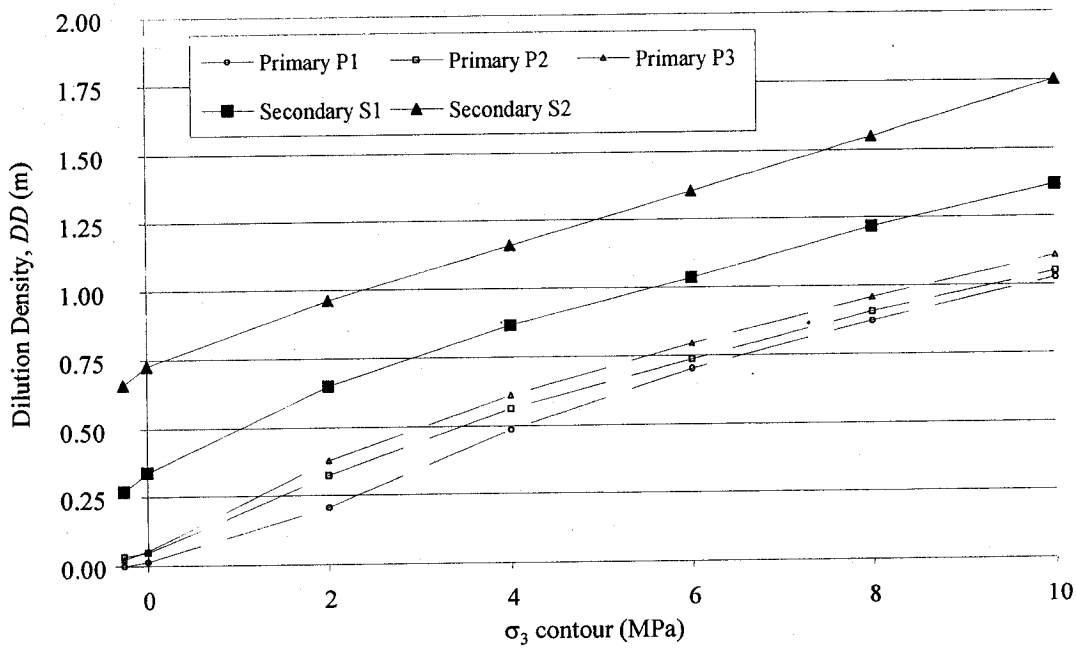

Figure 6.53 Average *DD* versus σ_3 contours, all Zone 3-1stopes

Linear trend lines for the *DD* versus σ_3 relationships stope types within each of the two zones closely follow the plotted data, provided in Figure 6.54 and 6.55, illustrate the near-parallel slopes of the modelled data. For Block 5 stopes, this relationship can be expressed as:

$$DD = 0.17 \cdot \sigma_3 + C \qquad (6\text{-}13)$$

where: *DD* = modelled dilution density (m)

σ_3 = iso-contour value of minimum principal confining stress (MPa), and

C = Stope type constant.

For Block 5 P-type stopes, C = 0.36m

For Block 5 S1-type stopes, C = 1.13m

For Block 5 S2-type stopes, C = 1.33m

Similarly, for Zone 3-1 stopes, this relationship can be expressed as:

$$DD = 0.10 \cdot \sigma_3 + C \qquad (6\text{-}14)$$

where: *DD* = modelled dilution density (m)

σ_3 = iso-contour value of minimum principal confining stress (MPa), and

C = Stope type constant.

For Zone 3-1 P-type stopes, C = 0.08m

For Zone 3-1 S1-type stopes, C = 0.43m

For Zone 3-1 S2-type stopes, C = 0.73m

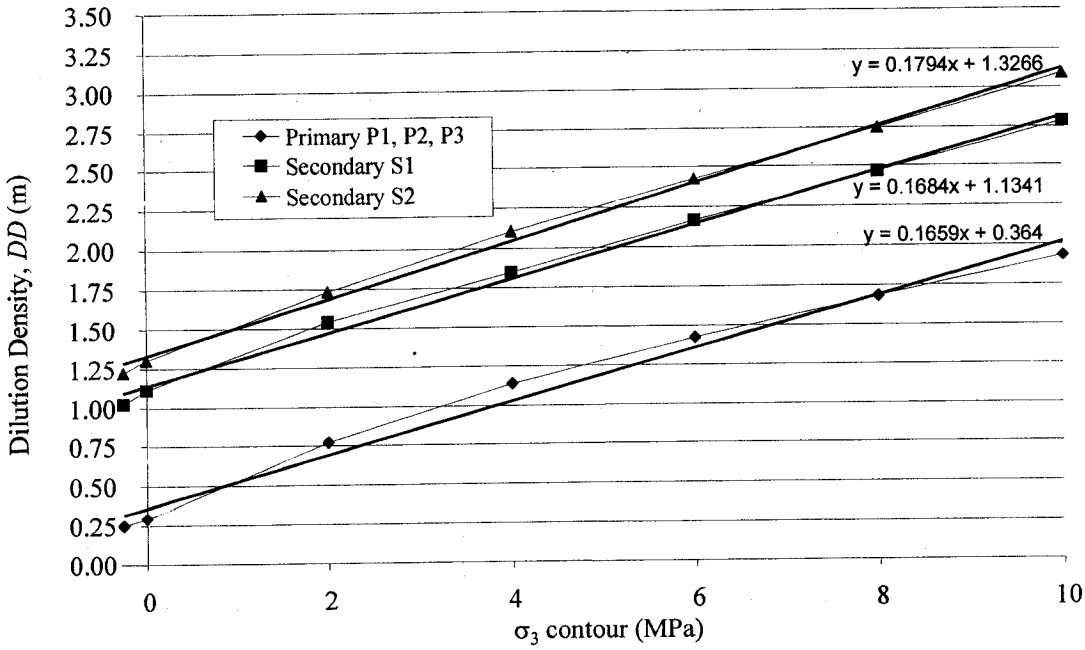

Figure 6.54 Trendlines, Block 5 stopes

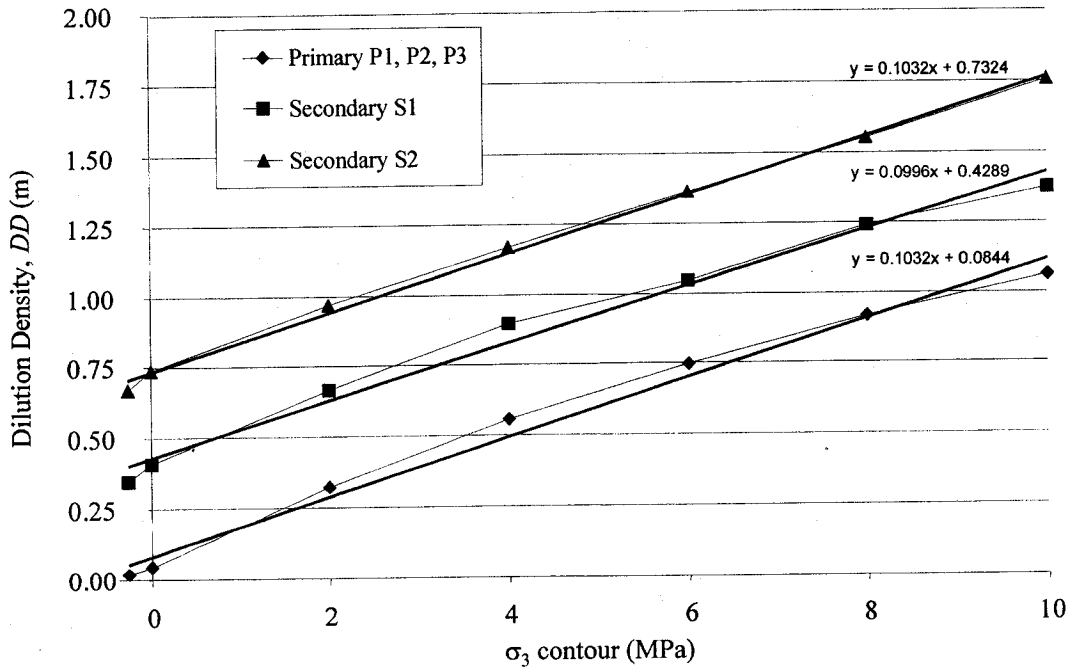

Figure 6.55 Trendlines, Zone 3-1 stopes

6.8.3 *DD* and DD_{cms} overbreak comparison

With this study, hanging-wall overbreak, expressed as dilution density has been determined using two approaches. Measured dilution density (DD_{cms}) represents a true assessment of hanging-wall overbreak, as determined using a physical CMS scan of the mined stope. The second approach uses 3-D numerical modelling techniques to estimate potential dilution density (*DD*) based on the extent of an envelope of low confinement stress, defined by the extents of σ_3.

To assess linkage between the DD_{cms} and *DD* approaches, *DD* versus σ_3 relationships were compared against the average DD_{cms} values obtained from the CMS database (see Table 6.22) for each stope type. As described in the parametric study (Chapter 5), differences in *DD* values between stopes of the two orezones can be attributed to smaller dimensions of Zone 3-1 stopes. Other factors, such as orezone depth and rockmass quality of the ore and host rock also play a role. Measured dilution density (DD_{cms}) values of individual excavated stopes within the two Bousquet orezones are described in Section 6.7.

Table 6.22 Average DD_{cms} values, transverse stopes

Stope type	Orezone	
	Block 5	Zone 3-1
Primary (P1, P2, P3)	2.02 m	0.71m
Secondary S1	1.87m	0.81m
Secondary S2	2.18m	1.14m

Relationships between DD_{cms} and *DD* for Block 5 and Zone 3-1 stope types are plotted in Figures 6.56 and 6.57, respectively. The intercept of the measured DD_{cms} value with the DD/σ_3 distribution identifies what σ_3 contour value corresponds to an appropriate *DD* in the numerical model. As can be seen in both plots, the values of DD_{cms} for the primary and secondary stope types intercept the

corresponding *DD* curve at values of σ_3 exceeding zero, suggesting that the rockmass may fail under low values of compressive stress. For both orezones, the DD_{cms} value for primary stopes intercepts the *DD* curve at a σ_3 contour value exceeding that of either of the secondary stope types. Similarly, the DD_{cms} value for S1-type secondary stopes intercepts the *DD* curve at a σ_3 contour value lower than both the P-type and S2-type stopes. The modelled σ_3 contour values corresponding to the DD_{cms} for each stope type in Block 5 and Zone 3-1, summarized in Table 6.23, can be obtained by using Equations 6-13 and 6-14, and the averaged CMS-based data provided Table 6.22.

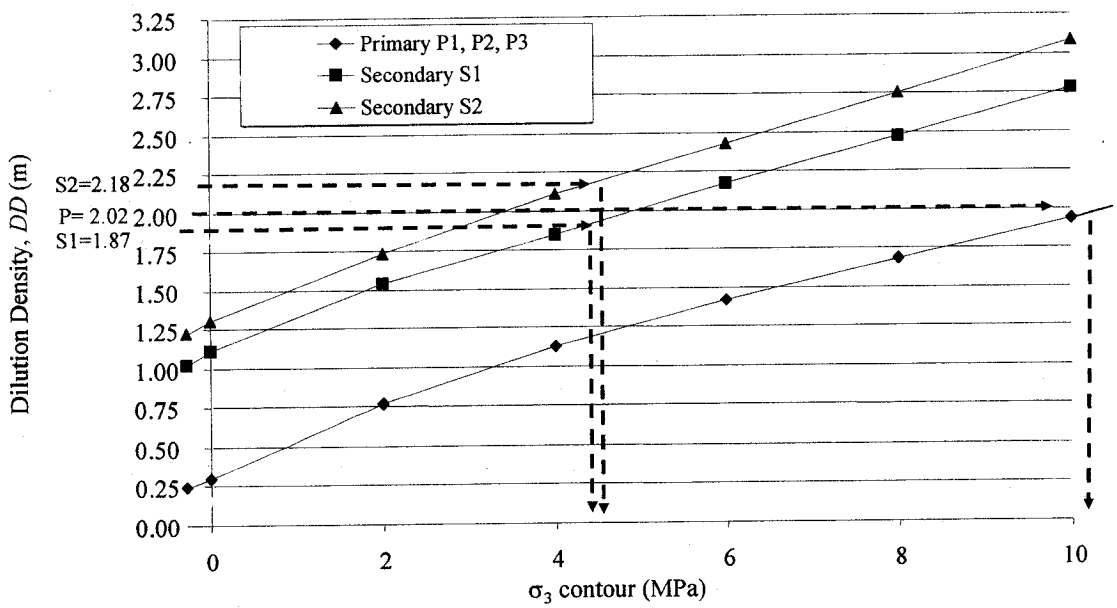

Figure 6.56 Average *DD* versus σ_3 contour, Block 5 transverse stopes

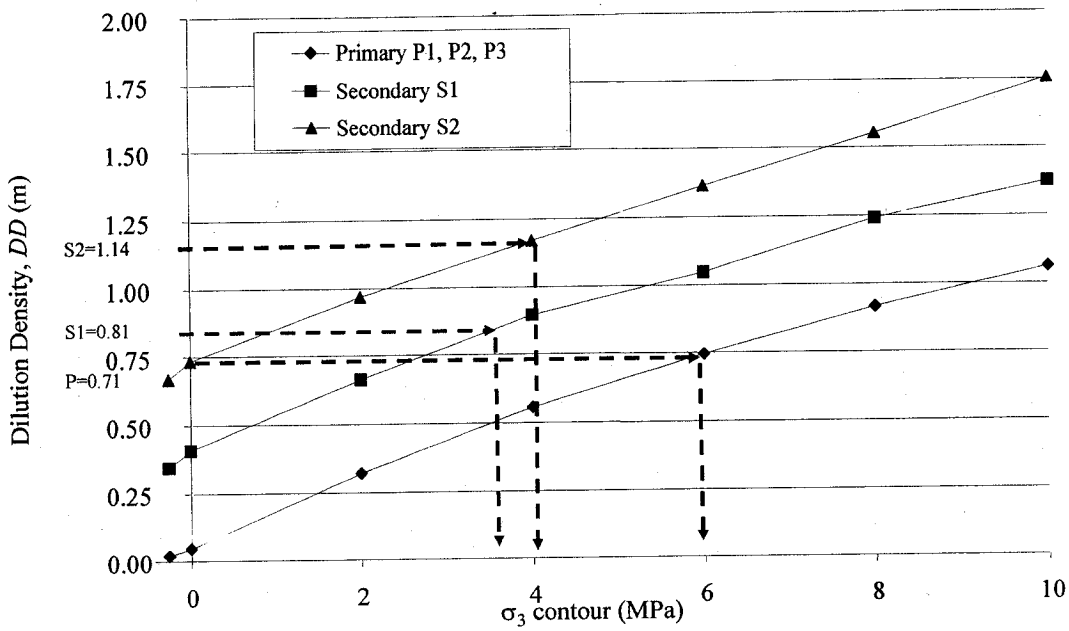

Figure 6.57 Average *DD* versus σ_3 contour, Zone 3-1 transverse stopes

Table 6.23 Modelled σ_3 contour corresponding to measured overbreak values

Stope type	Block 5		Zone 3-1	
	DD_{cms} value	Corresponding σ_3 contour value	DD_{cms} value	Corresponding σ_3 contour value
Primary (P1, P2, P3)	2.02 m	9.8 MPa	0.71m	6.3 MPa
Secondary S1	1.87m	4.4 MPa	0.81m	3.8 MPa
Secondary S2	2.18m	5.0 MPa	1.14m	4.1 MPa

6.8.4 Summary of model results

Intercepts of measured DD_{cms} with modelled *DD* curves for specific stope types, illustrated in Figure 6.56 and 6.57, and summarized in Table 6.23, are combined in Figure 6.58. As shown previously in Section 6.6, Block 5 and Zone 3-1 orezones had many common elements, such as stope height, orezone dip, orezone orientation with respect to pre-mining stresses, quality of the host rockmass, and the design and excavation of the individual stopes. Parametric investigations (Section 5.2), suggest that the increased depth at which mining occurs, such as that between Zone 3-1 and Block 5, plays only a minor role in increasing the severity of overbreak, as simulated by an elastic 3-D numerical model. As a result, it can be inferred that the differences in strike length of the stopes of Zone 3-1 and Block 5 are dominant factors influencing measured and modelled overbreak. As provided in Table 6.13, typical strike lengths for Zone 3-1 and Block 5 stopes are 10m and 15m, respectively.

Taking the elastic nature of the 3-D model into account, relationships can be defined between *DD* and DD_{cms}, based on ranges of modelled σ_3 contours. Figure 6.58 plots the contours of modelled σ_3 that correspond to measured average overbreak for primary (P-type) and secondary (S1 and S2-type) stopes. For example, when simulating overbreak associated with a Zone 3-1 primary stope (10m strike length), a modelled *DD* value calculated using the prolate ellipsoid axes defined by the σ_3 = 6.3 MPa contour corresponds to the measured DD_{cms} value for a typical Zone 3-1 primary stope.

Two clusters occur in Figure 6.58: primary stope and secondary stope. Primary stope values are associated with σ_3 contours exceeding 6MPa. Projecting a linear trend line between the 10m and 15m strike lengths, an inclined slope, increasing at a rise:run ratio of 0.4:1 is generated. Secondary stopes are associated with σ_3 contours in the range of 4 to 5MPa. Linear trend lines between 10m and 15m strike lengths are steeper than that of primary stopes. For S1-type stopes, the trend line increases at a rise:run ratio of 1.7:1. The trend line for S2-stopes increases at a rise:run ratio of 0.9:1. Contours of low confining stress (σ_3) vary

between primary and secondary stopes due to the influence of mined geometry on the 3-D elastic numerical model. As illustrated previously in Figure 6.51, the depth at which a low value σ_3 contour is generated in the hanging-wall is greater in a secondary stope than in a similarly sized primary stope hanging-wall.

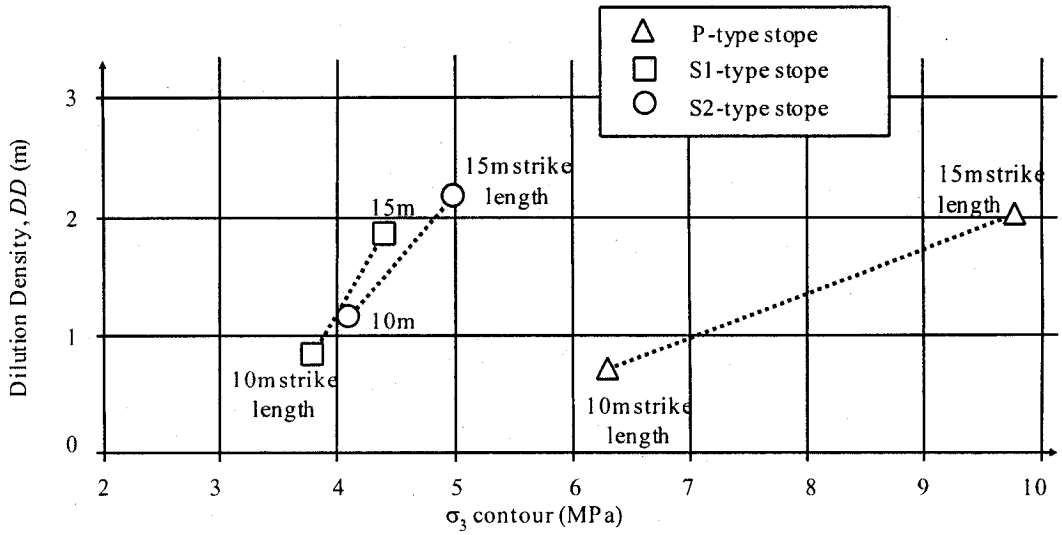

Figure 6.58 Modelled σ_3 contours corresponding to measured DD_{cms} overbreak values

6.8.4.1 Limitation of numerical modelling and calculation methodology

The approach adopted for this study can be used to predict reasonable estimates of overbreak severity for individual stope types with height of 30m and strike lengths ranging between 10m and 15m. The use of specific contours of σ_3 represents an adjustment factor between the measured overbreak and modelled simulation. By definition, numerical modelling represents an idealized simplification of physical characteristics. Simplifications and limitations of the numerical modelling approach used includes both the type of 3-D modelling tool utilized, and the methodology employed to calculate modelled overbreak.

Simulation of rockmass reinforcement and non-linear rockmass behaviour were beyond the capability of the 3-D elastic modelling software used (Map3D). As a result, the hanging-wall cablebolts used in Block 5 were not modelled, nor was non-linear failure.

The stopes in Block 5 and Zone 3-1 were constructed according to the designed stope geometry. Overbreak or potentially damaged ground from prior mining was not incorporated into the model. For example, the geometry of mined stopes was not modified to reflect mined geometry (as measured by CMS) prior mining of subsequent stopes.

The methodology employed to estimate modelled overbreak (*DD*) assumed that *DD* corresponds to the volume of one-half of a prolate ellipsoid. When modelled, the σ_3 iso-contours generated in the stope hanging-wall were not always parabolic. This was observed both in section view (see Figure 6.59), and in plan (see Figure 6.60). As a result, *DD* obtained from the numerical model may in some cases, represent a low-range estimate of overbeak.

In general, it was observed that the σ_3 iso-contours associated with primary stopes tended to be symmetrical in both plan and section views. With S1 and S2-type stopes, the vertical (section) σ_3 iso-contour profile was asymmetric, due to influence of adjacent mined stopes. In plan, the σ_3 iso-contour associated with the S1 stope were asymmetric, whereas S2-type stopes, located between two mined stopes generated symmetrical σ_3 iso-contours

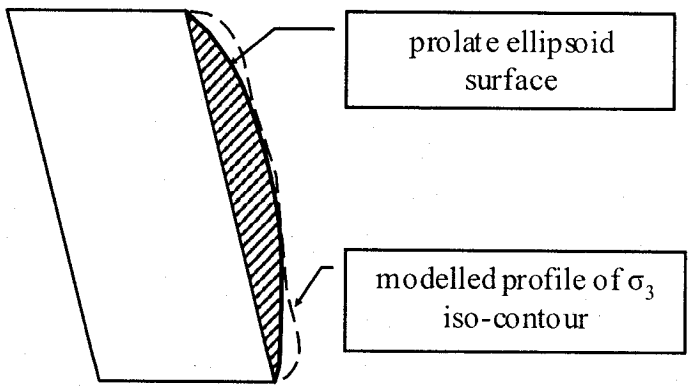

Figure 6.59 Section view showing σ_3 iso-contour profile and equivalent prolate ellipsoid surface, S2 type stope

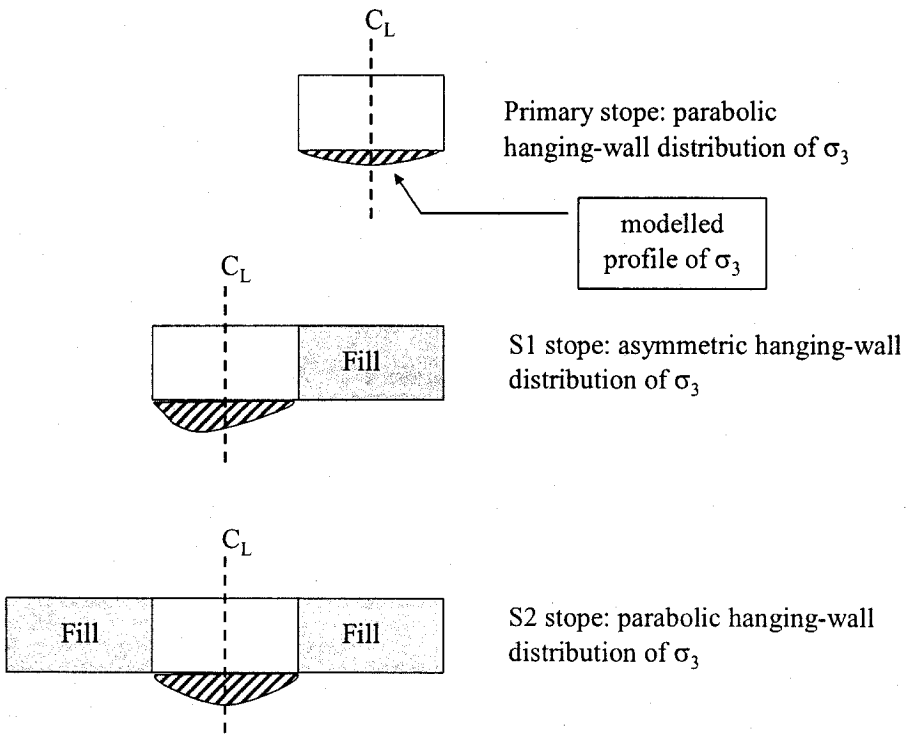

Figure 6.60 Plan view showing σ_3 iso-contour profiles for P, S1 and S2 type stopes

6.9 Primary and secondary stope failure modes

Measured overbreak varies with stope type, with secondary stopes generating a greater volume of hanging-wall dilution than primary stopes. This was observed in: (i) Parametric studies; (ii) the stopes of Zone 3-1 stopes, (iii) in stopes of Block 5 that had not been reinforced by downward fanning cablebolts, and (iv) in numerical modelling of Block 5 and Zone 3-1 sequencing. Typically, the following relationships were observed:

$$DD_{cms} \text{ (secondary stopes)} > DD_{cms} \text{ (primary stopes)} \quad (6\text{-}15)$$

$$DD \text{ (secondary stopes)} > DD \text{ (primary stopes)} \quad (6\text{-}16)$$

These observed contrasts between primary and secondary stopes suggest differing mechanisms associated with the generation of potential hanging-wall dilution.

6.9.1 Pre-conditioning of secondary stope hanging-walls

DD values for the secondary stopes are significantly greater than those associated with a primary stope. When viewing the results of 3-D numerical modelling, such as that shown in Figure 6.51, the depth that a given σ_3 iso-contour extends into the hanging-wall varies with stope type, and is greater with secondary-type stopes.

Physically, the S1 and S2 type stopes lie in a different stress setting than the primary (P1, P2 and P3 type) stopes. Primary stopes are, by definition, isolated from adjacent mined stopes by substantial rock pillars on both side walls. These pillars are mined at a later stage of the mining sequence as secondary stopes. Being isolated, much of the hanging-wall rockmass has not been significantly pre-conditioned by stress relaxation or stress-induced damage by prior mining. An exception is where undercutting of the top sill of the underlying stope results in localized rockmass relaxation at the base of the overlying primary stope.

With the secondary stopes, the hanging-wall rockmass is in an elevated state of relaxation due to prior mining of stopes on one or both sides, as well as below. Rockmass relaxation refers to stress reduction parallel to the excavation wall. As described by Kaiser et al. (1997), rockmass relaxation describes conditions where the stresses in the tangential direction to the excavation wall (the major and/or intermediate principal stress) are reduced in the rockmass. In practice, such conditions are encountered, for example when a hanging-wall is undercut, intentionally or by caving of the hanging-wall in an underlying stope, or by the prior extraction of the primary stopes (Bawden et al., 1998). This is most evident with the S2-type stopes, which are bound on three sides by mined stopes, as illustrated in Figure 6.61. Instability occurs when the rockmass has reached a critical relaxation threshold at which gravity-driven failure modes or slip along weakness planes is encountered. Hence, full relaxation causing zero or even tensile stress conditions is not required to cause failure.

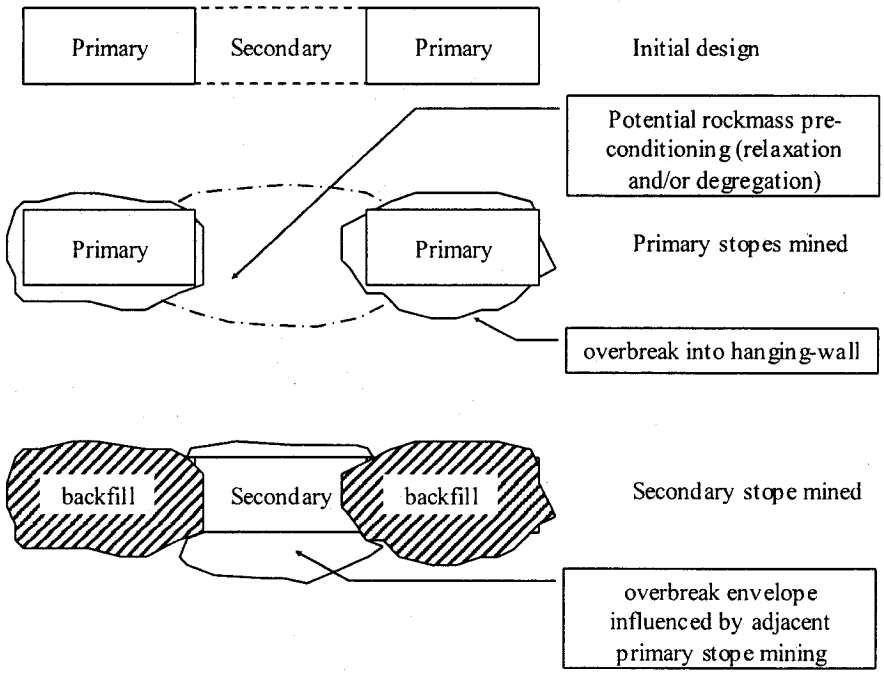

Figure 6.61 Rockmass relaxation in adjacent primary and secondary stopes, plan view

The rockmass of secondary stopes may be further pre-conditioned by stress-induced damages associated with prior mining of the primary stopes, by time-dependent weakening processes or by poor blasting practices. Rockmass degradation describes conditions where the rockmass quality and thus the rockmass strength has been reduced relative to its virgin state.

As discussed in Section 4.3.3, induced stresses are the result of excavation activity. When an excavation is made, stresses are shed onto adjacent material. The rock left standing has to take more load since the original confinement provided by the rock within the excavation has been removed. The impact of induced stress depends on: (i) the initial, pre-mining state of stress, (ii) the geometry of the excavation, and (iii) the constitutive (stress-strain) behaviour of the rockmass. According to Kaiser et al. (1997), rockmass degradation occurs as a result of stress-induced fracturing or fracture propagation, resulting in a reduced tensile strength or load bearing capacity of the rockmass.

6.9.2 Primary and secondary stope hanging-wall stress setting

Observations from the blast vibration monitoring (Section 5.8.1) suggested that mining of secondary stopes occur within a lower stress environment. Underground at Bousquet #2 mine, this stress relaxation was associated anecdotally by: (i) a reduced requirement for re-drilling of production blastholes, and (ii) fewer accounts of working ground.

To assess hanging-wall stress conditions, primary (P-type) and secondary (S1 and S2-type) stopes, located in Block 5 were examined using Map3D numerical modelling. The Block 5 Map3D model is described in Section 6.8.1. Modelled σ_1 and σ_3 stresses were obtained at points located at depths of 1.25m, 2.5m, and 5m from, and orthogonal to, the stope hanging-wall contact. The positions of the grid points, as well as the modelled stopes are shown in Figure 6.62. The stopes of Block 5 were mined according to the actual stope sequencing. Only one stope as mined per modelled step, that same stope was backfilled at the subsequent modelling stage.

For each stope, three stress setting were compiled: pre-mining stress, pre-stope stress and post-stope stress. Pre-mining stress refers to the natural stress setting, prior to the onset of orezone extraction. Pre-stope stress represents the local, induced stress state in the immediate vicinity of the planned stope at the time of the onset of mining a specific stope. Post-stope stress is the local stress state in the vicinity of the mined, unfilled stope. Modelled stresses are compiled in Table 6.24.

Table 6.24 Hanging-wall stress setting

Stope type	Distance from stope hanging-wall boundary	pre-mining stress (MPa)		pre-stope stress (MPa)		post-stope stress (MPa)	
		σ_1	σ_3	σ_1	σ_3	σ_1	σ_3
P	1.25 m	70.3	31.1	80.1	39.3	15.9	0.8
	2.5 m	70.3	31.1	80.4	39.4	28.1	1.6
	5 m	70.3	31.1	80.7	39.2	45.8	7.0
S1	1.25 m	68.5	30.3	104.2	50.2	18.9	-3.6
	2.5 m	68.5	30.3	102.7	47.7	27.7	-0.8
	5 m	68.5	30.3	99.2	42.2	44.2	6.3
S2	1.25 m	70.3	31.1	115.9	50.1	4.9	-6.7
	2.5 m	70.3	31.1	116.6	47.9	13.8	-3.1
	5 m	70.3	31.1	115.9	44.1	25.5	0.1

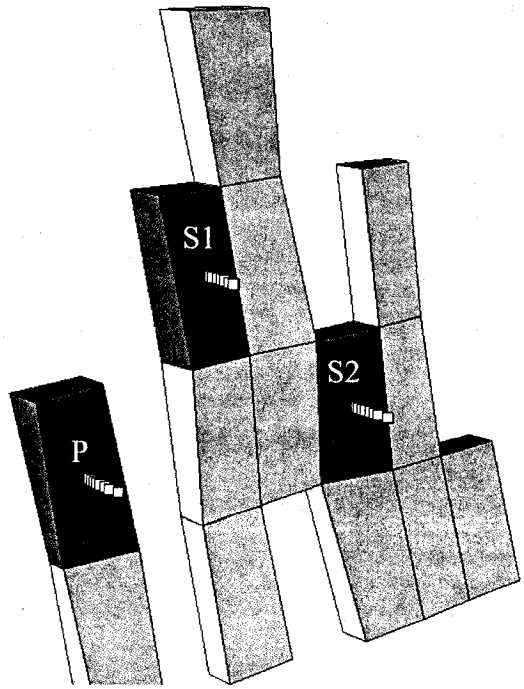

Figure 6.62 Plot of grid points projecting from stope center into hanging-wall

The calculated stresses are compared against Hoek-Brown failure criteria. The Hoek-Brown failure criterion was originally developed for application to rock around underground openings under confined conditions (Hoek and Brown, 1980). For most hard-rockmasses the failure criterion is usually expressed in the following form:

$$\sigma_1 = \sigma_3 + (m \cdot \sigma_c \cdot \sigma_3 + s \cdot \sigma_c^2)^{0.5} \qquad (6\text{-}17)$$

where: σ_1, σ_3 = principal effective stresses at failure

σ_c = unconfined compressive strength of the intact rock

m, s = parameters defined by Hoek and Brown (1998)

Hoek-Brown parameters are discussed in Section 4.3.4. Hoek-Brown parameters for the Bouquet #2 mine analyses are provided in Table 6.7, and described in Section 6.4.

Plots of major and minor principal pre-stoping stresses at the stope mid-height, provided in Figure 6.63, illustrate anticipated stability of the unexposed hanging-wall. Using conventional Hoek-Brown rockmass failure criterion, the hanging-walls of the unmined primary and secondary stopes are indicated as stable. The data points from the primary stope cluster closely together, indicating uniform stress setting. The data points have a greater distribution with the secondary stope, with the value of σ_3 increasing with closer proximity to the as-yet unmined stope. The primary stope hanging-wall values plot well below the Hoek-Brown threshold, suggesting stable pre-mining hanging-wall conditions. Secondary S1 and S2-type stope hanging-wall values, with increased σ_1 values, plot closer to the failure threshold, suggesting a potential for degradation of the rockmass by induced stresses. Values for the S2-type stope plot closest to the threshold.

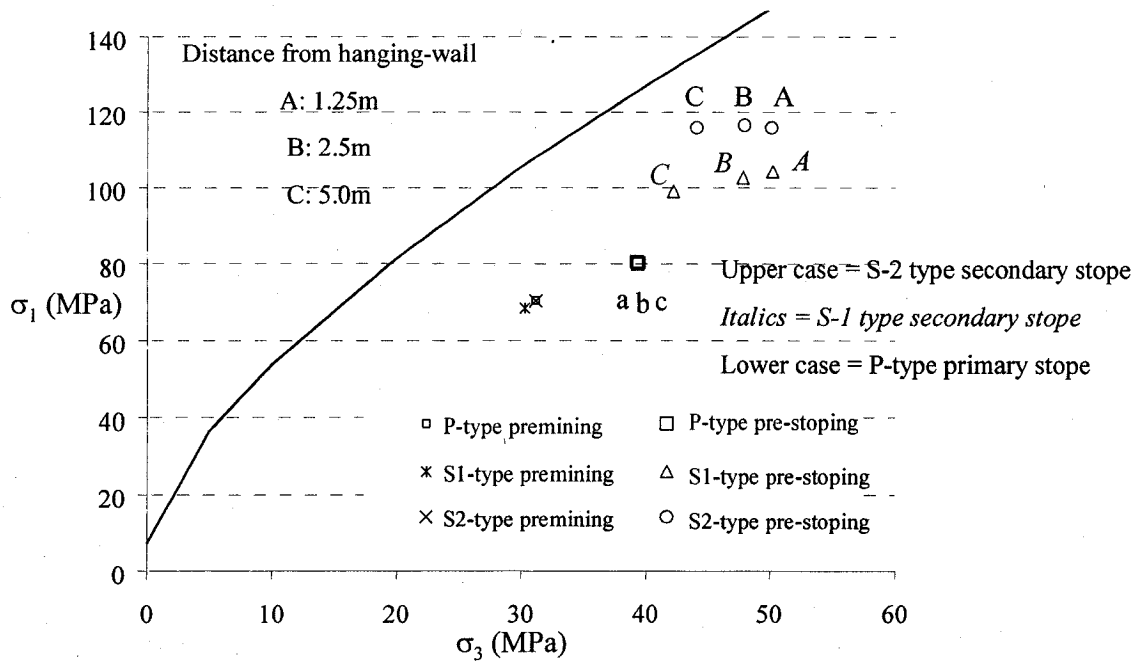

Figure 6.63 Pre-stoping stress conditions in hanging-wall

Following excavation, σ_1 and σ_3 stresses (post-stoping stress) have decreased for all stope types, indicating rockmass relaxation. See Figure 6.64. For the primary stope, values of σ_3 are near-zero, but marginally positive, at depths of 1.25 and

2.5m into the hanging-wall. At a depth of 5m into the hanging-wall, confined conditions are indicated by a positive value of σ_3. Values of σ_3 are negative to a depth of 5m into the hanging-wall of the secondary S2-type stope. The S1 stope lies between the P and S2 stopes. Negative σ_3 values were generated by the S1 stopes to a depth of 2.5m into the hanging-wall, while confined conditions were indicated at a 5m depth. In the region with confinement loss (σ_3=0 MPa) a potential for sloughage exists, however not all of this zone will fail if the rockmass has some self-supporting capacity.

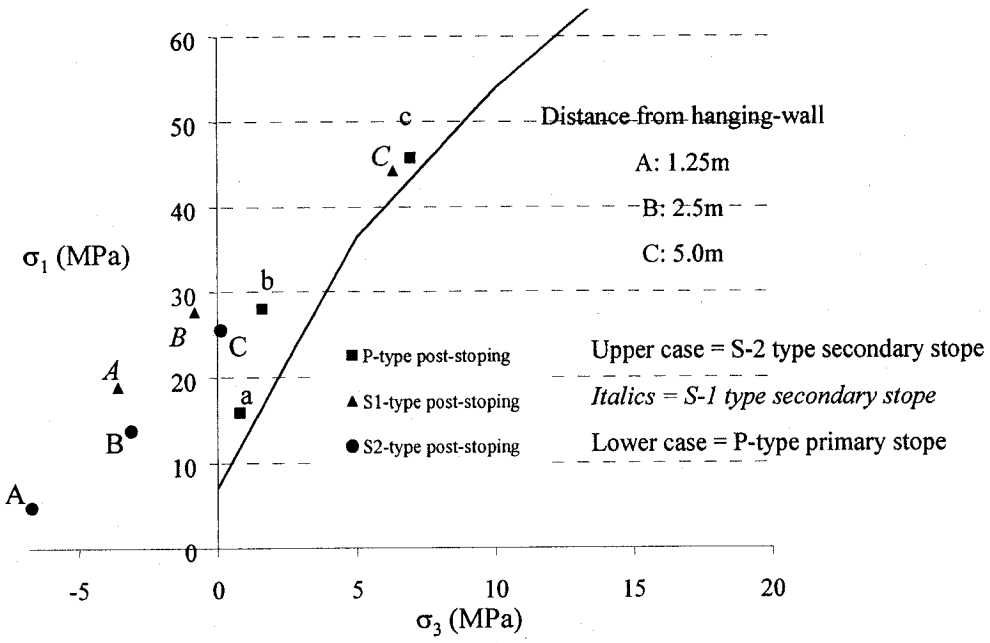

Figure 6.64 Hanging-wall stress conditions after mining

The potential stress paths that a rockmass around an underground opening experiences are illustrated in Figure 6.65. Inspection of Figure 6.65 illustrates that for most stress paths the rockmass is fundamentally unloaded. Stress paths associated with the pre-mining, pre-stope, and post-stope stages of P, S1 and S2-type stopes are illustrated in Figure 6.66. For each stope type, stresses generated at 2.5m depth into the hanging-wall are plotted. Figure 6.66 illustrates stress increase from pre-mined (in situ) conditions prior to stoping, due to other, prior,

stoping. Stresses are greater for the secondary stopes, reflecting the shedding of stress onto adjacent pillars and abutments following mining of the primary stopes. Depending on the competency of the rockmass, some degradation may occur. With mining, the stresses within the hanging-wall of all stope types decreases, indicating that the rockmass has unloaded. Tensile conditions ($\sigma_3 < 0$) are indicated at a depth of 2.5m into the hanging-wall for both the S2 and S1-type stopes. Decreases are greatest for the S2-type stope, followed by the S1 stope. Low confinement conditions are indicated for the P-type stope, where σ_3 stresses marginally above zero occur at a depth of 2.5m into the hanging-wall.

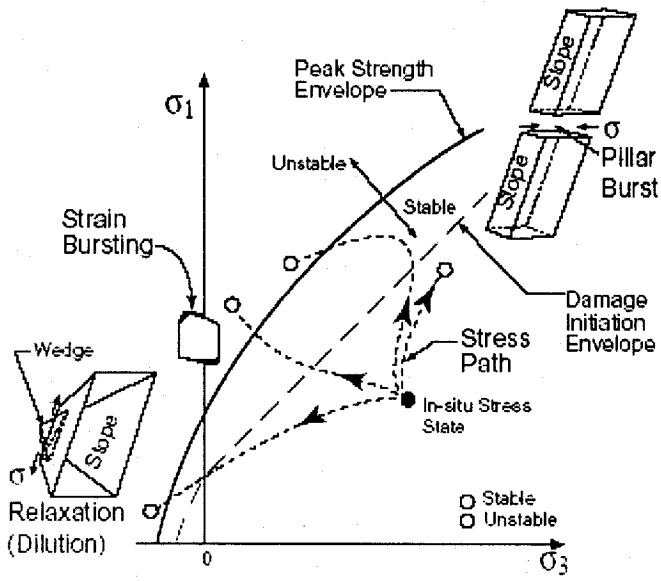

Figure 6.65 Illustration of possible stress paths near underground openings (Martin et al., 1999)

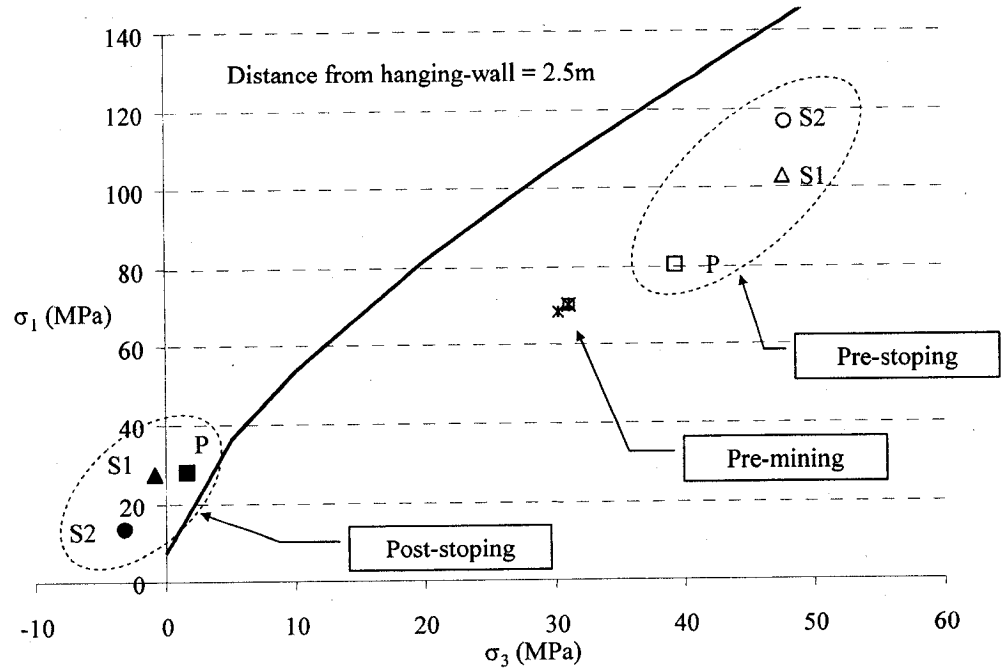

Figure 6.66 Modelled hanging-wall stress paths at point located 2.5m into hanging-wall

6.9.3 Summary

Intrinsic differences between primary and secondary stope performance, indicated by observed differences in blast vibration attenuation, and in excavated stope profile, demonstrates that the radial confining stress on secondary stope is reduced.

Stress path trends, shown schematically in Figure 6.67, identify differences between the performance of primary and secondary stope hanging-walls. In close proximity to the stope wall, it was noted that the secondary stopes experience a greater degree of pre-conditioning, in the form of both stress-induced damage by prior mining (pre-stoping) and by stress relaxation (post-stoping). Pre-conditioning was greatest with the S2-type stope.

Following production blasting of adjacent primary stopes, stresses were redistributed around the stope. Pre-conditioning of the secondary stope hanging-wall, due to these induced stresses resulted in rockmass yielding and an envelope

of de-stressed rock surrounding the stope. With mining of the secondary stope, additional stress relief occurs as induced stresses are redirected away from the adjacent backfilled stopes, onto the abutments.

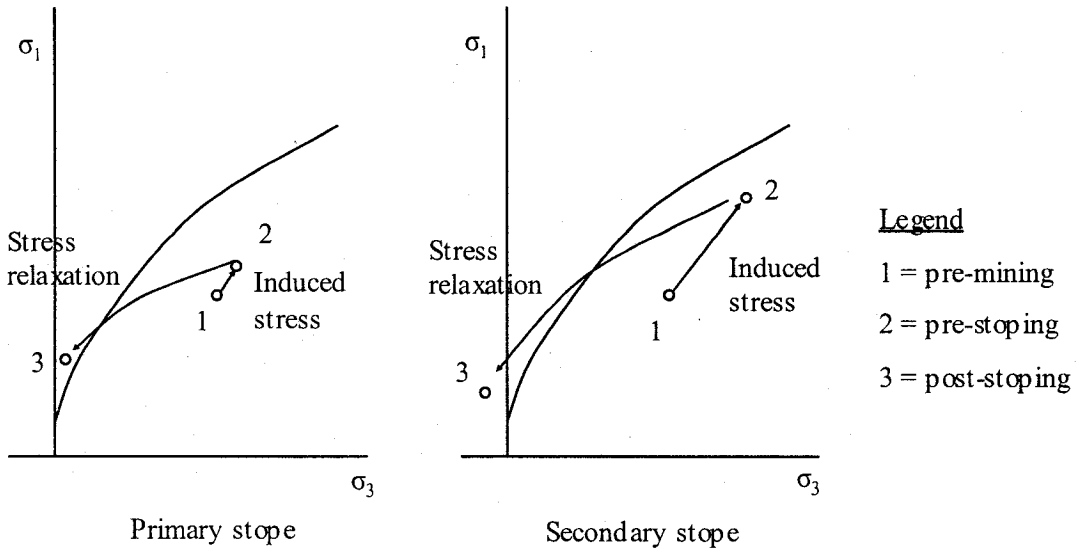

Figure 6.67 Schematic stress paths – primary and secondary stopes

CHAPTER 7

CONCLUDING REMARKS

Unplanned ore dilution or stope overbreak, which has a direct and large influence on the cost of a stope, and ultimately on the profitability of a mining operation, can be attributed to both the mining process and to geologic setting. The primary objective of the research undertaken was to establish new models for stope and orezone design, with respect to anticipated stope overbreak, focusing on the position and type of stope within the orezone extraction sequence. Identified factors influencing unplanned dilution, such as induced stress environment, stope geometry, and the setting of individual stopes were considered.

The research undertaken incorporates a variety of components, including (1) parametric 3-D numerical modelling to examine influences of individual factors on hanging-wall overbreak, (2) case example analysis, and (3) orezone extraction sequence simulation, using 3-D elastic numerical modelling.

The major achievements for this research include the following:

- Established a comprehensive geomechanics database
- Developed a simple methodology to assess potential overbreak from numerically modelled orezone geometry
- Evaluated the influence of mine depth, hanging-wall dimensions, hanging-wall dip angle, stress orientation, stope type, rockmass quality and stope construction factors on hanging-wall ore dilution

- A case study of two discrete orezones at the Bousquet #2 mine, identified as Block 5 and Zone 3-1 was described. Physical characteristics and measured stope dilutions associated with stopes from both zones were compared in detail.
- Analysed relationships between modelled overbreak (*DD*) and measured overbreak (DD_{cms})
- Defined relationships between identified dilution factors
- Compared stress paths associated with primary and secondary-type stopes

7.1 Establishment of a comprehensive database

Extensive stope construction and recovery data was obtained from two discrete orezones at the Bousquet #2 mine. The data for this research was compiled during numerous site visits to the Bousquet #2 mine between 2000 and 2002. Based on stope mining information, rockmass mapping and classification, as well as CMS survey data, a comprehensive empirical database, consisting of 172 stope histories was established for the study. The following information was included in the database:

- Stope construction details, including stope drilling and blast design,
- Stope excavation details, including CMS results and the stope cycle time between blasting and the CMS survey,
- Stope type category,
- Stope sequencing within the mining block,
- Geology and rockmass structures,
- Stress environment, and
- Rockmass classification

The database is an important resource for the dilution study. The comprehensive database is presented in Appendix B.

7.2 Quantifying ore dilution

A simple methodology was developed to assess potential overbreak from numerically modelled 3-D orezone geometry. Hanging-wall stresses of individual stopes were plotted onto grid planes placed at the mid-span and mid-height of the stope. The extent of the potential relaxation zone was determined from iso-contours of minimum principal stress (σ_3) associated with a given stope. For the parametric study, hanging-wall relaxation depth was defined as the maximum depth of the $\sigma_3 = 0$ MPa iso-contour

The volume of potential hanging-wall relaxation for a given 3-D stope geometry was represented as the volume of half a prolate ellipsoid, V_{pe}, which is defined as:

$$V_{pe} = 2/3\pi \cdot r_1 \cdot r_2 \cdot r_3 \ (m^3) \qquad (7\text{-}1)$$

where: r_1, r_2, and r_3 are radial distances from centre of stope to σ_3 stress iso-contour; r_1 = perpendicular radius distance, r_2 = vertical radius distance, r_3 = horizontal radius distance

For three-dimensional simulations, the ore Dilution Density (*DD*) is a term introduced in this study to denote potential hanging-wall overbreak. *DD* represents the volume of potential relaxation, bound by a specified minimum principal stress contour, such as the zero stress contour ($\sigma_3 = 0$ MPa).

$$DD = V_{pe} / (l' \cdot h') \qquad (7\text{-}2)$$

where: V_{pe} is the volume of half of a prolate ellipsoid (m^3), and

l' and h' represent modelled hanging-wall surface area (m^2); l' represents modelled strike length, and h' refers to the modelled stope height.

For overbreak data measured by cavity survey (CMS) from mined stopes, measured Dilution Density (DD_{cms}) is a term introduced in this study. It is the volume of overbreak on an exposed surface, and is expressed as:

$$DD_{cms} = \frac{\text{Surveyed Overbreak Volume } (m^3)}{\text{Surface area exposed } (m^2)} \quad (7\text{-}3)$$

The *DD* and DD_{cms} terms both express a measure of overbreak. However, they are calculated from differing sources: DD_{cms} is derived from observed overbreak volume, measured via a cavity survey of the excavated stope. *DD* represents overbreak simulated by the distribution of σ_3 stresses around stope blocks created in a 3-D elastic stress model.

7.3 Impact of individual factors on hanging-wall dilution

Parametric numerical modelling studies were undertaken to examine the impact of a variety of factors on hanging-wall ore dilution. The influence of mine depth, hanging-wall dimensions, hanging-wall dip angle, stress orientation, stope type, rockmass quality and stope construction factors on hanging-wall ore dilution were evaluated.

The parametric study considered two criteria for overbreak: (i) the volume of relaxed ground available for overbreak, assuming the rockmass has no tensile strength, represented by the $\sigma_3 = 0$ MPa; and (ii) the $\sigma_3 = \sigma_t$ contour, which considers the rockmass tensile strength.

7.3.1 Effect of mining depth

Stope mining depth was found not to play a significant role in the extent of $\sigma_3 = 0$ MPa contour within the hanging-wall as overbreak associated with σ_3=0 contour does not increase significantly with depth. For example, as the mining depth increases from 750m to 2250m, the increase in *DD* is only 0.05m or 8.6% for a 20m long stope.

However, for stopes with strike lengths exceeding 15 meters, overbreak associated with rockmass tensile strength (σ_t) contour increased with depth. With a 20m long stope, the severity of potential dilution associated with the $\sigma_3 = \sigma_t$ contour increased from 0.02m to 0.2m between shallow and moderate depth. As

mining depth increased from 1500m to 2250m depth, *DD* associated with the $\sigma_3 = \sigma_t$ contour increased from 0.2m to 0.28m.

7.3.2 Dilution density relationship with varying stope height and strike length

Stopes with large vertical and short horizontal dimensions or stopes having long horizontal and short vertical dimensions are more stable than large square-like stopes. Rectangular stopes with vertical height and strike lengths of 15m or less are more stable than large rectangular stopes. *DD* is reduced for stopes with Aspect Ratios of 0.5 or less, or rectangular stopes with vertical height and strike lengths less than 15m. Increased overbreak is associated with Aspect Ratios of 1.

7.3.3 Effect of hanging-wall dip angle on dilution density

Modelled overbreak increased as the hanging-wall dip angle becomes increasingly shallow. The influence on hanging-wall dip angle on overbreak is more pronounced as strike length increases. For a 30m high × 30 long stope, overbreak increases by 0.22m or 29% when the dip angle changes from 80° to 60°.

7.3.4 Effect of stress orientation on dilution density

Modelled overbreak is reduced when the orientation of pre-mining principal stress (σ_1) is parallel to the strike of the stope. A decrease in *DD* by 0.08m or 16% occurs when pre-mining stresses are parallel rather than perpendicular on a 20m long stope. Major principal stress orientation influences stope overbreak as strike length increases beyond 20m for a 30m high stope.

7.3.5 Effect of rockmass quality on dilution density

The influence of rockmass quality did not impact Dilution Density values associated with the $\sigma_3 = 0$ contour. With the elastic numerical modelling, the shape of the $\sigma_3 = 0$ contour varied with stope shape and was not influenced by rockmass quality. However, Dilution Density values associated with the $\sigma_3 = \sigma_t$ contours varied across the three quality ranges. A high quality rockmass has a more competent structure and will have greater tensile capacity prior to failure. As a result, the severity of anticipated overbreak diminishes as the rockmass quality of the host rock increases.

7.3.6 Effect of stope type on dilution density

Five stope types were identified, based on their position within a tabular blasthole mining sequence. Three stope types are classified as primary (P1, P2 and P3) and two are secondary stopes (S1 and S2). The type of stope influences the severity of modelled overbreak. Overbreak potential increased slightly between the three primary stope types, and increased significantly when comparing the primary and secondary stope types. In a general sense, this can be expressed as:

$$DD_P < DD_{S1} < DD_{S2} \qquad (7\text{-}4)$$

where: $DD_P = DD$ generated by primary (P1, P2 and P3) type stopes

$DD_{S1} = DD$ generated by S1-type stopes

$DD_{S2} = DD$ generated by S2-type stopes

7.3.7 Effect of Construction factors on dilution density

Stope construction refers to the techniques employed to prepare and extract a stope block. The various components involved with the design, drilling, and excavation of an individual stope play a critical role determining mining success.

Three construction factors (DD_{Cf}) were identified: Blasting, drillhole deviation and undercutting. Blast damage may generate a zone of decreased rockmass

quality at the stope boundary, to a depth exceeding one meter within the hanging-wall. The severity of blast vibration damage diminishes away from the stope boundary. With blasting, the severity of overbreak was reduced by limiting blast vibrations to less than 600 mm/second within hanging-wall rock. A good quality host rockmass is less susceptible to blast vibration damage.

Dilution associated with drill hole deviation is largely governed by human error and operator skill. Overbreak damages are reduced by good operator practices, such as avoiding set-up errors, and using good, well maintained equipment.

The extent of hanging-wall undercutting on both the top and bottom sill exposures directly influence overbreak. Overbreak increases as the depth and lateral extent of undercutting increases.

7.4 Case study of Bousquet #2 Mine

The Bousquet #2 mine operation was described in detail. Two individual orezones, identified as Block 5 and Zone 3-1 were described and compared. Physical differences between the two zones included depth below surface, method of hanging-wall reinforcement, hanging-wall dimensions and stope volume. Physical similarities included rockmass characteristics of the host rock, construction factors (such as workforce skill, equipment used, mining method and production drill patterns), orientation with respect to pre-mining stresses, and dip of the stope hanging-walls.

The severity of hanging-wall overbreak, as measured by CMS scans, was assessed for Zone 3-1 and Block 5. See Figure 7.1.

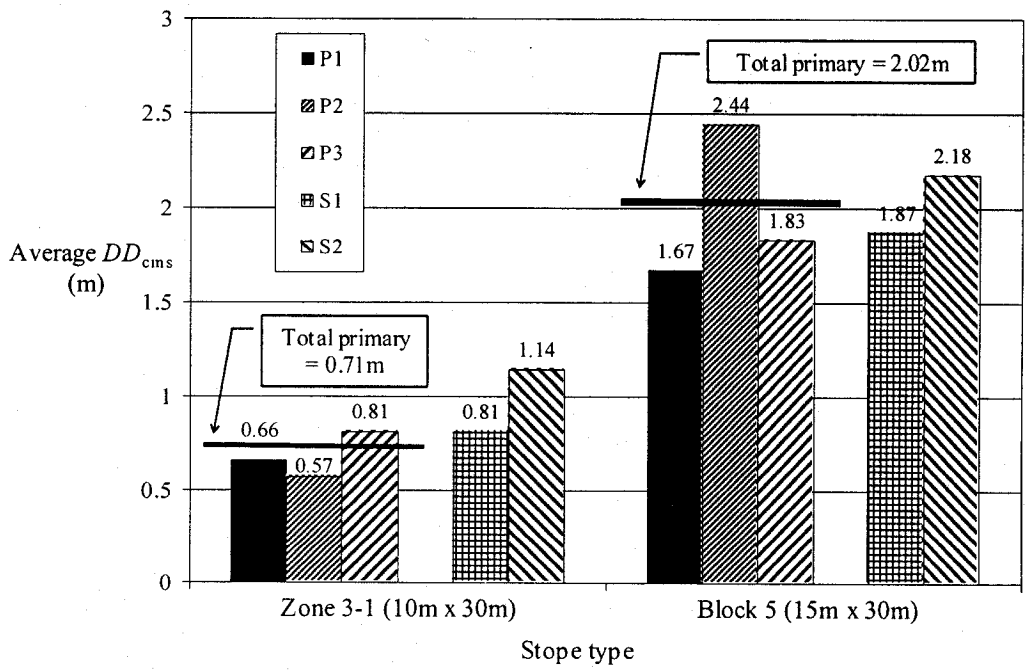

Figure 7.1 Average measured hanging-wall Dilution Density verses stope type

With Zone 3-1, average hanging-wall overbreak associated with secondary stopes was found to exceed that of primary stope types by 69%. In Block 5, hanging-wall overbreak associated with secondary stopes was found to exceed that of primary stope types by 9%. However, it was shown that the magnitude of Block 5 hanging-wall dilution was influenced by the presence of cablebolt reinforcement. When considering only those stopes supported by cablebolts installed in an unfavourable orientation (cablebolts fanning upwards), average hanging-wall overbreak associated with secondary stopes was found to exceed that of primary stope types by 16%.

Although at greater depth, Zone 3-1 stopes, with smaller hanging-wall dimensions, generated significantly less hanging-wall overbreak that did Block 5 stopes. Mean DD_{cms} values for Zone 3-1 stopes were 0.94m, values for Block 5 were DD_{cms} = 1.96m

The relationship between the hanging-wall hydraulic radius (*HR*) and the measured hanging-wall overbreak (DD_{cms}) of stopes from both Zone 3-1 and

Block 5 was examined. When the stope data was plotted according to the type of stope within the mining sequence, clustering of data suggested a linear relationship between the two factors. By plotting the upper bound of the primary and secondary stopes, conservative design estimates of DD_{cms}, based on hydraulic radius were developed. These design estimates are represented by the following relationships:

$$\text{Primary stopes: } DD_{cms} = (2.1 \cdot HR) - 5.2 \qquad (7\text{-}5)$$

$$\text{Secondary stopes: } DD_{cms} = (2.1 \cdot HR) - 4.5 \qquad (7\text{-}6)$$

where: HR = Hydraulic Radius (m), represented as true stope height multiplied by stope strike length.

7.5 Comparison of measured and modelled overbreak

With this research, hanging-wall overbreak, expressed as dilution density has been determined using two approaches. Measured dilution density (DD_{cms}) represents a true assessment of hanging-wall overbreak, as determined using a physical CMS scan of the mined stope. The second approach uses 3-D numerical modelling techniques to estimate potential dilution density (DD) based on the extent of an envelope of low confinement stress, defined by the extents of σ_3.

Detailed numerical models of the designed stopes of Block 5 and Zone 3-1 were constructed in Map3D, based on the initial planned stope design and geometries. Individual stopes were modelled according to the actual stope sequencing for the two zones. At each successive mining step, the extent of a given iso-contour of σ_3 was determined. A database, summarized in Appendix C, was constructed in which values of modelled stope hanging-wall dimensions, stope type, radius distances of the three axes of the prolate ellipsoid, and calculated Dilution Densities are compiled for individual stopes and averaged for each stope type.

The data trends revealed similarities between Block 5 and the smaller Zone 3-1 stopes. For both orezones, primary stope types cluster closely together, typically within a range of DD = 0.15m +/-. S2-type stopes exhibit the greatest modelled

overbreak, typically in the range of 0.62 to 1.06m *DD* greater than an averaged primary stope for a given σ_3 contour (varying between Zone 3-1 and Block 5). S1-type stopes occur between the S2 and P-type stopes. Typically, potential modelled overbreak values in the range of 0.31m to 0.75m *DD* greater than an averaged primary stope were generated (again, varying from Zone 3-1 to Block 5).

To assess linkage between the DD_{cms} and *DD* approaches, *DD* versus σ_3 relationships were compared against the average DD_{cms} values for each stope type. Figure 7.2 shows the example for Zone 3-1 stopes. Low range compresive stress conditions are represented σ_3 values exceeding σ_3 = 0 MPa. The intercept of the measured DD_{cms} value with the DD/σ_3 distribution identifies what σ_3 contour value corresponds to an appropriate *DD* in the numerical model. For both orezones, the DD_{cms} value for primary stopes intercepted the *DD* curve at a σ_3 contour value exceeding that of either of the secondary stope types. Similarly, the DD_{cms} value for S1-type secondary stopes intercept the *DD* curve at a σ_3 contour value lower than both the P-type and S2-type stopes.

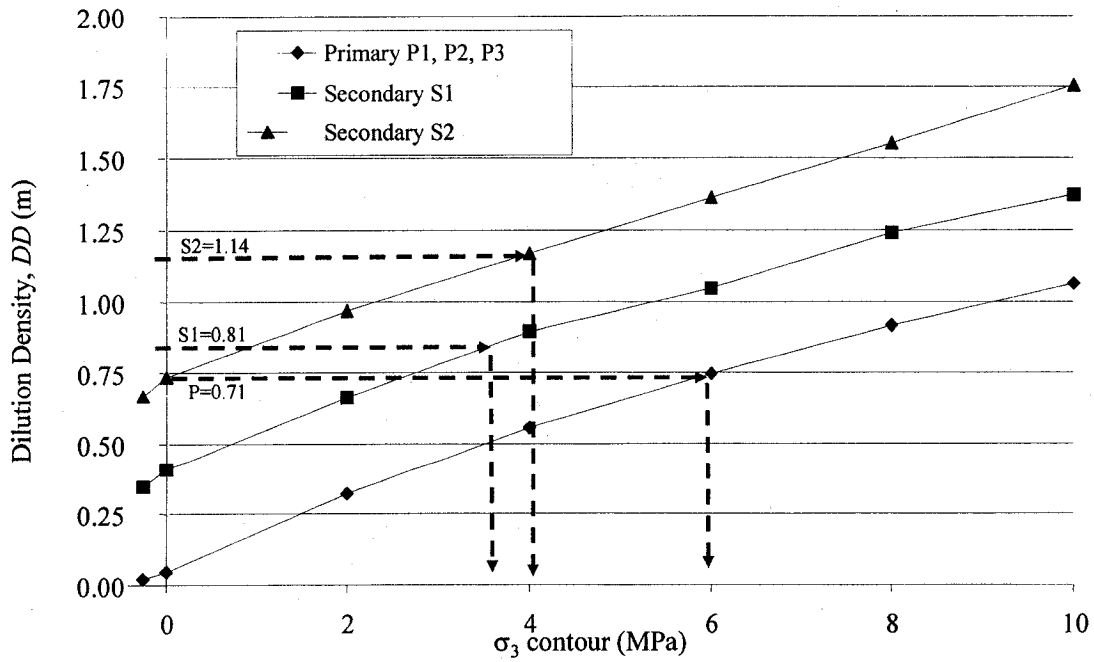

Figure 7.2 Average *DD* versus σ_3 contour, Zone 3-1 stopes

Relationships were established between DD and DD_{cms}, based on ranges of modelled σ_3 contours. Intercepts of measured DD_{cms} with modelled DD curves for specific stope types are combined in Figure 7.3, which plots the contours of modelled σ_3 that correspond to measured average overbreak for primary (P-type) and secondary (S1 and S2 –type) stopes.

Two clusters occur in Figure 7.3. Primary stope values are associated with σ_3 contours exceeding 6MPa. Projecting a linear trend line between the 10m and 15m strike lengths, an inclined slope is generated. Secondary stopes are associated with σ_3 contours in the range of 4 to 5MPa. Linear trend lines between 10m and 15m strike lengths are steeper than that of primary stopes.

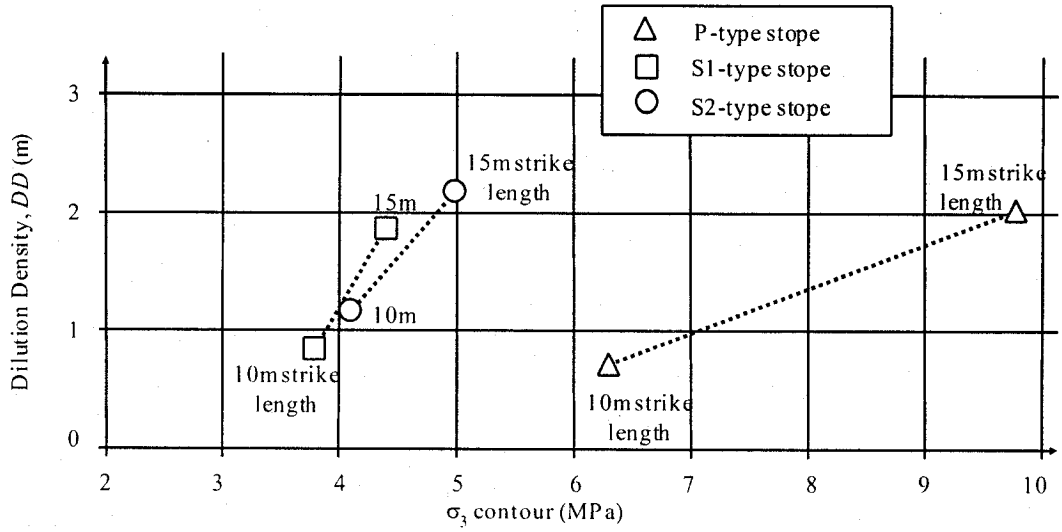

Figure 7.3 Modelled σ_3 contours corresponding to measured DD_{cms} overbreak values

7.5.1 Relationship between modelled and measured dilution density

A comparison of measured overbreak (DD_{cms}) and overbreak simulated by the numerical model (DD) reveals that the numerical modelling predictions, based solely on the σ_3= 0 MPa iso-contour, underestimate actual values. By definition, numerical modelling represents an idealized simplification of physical characteristics. Simplifications and limitations of the numerical modelling

approach used includes both the type of modelling tool used, and the methodology employed to calculate modelled overbreak.

The approach adopted for this study can be used to predict reasonable numerically modelled estimates of overbreak severity for individual stope types with height of 30m and strike lengths ranging between 10m and 15m. The use of specific contours of σ_3 represents an adjustment factor between the measured overbreak and modelled simulation.

7.6 Relationships between dilution parameters factors

Four categories of factors that influence overbreak are: (i) initial design, (ii) stope excavation, (iii) stope recovery, and (iv) data integration. Relationships between these factors are illustrated in Figure 7.4. Some factors, such as geology and rockmass quality, are inherent to a given mine setting. Others are due to large scale (mine-wide) and small scale (stope-wide) planning and design.

The relationship shown in Figure 7.4 is iterative. Initial design, followed by stope excavation, influence the success of stope recovery. Data integration, in the form of analysis of CMS data and/or numerical modelling, provides insight that can influence subsequent stope design.

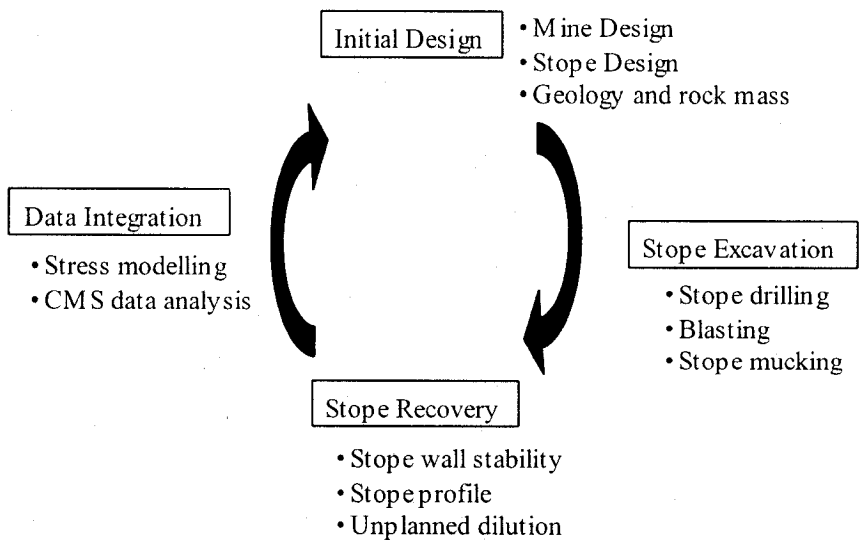

Figure 7.4 Stope overbreak categories

Hanging-wall overbreak was expressed as dilution density for both simulated overbreak (DD) and observed overbreak volume, measured via a cavity survey of the excavated stope (DD_{cms}).

From parametric study, two dilution parameters were identified: (i) Confinement overbreak (DD_T), corresponding with the $\sigma_3 = \sigma_t$ contour, represents dilution that will occur as a result of tensile failure of the hanging-wall rock, and (ii) No-tension overbreak (DD_0), corresponding to the $\sigma_3 = 0$ MPa contour, represents overbreak that may happen. The $\sigma_3 = 0$ MPa contour indicates transition from tension to compression state. The No-tension overbreak contour varies with stope geometry and hanging-wall dip, and is roughly independent of depth. The extent of Confinement overbreak increases with depth for a given stope geometry or hanging-wall dip angle. DD_T is a less conservative estimate of ore dilution density than DD_0

Two other factors influence the likelihood of dilution occurring within (and beyond) the envelope of No-tension overbreak. External Factors (DD_E) represent physical conditions of the stope setting that influence hanging-wall stability. These conditions include rockmass quality, orientation of principal stress, and stope type. Construction Factors (DD_{Cf}) are human influences impacting overbreak, such as blasting, drillhole deviation, and undercutting.

No-tension overbreak (DD_0) represents overbreak that may happen, depending largely on the severity of Construction Factors (DD_{Cf}) in damaging the tensile capacity of the rockmass. Confinement overbreak (DD_T), which increases with depth, represents dilution that will occur as a result of tensile failure of the hanging-wall rock into the mined stope. The magnitude of overbreak may be further increased by External Factors (DD_E).

Relationships between the factors DD, DD_{cms}, DD_0, DD_T, DD_{Cf}, and DD_E are illustrated in Figure 7.5. As previously mentioned, the relationship is iterative.

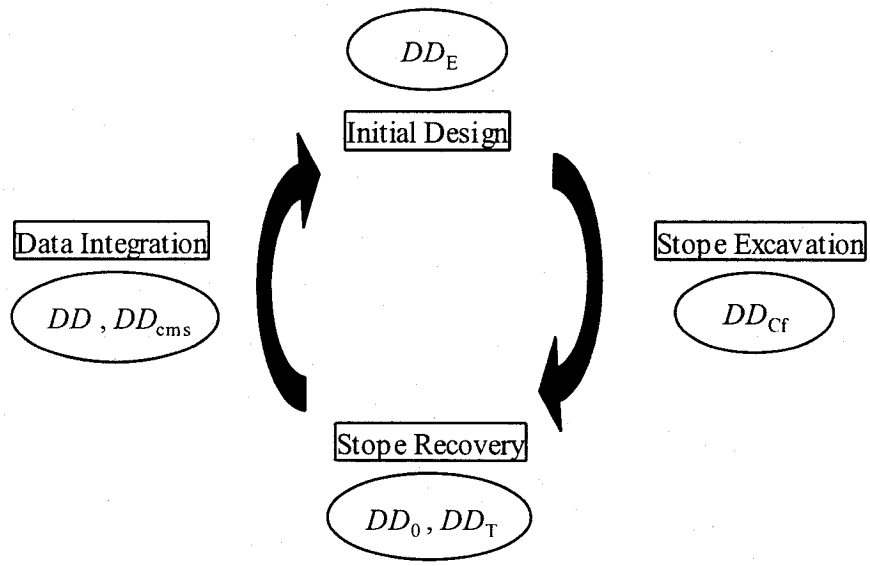

Figure 7.5 Stope overbreak factors

7.7 Comparison of primary and secondary stope failure modes

Measured overbreak varies with stope type, with secondary stopes generating a greater volume of hanging-wall dilution than do primary stopes. This was observed in: (i) Parametric studies; (ii) the stopes of Zone 3-1 stopes, (iii) in stopes of Block 5 that had not been reinforced by downward fanning cablebolts, and (iv) in numerical modelling stope types associated with the sequencing of Block 5 and Zone 3-1. Typically, the following relationships were observed:

$$DD_{cms} \text{ (secondary stopes)} > DD_{cms} \text{ (primary stopes)} \quad (7\text{-}7)$$

$$DD \text{ (secondary stopes)} > DD \text{ (primary stopes)} \quad (7\text{-}8)$$

Blast vibration monitoring results indicated that mining of secondary stopes occur within a lower stress environment. Underground at Bousquet #2 mine, this apparent stress reduction was associated anecdotally by a reduced requirement for re-drilling of production blastholes, and by fewer accounts of working ground.

The contrasts between primary and secondary stopes suggest differing mechanisms for associated with the generation of potential hanging-wall dilution.

Differences may be attributed to pre-conditioning, in the form of relaxation or degregation of the secondary stope hanging-wall. Rockmass relaxation refers to stress reduction parallel to the excavation wall. Rockmass degradation describes conditions where the rockmass quality and thus the rockmass strength has been reduced relative to its virgin state by stress-induced damages.

7.7.1 Hanging-wall stress setting

To assess hanging-wall stress conditions, primary (P-type) and secondary (S1 and S2-type) stopes were examined using Map3D numerical modelling. Modelled σ_1 and σ_3 stresses were measured at specific depths within the hanging-wall. For each stope, three stress setting were compiled: pre-mining stress, pre-stope stress and post-stope stress. Pre-mining stress refers to the natural stress setting, prior to the onset of orezone extraction. Pre-stope stress represents the local, induced stress state in the immediate vicinity of the planned stope at the time of the onset of stope mining. Post-stope stress is the local stress state in the vicinity of the mined, unfilled stope.

Stress path trends, associated with the pre-mining, pre-stope, and post-stope stages illustrate differences between the performance of primary and secondary stope hanging-walls. In close proximity to the stope wall, it was noted that the secondary stopes experience a greater degree of pre-conditioning – in the form of both stress-induced damage by prior mining (pre-stoping) and stress relaxation (post-stoping). Pre-conditioning was greatest with the S2-type stope.

Following production blasting of primary stopes, stresses are redistributed around the stope. Pre-conditioning of the secondary stope hanging-wall, due to these induced stresses resulted in rockmass yielding and an envelope of de-stressed rock surrounding the stope. With mining of the secondary stope, additional stress relief occurs as induced stresses are redirected away from the adjacent backfilled stopes, onto the abutments.

7.8 Summary

As indicated in Chapter 2, the impact of mining-induced dilution on mine scheduling is not properly accounted for in underground mine design. Mine design assumptions of dilution as a fixed value or percentage are incorrect. Influences of orezone extraction sequencing, and the design and construction of individual stope blocks are overlooked in common empirical assessments for mine and stope design. For example, most mine designs fail to consider the influence that the type of stope has on ore dilution.

Through parametric and case studies, it was demonstrated that, in addition to stope dimension, the amount of unplanned dilution differed according to stope type.

- Overbreak associated with secondary stopes exceeds that of primary stopes
- Overbreak associated with S2-type secondary stopes exceeds that of S1-type secondary stopes

If one were to emphasise minimization of unplanned dilution within a steeply dipping, tabular orebody with orezone widths of 4 to 15 meters, a pillarless mining sequence, comprised of primary and S1-type stopes, will generate less overall dilution that a primary stope – secondary pillar (primary and S2-type stopes) mining sequence.

Hanging-wall overbreak can be further managed through a reduction in the dimension the exposed hanging-wall, and by the installation of downwards-dipping cablebolt reinforcement. Upwards-dipping cablebolt reinforcement was shown to be less effective.

7.9 Recommendations for future research

This study has investigated and quantified relationships between modelled and measured hanging-wall overbreak. Extension of this present investigation in future work by others is recommended in such areas as:

- Compile detailed records of orezone extraction from a variety of orezones, at other mine sites, representing a diverse range of stoping environments.
- Using an elastic 3-D numerical model, expand on the numerical modelling methodology developed in this research for quantifying anticipated hanging-wall overbreak for stopes with dimensions outside the 30 x 10m to 30 x 15m range.
- Re-analyse the data documented in this study with 3-D non-linear numerical modelling software. Non-linear failure, being beyond the capability of the Map3D software, was identified as a limitation of the modelling.

REFERENCES

Adler, L., and Thompson, S.D., 1992. Mining methods classification system. SME Mining Engineering Handbook, 2nd Edition, Chapter 8.1. pg 531-537.

Alcott, J., 2002. Développements et défis en contrôle de terrain à la mine Campbell. In Proc. 17e A.M.Q. Colloque en Contrôle de Terrain, Val D`Or, Québec, March 2002, 8 pg.

Alcott, J.M., and Kaiser, P.K., 1999. Stability hazard and risk assessment (SHARK). Final report to Canadian Mining Research Organization (CAMIRO), Mining Division, 136 pg.

Alcott, J.M., Kaiser, P.K., Gauthier, M., Nelson, D., and Mah. P., 1999. SHARK: Stability hazard and risk assessment at Placer Dome's Campbell Mine. Proc. 14th A.M.Q. Colloque en Contrôle de Terrain, Val D`Or, Québec, March 1999.

Anderson, B., and Grebenc, B., 1995. Controlling dilution at the Golden Giant mine. In Proc. 12th CIM Mine Operators Conference, Timmins, February 1995.

Andrieux, P., and Rodgers, K., 1997. Controlled blasting for improved open stope wall stability at Brunswick mining. 13th CIM Mine Operators Conference, Sudbury, Ont. February 1997. 9 pg.

Andrieux, P., and Heilig, J., 1994. Near-field blast vibration monitoring - practical considerations and issues. 17e Session d'étude sur les techniques de sautage, Université Laval, Québec City, 3-4 November 1994.

Annels, A.E. 1996. Ore Reserves: Errors and Classification. Institution of Mining and Metallurgy, Section AS, Vol. 105 (A137-83, Sept. – Dec.), pp.A150-A162.

Arjang, B., and Herget, G., 1997. In situ ground stresses in the Canadian hardrock mines: an update. Int. J. of Rock Mech. & Min. Sci. 34: 3-4, Paper No. 015. 9 pg.

Arjang, B., 1996. In situ ground stresses in the Abitibi Mining District. CIM Bulletin Vol 89, No. 996.

Arjang, B., 1988. Pre-mining ground stresses at the Bousquet/Dumagami mines, Cadillac, Quebec. Division Report MRL 88-132 (TR), CANMET, Energy, Mines and Resources Canada.

Atlas Powder Company, 1987. Explosives and Rock Blasting. Dallas, TX, 662 pg. ISBN 0-9616284-0-5.

Barrett, J.R., Coulthard, M.A., and Dight, P.M., 1978. Determination of fill stability. Mining with Backfill, proc. 12th Canadian Rock Mechanics Symposium, Sudbury, Ont. 23-25 May 1978. CIM Special Volume 19.

Barton, N., Lien, I., and Lunde, J., 1974. Engineering classification of rock masses for the design of tunnel support. Rock Mechanics, 6(4): 186-236.

Bastien, J., 2001. Développement et exploitation souterraine, puits Penna. 103rd CIM Annual General Meeting, Québec City, Québec, 10 pg. (on CD).

Bauer, A., and Calder, P.N., 1978. Open Pit and Blast Seminar, Course #63-321. Queen's University Mining Engineering Department, Kingston, Ontario.

Bawden W.F., Hyett, A.J., Lausch, P., Moosavi, M., deGraaf, P., and Ruest, M., 1998. The S.M.A.R T. cable bolt: results from two initial field trials. In Proc. 100th CIM Annual General Meeting, Montreal, Québec, 3-7 May 1998, 11 pg (on CD).

Bawden, W.F., 1997. Optimization of Cable Bolt Reinforcement for Underground Mining. Interim Report #4, 1997 - 1998 NSERC/Industry CRD Progress Report. (Internal Report).

Bawden, W.F., and Hyett, A.J., 1994. A Field Cable Bolt Pull Test Programme - for LAC Minerals at Bousquet Division - Mineshaft 2. (Internal Report).

Bawden, W.F., 1993. The use of rock mechanics principals in Canadian underground hard rock mine design. Volume 5, Comprehensive Rock Engineering, Hudson, J.A., et al., eds., Pergamon Press.

Bawden, J.W., Nantel, J., and Sprott, D., 1989. Practical rock engineering in the optimization of stope dimensions – applications and cost effectiveness. CIM Bulletin, Vol. 82, No. 926, pp. 63-71.

Beauchamp, K.J., and Cameron, A.R., 1999. Optimizing underground stoping efficiency. In proc. 14th CIM Mine Operators Conference, 21-25 Feb 1999, Bathurst, N.B. 8 pg.

Belford, J.E., 1981. Sublevel stoping at Kidd Creek Mines. Design and Operation of Caving and Sublevel Stoping Mines, Chap. 42, D. Stewart, ed., SME-AIME, New York, pp. 577–584.

Bieniawski, Z.T., 1989. Engineering Rock Mass Classifications. 1989 John Wiley & Sons, Inc., New York. ISBN 0-471-60172-1. 251pg.

Bieniawski, Z.T., 1984. Rock Mechanics Design in Mining and Tunnelling. A.A. Balkema, Rotterdam, 1984. 272 pages

Bieniawski, Z.T., 1976. Rock mass classification in rock engineering. In: Bieniawski ZT, editor. Exploration for rock engineering, Proceedings of the Symposium, vol. 1. Rotterdam: Balkema. p. 97–106.

Board, M., Brummer, R., and Seldon, S., 2001. Use of numerical modeling for mine design and evaluation. Underground mining methods: engineering fundamentals and international case studies. Hustrulid, W.A., and Bullock, R.L., (eds), Society for Mining, Metallurgy, and Exploration, Inc., Littleton, Colorado, USA, pp 482-491.

Board, M., Brummer, R., Kaiser, P.K., and Tannant, D., 1996. Kidd Creek deep mining risk assessment – Phase 2 report. Internal report to Falconbridge Limited, Kidd Creek Division. 111p.

Boldt, J.R. and Queneau, P., 1967. The winning of nickel. Longmans Canada Limited, Toronto. 487p.

Brady, B.H.G. and Brown, E.T., 1985. Rock Mechanics for Underground Mining. Chapman and Hall, London.

Bronkhorst, D., and Brouwer, G., 2001. Sublevel stoping at the Williams mine. Underground mining methods: engineering fundamentals and international case studies. Hustrulid, W.A., and Bullock, R.L., (eds), Society for Mining, Metallurgy, and Exploration, Inc., Littleton, Colorado, USA, pp 235-238.

Bronkhorst, D., Rheault, J., and Ley, G.M.M., 1993. Geotechnical principals governing mine design at the Williams Mine. Innovative Mine Design for the 21st Century, Bawden and Archibald (eds), Balkema, Rotterdam, pp.433-442. ISBN 90 5410 325 6

Bruce, D.A., and Kord, F.M., 1992. The stabilization of loose backfill by drilling and grouting techniques. Rock Support in Mining and Underground Construction, Kaiser and McCreath eds, A.A. Balkema, Rotterdam, 227-236.

Butcher, R.J., 2000. Dilution Control in Southern African Mines. In proc. MassMin 2000, Brisbane, Australia, 29 October - 2 November 2000, pp. 113-118.

Cai, M., Kaiser, P.K., Uno, H., Tasaka, Y., and Minami, M., 2004. Estimation of rock mass strength and deformation modulus of jointed hard rock masses using the GSI system. Int. J. Rock Mech. Min. Sci. 41 (1), 3-19, 2004

Calvert, T.M., Simpson, J.B., and Sandy, M.P., 2000. Open Stope Design at Normandy Golden Grove Operations. In proc. MassMin 2000, Brisbane, Australia, 29 October - 2 November 2000. pp. 653-659.

Cambior, 1997. Second quarter 1997 financial report. Cambior Inc., 15 pg.

Cameron, A., Forsyth, B., and Steed, C., 1995. Blasting practices for the reduction of damage and dilution on open pit and underground mines. 12th CIM Mine Operators Conference, Timmins, Ont. February 1995. 14 pg.

Canadian Mining Journal, 2003. 2003 Mining Sourcebook, 112th annual edition. Scales, M., ed. Business Information Group, Don Mills, Ontario. ISSN 0840-6723.

Canadian Mining Journal, 2002. 2002 Mining Sourcebook, 111th annual edition. Scales, M., ed. Business Information Group, Don Mills, Ontario. ISSN 0840-6723.

Choquet, P., 1988. Rockbolting practical guide. CANMET SP88-15E. 266p.

Clark, L., 1998. Minimizing dilution in open stope mining with a focus on stope design and narrow vein longhole blasting. M.Sc. Thesis, University of British Columbia.

Clark, L.M. and Pakalnis, R.C., 1997. An empirical design approach for estimating unplanned dilution from open stope hangingwalls and footwalls. In Proc. 99th CIM Annual General Meeting, Vancouver, British Columbia. 33pg.

Clow, G., 1991. Why gold mines fail. The Northern Miner Magazine, Vol. 6, No. 2, pp 31-34.

Connors, C., Wheeler, L., Forsyth, B., and Clark, L., 1996. Determination of blast damage mechanisms in low quality rock masses. CANMET DSS File 02SQ.23440-4-1046.

Corlett, A.V., 1970. Ore reserves and dilution. In Proc. 72nd CIM Annual General Meeting, Toronto, April 1970. 12pg.

Cotesta, L., Lidkea, W., and Martin, D. 1999. Quality control in drift development. 101st CIM Annual General Meeting, Calgary, Alberta. 2-6 May 1999. 11pg.

Deere, D.U., 1968. Geological consideration. In: Stagg KG, Zienkiewicz OC, editors. Rock mechanics in engineering practice. NewYork: Wiley, 1968.

De la Vergne, J., 2000. Hard rock miner's handbook, Edition 1. McIntosh Redpath Engineering, North Bay, Ontario, 430 pp. ISBN 0-9687006-0-8.

Diederichs, M.S, Kaiser, P.K., and Suorineni, F., 2000. The impact of abutment relaxation on stability of underground mine openings. In Proc. 4th Northern American Rock Mechanics Symp. (NARMS), Seattle, Washington, pp 481-488.

Diederichs, M.S., 1999. Instability of hard rock masses: the role of tensile damage and relaxation. PhD Thesis, University of Waterloo, 566 p.

Diederichs, M.S., and Kaiser, P.K., 1999. Tensile strength and abutment relaxation as failure control mechanisms in underground excavations. Int. J. of Rock Mechanics and Mining Sciences & Geomechanical Abstracts, 36: 69-96.

Diederichs, M.S., and Kaiser, P.K. 1996. Rock Instability and risk analysis in open stope mine design. Canadian Geotechnical Journal. Vol 33, pp 431-439.

Doucet, C., and Harvey, A., 2001. Utilization du remblai en pâte dans les mines filioniennes: La Mine Doyon. In proc. International Symposium on Mining Techniques of Narrow-Vein Deposits, Val-d'Or, Québec, 1-4 October 2001, pp. 73-78.

Dunne, K., and Pakalnis, R.C., 1996. Dilution aspects of a sublevel retreat stope at Detour Lake Mine. Rock Mechanics, Aubertin, Hassani and Mitri (eds), 1996 Balkema, Rotterdam, pp. 305-313. ISBN 90 5410 838 X.

Dunne, K., Pakalnis, R., Mah, S., and Vongpaisal, S., 1996. Design analysis of an open stope at Detour Lake Mine. 98th CIM Annual General Meeting, Edmonton, Alberta, 16 pg.

Elbrond, J., 1994. Economic effects of orelosses and rock dilution. CIM Bulletin, Vol. 87, No. 978, pp. 131-134.

Fellows, G.L., 2001. Sublevel stoping at Echo Bay's Lamefoot Mine, Republic, Wash. Underground mining methods: engineering fundamentals and international case studies. Hustrulid, W.A., and Bullock, R.L., (eds), Society for Mining, Metallurgy, and Exploration, Inc., Littleton, Colorado, USA, pp 257-262.

Forsyth, W.W., Kleine, T.H., and Cameron, A.R., 1995. Inaccurate blasthole drilling. 21st Annual Conference of the Int. Soc. of Explosives Eng., Nashville, February, 1995. 8 pg.

Forsyth, W. W and Moss, A. E., 1990. Observations on blasting and damage around development openings. In Proc. 92nd CIM Annual General Meeting, Ottawa, Ontario, 6-10 May 1990. 12pg.

Friedrich, P., and Charette, F., 1997. Geomechanical assessment or rock mass at Mine Doyon. Internal report to Cambior Inc., La mine Doyon, 27 pg.

Gauthier, J., 1992. Controle de la dilution aux Mines Agnico-Eagle, Division Laronde. 7th AMQ colloque en Contrôle de terrain, Motel Alpin, Rouyn-Noranda, Quebec. 31 March 1992. 22pg.

Gauthier, P., 2001. Minage des zones étroites à la Mine Bousquet. In Proc. International Symposium on Mining Techniques of Narrow-Vein Deposits, Val-d'Or, Quebec, 1-4 October, 2001, pp 45-55.

Gauthier, P., 2000. Optimisation des câbles d'ancrage à la mine Bousquet. 15e AMQ Colloque on contrôle de terrain, Hôtel Confortel, Val-d'Or, 21-22 mars 2000. 29pg.

Germain., P., and Hagjigeorgiou, J., 1998. Influence of stope geometry on mining performance. 100th CIM Annual General Meeting, Montreal, Quebec, 1998, 7 pg.

Germain, P., and Hadjigeorgiou, J., 1997. Influence of stope geometry and blasting patterns on recorded overbreak. Int. J. Rock Mech. & Min. Sci. 34:3-4, paper No. 115.

Germain, P., Hadjigeorgiou. J., and Lessard, J.F., 1996. On the relationship between stability prediction and observed stope overbreak. Rock Mechanics, Aubertin, Hassani and Mitri (eds), 1996 Balkema, Rotterdam, pp. 277-283. ISBN 90 5410 838 X.

Golder Associates, 1999. Review visit to la mine Bousquet July 1999. Internal report to Barrick Gold Corporation, Bousquet 2 mine.

Golder Associates Ltd., 1989. NFOLD program user manual.

Golder Associates, 1988. Detailed Geotechnical Mapping and Rock Mass Classification, Donald J. Laronde Mine, Cadillac, Quebec.

Goris, J.M., Martin, L.A., and Brady, T.M., 1993. Field Evaluation of Cable Bolt Supports. Int. J. Rock Mech. Min. Sci. & Geomech. Abstr. Volume 30, No. 7, pp. 1431-1434.

Goulet, C., and Blais, S., 2001. Utilization du remblai en pâte à la Mine Bouchard-Hébert. 16e AMQ colloque en Contrôle de terrain. 20-21 March 2001, Val-d'Or, Quebec, 21 pg.

Graham, E.P., 1968. Low cost, high dilution mining. CIM Bulletin, Vol. 61, No. 675, pp 847-853.

Grant, D., and DeKruijff, S., 2000. Mount Isa Mines - 1100 Orebody, 35 Years On. In proc. MassMin 2000, Brisbane, Queensland, 29 October - 2 November 2000, pp 591-600.

Grenier, A., and Gauthier, L., 2001. Narrow vein mining method (trials and results). In proc. International Symposium on Mining Techniques of Narrow-Vein Deposits, Val d'Or, Québec, 1-4 October 2001, pp. 25-29.

Grice, A G, 1989. Fill research at Mount Isa Mines, Innovations in mining backfill technology, (Ed: Hassani et al) pp 15-22 (Balkema: Rotterdam).

Grimstad, E. and Barton, N. 1993. Updating the Q-System for NMT. Proc. int. symp. on sprayed concrete - modern use of wet mix sprayed concrete for

underground support, Fagernes, (eds Kompen, Opsahl and Berg). Oslo: Norwegian Concrete Assn.

Hadjigeorgiou, J., Lessard, J, and Turcotte, P., 2002. Analyse des problèmes opérationnels reliés aux cheninées à minerai dans les mines du Quebéc. 17e colloque en Contrôle de terrain, Hôtel Forestel, Val-d'Or, 19-20 March, 19pg.

Hall, O., 1937. Mining at Noranda. CIM Bulletin 1937 Trans., Vol. 40, pp. 141-164.

Hamrin, H., 2001. Underground mining methods and applications. Underground mining methods: engineering fundamentals and international case studies. Hustrulid, W.A., and Bullock, R.L., (eds), Society for Mining, Metallurgy, and Exploration, Inc., Littleton, Colorado, USA, pp 3-14.

Hamrin, H., 1980. Guide to underground mining methods and applications. Atlas Copco MCT, Stockholm, Sweden. 39 Pg.

Hassani, F., and Archibald, J., 1998. Mine Backfill 1998. Canadian Institute of Mining, Metallurgy and Petroleum, CD-ROM. 263 Pg.

Heal, D., Hudyma, M., and Vézina, F., 2005. Seismic Hazard at Agnico-Eagle's Laronde Mine Using MS-RAP. In Proc. CIM Maintenance Engineering / Mine Operators conference, 21-24 February 2005, Sudbury, Ontario. 31pg.

Henning, J.G., Gauthier, P., and Mitri, H.S., 2001a. Stope blast designs at Bousquet 2 mine. 24e Session d'étude sur les techniques de sautage, Université Laval, Québec City, November 1-2, 2001. 16 pg.

Henning, J.G., Kaiser, P.K., and Mitri, H.S., 2001b. Evaluation of stress influences on ore dilution: a case study. 38th U.S. Rock Mechanics Symposium, Washington D.C., USA, July 2001. 8 pg.

Henning, J.G., and Mitri H.S., 1999. Examination of hanging-wall stability in a weak rock mass. CIM Bulletin, Vol 92, No. 1032, pp 40-44.

Henning, J.G., 1998. Ground control strategies at the Bousquet 2 mine. M. Eng. Thesis, McGill University, Montreal, Quebec. 126 Pg.

Henning, J.G., 1997. CMS – Stability graph assessment from Zone T10, T11, T15, T20 & T30 data. Internal memo, Cambior Inc., La mine Doyon. 4 pg.

Henning, J.G., Gauthier, P., Ruest, M., and Provencher, C., 1997. Étude sur la stabilité des épontes supérieures au Complexe Bousquet. 20^{e} Session d'étude sur les techniques de sautage, Université Laval, Québec City, October 1997. 12 pg.

Henning, J.G., 1996. 3-1 Zone rock mechanics assessment – summary report. Internal report, Bousquet 2 mine, 21 pg.

Herget, G., 1988. Stresses in rock. Rotterdam: Balkema.

Hoek, E., and Brown, E.T., 1998. Practical estimates of rock mass strength. International Journal Rock Mechanics and Mining Science, 34(8):1165–1186.

Hoek, E., and Brown, E.T., 1988. The Hoek-Brown failure criterion - a 1988 update. Proc. 15th Canadian Rock Mechanics Symp. (ed. J.C. Curran), 31-38. Toronto, Dept. Civil Engineering, University of Toronto.

Hoek, E., and Brown, E.T., 1980. Underground Excavations in Rock. London: Institution of Mining and Metallurgy, 527 pages.

Hoek, E., Carranza-Torres, C., and Corkum, B, 2002. Hoek-Brown failure criterion – 2002 edition. Proceedings of the 5th North American Rock Mechanics Symposium and the 17th Tunnelling Association of Canada Conference: NARMS-TAC 2002, 7-10 July 2002. Hammah, R., Bawden, W., Curran, J., and Relesnicki, M. (eds.), University of Toronto press, Toronto, Ontario.

Hoek, E., Gabrinsky, M., and Diederichs, M., 1989. Numerical modelling in rock engineering. Report to Mining Research Directorate, 18 pg.

Hoek, E., Kaiser, P.K., and Bawden, W.F., 1995. Support of Underground Excavations in Hard Rock. A.A. Balkema, Rotterdam, 215 p.

Holmberg, R. and Persson, P. A., 1979, Design of Tunnel Perimeter Blasthole Pattern to Prevent Rock Damage, IMM Proc., Tunneling, pp. 280-283.

Hutchinson, D.J., and Diederichs, M.S., 1996. Cablebolting in Underground Mines. 1996 BiTech Publishers Ltd., Richmond, British Columbia. ISBN 0-921095-37-6.

Hyett A.J., Bawden W.F., Lausch P., Ruest M., Henning J., and Baillargeon M., 1997. The S.M.A.R.T. Cable Bolt. 99th CIM Annual General Meeting, Vancouver, May 1997. 8 pg.

Hyett, A.J., Bawden, W.F., Lausch, P., Moosavi, M., Ruest, M., and Pahkala, M., 1997b. The S.M.A.R.T. Cable Bolt: An instrument for the determination of tension in 7-wire strand cable bolts. International Symposium on Rock Support - Applied Solutions for Underground Structures, Lillehammer, Norway, June 22-25 1997. E.Broch, A. Myrvrang, G. Stjern (eds.), Helli Grafisk AS, Oslo. ISBN 82-91341-18-4.

Hyett, A., 1996. Uniaxial compressive strength testing of 3-1 Zone core samples. Internal memo to Bousquet mine, Queens University. 5pg.

Hyett, A.J., Bawden, W.F., Powers, R., and Rocque, P., 1993. The nutcase cable bolt. Innovative Mine Design for the 21st Century, Bawden & Archibald (eds). Balkema, Rotterdam. ISBN 90 5410 325 6

Hyett, A.J., Bawden, W.F., and Reichert, 1992. The Effect of Rock Mass Confinement on the Bond Strength of Fully Grouted Cable Bolts. Int. J. Rock Mech. Min. Sci. & Geomech. Abstr. Volume 29, No. 5, pp. 503-524.

Itasca, 2002. FLAC Version 3.4. Itasca Consulting Group Inc., Minneapolis. USA.

Itasca, 2000. UDEC Version 3.1. Itasca Consulting Group Inc., Minneapolis. USA.

Itasca, 1995. PFC-Particle Flow Code modelling software Version 1.0. Itasca Consulting Group Inc., Minneapolis. USA.

INCO, 2002. Definitions: mineability and dilution. INCO MTS internal memo, 4 pg.

Kaiser, P.K., Suorineni, F.T., Henning, J.G., Diederichs, M.S., Cai, M., Tannant, D.D. and Hajiabdolmajid, V., 2003. Guidelines on Support Selection for Safe Rapid Drift Development. Project report to the Canadian Mining Industry Research Organization (CAMIRO), 237 p.

Kaiser, P.K., Henning, J.G., Cotesta. L., and Dasys, A., 2002. Innovations in mine planning and design utilizing Collaborative Immersive Virtual Reality (CIVR). 104th CIM Annual General Meeting, Vancouver, May 2002, 8 pg.

Kaiser, P.K., Yazici, S., and Maloney, S., 2001. Mining-induced stress change and consequences of stress path on excavation stability – a case study. Int. J. of Rock Mechanics and Mining Sciences, Vol. 38, Issue 2, pp. 167-180.

Kaiser, P.K., Falmagne, V., Suorineni, F.T., Diederichs, M.S., and Tannant, D.D., 1997. Incorporation of rock mass relaxation and degradation into empirical stope design. CIM'97, Vancouver, (CD) 18 pg.

Kaiser, P.K., Yazici, S., and Nosé, J., 1992. Effect of stress change on the bond strength of fully grouted cables. Int. J. of Rock Mechanics and Mining Sciences & Geomechanical Abstracts, 29(3): 293-306.

Kaiser, P.K., Diederichs, M., and Yazici, S., 1992. Cable bolt performance during mining induced stress change – Three case examples. Rock Support in Mining and Underground Construction, Kaiser and McCreath (eds.), 1992 Balkema, Rotterdam. ISBN 90 5410 044 3.

Kaiser, P.K., MacKay, C., and Gale, A.D., 1986. Evaluation of rock classifications B.C. Rail Tumbler Ridge tunnels. Rock Mechanics and Rock Engineering 19. pp 205-234.

Knoll, K., 1989. And now the bad news. The Northern Miner Magazine, Vol. 4, No. 6, pp. 48-52.

Lafarge Canada Inc., 1994. Bousquet #2 Mine - Cemented Rockfill Testing. Internal report, Project 94037.

Lanctôt, M., 2002. Récupération des piliers horizontaux à Niobec. 17e AMQ colloque en Contrôle de terrain. 19-20 March 2001, Val-d'Or, Quebec, 21 pg.

Lang, A.H., Goodwin, A.M., Mulligan, D.R.E., Gross, G.A., Boyle, R.W., Johnston, A.G., Chamberlain, J.A., and Rose, E.R., 1968. Economic minerals of the Canadian Shield. Geology and Economic Minerals of Canada. Economic geology report No. 1, R.J.W. Douglas (editor). Department of Energy, Mines and Resources Canada, pp152-226.

Lang, L.C., 1998. Vertical Crater Retreat: an important mining method. Techniques in Underground Mining: selections from underground mining methods handbook. Ed: R.E. Gertsch and R.L. Bullock, SME publication, Littleton, Co, USA. Pp 329-342, ISBN 0-87335-163-0.

Langefors, U., and Kihlstrom, B., 1978. The Modern Technique of Rock Blasting, 3rd ed. John wiley & Sons, ISBN 0-470-99282-4, 438pp.

Laubscher D.H., 1990. A geomechanics classification system for the rating of rock mass in mine design. J South Afr Inst Min Metall 1990; 90(10):257–73.

Ley, G.M., Steed, C.M., Bronkhorst, D., and Gustas, R., 1998. Mining under backfill. CIM Bulletin, Vol. 91, No. 1020, pp. 65-71.

Liu, Q., Lizotte, Y., and Proulx, R., 1995. Les causes du dommage au massif rocheau dans les tiers longs trous. 18e SEEQ session d'étude sur les techniques de sautage, Université Laval. 2 - 3 November 1995. 17 pg.

Lizotte, Y. and Scoble, M. J., 1994. Geological control over blast fragmentation. CIM Bulletin, Volume 87, No. 983, pp. 57-71.

Mackenzie, C.K., 1987. Blasting in hard rock: techniques for diagnosis and modelling for damage and fragmentation. Proc. 6th Int. ISRM Congress on Rock Mechanics, Montreal, Canada. pp. 1425-1431.

Mah, S.G.L., 1997. Quantification and prediction of wall slough in open stope mining methods. M.Sc. Thesis, University of British Columbia. 290pg.

Mah, S.G.L., Pakalnis, R.T., Poulin, R., and Clark, L,M., 1995. Obtaining quality cavity monitoring survey data. In Proc. CAMI'95: 3rd Canadian Conference on Computer Applications in the Mineral Industry, Montréal, Québec, Oct 22-25, pp. 400-407.

Makuch, T.P., 2001. No job takes priority over safety – Dynatec's approach to narrow-vein longhole stoping at Midas, Nevada. In Proc. International Symposium on Mining Techniques of Narrow-Vein Deposits, Val-d'Or, Quebec, 1-4 October, 2001, pp 7-10.

Malek, F., Espley, S., O'Donnell, D., and Suorineni, F., 2001. Open stope design at Inco's Stobie mine. 15th CIM Mine Operators Conference, Sudbury, Ont. 10 pg.

Maloney, S., Fearon, R., Nose, J., and Kaiser, P.K., 1992. Investigations into the effect of stress change on support capacity. Rock Support in Mining and Underground Construction, Kaiser and McCreath (eds.), 1992 Balkema, Rotterdam. ISBN 90 5410 044 3.

Martin, C.D., Yazici, S., Espley, S., and Tan, G., 2000. Using numerical models to quantify stope dilution. 102nd CIM Annual General Meeting, Toronto, Ontario, 5-10 March, 8 pg.

Martin, C.D., Tannant, D.D., Yazici, S., and Kaiser, P.K., 1999. Stress path and instability around mine openings. In Proc. 9th ISRM Congress on Rock Mechanics, Paris, Edited by G. Vouille and P. Berest, Vol. 1, pp. 311–315. A.A. Balkema, Rotterdam.

Mathews, K.E., Hoek, E., Wyllie, D.C., and Steward, S.B.V., 1981. Prediction of stable excavations for mining at depths below 1000 Metres in hard rock.

CANMET Report DSS Serial No. OSQ80-00081, DSS File No. 17SQ.23440-0-9020. Ottawa : Dept. Energy, Mines and Resources.

Mawdesley, C., Trueman, R., and Whiten, W.J., 2001. Extending the Mathews stability graph for open-stope design. Trans. Instn Min. Metall. (Section A), Volume 110, January-April 2001, p A27-39.

Melong, K., and Naylor, J., 1997. Paste backfill usage at Macassa mine: planning, design and implementation. 13th CIM Mine Operators Conference, February 16 - 19, 1997, Sudbury, Ontario.

Miller, F., Potvin, Y., and Jacob, D., 1992. Laser measurement for open stope dilution. CIM Bulletin, Vol. 85, No. 962, pp. 96-102.

Milne, D., Hadjigeorgiou, J., and Pakalnis, R., 1998. Rock mass characterization for underground hard rock mines. Tunnelling and Underground Space Technology, Oct. 1998, vol 13, no 4, pp 383-391.

Milne, D., and Pakalnis, R., 1997. Theory behind empirical design techniques. In Proc. 12th A.M.Q. Colloque en Contrôle de Terrain, Val D`Or, Québec, March 1997, 21 pg.

Milne, D.M., Pakalnis, R.C., and Lunder P.J., 1996. Approach to the quantification of hanging-wall behaviour. Trans. Instn Min. Metall. (Sect. A.: Min. industry), Vol. 105, January-April 1996. pp A69-A74.

Mitri, H.S., Rispoli, A., and Bétournay, M.C., 2005. Strength and behavior of biaxially loaded limestone rock. Proc. 40th U.S. Symposium on Rock Mechanics, Anchorage, Alaska, June 25-29, 2005. 7 pg.

Mitri, H.S., and Bétournay, M.C., 2005. Progressive failure of norite rock under biaxial loading condition. 107th CIM Annual General Meeting, April 2005, 7pg.

Mitri, H.S., Ma, J., Mohammed, M.M, and Bouteldja, M., 1998. Design of cable bolts using numerical modelling. Design and Construction in Mining, Petroleum and Civil Engineering, Ayres da Silva et al. (eds) pp. 269-275, ISRM Regional Symposium.

Morrison, R.G.K., 1976. A philosophy of ground control. Department of Mining and Metallurgical Engineering, McGill University. T.H. Best Printing Company, Montreal. 182 Pg. ISBN 0-9690582-0-9

Nickson, S.D., 1992. Cable Support Guidelines for Underground Hard Rock Mine Operations. M.A.Sc. Thesis, Department Mining and Mineral Processing, University of British Columbia. 223 Pg.

O'Hara, T.A., 1980. Quick guides to the evaluation of orebodies. CIM Bulletin, Vol. 73, No. 814, pp. 87-99.

Olsson, M., and Thorshag. H., 1986. Mining Technique for Narrow Orebodies. Swedish Detonic Research Foundation.

Oriard, L.L., 1982. Blasting effects and their control. Underground Mining Methods handbook, SME, pp. 1590-1603.

Pakalnis, R.C., 1986. Empirical Stope Design in Canada. Ph.D. Thesis. University of British Columbia, 276pp.

Pakalnis, R., Sandhu, M., and Clark, L., 1998. Development of stope design guidelines for narrow vein open stope mining in terms of minimizing dilution. Final report by Echo Bay Mines Ltd. – Lupin Mine in association with Pakalnis and Associates. CANMET Project Number: 5-1228. 314 pg.

Pakalnis, R.C., Poulin, R., and Hadjigeorgiou J., 1995. Quantifying the cost of dilution in underground mines. Mining Engineering, December 1995, pp: 1136-1141.

Pakalnis, R. and Vongpaisal, S., 1998. Empirical Design Methods - UBC Geomechanics. Proc. 100th CIM Annual General Meeting, Montréal, Québec, 3-7 May 1998.

Pakalnis, R., and Vongpaisal, S., 1993. Mine design - an empirical approach. Innovative Mine Design for the 21st Century, Bawden and Archibald (eds), Balkema, Rotterdam, pp.455-467. ISBN 90 5410 325 6.

Palmstrøm, A., 1996. Characterizing rock masses by the RMi for use in practical rock engineering, Part 1: the development of the rock mass index (RMi). Tunnelling Underground Space Technology 1996; 11(2):175–88.

Patton, F.E., 1952. Back filling at Noranda. CIM Bulletin Vol. 45, No. 480, pp. 191-197.

Paventi, M., 1995. Rock mass characteristics and damage at the Birchtree mine. Unpublished PhD thesis, McGill University. 441 pg.

Pelley, C.W., 1994. A study of sequencing strategy for steep, tabular, hardrock orebodies. Ph.D. Thesis. McGill University, 310pp.

Pera, P., Tuovinen, S., Korteniemi, Matinlassi, M., and Nilranen, S., 2001. Stoping at the Pyhäsalmi Mine. Underground mining methods: engineering fundamentals and international case studies. Hustrulid, W.A., and Bullock, R.L., (eds), Society for Mining, Metallurgy, and Exploration, Inc., Littleton, Colorado, USA, pp 215-220.

Perron, J., 1999. Simple solutions and employee's involvement reduced the operating cost and improved the productivity at Langlois mine. In Proc. 14th CIM Mine Operator's Conference, 21-25 February 1999, Bathurst, New Brunswick. 20pg.

Piché, A., Liu, Q., Tran, H., van Hijfte, L., 1998. Drilling and blasting research at the Noranda Technology Centre. 100th CIM Annual General Meeting, Montreal, PQ., 3-7 May 1998. (on CD), 9 pg.

Pierce, M., 1998. Modeling of alternative individual stope modeling sequences at Bousquet #2 mine. Internal report to Barrick Gold Corp., Bousquet #2 Mine. 31 pg.

Planeta, S., Bourgoin, C., and Laflamme, M., 1990. The impact of rock dilution on underground mining: operational and financial considerations. In Proc. 92nd CIM Annual General Meeting, Ottawa, Ontario, 6-10 May 1990. 15pg.

Potvin, Y., 1998. Rock Mechanics Principles for Open Stope Mining at Mount Isa Mines. 100th CIM Annual General Meeting, Montreal, 3-7 May 1998. (on CD), 11 pg.

Potvin, Y.,1988. Empirical open stope design in Canada. Ph.D. thesis. Dept. Mining and Mineral Processing, University of British Columbia.

Potvin,Y., and Hadjigorgiou, J., 2001. The stability graph method for open stope design. Underground mining methods: engineering fundamentals and international case studies. Hustrulid, W.A., and Bullock, R.L., (eds), Society for Mining, Metallurgy, and Exploration, Inc., Littleton, Colorado, USA, pp 513-520.

Potvin, Y., and Hudyma, M., 2000. Open stope mining in Canada. MassMin 2000, Brisbane, Australia, 29 October - 2 November 2000, pp. 661-674.

Prasad, K.,1996. Elastic and Plastic Material Properties of Core Samples From Bousquet #2. Internal memo to Bousquet mine, Queen's University. 15 pg.

Quesnel, W.J.F., and Ley, G.M.M., 1991. The development of mine design guidelines for dilution control, Bousquet Division, No. 1 shaft, Lac Minerals Ltd. 93rd CIM Annual General Meeting, Vancouver, B.C., April 28 – May 1. 20 pg.

Ran, J., 2002. Hanging-wall sloughing mechanism in open stope mining. CIM Bulletin Vol. 95, No. 1064, pp. 74-77.

Redpath, J.S., Ltd., 1986. Estimating preproduction and operating costs of small underground deposits. CANMET Report SP 86-11E, Energy, Mines and Resources Canada.

Rocscience, 2004. ExamineTAB, Version 2.1. 3D Stress Analysis for Tabular Ore Bodies. Rocscience Inc., Toronto, Ontario.

Rocscience, 2002. Phase2 Version 5. A 2D finite element program for calculating stresses and estimating support around underground excavations. Rocscience Inc., Toronto, Ontario.

Rocscience, 1998. Examine3D Version 4.0. A 3D computer-aided engineering analysis package for underground excavations in rock. Rocscience Inc., Toronto, Ontario.

Ruest, M., 1988. Back analysis of instrumented hanging wall cable bolt reinforcement at complexe bousquet using smart cable technology. Unpublished M. Sc. thesis. Queen's University, Kingston, Ontario. 250 pg.

Scoble, M. J., Lizotte, M., Paventi, M., Mohanty, B. B., 1997. Measurement of blast damage. Mining Engineering, pp. 103-108.

Scoble, M.J., and Moss, A., 1994. Dilution in underground bulk mining: Implications for Production Management, mineral resource evaluation II, methods and case histories, Geological Society Special Publication No. 79, 95-108.

Skeeles, B.E., and Semier, R., 1991. Open stope surveys at Lupin Mine. 10th CIM Underground Operators Conference, Val d'Or, Quebec. 4 pg.

Sprott, D.L., Toppi, M.A., Yi, X., and Bawden, W.F., 1999. The incorporation of stress induced damage factor into Mathew's Stability graph. In Proc. 101st CIM Annual General Meeting, Calgary, Alberta, 10p.

Stewart, P.C., and Trueman, R., 2004. Quantifying the effect of stress relaxation on excavation stability. Trans. Instn Min. Metall. (Sect. A; Min. industry), Vol. 113, June 2004. pp A107-A117.

Suorineni, F.T., Henning, J.G., and Kaiser, P.K., 2005. Strategy for safe rapid drift development - support selection. CIM Maintenance Engineering / Mine Operators Conference (ME/MO 2005), Sudbury, February 2005, 12pg.

Suorineni, F.T., and Kaiser, P.K., 2002. Dependence of stand-up time of stopes on size and rock quality. Proceedings of the 5th North American Rock Mechanics Symposium and the 17th Tunnelling Association of Canada Conference: NARMS-TAC 2002, 7-10 July 2002. Hammah, R., Bawden,

W., Curran, J., and Relesnicki, M. (eds.), University of Toronto press, Toronto, Ontario. pp 133-140.

Suorineni, F.T., Tannant, D.D., and Kaiser, P.K., 1999. Fault factor for the stability graph method of open-stope design. Trans. Instn. Min. Metall., (Section A: Mining industry), London, pp. Vol. 108, pp. A92-104.

Suorineni, F.T., Tannant, D.D., and Kaiser, P.K., 1999b. Determination of fault-related sloughage in open stopes. Int J Rock Mech Min Sci. 1999; 36: pp 891-906.

Suorineni, F.T., 1998. Effects of Faults and Stress on Open Stope Design. Ph.D. Thesis, Dept. of Earth Sciences, University of Waterloo, 344p.

Tannant, D.D., Diederichs, M., and Seldon, S., 1998. Hangingwall relaxation and cablebolt support for deep stopes at Kidd Mine. In Proc. 100th CIM Annual General Meeting, Montreal, PQ. 8pg.

Tannant, D.D., Martin, C.D., and Yazici, S., 1998b. Geomechanics study for Hoyle Pond 1060 zone. Internal report to Kinross Gold Corporation, 88 pg.

Tatman, C.R., 2001. Mining dilution in moderate- to narrow-width deposits. Underground mining methods: engineering fundamentals and international case studies. Hustrulid, W.A., and Bullock, R.L., (eds), Society for Mining, Metallurgy, and Exploration, Inc., Littleton, Colorado, USA, pp 615-626.

Taylor, H.K., 1994. Ore reserves, mining and profit. CIM Bulletin, Vol. 87, No. 983, pp. 38-46.

Tintor, N., 1988. Why some mines fail to work. The Northern Miner, Vol. 74, No. 30, 3 October 1988.

Tourigny, G., Doucet, D., and Bourget, A., 1993. Geology of the Bousquet 2 Mine: An Example of a Deformed, Gold-Bearing Polymetallic Sulphide Deposit. Economic Geology, Vol. 88. pp. 1578-1597.

Trahan, M., 1995. Méthode de Minage ''Eureka''. 10th AMQ colloque en contrôle de terrain, Val d'Or, Quebec, Canada. 4 pg.

Trevor, S.M., 1991. Dilution control at Hudson Bay Mining & Smelting, Flin Flon Operations. In Proc. 93rd CIM Annual General Meeting, Vancouver, British Columbia.

Uggalla, S., 2001. Sublevel Open Stoping – Design and planning at the Olympic Dam Mine. Underground mining methods: engineering fundamentals and international case studies. Hustrulid, W.A., and Bullock, R.L., (eds), Society for Mining, Metallurgy, and Exploration, Inc., Littleton, Colorado, USA, pp 239-244.

Vallée, M., David, M., Dagbert, M., and Desrochers, C., 1992. Guide to the evaluation of gold deposits; CIM Special Volume 45. ISBN 0-919086-31-4.

Villaesusa, E., Onederra, I., and Scott, C., 2004. Blast induced damage and dynamic behaviour of hangingwalls in bench stoping. Fragblast 2004. Vol. 8, No. 1, pp 23-40.

Villaescusa, E., 2000. A Review of Sublevel Stoping. In proc. MassMin 2000, Brisbane, Australia, 29 October - 2 November 2000, pp 577-590.

Wang, J., 2004. Influence of stress, undercutting, blasting and time on open stope stability and dilution. Unpublished PhD thesis, University of Saskatchewan. 279 pg.

Wang, J., Milne, D., Yao, M., and Allen, G., 2002a. Quantifying the effect of hanging wall undercutting on stope dilution. In Proc. 104th CIM Annual General Meeting, Vancouver BC. 8pg.

Wang, J., Milne, D., Yao, M., and Allen, G., 2002b. Factors influencing stope dilution at Hudson Bay Mining & Smelting. Proceedings of the 5th North American Rock Mechanics Symposium and the 17th Tunnelling Association of Canada Conference: NARMS-TAC 2002, 7-10 July 2002.

Hammah, R., Bawden, W., Curran, J., and Relesnicki, M. (eds.), University of Toronto press, Toronto, Ontario. pp 195-202.

Whiteway, P., 1988. Cookie Jar Mining. The Northern Miner Magazine, Vol. 3, No. 10, pp 47-50.

Wiles, T., 2005. Map3D Version 51. A mining analysis program in three dimensions. Mine Modelling Pty Ltd. Mt. Eliza, Victoria, Australia. www.map3d.com

Xishan, C., 1998. Resuing shrinkage stoping. Engineering and Mining Journal, Vol. 199, No. 10, pp 34-36.

Yang, R.L., Rocque, P., Katsabanis, P., and Bawden, J.F., 1994. Measurement and analysis of near-field blast vibration and damage. Geotechnical and Geological Engineering, Vol 12, pp 169-182.

Yang, R.L., Bawden, J.F., Talebi, S., and Rocque, P., 1993. An integrated technique for vibration monitoring adjacent to a blast hole. CIM Bulletin, Vol. 86, No. 972, pp 45-52.

Yao, X., Allen, G., and Willett, M., 1999. Dilution evaluation using Cavity Monitoring System at HBMS – Trout Lake Mine. In Proc. 101st CIM Annual General Meeting, Calgary, Alberta, 10p.

Yu, T.R., and Vongpaisal, S., 1996. New blast damage criteria for underground blasting. CIM Bulletin, Vol. 89, No. 998, pp 139-145.

Yu, T.R., 1993. The development of new blast damage criteria for blasthole mining operations. Report prepared by Falconbridge Ltd., Kidd Creek Division, CANMET Project No. 1-9050, 152 pg.

Yu, T.R., 1992. Mechanisms of fill failure and fill strength requirements. In proc. 16th Canadian Rock Mechanics Symposium, Sudbury, Ontario, 15 June 1992, pp. 43-48.

Yu, T.R., and Counter, D.B., 1983. Backfill practices and technology at Kidd Creek Mines. CIM Bulletin, Vol. 76, No., 856, pp 56-65.

Yu, T.R., 1980. Ground control at Kidd Creek mine. Underground Rock Engineering, 13th Canadian Rock Mechanics Symposium, Toronto, Ont. 28-29 May 1980. CIM Special Volume 22.

APPENDIX A

Parametric numerical modelling - summarized results

Table A1.1 Modelled dilution density values; 80° hanging-wall dip, GSI=65, σ_1° perpendicular to hanging-wall

Dimensions (m)			DD at σ_3 = 0 contour Depth (m)			DD at σ_3 = -0.5MPa contour Depth (m)		
Height	Strike Length	Dip	750	1500	2250	750	1500	2250
	10	80°	0	0	0.02	0	0	0
	15	80°	0	0	0.02	0	0	0
10	20	80°	0.15	0.09	0.11	0	0	0.03
	30	80°	0.14	0.09	0.09	0	0	0.02
	40	80°	0.2	0.18	0.15	0	0.02	0.04
	10	80°	0.1	0.1	0.1	0	0	0.01
	15	80°	0.2	0.18	0.18	0	0.01	0.04
20	20	80°	0.52	0.44	0.43	0	0.1	0.16
	30	80°	0.65	0.52	0.51	0.03	0.24	0.29
	40	80°	0.65	0.53	0.52	0.03	0.17	0.24
	10	80°	0.12	0.12	0.18	0	0.01	0.02
	15	80°	0.26	0.2	0.3	0	0.02	0.04
30	20	80°	0.62	0.5	0.69	0.02	0.2	0.28
	30	80°	0.92	0.71	0.96	0.06	0.29	0.44
	40	80°	1.12	0.92	1.16	0.08	0.39	0.47
	10	80°	0.12	0.12	0.12	0	0	0.01
	15	80°	0.22	0.22	0.19	0	0.01	0.03
40	20	80°	0.47	0.47	0.44	0	0.06	0.18
	30	80°	0.87	0.83	0.74	0.01	0.3	0.45
	40	80°	1.24	1.06	1	0.03	0.27	0.39

Table A1.2 Modelled dilution density values; 60° hanging-wall dip, GSI=65, σ_1° perpendicular to hanging-wall

Dimensions (m)			DD at σ_3 = 0 contour Depth (m)			DD at σ_3 = -0.5MPa contour Depth (m)		
Height	Strike Length	Dip	750	1500	2250	750	1500	2250
	10	60°	0.13	0.06	0.06	0	0	0
	15	60°	0.21	0.09	0.08	0	0	0
10	20	60°	0.43	0.24	0.2	0	0	0.05
	30	60°	0.48	0.28	0.24	0	0.04	0.06
	40	60°	0.62	0.44	0.36	0	0.09	0.11
	10	60°	0.07	0.04	0.04	0	0	0
	15	60°	0.17	0.12	0.1	0	0	0.01
20	20	60°	0.72	0.56	0.48	0	0.17	0.23
	30	60°	1.29	0.89	0.82	0	0.3	0.41
	40	60°	1.58	1.25	1.16	0	0.66	0.79
	10	60°	0.1	0.04	0.07	0	0	0
	15	60°	0.25	0.15	0.17	0	0	0.03
30	20	60°	0.63	0.54	0.49	0	0.01	0.12
	30	60°	1.43	1.09	1.09	0	0.46	0.76
	40	60°	2.19	1.58	1.48	0	0.4	0.96
	10	60°	0.03	0.01	0.03	0	0	0
	15	60°	0.17	0.1	0.12	0	0	0.01
40	20	60°	0.53	0.48	0.45	0	0.05	0.13
	30	60°	1.22	0.99	0.95	0	0.18	0.34
	40	60°	2.02	1.4	1.27	0	0.33	0.63

Table A1.3 Modelled dilution density values; 80° hanging-wall dip, GSI=65, σ_1° parallel to hanging-wall

Dimensions (m)			DD at σ_3 = 0 contour)	DD at σ_3 = -0.5MPa contour
Height	Strike Length	Dip	1500m depth	1500m depth
	10	80°	0.12	0.01
	15	80°	0.18	0.02
30	20	80°	0.42	0.13
	30	80°	0.68	0.16
	40	80°	0.78	0.22

Table A1.4 Modelled dilution density values; 60° hanging-wall dip, GSI=65, σ_1° parallel to hanging-wall

Dimensions (m)			DD at σ_3= 0 contour	DD at σ_3 = -0.5MPa contour
Height	Strike Length	Dip	1500m depth	1500m depth
	10	60°	0.03	0
	15	60°	0.12	0
30	20	60°	0.43	0.01
	30	60°	0.9	0.24
	40	60°	1.11	0.1

Table A1.5 Modelled dilution density values per stope type; 80° hanging-wall dip, GSI=65, σ_1° perpendicular to hanging-wall

Dimensions (m)			DD at σ_3 = 0 contour			DD at σ_3 = -0.5MPa contour		
Height	Strike Length	Dip	Depth (m)			Depth (m)		
			750	1500	2250	750	1500	2250
P1 (primary) stope								
	10	80°	0.12	0.12	0.18	0	0.01	0.02
	15	80°	0.26	0.2	0.3	0	0.02	0.04
30	20	80°	0.62	0.5	0.69	0.02	0.2	0.28
	30	80°	0.92	0.71	0.96	0.06	0.29	0.44
	40	80°	1.12	0.92	1.16	0.08	0.39	0.47
P2 (primary) stope								
	10	80°		0.18			0.1	
	15	80°		0.35			0.18	
30	20	80°		0.66			0.37	
	30	80°		1.14			0.72	
	40	80°		1.52			1	
P3 (primary) stope								
	10	80°		0.19			0.1	
	15	80°		0.36			0.16	
30	20	80°		0.68			0.37	
	30	80°		1.23			0.94	
	40	80°		1.55			1.03	
S1 (secondary) stope								
	10	80°		0.48			0.29	
	15	80°		0.79			0.6	
30	20	80°		1.16			0.94	
	30	80°		1.79			1.45	
	40	80°		2.09			1.55	
S2 (secondary) stope								
	10	80°		0.96			0.8	
	15	80°		1.5			1.29	
30	20	80°		2.1			1.83	
	30	80°		2.7			2.39	
	40	80°		2.8			2.53	

Table A1.6 Dilution Density as a function of strike length of base-case stope at varying mine depths*, see Figures 5.3 and 5.4

	750m mine depth		1500m mine depth		2250m mine depth	
Strike length	DD at σ_3 = 0 MPa contour	DD at σ_3 = -0.5 MPa contour	DD at σ_3 = 0 MPa contour	DD at σ_3 = -0.5 MPa contour	DD at σ_3 = 0 MPa contour	DD at σ_3 = -0.5 MPa contour
10m strike	0.12 m	0 m	0.12 m	0.01 m	0.18 m	0.02 m
15m strike	0.26	0	0.2	0.02	0.3	0.04
20m strike	0.62	0.02	0.5	0.2	0.69	0.28
30m strike	0.92	0.06	0.77	0.3	0.96	0.44
40m strike	1.12	0.08	0.92	0.38	1.16	0.47

* Vertical height = 30m, 80° dip, GSI = 65, σ_1° perpendicular to hanging-wall, P1-type stope

Table A1.7 Dilution Density as a function of stope dimension*, see Figure 5.6

Vertical height (m)	Strike length (m)	Mine Depth (m)			Average DD (m)
		750 m	1500 m	2250 m	
		DD (m) at σ_3 = 0 MPa contour			
10	10	0	0	0.02	0
	15	0	0	0.02	0
	20	0.15	0.09	0.11	0.11
	30	0.14	0.09	0.09	0.11
	40	0.20	0.18	0.15	0.18
20	10	0.10	0.10	0.10	0.10
	15	0.20	0.18	0.18	0.19
	20	0.52	0.44	0.43	0.45
	30	0.65	0.52	0.51	0.51
	40	0.65	0.53	0.52	0.52
30	10	0.12	0.12	0.18	0.14
	15	0.26	0.20	0.30	0.23
	20	0.62	0.50	0.69	0.60
	30	0.92	0.77	0.96	0.88
	40	1.12	0.92	1.16	1.07
40	10	0.12	0.12	0.12	0.12
	15	0.22	0.22	0.19	0.18
	20	0.47	0.46	0.44	0.46
	30	0.87	0.83	0.74	0.81
	40	1.24	1.06	1.00	1.10

* GSI = 65, $\sigma_1{}^{\circ}$ perpendicular to hanging-wall, P1-type stope

Table A1.8 Dilution Density as a function of hanging-wall dip angle of base case stope*, see Figure 5.11

Vertical height	Hanging-wall dip angle	Strike Length (m)				
		10	15	20	30	40
		DD (m) at σ_3 = 0 MPa contour				
20m	80° hanging-wall dip	0.10	0.18	0.44	0.52	0.53
	60° hanging-wall dip	0.04	0.12	0.56	0.89	1.25
30m	80° hanging-wall dip	0.12	0.20	0.50	0.77	0.92
	60° hanging-wall dip	0.04	0.15	0.54	0.99	1.40
40m	80° hanging-wall dip	0.12	0.22	0.45	0.76	1.02
	60° hanging-wall dip	0.01	0.10	0.48	1.09	1.58

* Vertical height = 30m, depth = 1500m, GSI = 65, σ_1° perpendicular to hanging-wall, P1-type stope

Table A1.9 Dilution Density as a function of major principal stress orientation*, see Figure 5.12

	Strike Length (m)				
	10	15	20	30	40
	DD at σ_3 = 0 MPa contour				
Sig1 Perpendicular - 80deg	0.12	0.2	0.5	0.77	0.92
Sig1 Parallel - 80deg	0.12	0.18	0.42	0.68	0.78
Sig1 Perpendicular - 60deg	0.04	0.15	0.54	0.99	1.40
Sig1 Parallel - 60deg	0.03	0.12	0.43	0.9	1.11

* Vertical height = 30m, depth = 1500m, GSI = 65, P1-type stope

Table A1.10 Dilution Density as a function of stope type*, see Figures 5.13 and 5.14

Stope type	Strike Length (m)									
	10		15		20		30		40	
	DD at σ_3 = 0 MPa contour	DD at σ_3 = -0.5 MPa contour	DD at σ_3 = 0 MPa contour	DD at σ_3 = -0.5 MPa contour	DD at σ_3 = 0 MPa contour	DD at σ_3 = -0.5 MPa contour	DD at σ_3 = 0 MPa contour	DD at σ_3 = -0.5 MPa contour	DD at σ_3 = 0 MPa contour	DD at σ_3 = -0.5 MPa contour
P1	0.12	0.01	0.2	0.02	0.5	0.2	0.77	0.29	0.92	0.39
P2	0.18	0.1	0.35	0.18	0.66	0.37	1.14	0.72	1.52	1
P3	0.19	0.1	0.36	0.16	0.68	0.37	1.23	0.94	1.55	1.03
S1	0.48	0.29	0.79	0.6	1.16	0.94	1.79	1.45	2.09	1.55
S2	0.96	0.8	1.5	1.29	2.1	1.83	2.7	2.39	2.8	2.53

* Vertical height = 30m, depth = 1500m, GSI = 65, σ_1° perpendicular to hanging-wall

APPENDIX B

Bousquet #2 mine details

APPENDIX B1

Block 5 stope design and CMS database

Table B1.1 Block 5 stope design details, 9-3 horizon stopes

				Stope Design																Stope Type					Drill Pattern		
STOPE NAME	HW Sequence mined	HW cables - fan upward	HW cables- fan downward	Stope size (tonnes) - planned	Stope muck grade (gm/tonne)	Stope base (floor elevation)	Stope top(top sill floor elevation)	Strike Azimuth	Stope Width on strike (@midspan)	Vertical Height (m)	Stope HW angle	True HW height	HW area (m2)	HW Hydraulic Radius (m)	Stope FW angle	True FW height	FW area (m2)	FW Hydraulic Radius (m)	Primary (P1)	P2	P3	Secondary (S1)	S2	parallel (primary)	ring (secondary)	Longitudinal
9-3 horizon																											
9-3-1	21	x		9602	7.1	3886.0	3917.0	88	14	31	77	31.8	445.4	4.9	82	31.3	438.3	4.8		x					x	
9-3-2	42	x		8615	9.1	3886.0	3917.5	90	11	31.5	77	32.3	355.6	4.1	78	32.2	354.2	4.1					x		x	
9-3-3	32	x		11624	11.1	3886.0	3917.5	92	15.5	31.5	75	32.6	505.5	5.3	78	32.2	499.2	5.2		x					x	
9-3-4	53	x		14388	9	3885.5	3917.0	90	17	31.5	72	33.1	563.1	5.6	74	32.8	557.1	5.6				x			x	
9-3-5	66	x		10818	7.9	3886.0	3917.0	91	14.5	31	73	32.4	470	5.0	70	33.0	478.3	5.0				x			x	
9-3-6	76	x		9934	7.8	3886.0	3916.5	96	12.5	30.5	74	31.7	396.6	4.5	74	31.7	396.6	4.5				x			x	
9-3-7	81	x		14138	6.7	3885.5	3915.5	96	13.5	30	75	31.1	419.3	4.7	73	31.4	423.5	4.7					x		x	
9-3-8	56	x		16026	8.9	3885.5	3916.0	97	13	30.5	75	31.6	410.5	4.6	74	31.7	412.5	4.6			x				x	
9-3-9	68	x		17999	11.2	3884.5	3916.0	97	14.5	31.5	74	32.8	475.2	5.0	82	31.8	461.2	5.0					x		x	
9-3-10	34	x		34060	11.3	3884.5	3915.0	90	15	30.5	74	31.7	475.9	5.1	80	31.0	464.6	5.1			x				x	
9-3-11	46	x		14075	12.1	3885.5	3914.5	98	14.5	29	75	30.0	435.3	4.9	81	29.4	425.7	4.9					x		x	
9-3-12	30	x		23095	10.7	3884.5	3914.0	105	14	29.5	76	30.4	425.6	4.8	76	30.4	425.6	4.8			x				x	
9-3-13	55	x		23910	10.5	3884.0	3914.5	96	15	30.5	76	31.4	471.5	5.1	77	31.3	469.5	5.1				x			x	
9-3-14	80	x		20057	4.6	3884.0	3913.5	112	14.5	29.5	76	30.4	440.8	4.9	80	30.0	434.3	4.9					x		x	
9-3-15	64	x		21238	7.2	3884.5	3914.5	98	15	30	76	30.9	463.8	5.1	84	30.2	452.5	5.0			x				x	
9-3-16	89	x		19447	5.5	3884.0	3914.5	90	14.5	30.5	80	31.0	449.1	4.9	80	31.0	449.1	4.9					x		x	
9-3-17	75	x		19985	5.6	3885.0	3914.0	92	15	29	82	29.3	439.3	5.0	80	29.4	441.7	5.0			x				x	
9-3-18	92	x		6900	6.4	3885.0	3915.0	87	11.5	30	85	30.1	346.3	4.2	85	30.1	346.3	4.2					x		x	
9-3-19	87	x		6963	5.6	3885.5	3914.5	81	12	29	85	29.1	349.3	4.2	85	29.1	349.3	4.2			x				x	
9-3-20	97			5100	6.6	3886.5	3915.0	80	13	28.5	87	28.5	371	4.5	85	28.6	371.9	4.5					x			x
9-3-21	96			5300	5.2	3886.5	3915.0	93	14	28.5	85	28.6	400.5	4.7	83	28.7	402	4.7	x							x

Table B1.1 Block 5 stope design details, 9-2 horizon stopes

	Stope Design																		Stope Type					Drill Pattern		
STOPE NAME	HW Sequence mined	HW cables - fan upward	HW cables- fan downward	Stope size (tonnes) - planned	Stope muck grade (gm/tonne)	Stope base (floor elevation)	Stope top(top sill floor elevation)	Strike Azimuth	Stope Width on strike (@midspan)	Vertical Height (m)	Stope HW angle	True HW height	HW area (m2)	HW Hydraulic Radius (m)	Stope FW angle	True FW height	FW area (m2)	FW Hydraulic Radius (m)	Primary (P1)	P2	P3	Secondary (S1)	S2	parallel (primary)	ring (secondary)	Longitudinal
9-2 horizon																										
9-2-1	12		x	8867	6.6	3856.5	3886.0	88	15	29.5	80	30.0	449.3	5.0	73	30.8	462.7	5.0	x					x		
9-2-2	39		x	8097	8.6	3856.0	3886.0	87	14.5	30	80	30.5	441.7	4.9	75	31.1	450.3	4.9					x		x	
9-2-3	29		x	8844	10.3	3856.0	3886.0	85	15	30	78	30.7	460.1	5.0	77	30.8	461.8	5.0	x					x		
9-2-4	50		x	13002	7.7	3856.5	3885.5	88	17	29	74	30.2	512.9	5.4	74	30.2	512.9	5.4				x			x	
9-2-5	60		x	9323	7.1	3856.0	3886.0	90	14	30	74	31.2	436.9	4.8	76	30.9	432.9	4.8				x			x	
9-2-6	72		x	8837	7.5	3854.5	3886.0	96	11	31.5	73	32.9	362.3	4.1	73	32.9	362.3	4.1				x			x	
9-2-7	79		x	8423	7.5	3854.5	3885.5	96	11.5	31	72	32.6	374.8	4.3	74	32.2	370.9	4.2					x		x	
9-2-8	49		x	18370	7.1	3854.0	3885.5	99	13	31.5	74	32.8	426	4.7	77	32.3	420.3	4.6		x				x		
9-2-9	65		x	19998	5.7	3854.5	3885.5	101	11	31	78	31.7	348.6	4.1	79	31.6	347.4	4.1			x				x	
9-2-10	26		x	21635	8.3	3853.5	3884.5	99	15	31	80	31.5	472.2	5.1	78	31.7	475.4	5.1		x				x		
9-2-11	43		x	21485	9.2	3853.0	3884.0	90	15	31	79	31.6	473.7	5.1	82	31.3	469.6	5.1					x		x	
9-2-12	16		x	17732	13.3	3852.5	3884.5	115	15	32	79	32.6	489	5.1	79	32.6	489	5.1		x				x		
9-2-13	52		x	14973	17.4	3852.0	3884.0	95	15	32	77	32.8	492.6	5.1	80	32.5	487.4	5.1				x			x	
9-2-14	78		x	31345	7.4	3852.0	3884.0	102	14.5	32	77	32.8	476.2	5.0	80	32.5	471.2	5.0					x		x	
9-2-15	59		x	27054	5.5	3852.5	3884.5	96	15	32	78	32.7	490.7	5.1	80	32.5	487.4	5.1					x	x		
9-2-16	88		x	20434	5.4	3852.0	3884.0	98	10.5	32	79	32.6	342.3	4.0	82	32.3	339.3	4.0					x		x	
9-2-17	70		x	21867	4.4	3854.0	3885.5	92	15	31.5	77	32.3	484.9	5.1	79	32.1	481.3	5.1			x			x		
9-2-18	91		x	8600		3853.0	3885.5	90	13	32.5	80	33.0	429	4.7	78	33.2	431.9	4.7					x		x	
9-2-19	83		x	20387	4.7	3853.5	3885.5	93	13	32	85	32.1	417.6	4.6	80	32.5	422.4	4.6			x			x		
9-2-20	94			5650	4.8	3854.5	3886.5	86	14	32	84	32.2	450.5	4.9	84	32.2	450.5	4.9					x		x	
9-2-21	90			22941	3.1	3854.0	3886.5	90	15	32.5	85	32.6	489.4	5.1	80	33.0	495	5.2			x			x		
9-2-22	95			16600	3.4	3854.0	3887.5	94	14.5	33.5	86	33.6	486.9	5.1	78	34.2	496.6	5.1				x			x	

Table B1.1 Block 5 stope design details, 9-1 horizon stopes

	Stope Design																			Stope Type					Drill Pattern		
STOPE NAME	HW Sequence mined	HW cables - fan upward	HW cables- fan downward	Stope size (tonnes) - planned	Stope muck grade (gm/tonne)	Stope base (floor elevation)	Stope top(top sill floor elevation)	Strike Azimuth	Stope Width on strike (@midspan)	Vertical Height (m)	Stope HW angle	True HW height	HW area (m2)	HW Hydraulic Radius (m)	Stope FW angle	True FW height	FW area (m2)	FW Hydraulic Radius (m)	Primary (P1)	P2	P3	Secondary (S1)	S2	parallel (primary)	ring (secondary)	Longitudinal
9-1 horizon																											
9-1-2	10			4721	3.8	3823.5	3856.0	86	14	32.5	78	33.2	465.2	4.9	78	33.2	465.2	4.9	x					x		
9-1-3	18			7241	3.7	3824.0	3856.5	87	19	32.5	80	33.0	627	6.0	78	33.2	631.3	6.0					x	x		
9-1-4	3			7102	4.3	3824.0	3856.5	88	15	32.5	80	33.0	495	5.2	78	33.2	498.4	5.2		x				x		
9-1-5	41			7721	5.2	3824.5	3856.0	88	15	31.5	82	31.8	477.1	5.1	77	32.3	484.9	5.1				x			x	
9-1-6	58	x		8555	7.4	3824.5	3856.0	90	15	31.5	84	31.7	475.1	5.1	77	32.3	484.9	5.1				x			x	
9-1-7	67	x		8452	7.0	3824.0	3855.0	96	16	31	83	31.2	499.7	5.3	75	32.1	513.5	5.3					x		x	
9-1-8	38	x		19476	5.0	3823.0	3854.0	102	15	31	82	31.3	469.6	5.1	85	31.1	466.8	5.1		x				x		
9-1-9	54	x		19397	4.3	3823.0	3854.5	100	13.5	31.5	80	32.0	431.8	4.7	73	32.9	444.7	4.8					x		x	
9-1-10	15	x		15827	5.0	3822.5	3853.5	96	14.5	31	80	31.5	456.4	5.0	75	32.1	465.4	5.0			x			x		
9-1-11	36	x		19939	4.6	3822.0	3853.5	103	14	31.5	78	32.2	450.9	4.9	70	33.5	469.3	4.9					x		x	
9-1-12	5	x		20260		3822.0	3853.0	98	14.5	31	75	32.1	465.4	5.0	70	33.0	478.3	5.0		x				x		
9-1-13	23	x		12951	14.2	3821.0	3852.0	97	14	31	77	31.8	445.4	4.9	74	32.2	451.5	4.9				x		x		
9-1-14	61	x		13693	21.4	3821.0	3852.0	93	13	31	82	31.3	407	4.6	77	31.8	413.6	4.6					x		x	
9-1-15	27	x		12461	12.5	3821.0	3852.0	104	15	31	78	31.7	475.4	5.1	76	31.9	479.2	5.1		x				x		
9-1-16	73	x		9693	8.6	3821.0	3852.0	97	15	31	75	32.1	481.4	5.1	76	31.9	479.2	5.1					x		x	
9-1-17	37	x		9464	5.2	3822.0	3854.0	95	15	32	77	32.8	492.6	5.1	77	32.8	492.6	5.1			x			x		
9-1-18	85	x		8350	8.4	3822.0	3853.0	96	12	31	77	31.8	381.8	4.4	77	31.8	381.8	4.4					x		x	
9-1-19	69	x		8557	6.2	3822.5	3854.0	92	15	31.5	76	32.5	487	5.1	77	32.3	484.9	5.1			x			x		
9-1-20	93	x		7550		3822.5	3854.0	91	14	31.5	82	31.8	445.3	4.9	80	32.0	447.8	4.9					x		x	
9-1-21	84			5744	3.1	3823.0	3854.0	90	15	31	85	31.1	466.8	5.1	84	31.2	467.6	5.1		x				x		

Table B1.1 Block 5 stope design details, 9-0 horizon stopes

	Stope Design																		Stope Type					Drill Pattern		
STOPE NAME	HW Sequence mined	HW cables - fan upward	HW cables- fan downward	Stope size (tonnes) - planned	Stope muck grade (gm/tonne)	Stope base (floor elevation)	Stope top(top sill floor elevation)	Strike Azimuth	Stope Width on strike (@midspan)	Vertical Height (m)	Stope HW angle	True HW height	HW area (m2)	HW Hydraulic Radius (m)	Stope FW angle	True FW height	FW area (m2)	FW Hydraulic Radius (m)	Primary (P1)	P2	P3	Secondary (S1)	S2	parallel (primary)	ring (secondary)	Longitudinal
9-0 horizon																										
9-0-3	7			5190		3795.0	3823.5	89	16	28.5	75	29.5	472.1	5.2	75	29.5	472.1	5.2				x				x
9-0-4	1			6128	6.8	3784.5	3823.5	89	13.5	39	76	40.2	542.6	5.1	76	40.2	542.6	5.1	x							x
9-0-5	6			5566		3795.0	3824.5	89	15	29.5	76	30.4	456	5.0	76	30.4	456	5.0				x				x
9-0-6	11	x		4598	7.8	3794.0	3824.5	91	16	30.5	78	31.2	498.9	5.3	78	31.2	498.9	5.3				x				x
9-0-7	47	x		4363	10.2	3794.0	3824.0	96	16	30	80	30.5	487.4	5.2	80	30.5	487.4	5.2					x	x		
9-0-8	35	x		4667	8.2	3794.0	3823.0	103	15	29	80	29.4	441.7	5.0	80	29.4	441.7	5.0	x					x		
9-0-9	44	x		16576	6.1	3793.5	3823.0	98	15	29.5	77	30.3	454.1	5.0	80	30.0	449.3	5.0					x		x	
9-0-10	9	x		12811	6.0	3793.5	3822.5	96	15	29	75	30.0	450.3	5.0	77	29.8	446.4	5.0		x				x		
9-0-11	25	x		18001	5.5	3791.5	3822.5	102	16	31	83	31.2	499.7	5.3	84	31.2	498.7	5.3					x		x	
9-0-12	2	x		7741	5.3	3792.0	3822.5	100	15	30.5	85	30.6	459.2	5.0	88	30.5	457.8	5.0	x					x		
9-0-13	13	x		8193	5.6	3792.5	3821.0	97	15.5	28.5	83	28.7	445.1	5.0	78	29.1	451.6	5.1				x		x		
9-0-14	40	x		7813	4.4	3792.5	3821.0	94	12.5	28.5	76	29.4	367.2	4.4	70	30.3	379.1	4.4					x		x	
9-0-15	19	x		8219	9.7	3793.0	3821.0	97	15	28	73	29.3	439.2	5.0	66	30.6	459.7	5.0		x				x		
9-0-16	51	x		10215	12.4	3793.0	3821.0	97	15	28	76	28.9	432.9	4.9	76	28.9	432.9	4.9					x		x	
9-0-17	33	x		10090	14.0	3793.5	3822.0	96	15	28.5	76	29.4	440.6	5.0	79	29.0	435.5	4.9		x				x		
9-0-18	74	x		9681	10.2	3793.5	3822.5	96	13	29	75	30.0	390.3	4.5	80	29.4	382.8	4.5					x		x	
9-0-19	48	x		9177	12.3	3794.0	3822.5	93	15	28.5	77	29.2	438.7	5.0	81	28.9	432.8	4.9		x				x		
9-0-20	86	x		10412	8.2	3794.5	3822.5	92	16	28	80	28.4	454.9	5.1	87	28.0	448.6	5.1					x		x	
9-0-21	71			5984	7.1	3795.0	3823.0	97	15	28	82	28.3	424.1	4.9	85	28.1	421.6	4.9		x				x		

Table B1.1 Block 5 stope design details, 10-3 horizon stopes

				Stope Design															Stope Type					Drill Pattern		
STOPE NAME	HW Sequence mined	HW cables - fan upward	HW cables- fan downward	Stope size (tonnes) - planned	Stope muck grade (gm/tonne)	Stope base (floor elevation)	Stope top(top sill floor elevation)	Strike Azimuth	Stope Width on strike (@midspan)	Vertical Height (m)	Stope HW angle	True HW height	HW area (m2)	HW Hydraulic Radius (m)	Stope FW angle	True FW height	FW area (m2)	FW Hydraulic Radius (m)	Primary (P1)	P2	P3	Secondary (S1)	S2	parallel (primary)	ring (secondary)	Longitudinal
10-3 horizon																										
10-3-8	28			4381	7.5	3762.5	3794.0	95	13	31.5	72	33.1	430.6	4.7	72	33.1	430.6	4.7				x				x
10-3-9	20			4813	6.1	3763.0	3793.5	97	16.5	30.5	72	32.1	529.1	5.4	72	32.1	529.1	5.4				x				x
10-3-10	5			7659		3763.0	3793.5	102	15	30.5	72	32.1	481	5.1	68	32.9	493.4	5.2	x					x		
10-3-11	17			13993	6.4	3762.5	3791.5	102	16	29	72	30.5	487.9	5.2	72	30.5	487.9	5.2				x			x	
10-3-12	31			12114	8.8	3763.0	3793.0	102	15	30	72	31.5	473.2	5.1	78	30.7	460.1	5.0					x		x	
10-3-13	8			7304		3761.5	3792.5	94	15	31	75	32.1	481.4	5.1	77	31.8	477.2	5.1	x					x		
10-3-14	24			6696	10.8	3761.0	3792.0	93	15	31	75	32.1	481.4	5.1	78	31.7	475.4	5.1					x		x	
10-3-15	14			6329	7.6	3763.0	3793.0	97	15	30	78	30.7	460.1	5.0	80	30.5	456.9	5.0	x							x
10-3-16	62			9661	8.1	3762.0	3792.5	96	15	30.5	73	31.9	478.4	5.1	68	32.9	493.4	5.2					x		x	
10-3-17	22			9320	13.0	3762.5	3793.5	96	15	31	72	32.6	488.9	5.1	67	33.7	505.2	5.2	x					x		
10-3-18	57			13731	12.4	3762.5	3793.5	99	16	31	73	32.4	518.7	5.4	74	32.2	516	5.3					x		x	
10-3-19	45			12075	9.2	3763.0	3794.0	98	15	31	74	32.2	483.7	5.1	74	32.2	483.7	5.1	x					x		
10-3-20	77			12128	10.3	3764.5	3794.5	96	15	30	75	31.1	465.9	5.1	72	31.5	473.2	5.1					x		x	
10-3-21	63			9254	10.3	3764.0	3795.0	99	15	31	76	31.9	479.2	5.1	74	32.2	483.7	5.1	x					x		
10-3-22	82			4338	3.5	3764.5	3794.5	100	12	30	80	30.5	365.6	4.3	80	30.5	365.6	4.3				x			x	

Table B1.2 Block 5 stope recovery details, 9-3 horizon stopes

Stope Recovery Details

STOPE NAME	Survey date	mineral broken/blasted (tonnes)	CMS HW slough (tonnes)	CMS FW slough (tonnes)	CMS sidewall ore slough (tonnes)	CMS backfill - sidewall slough (tonnes)	CMS HW slough (m3)	CMS FW slough (m3)	HW - Dilution Density (m)	FW - Dilution Density (m)	total DDems (HW + FW)	% DD from HW	Vol Backfill (m3)	Milled Dilution %	Dil'n % unplanned waste/ore mined (tonnes)	Recovery %	Stope Cycle (#days)
9-3 horizon																	
9-3-1	12-Mar-97	9064	5014	1816	1069	0	1790.7	648.57	4.0	1.5	5.5	73.1		46.0	67.4	89.4	48
9-3-2	17-Jul-98	8460	3391	1392	0	1428	1211.1	497.14	3.4	1.4	4.8	70.8	3971	68.8	56.5	84.3	39
9-3-3	05-Jan-98	11201	3774	1750	1343	0	1347.9	625	2.7	1.3	3.9	68.0	4141	25.7	44.0	96.4	40
9-3-4	27-Apr-99	13469	3541	880	201	25	1264.6	314.29	2.2	0.6	2.8	79.9	4717	29.0	32.3	93.1	83
9-3-5	05-Jan-00	9305	5398	494	775	14	1927.9	176.43	4.1	0.4	4.5	91.7	3883	31.3	58.5	78.6	39
9-3-6	08-Aug-00	9552	3662	198	34	228	1307.9	70.714	3.3	0.2	3.5	94.9	3407	32.5	40.3	94.6	28
9-3-7	18-Jan-01	14095	3033	0	0	1015	1083.2	0	2.6	0.0	2.6	100.0	4982	64.4	21.5	99.7	51
9-3-8	01-Jun-99	15339	2960	0	1164	0	1057.1	0	2.6	0.0	2.6	100.0	4122	18.5	17.9	89.5	53
9-3-9	29-Feb-00	16334	0	0	4500	301	0	0	Ore left in HW				4907	2.3	0.0	89.9	46
9-3-10	28-Feb-98	32345	2148	0	2193	0	767.14	0	1.6	0.0	1.6	100.0	9596	2.8	6.2	92.0	59
9-3-11	04-Nov-98	13788	11888	1105	0	3968	4245.7	394.64	9.8	0.9	10.7	91.3	7763	57.6	94.2	94.4	54
9-3-12	17-Nov-97	20902	5306	986	992	0	1895	352.14	4.5	0.8	5.3	84.3	7231	21.6	28.7	86.2	52
9-3-13	05-May-99	22624	1878	526	390	92	670.71	187.86	1.4	0.4	1.8	78.0	6779	13.3	10.4	94.3	60
9-3-14	16-Mar-01	19940	2957	2718	0	2948	1056.1	970.71	2.4	2.2	4.6	51.7	7841	40.7	28.5	98.7	121
9-3-15	17-Dec-99	20155	3434	790	3288	0	1226.4	282.14	2.6	0.6	3.3	80.9	7301	22.6	18.0	93.0	56
9-3-16	02-Oct-01	19236	3256	1200	0	3608	1162.9	428.57	2.6	1.0	3.5	73.1	6881	38.3	23.2	96.9	58
9-3-17	15-Nov-00	19305	2266	287	2829	0	809.29	102.5	1.8	0.2	2.1	88.8	6167	10.7	11.5	95.8	127
9-3-18	10-Jan-02	6796	1029	1241	0	1045	367.5	443.21	1.1	1.3	2.3	45.3	2899	45.6	33.4	98.5	30
9-3-19	30-Apr-01	6833	2001	2947	2662	0	714.64	1052.5	2.0	3.0	5.1	40.4	2923	16.6	52.1	98.1	21
9-3-20	23-Sep-02	4138	283	322	0	0	101.07	115	0.3	0.3	0.6	46.8	1178	14.6	14.6	81.1	17
9-3-21	08-Jul-02	6596	425	2545	0	0	151.79	908.93	0.4	2.3	2.6	14.4	2295	4.8	45.0	167.1	26

Table B1.2 Block 5 stope recovery details, 9-2 horizon stopes

Stope Recovery Details

STOPE NAME	Survey date	mineral broken/blasted (tonnes)	CMS HW slough (tonnes)	CMS FW slough (tonnes)	CMS sidewall ore slough (tonnes)	CMS backfill - sidewall slough (tonnes)	CMS HW slough (m3)	CMS FW slough (m3)	HW - Dilution Density (m)	FW - Dilution Density (m)	total DDcms (HW + FW)	% DD from HW	Vol Backfill (m3)	Milled Dilution %	Dil'n % unplanned waste/ore mined (tonnes)	Recovery %	Stope Cycle (#days)
9-2 horizon																	
9-2-1	23-Sep-96	8195	1849		305	0	660.4		1.5	0.0	1.5	100.0		14.8	21.8	92.4	85
9-2-2	22-May-98	7761	2189	351	0	647	781.79	125.36	1.8	0.3	2.0	86.4	2840	45.5	32.7	94.0	44
9-2-3	22-Oct-97	7993	2517	88	351	0	898.93	31.429	2.0	0.1	2.0	96.6	3136	29.5	31.2	88.1	43
9-2-4	17-Jan-99	11849	1571	217	40	302	561.07	77.5	1.1	0.2	1.2	87.9	3277	17.1	15.0	84.6	50
9-2-5	15-Sep-99	8982	5700	114	2909	35	2035.7	40.714	4.7	0.1	4.8	98.0	4487	40.4	48.9	91.0	27
9-2-6	07-Jun-00	8080	2826	25	580	382	1009.3	8.9286	2.8	0.0	2.8	99.1	3254	24.5	32.9	91.4	32
9-2-7	30-Oct-00	8036	1812	403	276	237	647.14	143.93	1.7	0.4	2.1	81.6	2841	30.4	26.6	94.8	22
9-2-8	24-Dec-98	17347	4057	488	2030	0	1448.9	174.29	3.4	0.4	3.8	89.1	5506	17.6	23.5	92.5	37
9-2-9	17-Dec-99	19484	1019	620	0	1753	363.93	221.43	1.0	0.6	1.7	62.1	5851	16.6	8.4	96.4	50
9-2-10	18-Aug-97	20595	4594	527	1714	0	1640.7	188.21	3.5	0.4	3.9	89.8	7176	0.0	23.0	68.1	41
9-2-11	14-Aug-98	21054	4938	346	0	3038	1763.6	123.57	3.7	0.3	4.0	93.4	9364	12.4	25.1	75.7	66
9-2-12	08-Nov-96	16604	4111	306	828	0	1468.2	109.29	3.0	0.2	3.2	93.1		24.3	25.3	91.9	37
9-2-13	25-Jan-99	14300	1164	1502	467	210	415.71	536.43	0.8	1.1	1.9	43.4	4224	17.2	18.1	92.8	32
9-2-14	20-Oct-00	30889	4295	1233	0	912	1533.9	440.36	3.2	0.9	4.2	77.5	9663	20.8	17.9	98.4	66
9-2-15	30-Jul-99	26005	7202	2796	3254	0	2572.1	998.57	5.2	2.0	7.3	71.9	10478	21.5	34.2	95.0	72
9-2-16	15-Jun-01	19869	2205	909	0	1972	787.5	324.64	2.3	1.0	3.3	70.6	7008	31.5	15.7	97.0	59
9-2-17	19-Apr-00	20542	1549	89	2610	0	553.21	31.786	1.1	0.1	1.2	94.5	6358	7.0	7.1	93.9	47
9-2-18	18-Nov-01	No CMS	0	50	0	0	0	17.857									34
9-2-19	13-Feb-01	20223	1092	2605	5127	0	390	930.36	0.9	2.2	3.1	29.8	7560	9.2	14.6	99.2	60
9-2-20	25-Feb-02	5312	480	3455	0	140	171.43	1233.9	0.4	2.7	3.1	12.2	2711	74.1	74.1	94.0	25
9-2-21	19-Nov-01	21798	873	1383	1198	0	311.79	493.93	0.6	1.0	1.6	39.0	7222	9.8	9.8	94.1	59
9-2-22	26-Apr-02	14422	903	508	0	624	322.5	181.43	0.7	0.4	1.0	64.4	4937	14.1	9.8	86.9	41

Table B1.2 Block 5 stope recovery details, 9-1 horizon stopes

Stope Recovery Details

STOPE NAME	Survey date	mineral broken/blasted (tonnes)	CMS HW slough (tonnes)	CMS FW slough (tonnes)	CMS sidewall ore slough (tonnes)	CMS backfill - sidewall slough (tonnes)	CMS HW slough (m3)	CMS FW slough (m3)	HW - Dilution Density (m)	FW - Dilution Density (m)	total DDems (HW + FW)	% DD from HW	Vol Backfill (m3)	Milled Dilution %	Dil'n % unplanned waste/ore mined (tonnes)	Recovery %	Stope Cycle (#days)
9-1 horizon																	
9-1-2	30-May-96	4444	2976		79	0	1062.9		2.3	0.0	2.3	100.0		64.5	65.8	77.2	17
9-1-3	31-Dec-96	5535	4308	702	43	138	1538.6	250.71	2.5	0.4	2.9	86.1		67.8	89.8	76.4	48
9-1-4	30-Oct-95	6801	3165				1130.4		2.3	0.0	2.3	100.0			46.5	95.8	45
9-1-5	08-Jun-98	6355	782	550	132	46	279.29	196.43	0.6	0.4	1.0	59.1	2269	23.2	20.5	75.2	18
9-1-6	04-Jun-99	7570	838	450	258	216	299.29	160.71	0.6	0.3	1.0	65.5	2412	14.1	16.5	88.5	37
9-1-7	21-Jan-00	8452	1996	0	0	174	712.86	0	1.4	0.0	1.4	100.0	2612	30.0	23.6	82.6	30
9-1-8	18-May-98	17321	4088	27	1302	0	1460	9.6429	3.1	0.0	3.1	99.3	6911	19.4	22.1	88.2	48
9-1-9	17-Mar-99	18905	3509	447	685	2159	1253.2	159.64	2.9	0.4	3.3	89.0	7070	30.7	20.2	97.5	36
9-1-10	04-Sep-96	14459	766		293	0	273.6		0.6	0.0	0.6	100.0		5.2	5.2	91.4	28
9-1-11	18-Mar-98	18401	2541	393	0	566	907.5	140.36	2.0	0.3	2.3	87.1	6158	14.5	15.9	92.3	45
9-1-12	20-Dec-95	19717	3068		0	0	1095.7		2.4	0.0	2.4	100.0		14.2	15.6	97.2	88
9-1-13	08-Apr-97	11972	948	822	518	351	338.57	293.57	0.8	0.7	1.4	53.9		17.2	14.2	91.3	33
9-1-14	04-Oct-99	12112	16	148	0	312	5.7143	52.857	Ore left in HW				3084	5.0	1.4	88.5	34
9-1-15	18-Sep-97	11968	4117	70	1279	0	1470.4	25	3.1	0.1	3.1	98.3	5088	31.2	31.6	96.0	41
9-1-16	07-Jul-00	8823	113	428	0	209	40.357	152.86	0.1	0.3	0.4	20.8	2323	8.3	6.1	90.5	29
9-1-17	02-Apr-98	8562	3942	8	484	0	1407.9	2.8571	2.9	0.0	2.9	99.8	3812	32.4	43.7	89.6	27
9-1-18	26-Mar-01	6126	0	255	0	95	0	91.071	Ore left in HW				1559	5.6	4.2	73.4	30
9-1-19	12-May-00	7856	1939	896	637	0	692.5	320	1.4	0.7	2.1	68.3	2988	33.4	33.4	91.8	75
9-1-20	31-Dec-01	7400	500	0			178.57	0	0.4	0.0	0.4	100.0			6.8		21
9-1-21	26-Jan-01	5617	1302	2520	346	0	465	900	1.0	1.9	2.9	34.1	1726	36.9	64.1	90.8	28

Table B1.2 Block 5 stope recovery details, 9-0 horizon stopes

Stope Recovery Details

STOPE NAME	Survey date	mineral broken/blasted (tonnes)	CMS HW slough (tonnes)	CMS FW slough (tonnes)	CMS sidewall ore slough (tonnes)	CMS backfill - sidewall slough (tonnes)	CMS HW slough (m3)	CMS FW slough (m3)	HW - Dilution Density (m)	FW - Dilution Density (m)	total DDems (HW + FW)	% DD from HW	Vol Backfill (m3)	Milled Dilution %	Dil'n %: unplanned waste/ore mined (tonnes)	Recovery %	Stope Cycle (#days)
9-0 horizon																	
9-0-3	15-Mar-96	4089	2214		0	32	790.7		1.7	0.0	1.7	100.0		47.9	54.1	55.7	30
9-0-4	14-Nov-95	5095	1157		0	32	413.2		0.8	0.0	0.8	100.0			22.7	83.1	120
9-0-5	20-Mar-96	4755	1385		0	0	494.6		1.1	0.0	1.1	100.0		22.8	29.1	85.4	68
9-0-6	20-Jun-96	4355	1323		0	11	472.5		0.9	0.0	0.9	100.0		30.6	30.4	94.7	27
9-0-7	29-Oct-98	3678	1381	336	0	0	493.21	120	1.0	0.2	1.3	80.4	1646	45.6	46.7	83.8	34
9-0-8	10-Mar-98	4123	2631	67	61	0	939.64	23.929	2.1	0.1	2.2	97.5	1843	66.4	64.5	63.7	51
9-0-9	07-Aug-98	14711	2563	158	0	196	915.36	56.429	2.0	0.1	2.1	94.1	5250	21.8	18.5	88.1	50
9-0-10	17-May-96	11734	2788		135	0	995.7		2.2	0.0	2.2	100.0		11.3	23.5	89.3	23
9-0-11	11-Aug-97	17132	1541	1383	196	702	550.36	493.93	1.1	1.0	2.1	52.7	6252	21.0	16.9	94.9	45
9-0-12	19-Aug-95	7100	800	150	0	0	285.71	53.571	0.6	0.1	0.7	84.2			13.4		25
9-0-13	03-Aug-96	7743	2662		1317	0	950.7		2.1	0.0	2.1	100.0		14.4	29.4	89.6	23
9-0-14	11-May-98	7265	184	427	0	175	65.714	152.5	0.2	0.4	0.6	30.8	2229	11.0	8.4	91.7	27
9-0-15	31-Dec-96	7861	3239	404	807	0	1156.8	144.29	2.6	0.3	2.9	89.4		36.1	42.0	87.1	34
9-0-16	12-Jan-99	8195	0	1305	112	65	0	466.07	Ore left in HW				2411	16.6	15.7	79.7	34
9-0-17	28-Jan-98	9703	2361	384	331	0	843.21	137.14	1.9	0.3	2.2	85.9	3528	21.9	27.4	96.2	41
9-0-18	10-Jul-00	9119	335	198	111	231	119.64	70.714	0.3	0.2	0.5	62.4	2416	8.3	5.8	94.2	24
9-0-19	04-Nov-98	8397	817	393	934	0	291.79	140.36	0.7	0.3	1.0	67.2	2602	13.0	13.0	91.5	29
9-0-20	03-May-01	9144	497	18	0	97	177.5	6.4286	0.4	0.0	0.4	96.5	2355	6.6	5.6	87.8	28
9-0-21	10-Apr-00	5568	993	504	0	0	354.64	180	0.8	0.4	1.3	66.2	1830	25.0	26.9	93.0	23

Table B1.2 Block 5 stope recovery details, 10-3 horizon stopes

Stope Recovery Details

STOPE NAME	Survey date	mineral broken/blasted (tonnes)	CMS HW slough (tonnes)	CMS FW slough (tonnes)	CMS sidewall ore slough (tonnes)	CMS backfill - sidewall slough (tonnes)	CMS HW slough (m3)	CMS FW slough (m3)	HW - Dilution Density (m)	FW - Dilution Density (m)	total DDcms (HW + FW)	% DD from HW	Vol Backfill (m3)	Milled Dilution %	Dil'n %: unplanned waste/ore mined (tonnes)	Recovery %	Stope Cycle (#days)
10-3 horizon																	
10-3-8	04-Sep-97	3331	2865	165	0	0	1023.2	58.929	2.4	0.1	2.5	94.6	1781	15.7	91.0	76.0	26
10-3-9	31-Jan-97	4559	3408	305	270	2	1217.1	108.93	2.3	0.2	2.5	91.8		37.3	76.9	75.0	48
10-3-10	19-Dec-95	6791	3337		0	0	1191.8		2.5	0.0	2.5	100.0		30.9	49.1	88.7	42
10-3-11	27-Nov-96	13159	3168	237	294	21	1131.4	84.643	2.3	0.2	2.5	93.0		11.9	25.3	94.0	36
10-3-12	05-Jan-98	11540	3492	910	0	4186	1247.1	325	2.6	0.7	3.3	78.9	5054	39.9	38.1	95.3	62
10-3-13	28-Mar-96	6037	1580		0	0	564.3		1.2	0.0	1.2	100.0		10.1	26.2	82.7	21
10-3-14	27-May-97	6366	2587	875	0	118	923.93	312.5	1.9	0.7	2.6	74.5		50.9	54.4	95.1	20
10-3-15	07-Aug-96	4256	2647		76	0	945.4		2.1	0.0	2.1	100.0		55.5	61.1	67.2	26
10-3-16	01-Oct-99	8695	3806	58	0	110	1359.3	20.714	2.8	0.0	2.9	98.5	3402	44.7	44.4	88.4	29
10-3-17	12-Mar-97	8610	2976	347	234	0	1062.9	123.93	2.2	0.2	2.4	89.9		29.3	37.6	92.4	38
10-3-18	17-May-99	12964	1412	765	472	126	504.29	273.21	1.0	0.5	1.5	64.7	3959	17.0	16.2	94.4	31
10-3-19	30-Jul-98	11167	2746	186	677	0	980.71	66.429	2.0	0.1	2.2	93.7	4174	23.1	24.8	91.9	29
10-3-20	01-Sep-00	11231	1569	72	0	40	560.36	25.714	1.2	0.1	1.3	95.7	3216	14.6	14.6	92.6	29
10-3-21	28-Oct-99	7886	468	0	24	0	167.14	0	0.3	0.0	0.3	100.0	2007	5.6	5.9	85.2	25
10-3-22	21-Dec-00	3788	492	153	0	0	175.71	54.643	0.5	0.1	0.6	76.3	1111	17.0	17.0	87.3	24

Table B1.3 Block 5 stope blasting details, 9-3 horizon stopes

	Blasting Details																									
	Blast #1					Blast #2					Blast #3					Blast #4					Blast #5				
STOPE NAME	Date Blast #1	Tonnes Blasted	Tonnes Powder (kg)	PF (kg/TM)	Powder Factor (kg/m3)	Date Blast #2	Tonnes Blasted	Tonnes Powder	PF (kg/TM)	Powder Factor (kg/m3)	Date Blast #3	Tonnes Blasted	Tonnes Powder	PF (kg/TM)	Powder Factor (kg/m3)	Date Blast #4	Tonnes Blasted	Tonnes Powder	PF (kg/TM)	Powder Factor (kg/m3)	Date Blast #5	Tonnes Blasted	Tonnes Powder	PF (kg/TM)	Powder Factor (kg/m3)
9-3 horizon																									
9-3-1	24-Jan-97	3000	1275	0.43	1.83	31-Jan-97	1000	405	0.4	1.74	10-Feb-97	4800	2153	0.45	1.93										
9-3-2	08-Jun-98	3100	810	0.26	1.12	19-Jun-98	2500	646	0.26	1.11	03-Jul-98	5700	1598	0.28	1.2										
9-3-3	25-Nov-97	1100	1058	0.5	2.16	12-Dec-97	4900	1218	0.34	1.45	17-Dec-97	3100	1063	0.35	1.525										
9-3-4	04-Feb-99	1000	595	0.6	2.56	09-Feb-99	2300	1063	0.46	1.99	18-Feb-99	4400	2148	0.49	2.1	25-Feb-99	7000	4276	0.61	2.63					
9-3-5	26-Nov-99	1550	608	0.39	1.69	02-Dec-99	3900	1199	0.31	1.32	14-Dec-99	5550	3035	0.54	2.34										
9-3-6	10-Jul-00	1850	810	0.44	1.88	17-Jul-00	2800	901	0.32	1.38	21-Jul-00	5150	1522	0.3	1.27										
9-3-7	27-Nov-00	1300	811	0.62	2.68	04-Dec-00	3700	1561	0.42	1.73	15-Dec-00	8500	2847	0.47	2										
9-3-8	08-Apr-99	750	666	0.89	3.82	14-Apr-99	2700	1079	0.4	1.72	06-May-99	4700	2346	0.5	1.9	17-May-99	7250	3083	0.43	1.74					
9-3-9	13-Jan-00	1100	946	0.86	3.7	19-Jan-00	5200	2457	0.47	2.03	04-Feb-00	6500	3042	0.47	2.01										
9-3-10	29-Dec-97	1025	645	0.63	2.71	09-Jan-98	3000	1929	0.64	2.76	22-Jan-98	16400	5270	0.32	1.29										
9-3-11	10-Sep-98	7500	2397	0.32	1.37	21-Sep-98	4600	2535	0.55	2.37															
9-3-12	25-Sep-97	5000	2374	0.47	2.04	10-Oct-97	6950	3245	0.47		23-Oct-97	6950	3222	0.46	1.98										
9-3-13	05-Mar-99	1800	934	0.52	2.23	10-Mar-99	2800	1610	0.58	2.47	22-Mar-99	4600	2374	0.52	2.22	10-Apr-99	17300	5963	0.34	1.38					
9-3-14	15-Nov-00	2300	642	0.28	1.2	18-Nov-00	2000	540	0.27	1.16	24-Nov-00	2700	960	0.36	1.53	06-Dec-00	13350	3946	0.3	1.22					
9-3-15	21-Oct-99	1050	690	0.66	2.83	01-Nov-99	3100	1096	0.35	1.52	05-Nov-99	5800	2673	0.46	1.98	10-Nov-99	12450	3361	0.27	1					
9-3-16	04-Aug-01	1400	805	0.58	2.47	12-Aug-01	6300	2551	0.47	2.03	03-Sep-01	4100	1250	0.3											
9-3-17	08-Jul-00	1000	712	0.71	3.06	23-Jul-00	3200	977	0.31	1.31	01-Sep-00	3500	1373	0.39	1.69	25-Sep-00	12300	5221	0.42	1.6					
9-3-18	10-Dec-01	1700	792	0.47	2	12-Dec-01	1500	423	0.28	1.21	20-Dec-01	3700	1530	0.41	1.78										
9-3-19	09-Apr-01	5400	2268	0.42	1.81																				
9-3-20	06-Sep-02	1100	687	0.62	2.69	11-Sep-02	1300	497	0.38	1.64	16-Sep-02	2700	937	0.35	1.49										
9-3-21	12-Jun-02	1500	454	0.3	1.3	15-Jun-02	800	477	0.6	2.56	20-Jun-02	3000	1856	0.62	2.66										

Table B1.3 Block 5 stope blasting details, 9-2 horizon stopes

	Blasting Details																								
	Blast #1					Blast #2					Blast #3					Blast #4					Blast #5				
STOPE NAME	Date Blast #1	Tonnes Blasted	Tonnes Powder (kg)	PF (kg/TM)	Powder Factor (kg/m3)	Date Blast #2	Tonnes Blasted	Tonnes Powder	PF (kg/TM)	Powder Factor (kg/m3)	Date Blast #3	Tonnes Blasted	Tonnes Powder	PF (kg/TM)	Powder Factor (kg/m3)	Date Blast #4	Tonnes Blasted	Tonnes Powder	PF (kg/TM)	Powder Factor (kg/m3)	Date Blast #5	Tonnes Blasted	Tonnes Powder	PF (kg/TM)	Powder Factor (kg/m3)
9-2 horizon																									
9-2-1	28-Jun-96	2000	748	0.37		30-Jun-96	6000	3118	0.52																
9-2-2	08-Apr-98	850	705	0.71	2.81	16-Apr-98	2800	1190	0.43	1.7	29-Apr-98	4250	1689	0.4	1.71										
9-2-3	09-Sep-97	1000	690	0.69	2.69	10-Sep-97	1600	780	0.49	1.9	03-Oct-97	5700	1112	0.24	1.02										
9-2-4	27-Nov-98	550	322	0.59	2.28	02-Dec-98	1250	615	0.49	2.01	11-Dec-98	2000	501	0.25	1.02	17-Dec-98	2550	842	0.33	1.42	30-Dec-98	6800	3612	0.53	2.17
9-2-5	18-Aug-99	1300	919	0.7	3.04	23-Aug-99	2700	1556	0.58		28-Aug-99	3800	1885	0.49	2.13										
9-2-6	05-May-00	1400	683	0.49	2.05	15-May-00	2100	653	0.31	1.31	18-May-00	4900	1941	0.4	1.66										
9-2-7	08-Oct-00	1500	932	0.62	2.67	13-Oct-00	3000	653	0.33	1.4	20-Oct-00	4100	1793	0.44	1.8										
9-2-8	17-Nov-98	1000	730	0.73	3.14	19-Nov-98	900	551	0.61	2.51	29-Nov-98	4400	1319	0.38	2.58	07-Dec-98	10600	3443	0.32	4.8					
9-2-9	27-Oct-99	1200	939	0.78	3.36	31-Oct-99	3000	1488	0.47	2.03	07-Nov-99	6200	1654	0.27	1.12	16-Nov-99	9600	2507	0.26	1.17					
9-2-10	07-Jul-97	900	628	0.7	2.65	08-Jul-97	1400	654	0.47	1.77	09-Jul-97	4650	2155	0.46	1.99	18-Jul-97	5200	1789	0.34	1.48	23-Jul-97	9350	3537	0.38	1.63
9-2-11	08-Jun-98	2800	763	0.27	1.06	15-Jun-98	3300	820	0.25	1.04	23-Jun-98	5950	2707	0.45	1.9	10-Jul-98	8150	2289	0.28	1.21					
9-2-12	01-Oct-96	1300	797	0.61	2.45	03-Oct-96	1250	604	0.48	2.08	07-Oct-96	7500	2563	0.34	1.47	08-Oct-96	6950	1807	0.26	1.12					
9-2-13	23-Dec-98	1100	455	0.41	1.65	04-Jan-99	2000	840	0.42		08-Jan-99	4700	2151	0.46	1.87	17-Jan-99	6300	3598	0.57	2.46					
9-2-14	14-Aug-00	1750	798	0.46	1.96	18-Aug-00	6500	997	0.25	1.07	30-Aug-00	6100	2398	0.39	1.69	19-Sep-00	6850	2295	0.34	1.47	27-Sep-00	7400	2309	0.31	1.19
9-2-15	18-May-99	1000	808	0.808	3.15	24-May-99	1800	946	0.53	2.26	03-Jun-99	6300	1759	0.28	1.12	17-Jun-99	7800	3855	0.49	1.83	29-Jun-99	11700	6428	0.55	1.92
9-2-16	16-Apr-01	950	528	0.56	2.39	23-Apr-01	2250	588	0.31	1.33	02-May-01	3000	1325	0.44	1.9	22-May-01	13200	5206	0.47	1.84					
9-2-17	02-Mar-00	1650	979	0.59	2.55	05-Mar-00	1250	820	0.66	2.82	08-Mar-00	6300	1870	0.3	1.28	18-Mar-00	11800	4009	0.34	1.3					
9-2-18	14-Oct-01	1500	783	0.52	2.24	24-Oct-02	3300	1133	0.34	1.51	02-Nov-01	3800	1294	0.34	1.46										
9-2-19	13-Dec-00	1000	661	0.66	2.84	17-Dec-00	1900	1297	0.59	2.53	24-Dec-00	7000	2345	0.34	1.44	04-Jan-01	8800	3732	0.42	1.48					
9-2-20	31-Jan-02	1200	493	0.41	1.77	05-Feb-02	1850	750	0.41	1.74	08-Feb-02	2600	1257	0.48	2.08										
9-2-21	20-Sep-01	1400	752	0.54	1.99	25-Sep-01	1700	1197	0.7	2.44	02-Oct-01	3700	1529	0.41	1.53	10-Oct-01	7800	3568	0.46	1.6	29-Oct-01	7800	3472	0.45	1.6
9-2-22	15-Mar-02	1100	796	0.72	2.53	19-Mar-02	2300	909	0.4	1.38	25-Mar-02	3900	2125	0.55	1.74	02-Apr-02	9300	4788	0.51	1.65					

Table B1.3 Block 5 stope blasting details, 9-1 horizon stopes

	Blasting Details																									
	Blast #1					Blast #2					Blast #3					Blast #4					Blast #5				
STOPE NAME	Date Blast #1	Tonnes Blasted	Tonnes Powder (kg)	PF (kg/TM)	Powder Factor (kg/m3)	Date Blast #2	Tonnes Blasted	Tonnes Powder	PF (kg/TM)	Powder Factor (kg/m3)	Date Blast #3	Tonnes Blasted	Tonnes Powder	PF (kg/TM)	Powder Factor (kg/m3)	Date Blast #4	Tonnes Blasted	Tonnes Powder	PF (kg/TM)	Powder Factor (kg/m3)	Date Blast #5	Tonnes Blasted	Tonnes Powder	PF (kg/TM)	Powder Factor (kg/m3)
9-1 horizon																									
9-1-2	13-May-96	800	657	0.82		14-May-96	950	641	0.67		21-5-96	2900	1582	0.55											
9-1-3	13-Nov-96	200	271	1.35	4.74	14-Nov-96	700	484	0.69	2.42	12-Jun-96	4800	2320	0.48	1.69										
9-1-4	15-Sep-95	1100	936	0.85		19-Sep-95	1200	786	0.66		22-9-95	4900	1594	0.33											
9-1-5	20-May-98	2500	1199	0.48		29-May-98	4250	1486	0.35	1.44															
9-1-6	27-Apr-99	200	250			05-Apr-99	1500	481	0.32	1.12	13-5-99	6300	3221	0.51	1.99										
9-1-7	21-Dec-99	1350	743	0.55	2.37	24-Dec-99	2150	1057	0.49	1.92	07-Jan-00	5150	2564	0.49	1.91										
9-1-8	30-Mar-98	800	477	0.6	2.08	03-Apr-98	1150	436	0.48	1.69	06-Apr-98	4150	1129	0.27	1.18	23-Apr-98	5274	1250	0.42	1.81					
9-1-9	11-Feb-99	2000	1312	0.66	2.56	16-Feb-99	2600	1139	0.44	1.75	19-2-99	4000	2669	0.67	2.12	01-Mar-99	9400	5689	0.61	2.12					
9-1-10	06-Aug-96	1400	961	0.69		09-Aug-96	4400	1544	0.35		15-8-96	9200	3547	0.39											
9-1-11	03-Feb-98	1550	882	0.57	1.99	09-Feb-98	1400	642	0.46	1.6	13-Feb-98	4050	1796	0.44	1.55	24-Feb-98	12400	5121	0.41	1.45					
9-1-12	22-Sep-95	1200	824	0.69		23-Sep-95	1100	686	0.62		02-Oct-95	6850	1940	0.28		04-Oct-95	9350	3180	0.34						
9-1-13	05-Mar-97	700	774	1.1	4.75	06-Mar-97	1700	986	0.58	2.26	14-Mar-97	4000	1946	0.49	1.9	21-Mar-97	5250	2438	0.46	2					
9-1-14	31-Aug-99	1700	905	0.53	2.08	09-Sep-99	5650	2202	0.39	1.52	17-Sep-99	6150	2699	0.44	1.8										
9-1-15	07-Aug-97	850	646	0.76	3.27	20-Aug-97	3100	1578	0.51	2.18	26-Aug-97	7800	3121	0.4	1.72										
9-1-16	08-Jun-00	1400	622	0.44	1.91	09-Jun-00	4200	1242	0.3	1.24	20-Jun-00	4200	1742	0.41	1.78										
9-1-17	05-Mar-98	1200	613	0.51	2.18	17-Mar-98	1800	741	0.41	1.77	23-Mar-98	6050	1745	0.29	1.27										
9-1-18	26-Feb-01	1200	561	0.47	2.01	02-Mar-01	2600	729	0.28	1.21	12-Mar-01	4400	1274	0.29	1.25										
9-1-19	27-Feb-00	1000	627	0.63	2.7	26-Mar-00	2150	635	0.3	1.27	07-Apr-00	1850	657	0.36	1.53	10-Apr-00	3200	1266	0.4	1.7					
9-1-20	10-Dec-01	750	289	0.38	1.46	14-Dec-01	2700	834	0.31	1.33	21-Dec-01	4000	1551	0.39	1.67										
9-1-21	28-Dec-00	800	452	0.57	2.43	29-Dec-00	1150	553	0.48	2.07	09-Jan-01	3400	1017	0.3	1.26										

Table B1.3 Block 5 stope blasting details, 9-0 horizon stopes

	Blasting Details																								
	Blast #1					Blast #2					Blast #3					Blast #4					Blast #5				
STOPE NAME	Date Blast #1	Tonnes Blasted	Tonnes Powder (kg)	PF (kg/TM)	Powder Factor (kg/m3)	Date Blast #2	Tonnes Blasted	Tonnes Powder	PF (kg/TM)	Powder Factor (kg/m3)	Date Blast #3	Tonnes Blasted	Tonnes Powder	PF (kg/TM)	Powder Factor (kg/m3)	Date Blast #4	Tonnes Blasted	Tonnes Powder	PF (kg/TM)	Powder Factor (kg/m3)	Date Blast #5	Tonnes Blasted	Tonnes Powder	PF (kg/TM)	Powder Factor (kg/m3)
9-0 horizon																									
9-0-3	15-Feb-96	500	503	1.01		19-Feb-96	700	375	0.54		26-Feb-96	3100	1924	0.62											
9-0-4	14-Jul-95	1000	632	0.63		18-Jul-95	950	469	0.55		21-Jul-95	3750	1201	0.32											
9-0-5	12-Jan-96	1450	891	0.61		16-Jan-96	2350	1604	0.68		24-Jan-96	1350	704	0.52											
9-0-6	23-May-96	170	218	1.28		25-May-96	900	539	0.6		06-Jun-96	500	341	0.68		04-Oct-95	3580	1779	0.49						
9-0-7	25-Sep-98	450	356	0.79	2.77	05-Oct-98	1050	654	0.62	2.18	07-Oct-98	2600	1510	0.58	2.03										
9-0-8	19-Jan-98	550	318	0.58	2.02	21-Jan-98	1000	432	0.43	1.51	23-Jan-98	2800	1150	0.41	1.44										
9-0-9	17-Jun-98	2300	713	0.31	1.2	23-Jun-98	3500	704	0.2	1.24	09-Jul-98	2900	1431	0.49	1.92	22-Jul-98	9900	2895	0.29	1.26					
9-0-10	24-Apr-96	1000	849	0.85		26-Apr-96	3800	1427	0.38		03-May-96	6350	2655	0.42											
9-0-11	26-Jun-97	850	600	0.7	3.03	27-Sep-97	2250	1175	0.52	2.24	09-Jul-97	2900	2103	0.72	2.76	23-Jul-97	7300	3230	0.44	1.9	29-Jul-97	3400	1586	0.47	2
9-0-12	24-Jul-95	1600	702	0.44		25-Jul-95	600	392	0.65		28-Jul-95	4400	1258	0.29											
9-0-13	10-Jul-96	1000	614	0.61		15-Jul-96	3000	1135	0.38		22-Jul-96	4200	2058	0.49											
9-0-14	14-Apr-98	1700	995	0.59	2.52	17-Apr-98	1600	512	0.32	1.38	27-Apr-98	4650	1648	0.35	1.52										
9-0-15	27-Nov-96	700	322	0.46	1.98	28-Nov-96	1500	639	0.43	1.83	09-Dec-96	5550	2509	0.45	1.94										
9-0-16	08-Dec-98	200	317	1.58	6.8	14-Dec-98	2800	910	0.33	1.4	18-Dec-98	2500	1724	0.69	2.96	06-Jan-99	4500	2235	0.5						
9-0-17	17-Dec-97	1000	674	0.67	2.9	19-Dec-97	2400	880	0.37	1.57	05-Jan-98	6400	2621	0.41	1.76										
9-0-18	16-Jun-00	1300	699	0.54	2.31	22-Jun-00	4500	1468	0.33	1.4	04-Jul-00	3600	2172	0.6	2.59										
9-0-19	05-Oct-98	1200	839	0.7	3	08-Oct-98	1750	836	0.48	2.05	15-Oct-98	6500	1887	0.29											
9-0-20	05-Apr-01	1800	848	0.47	2.03	20-Apr-01	3500	1211	0.35	1.49		5250													
9-0-21	17-Mar-00	900	574	0.64	1.74	22-Mar-00	1000	644	0.64	2.77	28-Mar-00	3700	1212	0.33	1.41										

Table B1.3 Block 5 stope blasting details, 10-3 horizon stopes

	Blasting Details																								
	Blast #1					Blast #2					Blast #3					Blast #4					Blast #5				
STOPE NAME	Date Blast #1	Tonnes Blasted	Tonnes Powder (kg)	PF (kg/TM)	Powder Factor (kg/m3)	Date Blast #2	Tonnes Blasted	Tonnes Powder	PF (kg/TM)	Powder Factor (kg/m3)	Date Blast #3	Tonnes Blasted	Tonnes Powder	PF (kg/TM)	Powder Factor (kg/m3)	Date Blast #4	Tonnes Blasted	Tonnes Powder	PF (kg/TM)	Powder Factor (kg/m3)	Date Blast #5	Tonnes Blasted	Tonnes Powder	PF (kg/TM)	Powder Factor (kg/m3)
10-3 horizon																									
10-3-8	08-Aug-97	1085	562	0.52	1.81	18-Aug-97	1015	591	0.58	2.04	19-Aug-97	1700	779	0.46	1.6										
10-3-9	13-Dec-96	350	260	0.74	2.6	17-Dec-96	950	626	0.66	2.31	18-Dec-96	3400	2481	0.73	2.55										
10-3-10	07-Nov-95	875	756	0.86		09-Nov-95	1100	656	0.6		10-Nov-95	4625	1260	0.27											
10-3-11	21-Oct-96	1225	949	0.77	3.33	25-Oct-96	1575	1129	0.71	2.5	04-Nov-96	4500	1820	0.4	1.74	11-Nov-96	7200	2918	0.41	1.42					
10-3-12	03-Nov-97	1900	1116	0.59	2.06	07-Nov-97	3000	942	0.31	1.22	20-Nov-97	5157	3948	0.76	3.3										
10-3-13	07-Mar-96	1200	636	0.53		08-Mar-96	1850	796	0.43		15-Mar-96	3750	1687	0.45											
10-3-14	07-May-97	1000	419	0.42	1.8	13-May-97	2300	1014	0.44	1.9	15-May-97	2850	1896	0.66	2.86										
10-3-15	11-Jul-96	800	512	0.64		12-Jul-96	600	334	0.56		16-Jul-96	2600	949	0.37											
10-3-16	02-Sep-99	1000	627	0.63	2.7	07-Sep-99	4000	826	0.21	1.13	13-Sep-99	5250	1546	0.29	1.27										
10-3-17	04-Feb-97	950	661	0.7	2.99	05-Feb-97	1900	915	0.48	2.07	14-Feb-97	6300	3313	0.53	2.26										
10-3-18	16-Apr-99	1100	419	0.38	1.64	19-Apr-99	1500	477	0.32	1.37	23-Apr-99	5200	1938	0.37	1.6	03-May-99	6600	3622	0.55	2.36					
10-3-19	01-Jul-98	1050	629	0.6	2.57	08-Jul-98	2550	953	0.37	1.61	16-Jul-98	8800	2544	0.29	1.24										
10-3-20	02-Aug-00	1500	1128	0.752	3.23	09-Aug-00	4600	920	0.3	1.26	17-Aug-00	6100	2003	0.33	1.41										
10-3-21	03-Oct-99	1350	865	0.64	2.75	05-Oct-99	1300	762	0.59	2.52	12-Oct-99	6850	2097	0.31	1.33										
10-3-22	27-Nov-00	950	664	0.7	3	01-Dec-00	1400	853	0.61	2.62	13-Dec-00	1850	1083	0.59	2.52										

APPENDIX B2

Zone 3-1 stope design and CMS database

Table B2.1 Zone 3-1 stope design details, 3560m and 3590m horizon stopes

				Stope Design															Stope Type					Drill Pattern		
STOPE NAME	HW Sequence mined	HW cables - fan upward	HW cables- fan downward	Stope size (tonnes) - planned	Stope muck grade (gm/tonne)	Stope base (floor elevation)	Stope top(top sill floor elevation)	Strike Azimuth	Stope Width on strike (@midspan)	Vertical Height (m)	Stope HW angle	True HW height	HW area (m2)	HW Hydraulic Radius (m)	Stope FW angle	True FW height	FW area (m2)	FW Hydraulic Radius (m)	Primary (P1)	P2	P3	Secondary (S1)	S2	parallel (primary)	ring (secondary)	Longitudinal
3590 horizon																										
3590-19	52			2850	6.5	3593.5	3624.5	98	10	31	94	31.1	310.8	3.8	93	31.0	310.4	3.8	x							x
3590-20	64			2650	5.0	3593.0	3624.0	95	9	31	88	31.0	279.2	3.5	90	31.0	279.0	3.5				x				x
3590-21	72			4400	8.2	3593.0	3624.0	101	12.5	31	88	31.0	387.7	4.5	89	31.0	387.6	4.5					x			x
3590-22	59			4000	8.4	3593.0	3624.0	101	11	31	86	31.1	341.8	4.1	88	31.0	341.2	4.1		x						x
3590-23	70			4700	13.2	3593.5	3625.0	96	11	31.5	89	31.5	346.6	4.1	90	31.5	346.5	4.1					x			x
3590-24	48			4350		3594.0	3624.0	93	10	30	91	30.0	300.0	3.8	92	30.0	300.2	3.8			x					x
3590-25	75			No Record		3593.5	3623.5	93	8	30	88	30.0	240.1	3.2	92	30.0	240.1	3.2					x		x	
3590-26	60			3300	10.1	3593.5	3623.5	97	10	30	88	30.0	300.2	3.8	91	30.0	300.0	3.8		x						x
3590-27	71			2500	6.7	3592.5	3625.0	95	8.5	32.5	87	32.5	276.6	3.4	87	32.5	276.6	3.4					x		x	
3590-28	55			3350	7.1	3592.5	3625.0	97	10	32.5	83	32.7	327.4	3.8	85	32.6	326.2	3.8			x					x
3560 horizon																										
3560-21	57			3200	5.0	3562.5	3593.0	100	9	30.5	81	30.9	277.9	3.5	83	30.7	276.6	3.5				x				x
3560-22	49			2950	6.9	3563.0	3593.0	100	9	30	82	30.3	272.7	3.5	80	30.5	274.2	3.5	x						x	
3560-23	66			6000	7.2	3562.0	3593.5	101	11	31.5	91	31.5	346.6	4.1	88	31.5	346.7	4.1					x	x		
3560-24	42			3937	9.8	3562.5	3594.0	93	10	31.5	93	31.5	315.4	3.8	89	31.5	315.0	3.8			x				x	
3560-25	68			6000	13.6	3560.5	3593.5	94	11.5	33	93	33.0	380.0	4.3	88	33.0	379.7	4.3					x	x		
3560-26	38			6101	14.6	3560.5	3594.0	98	10	33.5	91	33.5	335.1	3.9	90	33.5	335.0	3.9			x				x	
3560-27	67			5550	8.0	3560.0	3593.0	97	11.5	33	93	33.0	380.0	4.3	91	33.0	379.6	4.3					x		x	
3560-28	40			4612	6.2	3560.5	3592.5	98	10	32	88	32.0	320.2	3.8	90	32.0	320.0	3.8			x				x	
3560-29	74			5000	6.8	3560.0	3592.5	97	13.5	32.5	90	32.5	438.8	4.8	90	32.5	438.8	4.8				x			x	
3560-30				PILLAR																						
3560-31	69			2650	5.4	3559.5	3593.0	96	8.5	33.5	84	33.7	286.3	3.4	85	33.6	285.8	3.4				x				x
3560-32	62			2450	3.2	3559.5	3593.0	95	9.5	33.5	86	33.6	319.0	3.7	86	33.6	319.0	3.7	x							x

Table B2.1 Zone 3-1 stope design details, 3500m and 3530m horizon stopes

				Stope Design															Stope Type				Drill Pattern		
STOPE NAME	HW Sequence mined	HW cables - fan upward	HW cables- fan downward	Stope size (tonnes) - planned	Stope muck grade (gm/tonne)	Stope base (floor elevation)	Stope top(top sill floor elevation)	Strike Azimuth	Stope Width on strike (@midspan)	Vertical Height (m)	Stope HW angle	True HW height	HW area (m2)	HW Hydraulic Radius (m)	Stope FW angle	True FW height	FW area (m2)	FW Hydraulic Radius (m)	Primary (P1)	P2	P3	Secondary (S1)	S2	parallel (primary)	ring (secondary)	Longitudinal
3530 horizon																										
3530-24	37			4122	5.2	3526.5	3562.5	93	11.5	36	88	36.0	414.3	4.4	88	36.0	414.3	4.4	x					x		
3530-25	51			4850	5.9	3526.5	3560.5	95	11	34	85	34.1	375.4	4.2	84	34.2	376.1	4.2					x		x	
3530-26	34			4372	7.2	3527.0	3560.5	98	10	33.5	80	34.0	340.2	3.9	79	34.1	341.3	3.9		x				x		
3530-27	46			4050	5.6	3527.0	3560.5	93	10	33.5	81	33.9	339.2	3.9	78	34.2	342.5	3.9					x		x	
3530-28	22			9698	7.7	3526.5	3560.5	94	10	34	82	34.3	343.3	3.9	84	34.2	341.9	3.9		x				x		
3530-29	63			8150	8.1	3527.0	3560.5	94	9	33.5	76	34.5	310.7	3.6	82	33.8	304.5	3.6					x		x	
3530-30	19			7900	9.7	3527.5	3559.0	99	10	31.5	77	32.3	323.3	3.8	83	31.7	317.4	3.8			x			x		
3530-31	54			5500	7.3	3528.5	3559.0	94	11	30.5	80	31.0	340.7	4.1	89	30.5	335.6	4.0					x		x	
3530-32	20			6227	5.8	3528.0	3559.5	98	10	31.5	82	31.8	318.1	3.8	85	31.6	316.2	3.8		x					x	
3530-33	32			4914	6.1	3529.0	3560.0	101	10.5	31	79	31.6	331.6	3.9	86	31.1	326.3	3.9					x	x		
3530-34	23			2357	7.2	3528.0	3559.5	97	8.5	31.5	82	31.8	270.4	3.4	83	31.7	269.8	3.4		x				x		
3500 horizon																										
3500-26	30			3336	4.2	3497.0	3526.5	90	11	29.5	84	29.7	326.3	4.0	80	30.0	329.5	4.0	x							x
3500-27				PILLER																						
3500-28	17			3130	9.1	3499.0	3526.5	95	10	27.5	78	28.1	281.1	3.7	81	27.8	278.4	3.7	x					x		
3500-29	24			5245	8.4	3499.0	3527.0	95	11.5	28	83	28.2	324.4	4.1	84	28.2	323.8	4.1					x		x	
3500-30	15			10106	10.6	3499.0	3527.5	99	10	28.5	83	28.7	287.1	3.7	77	29.2	292.5	3.7			x			x		
3500-31	27			13772	7.8	3499.0	3528.5	99	10	29.5	84	29.7	296.6	3.7	76	30.4	304.0	3.8					x		x	
3500-32	10			9965	12.2	3499.0	3528.0	94	10	29	87	29.0	290.4	3.7	85	29.1	291.1	3.7			x			x		
3500-33	29			10847	8.2	3500.5	3529.0	99	10	28.5	84	28.7	286.6	3.7	82	28.8	287.8	3.7					x		x	
3500-34	8			5251	9.1	3500.0	3528.5	101	10	28.5	75	29.5	295.1	3.7	82	28.8	287.8	3.7			x			x		
3500-35	26			4812	4.7	3500.0	3529.0	99	10	29	75	30.0	300.2	3.8	82	29.3	292.8	3.7					x	x		
3500-36	12			3158	3.3	3500.0	3529.0	98	10	29	87	29.0	290.4	3.7	88	29.0	290.2	3.7			x				x	

Table B2.1 Zone 3-1 stope design details, 3440m and 3470m horizon stopes

	Stope Design																		Stope Type					Drill Pattern		
STOPE NAME	HW Sequence mined	HW cables - fan upward	HW cables- fan downward	Stope size (tonnes) - planned	Stope muck grade (gm/tonne)	Stope base (floor elevation)	Stope top(top sill floor elevation)	Strike Azimuth	Stope Width on strike (@midspan)	Vertical Height (m)	Stope HW angle	True HW height	HW area (m2)	HW Hydraulic Radius (m)	Stope FW angle	True FW height	FW area (m2)	FW Hydraulic Radius (m)	Primary (P1)	P2	P3	Secondary (S1)	S2	parallel (primary)	ring (secondary)	Longitudinal
3470 horizon																										
3470-29	21			4326	3.7	3468.0	3498.5	94	10	30.5	80	31.0	309.7	3.8	78	31.2	311.8	3.8				x			x	
3470-30	11			4209	4.3	3468.5	3498.5	100	10	30	79	30.6	305.6	3.8	77	30.8	307.9	3.8	x					x		
3470-31	18			10067	6.5	3468.5	3499.0	94	10	30.5	80	31.0	309.7	3.8	77	31.3	313.0	3.8					x		x	
3470-32	5			8449	9.4	3468.5	3499.0	105	10	30.5	78	31.2	311.8	3.8	79	31.1	310.7	3.8		x				x		
3470-33	13			10865	12.2	3469.0	3500.5	101	11.5	31.5	88	31.5	362.5	4.2	80	32.0	367.8	4.2					x		x	
3470-34	4			6259	16.5	3469.0	3500.5	100	10	31.5	79	32.1	320.9	3.8	80	32.0	319.9	3.8		x				x		
3470-35	16			7116	18.2	3470.5	3500.0	99	10	29.5	80	30.0	299.6	3.7	81	29.9	298.7	3.7					x		x	
3470-36	6			10339	7.9	3470.0	3500.5	97	10	30.5	82	30.8	308.0	3.8	90	30.5	305.0	3.8		x				x		
3440 horizon																										
3440-31	14			2192	6.5	3440.5	3468.5	93	10	28	85	28.1	281.1	3.7	83	28.2	282.1	3.7				x			x	
3440-32	1			1850	4.2	3440.5	3468.5	92	10	28	84	28.2	281.5	3.7	82	28.3	282.8	3.7	x					x		
3440-33	7			5928	4.8	3440.0	3469.0	100	11.5	29	80	29.4	338.6	4.1	70	30.9	354.9	4.2					x		x	
3440-34	2			6477	6.6	3440.0	3469.5	100	10	29.5	80	30.0	299.6	3.7	80	30.0	299.6	3.7	x					x		
3440-35	9			6653	13.9	3439.5	3470.5	100	11	31	80	31.5	346.3	4.1	74	32.2	354.7	4.1					x		x	
3440-36	3			4186	13.8	3439.5	3470.0	100	10	30.5	80	31.0	309.7	3.8	75	31.6	315.8	3.8	x					x		
3440-37	56			4400	8.4	3438.5	3470.0	98	12.5	31.5	83	31.7	396.7	4.5	79	32.1	401.1	4.5				x		x		

Table B2.1 Zone 3-1 stope design details, 3380m and 3410m horizon stopes

	Stope Design																		Stope Type					Drill Pattern		
STOPE NAME	HW Sequence mined	HW cables - fan upward	HW cables- fan downward	Stope size (tonnes) - planned	Stope muck grade (gm/tonne)	Stope base (floor elevation)	Stope top(top sill floor elevation)	Strike Azimuth	Stope Width on strike (@midspan)	Vertical Height (m)	Stope HW angle	True HW height	HW area (m2)	HW Hydraulic Radius (m)	Stope FW angle	True FW height	FW area (m2)	FW Hydraulic Radius (m)	Primary (P1)	P2	P3	Secondary (S1)	S2	parallel (primary)	ring (secondary)	Longitudinal
3410 horizon																										
3410-32	73			2000	5.0	3411.0	3440.5	94	9	29.5	83	29.7	267.5	3.5	83	29.7	267.5	3.5				x			x	
3410-33	58			2400	6.4	3411.5	3440.5	100	10.5	29	81	29.4	308.3	3.9	80	29.4	309.2	3.9				x			x	
3410-34	45			2947	7.4	3411.5	3440.5	95	12	29	76	29.9	358.7	4.3	76	29.9	358.7	4.3				x			x	
3410-35	39			3076	9.6	3412.0	3439.5	97	11	27.5	76	28.3	311.8	4.0	75	28.5	313.2	4.0			x				x	
3410-36	31			2177	10.8	3412.0	3439.0	99	10	27	75	28.0	279.5	3.7	75	28.0	279.5	3.7	x						x	
3410-37	50			4850	8.9	3411.0	3438.5	97	11.5	27.5	72	28.9	332.5	4.1	79	28.0	322.2	4.1					x		x	
3410-38	36			3940	11.6	3411.0	3438.5	97	10	27.5	72	28.9	289.2	3.7	78	28.1	281.1	3.7		x				x		
3410-39	61			4500	11.7	3410.0	3439.0	96	10	29	74	30.2	301.7	3.8	76	29.9	298.9	3.7					x	x		
3410-40	47			2550	10.2	3410.0	3439.0	98	8.5	29	77	29.8	253.0	3.3	78	29.6	252.0	3.3		x				x		
3380 horizon																										
3380-33	43			2443	4.8	3380.5	3411.5	90	8.5	31	86	31.1	264.1	3.3	85	31.1	264.5	3.3				x				x
3380-34	35			1506	4.3	3381.0	3412.0	90	11	31	85	31.1	342.3	4.1	84	31.2	342.9	4.1				x				x
3380-35	28			3094	5.3	3381.5	3412.0	97	10	30.5	83	30.7	307.3	3.8	80	31.0	309.7	3.8				x				x
3380-36	25			2885	6.1	3381.5	3412.5	97	10	31	83	31.2	312.3	3.8	79	31.6	315.8	3.8	x							x
3380-37	44			7800		3379.5	3411.5	93	11	32	81	32.4	356.4	4.1	83	32.2	354.6	4.1					x		x	
3380-38	33			5647	12.3	3378.5	3411.0	97	10	32.5	80	33.0	330.0	3.8	77	33.4	333.5	3.8	x					x		
3380-39	53			5450	9.7	3378.0	3411.5	95	11	33.5	79	34.1	375.4	4.2	77	34.4	378.2	4.2					x		x	
3380-40	41			10956	6.7	3378.0	3411.5	94	10	33.5	75	34.7	346.8	3.9	75	34.7	346.8	3.9	x						x	
3380-41	65			10400	5.6	3378.0	3410.0	95	12	32	84	32.2	386.1	4.4	85	32.1	385.5	4.4				x			x	

Table B2.2 Zone 3-1 stope recovery details, 3560m and 3590m horizon stopes

Stope Recovery Details

STOPE NAME	Survey date	mineral broken/blasted (tonnes)	CMS HW slough (tonnes)	CMS FW slough (tonnes)	CMS sidewall ore slough (tonnes)	CMS backfill - sidewall slough (tonnes)	CMS HW slough (m3)	CMS FW slough (m3)	HW - Dilution Density (m)	FW - Dilution Density (m)	total DDcms (HW + FW)	% DD from HW	Vol Backfill (m3)	Milled Dilution %	Dil'n % unplanned waste/ore mined (tonnes)	Recovery %	Stope Cycle (#days)
3590 horizon																	
3590-19	21-Feb-02	2721	980	1019	0	0	350	363.9	1.1	1.2	2.3	49.0	1462	56.3	73.5	95.5	14
3590-20	07-Jun-02	2589	950	67	0	0	339.3	23.93	1.2	0.1	1.3	93.4	1121	35.4	39.3	97.7	13
3590-21	23-Oct-02	3868	2044	815	0	0	730	291.1	1.9	0.8	2.6	71.5	1936	55.7	73.9	83.4	19
3590-22	08-May-02	3977	2029	690	0	0	724.6	246.4	2.1	0.7	2.8	74.6	2214	68.4	68.4	99.4	26
3590-23	15-Aug-02	4131	0	1047	0	81	0		Ore left in HW				1705	27.3	25.3	87.9	19
3590-24	22-Nov-01	CMS data					0	0									
3590-25	CMS performed																
3590-26	10-May-02	3670	1605	475	0	0	573.2	169.6	1.9	0.6	2.5	77.2	1839	53.9	56.7	111.2	17
3590-27	27-Aug-02	2670	1483	224	0	36	529.6	80	1.9	0.3	2.2	86.9	1338	58.9	63.9	104.8	18
3590-28	14-Mar-02	2808	575	847	0	0	205.4	302.5	0.6	0.9	1.6	40.3	1385	50.6	50.6	83.8	18
3560 horizon																	
3560-21	28-Mar-02	3352	1544	559	0	178	551.4	199.6	2.0	0.7	2.7	73.3	1581	50.1	62.7	104.8	17
3560-22	21-Jan-02	2927	631	312	0	0	225.4	111.4	0.8	0.4	1.2	67.0	1251	32.2	32.2	99.2	23
3560-23	27-Jun-02	5435	622	169	0	35	222.1	60.36	0.6	0.2	0.8	78.6	1999	15.2	14.6	90.6	20
3560-24	05-Oct-01	3585	446	318	23	0	159.3	113.6	0.5	0.4	0.9	58.3	1360	21.5	21.2	89.8	21
3560-25	03-Sep-02	5581	612	504	0	268	218.6	180	0.6	0.5	1.0	54.8	2277	24.8	20.0	93.0	51
3560-26	22-Aug-01	5232	1141	511	0	0	407.5	182.5	1.2	0.5	1.8	69.1	2035	21.1	31.6	85.8	39
3560-27	17-Jul-02	5403	45	1429	0	447	16.07	510.4	0.0	1.3	1.4	3.0	2387	30.2	27.3	97.3	20
3560-28	18-Sep-01	4216	868	1699	57	0	310	606.8	1.0	1.9	2.9	33.8	2191	60.1	60.1	91.4	28
3560-29	14-Nov-02	4624	1191	2500	0	56	425.4	892.9	1.0	2.0	3.0	32.3	2287	59.2	79.8	90.5	26
3560-30																	
3560-31	31-Jul-02	2359	251	728	0	0	89.64	260	0.3	0.9	1.2	25.6	1087	41.5	41.5	89.0	12
3560-32	03-Jun-02	2450	1625	1858	0	0	580.4	663.6	1.8	2.1	3.9	46.7	2010	132.9	142.2	101.8	23

Table B2.2 Zone 3-1 stope recovery details, 3500m and 3530m horizon stopes

Stope Recovery Details

STOPE NAME	Survey date	mineral broken/blasted (tonnes)	CMS HW slough (tonnes)	CMS FW slough (tonnes)	CMS sidewall ore slough (tonnes)	CMS backfill - sidewall slough (tonnes)	CMS HW slough (m3)	CMS FW slough (m3)	HW - Dilution Density (m)	FW - Dilution Density (m)	total DDcms (HW + FW)	% DD from HW	Vol Backfill (m3)	Milled Dilution %	Dil'n % unplanned waste/ore mined (tonnes)	Recovery %	Stope Cycle (#days)
3530 horizon																	
3530-24	30-Jul-01	3852	311	1456	36	0	111.1	520	0.3	1.3	1.5	17.6	1261	14.0	45.4	88.6	25
3530-25	14-Feb-02	4490	312	1273	0	270	111.4	454.6	0.3	1.2	1.5	19.7	2002	36.8	35.3	92.6	19
3530-26	06-Jun-01	4048	373	452	41	0	133.2	161.4	0.4	0.5	0.9	45.3	1429	10.1	20.2	92.6	18
3530-27	17-Jan-02	3721	654	932	0	516	233.6	332.9	0.7	1.0	1.7	41.5	1987	56.5	42.6	91.9	68
3530-28	27-Sep-00	9056	1073	441	816	0	383.2	157.5	1.1	0.5	1.6	70.8	3567	13.9	15.3	92.9	34
3530-29	28-Jun-02	8450	990	1225	0	964	353.6	437.5	1.1	1.4	2.6	44.2	2817	16.7	26.2	98.8	41
3530-30	17-Jul-00	6723	705	1352	341	0	251.8	482.9	0.8	1.5	2.3	33.9	2543	12.7	29.1	83.8	31
3530-31	22-Mar-02	5155	613	1474	0	395	218.9	526.4	0.6	1.6	2.2	29.1	2044	28.8	40.5	93.7	30
3530-32	14-Aug-00	5539	350	97	110	0	125	34.64	0.4	0.1	0.5	78.2	1807	4.4	7.9	88.9	20
3530-33	30-Apr-01	4901	2300	1908	0	1036	821.4	681.4	2.5	2.1	4.6	54.3	2391	67.2	85.9	97.7	19
3530-34	21-Nov-00	2136	365	869	49	0	130.4	310.4	0.5	1.2	1.6	29.5	1094	56.4	56.5	90.6	24
3500 horizon																	
3500-26	10-Apr-01	3034	534	225	0	0	190.7	80.36	0.6	0.2	0.8	70.6	1201	25.0	25.0	90.9	19
3500-27																	
3500-28	23-May-00	2991	645	357	179	0	230.4	127.5	0.8	0.5	1.3	64.1	1325	31.6	31.6	95.6	19
3500-29	12-Dec-00	5182	652	2319	283	651	232.9	828.2	0.7	2.6	3.3	21.9	2905	47.1	54.4	98.9	35
3500-30	17-Apr-00	9403	584	153	509	0	208.6	54.64	0.7	0.2	0.9	79.5	3343	7.3	7.4	93.0	24
3500-31	06-Feb-01	13668	1843	509	0	2125	658.2	181.8	2.2	0.6	2.8	78.8	6021	29.5	17.2	99.2	44
3500-32	29-Dec-99	8791	415	266	219	0	148.2	95	0.5	0.3	0.8	61.0	2837	2.9	7.6	86.7	26
3500-33	16-Mar-01	10147	1652	86	0	1343	590	30.71	2.1	0.1	2.2	95.1	3810	18.6	17.1	93.5	34
3500-34	01-Nov-99	4470	538	749	22	0	192.1	267.5	0.7	0.9	1.6	41.2	1833	11.0	28.7	85.1	23
3500-35	11-Jan-01	4673	1514	329	131	312	540.7	117.5	1.8	0.4	2.2	81.8	2257	51.8	38.4	97.1	26
3500-36	16-Feb-00	2558	131	1344	0	0	46.79	480	0.2	1.7	1.8	8.9	1291	54.9	57.7	81.0	25

Table B2.2 Zone 3-1 stope recovery details, 3440m and 3470m horizon stopes

Stope Recovery Details

STOPE NAME	Survey date	mineral broken/blasted (tonnes)	CMS HW slough (tonnes)	CMS FW slough (tonnes)	CMS sidewall ore slough (tonnes)	CMS backfill - sidewall slough (tonnes)	CMS HW slough (m3)	CMS FW slough (m3)	HW - Dilution Density (m)	FW - Dilution Density (m)	total DDcms (HW + FW)	% DD from HW	Vol Backfill (m3)	Milled Dilution %	Dil'n %: unplanned waste/ore mined (tonnes)	Recovery %	Stope Cycle (#days)
3470 horizon																	
3470-29	30-Aug-00	3834	282	152	0	141	100.7	54.29	0.3	0.2	0.5	65.1	1406	15.3	11.3	88.6	30
3470-30	19-Jan-00	3915	833	1017	1096	0	297.5	363.2	1.0	1.2	2.2	45.2	2182	36.9	36.9	93.0	26
3470-31	26-Jun-00	9491	1481	104	0	894	528.9	37.14	1.7	0.1	1.8	93.5	3875	30.2	16.7	94.3	30
3470-32	23-Jul-99	7856	923	409	215	0	329.6	146.1	1.1	0.5	1.5	69.2	2838	13.4	16.5	93.0	18
3470-33	20-Mar-00	10595	210	930	878	1019	75	332.1	0.2	0.9	1.1	18.6	4224	15.3	9.9	97.5	36
3470-34	18-Jun-99	5631	585	649	24	0	208.9	231.8	0.7	0.7	1.4	47.3	2025	16.5	21.8	90.0	16
3470-35	08-May-00	7012	1032	371	0	786	368.6	132.5	1.2	0.4	1.7	73.5	2812	25.9	20.0	98.5	24
3470-36	02-Sep-99	9084	33	113	57	0	11.79	40.36	Ore left in HW				2905	1.6	1.6	87.9	22
3440 horizon																	
3440-31	06-Mar-00	2071	495	193	34	112	176.8	68.93	0.6	0.2	0.9	72.0	890	36.5	32.7	92.2	15
3440-32	25-Jan-99	1583	701	434	0	0	250.4	155	0.9	0.5	1.4	61.9	873	71.7	71.7	85.6	13
3440-33	04-Oct-99	5628	1003	292	135	169	358.2	104.3	1.1	0.3	1.4	78.3	2239	27.7	22.5	95.3	24
3440-34	30-Mar-99	5619	634	601	26	0	226.4	214.6	0.8	0.7	1.5	51.3	2176	21.8	21.9	86.8	18
3440-35	24-Nov-99	6417	920	50	0	336	328.6	17.86	0.9	0.1	1.0	95.0	2481	17.1	15.1	96.4	23
3440-36	26-Apr-99	3942	454	578	161	0	162.1	206.4	0.5	0.7	1.2	44.5	1626	25.1	25.2	94.2	17
3440-37	08-Apr-02	4908	622	2768	0	102	222.1	988.6	0.6	2.5	3.0	18.5	1220	3.7	69.1	109.3	37

Table B2.2 Zone 3-1 stope recovery details, 3380m and 3410m horizon stopes

Stope Recovery Details

STOPE NAME	Survey date	mineral broken/blasted (tonnes)	CMS HW slough (tonnes)	CMS FW slough (tonnes)	CMS sidewall ore slough (tonnes)	CMS backfill - sidewall slough (tonnes)	CMS HW slough (m3)	CMS FW slough (m3)	HW - Dilution Density (m)	FW - Dilution Density (m)	total DDcms (HW + FW)	% DD from HW	Vol Backfill (m3)	Milled Dilution %	Dil'n %: unplanned waste/ore mined (tonnes)	Recovery %	Stope Cycle (#days)
3410 horizon																	
3410-32	25-Oct-02	2154	998	450	0	152	356.4	160.7	1.3	0.6	1.9	68.9	1251	60.0	67.2	107.7	17
3410-33	23-Apr-02	1910	188	492	0	0	67.14	175.7	0.2	0.6	0.8	27.7	839	35.6	35.6	79.6	15
3410-34	27-Nov-01	2730	1632	182	0	26	582.9	65	1.6	0.2	1.8	90.0	1470	69.3	66.4	92.6	27
3410-35	28-Aug-01	2306	1511	0	0	75	539.6	0	1.7	0.0	1.7	100.0	1233	76.1	65.5	75.0	27
3410-36	11-Apr-01	1916	777	112	0	0	277.5	40	1.0	0.1	1.1	87.4	895	46.4	46.4	88.0	18
3410-37	07-Feb-02	4495	798	908	0	468	285	324.3	0.9	1.0	1.9	46.0	2203	47.5	38.0	90.6	27
3410-38	17-Jul-01	3252	129	1525	0	0	46.07	544.6	0.2	1.9	2.1	7.6	1568	50.9	50.9	82.5	21
3410-39	28-May-02	3732	1127	110	0	63	402.5	39.29	1.3	0.1	1.5	91.0	1640	34.8	33.1	82.9	25
3410-40	03-Jan-02	2674	217	526	0	0	77.5	187.9	0.3	0.7	1.1	29.1	852	13.3	27.8	100.9	33
3380 horizon																	
3380-33	10-Oct-01	1988	244	675	0	113	87.14	241.1	0.3	0.9	1.2	26.6	902	47.4	46.2	81.4	19
3380-34	06-Jun-01	1357	77	0	0	1894	27.5	0	0.1	0.0	0.1	100.0	813	29.3	5.7	76.9	18
3380-35	28-Feb-01	3070	1838	402	0	249	656.4	143.6	2.1	0.5	2.6	82.2	1768	77.8	73.0	99.2	28
3380-36	03-Jan-01	2824	1680	66	0	0	600	23.57	1.9	0.1	2.0	96.3	1465	57.4	61.8	97.9	25
3380-37	13-Dec-01	7600	250	400	0	50	89.29	142.9	0.3	0.4	0.7	38.3			8.6		48
3380-38	25-May-01	4736	410	144	0	0	146.4	51.43	0.4	0.2	0.6	74.2	1665	11.7	11.7	83.9	28
3380-39	19-Mar-02	5010	1146	453	0	272	409.3	161.8	1.1	0.4	1.5	71.8	2221	35.5	31.9	91.9	38
3380-40	05-Nov-01	9644	109	610	453	0	38.93	217.9	0.1	0.6	0.7	15.2	3395	7.1	7.1	88.0	65
3380-41	10-Oct-02	9493	0	1068	0	293	0	381.4	Ore left in HW				3495	14.3	11.3	91.3	127

Table B2.3 Zone 3-1 stope blasting details, 3560m and 3590m horizon stopes

	Blasting Details																			
	Blast #1					Blast #2					Blast #3					Blast #4				
STOPE NAME	Date Blast #1	Tonnes Blasted	Tonnes Powder (kg)	PF (kg/TM)	Powder Factor (kg/m3)	Date Blast #2	Tonnes Blasted	Tonnes Powder	PF (kg/TM)	Powder Factor (kg/m3)	Date Blast #3	Tonnes Blasted	Tonnes Powder	PF (kg/TM)	Powder Factor (kg/m3)	Date Blast #4	Tonnes Blasted	Tonnes Powder	PF (kg/TM)	Powder Factor (kg/m3)
3590 horizon																				
3590-19	7-Feb-02	400	421	1.04	3.34	8-Feb-02	750	583	0.78	2.49	12-Feb-02	1700	1102	0.65	2.07					
3590-20	24-May-02	500	330	0.66	2.11	27-May-02	500	302	0.6	1.93	30-May-02	1650	907	0.55	1.76					
3590-21	4-Oct-02	900	486	0.54	1.73	11-Oct-02	900	540	0.6	1.92	15-Oct-02	1850	818	0.44	1.42					
3590-22	12-Apr-02	800	465	0.58	1.86	19-Apr-02	700	342	0.49	1.56	23-Apr-02	2500	893	0.36	1.14					
3590-23	26-Jul-02	850	549	0.65	2.07	1-Sep-02	1600	718	0.45	1.44	6-Aug-02	2250	738	0.33	1.05					
3590-24	3-Dec-01	900	604	0.67	2.15	7-Dec-01	850	512	0.6	1.93	10-Dec-01	2500	933	0.37	1.2					
3590-25	9-Dec-02	3700	1015	0.31	0.98	no 2nd blast- due to cave														
3590-26	23-Apr-02	600	322	0.54	1.72	25-Apr-02	600	421	0.7	2.25	29-Apr-02	2100	748	0.35	1.14					
3590-27	9-Aug-02	750	563	0.75	2.4	16-Aug-02	750	348	0.46	1.48	19-Aug-02	1250	485	0.39	1.24					
3590-28	26-Feb-02	650	466	0.72	2.29	5-Mar-02	850	522	0.61	1.97	8-Mar-02	1850	885	0.48	1.53					
3560 horizon																				
3560-21	11-Mar-02	150	137	0.91	2.92	13-Mar-02	400	325	0.81	2.6	18-Mar-02	1050	454	0.43	1.38	21-Mar-02	1600	893	0.56	1.79
3560-22	28-Dec-01	500	393	0.79	2.51	4-Jan-02	1050	338	0.55	1.76	11-Jan-02	1400	771	0.55	1.76					
3560-23	7-Jun-02	1500	882	0.59	1.88	11-Jun-02	1400	361	0.26	1.21	13-Jun-02	3100	1785	0.58	1.84					
3560-24	14-Sep-01	800	446	0.56	3.2	21-Sep-01	1100	588	0.53	1.71	26-Sep-01	2100	837	0.4	1.28					
3560-25	12-Jul-02	1600	795	0.5	1.59	2-Aug-02	1200	490	0.41	1.31	8-Aug-02	3200	2022	0.62	2.02					
3560-26	13-Jul-01	1600	980	0.61	1.96	27-Jul-01	1700	533	0.31	1	3-Aug-01	2950	1611	0.55	1.75					
3560-27	27-Jun-02	1250	830	0.66	2.12	28-Jun-02	1300	610	0.47	1.5	11-Jul-02	3000	1083	0.36	1.16					
3560-28	20-Aug-01	650	331	0.51	1.63	24-Aug-01	700	311	0.44	1.43	27-Aug-01	1000	288	0.29	0.92	4-Sep-01	1900	775	0.41	1.3
3560-29	18-Oct-02	1150	817	0.71	2.27	25-Oct-02	1300	917	0.71	2.26	31-Oct-02	2550	1251	0.49	1.37					
3560-30	PILLAR																			
3560-31	19-Jul-02	400	366	0.92	2.93	22-Jul-02	650	321	0.49	1.58	26-Jul-02	1600	652	0.41	1.31					
3560-32	10-May-02	700	588	0.84	2.69	17-May-02	750	686	0.91	2.93	23-May-02	1000	582	0.58	1.86					

Table B2.3 Zone 3-1 stope blasting details, 3500m and 3530m horizon stopes

	Blasting Details																			
	Blast #1					Blast #2					Blast #3					Blast #4				
STOPE NAME	Date Blast #1	Tonnes Blasted	Tonnes Powder (kg)	PF (kg/TM)	Powder Factor (kg/m3)	Date Blast #2	Tonnes Blasted	Tonnes Powder	PF (kg/TM)	Powder Factor (kg/m3)	Date Blast #3	Tonnes Blasted	Tonnes Powder	PF (kg/TM)	Powder Factor (kg/m3)	Date Blast #4	Tonnes Blasted	Tonnes Powder	PF (kg/TM)	Powder Factor (kg/m3)
3530 horizon																				
3530-24	05-Jul-01	750	494	0.66	2.11	11-Jul-01	1950	854	0.44	1.4	23-Jul-01	1400	1145	0.82	2.62					
3530-25	25-Jan-02	700	606	0.87	2.77	29-Jan-02	1650	430	0.26		01-Feb-02	2050	1559	0.76	2.43					
3530-26	18-May-01	1200	610	0.51	1.61	22-May-01	1300	510	0.39	1.26	25-May-01	2400	975	0.41	1.3					
3530-27	09-Nov-01	850	616	0.72	2.32	14-Nov-01	1000	406	0.41	1.3	16-Nov-01	2200	1187	0.54	1.73					
3530-28	23-Aug-00	1650	1220	0.73	2.37	04-Sep-00	3800	1116	0.29	0.94	08-Sep-00	4650	2050	0.44	1.41					
3530-29	17-May-02	600	428	0.71	2.28	23-May-02	5550	2577	0.46	1.49										
3530-30	16-Jun-00	1400	1115	0.79	2.54	22-Jun-00	3300	1457	0.44	1.41	26-Jun-00	3350	1510	0.45	1.58					
3530-31	22-Feb-02	1050	838	0.8	2.55	28-Feb-02	3000	1763	0.59	1.89										
3530-32	24-Jul-00	1100	872	0.79	2.54	26-Jul-00	1900	644	0.34	1.08	02-Aug-00	3200	1434	0.44	1.43					
3530-33	11-Apr-01	1000	836	0.84	2.67	13-Apr-01	1000	313	0.31	1	16-Apr-01	2500	872	0.35	1.12					
3530-34	27-Oct-00	1000	756	0.75	2.41	06-Nov-00	250	255	0.51	1.63	07-Nov-00	1050	688	0.65	2.09					
3500 horizon																				
3500-26	21-Mar-01	450	469	1.04	3.33	30-Mar-01	900	499	0.55	1.77	03-Apr-01	1600	1107	0.69	2.21					
3500-27	PILLAR																			
3500-28	04-May-00	950	695	0.73	2.34	05-May-00	800	335	0.42	1.34	11-May-00	1450	586	0.4	1.29					
3500-29	07-Nov-00	1200	860	0.72	2.29	08-Nov-00	1000	483	0.48	1.55	13-Nov-00	2900	1338	0.46	1.48					
3500-30	23-Mar-00	900	789	0.87	2.8	24-Mar-00	1200	429	0.36	1.14	28-Mar-00	2000	1188	0.59	1.9	04-Apr-00	6400	3013	0.47	1.51
3500-31	22-Dec-00	1900	1113	0.58	1.87	29-Dec-00	2100	1365	0.65	2.08	05-Jan-01	9000	3535	0.39	1.26					
3500-32	03-Dec-99	1000	460	0.46	1.47	07-Dec-99	1000	301	0.3	0.96	13-Dec-99	2000	790	0.39	1.26	15-Dec-99	5800	1885	0.33	1.04
3500-33	12-Feb-01	1500	1102	0.73	2.35	19-Feb-01	1500	520	0.34	1.11	23-Feb-01	2900	1686	0.58	1.86	02-Mar-01	4600	1758	0.38	1.22
3500-34	08-Oct-99	1000	785	0.79	2.51	12-Oct-99	1200	315	0.26	0.84	20-Oct-99	3000	1513	0.5	1.76					
3500-35	15-Dec-00	800	647	0.8	2.58	20-Dec-00	1900	874	0.46	1.47	22-Dec-00	2000	1202	0.6	1.92					
3500-36	21-Jan-00	750	606	0.8	2.59	28-Jan-00	800	418	0.52	1.67	03-Feb-00	1800	784	0.43	1.39					

Table B2.3 Zone 3-1 stope blasting details, 3440m and 3470m horizon stopes

	Blasting Details																			
	Blast #1					Blast #2					Blast #3					Blast #4				
STOPE NAME	Date Blast #1	Tonnes Blasted	Tonnes Powder (kg)	PF (kg/TM)	Powder Factor (kg/m3)	Date Blast #2	Tonnes Blasted	Tonnes Powder	PF (kg/TM)	Powder Factor (kg/m3)	Date Blast #3	Tonnes Blasted	Tonnes Powder	PF (kg/TM)	Powder Factor (kg/m3)	Date Blast #4	Tonnes Blasted	Tonnes Powder	PF (kg/TM)	Powder Factor (kg/m3)
3470 horizon																				
3470-29	31-Jul-00	700	522	0.74	2.39	04-Aug-00	650	352	0.54	1.73	18-Aug-00	2700	1798	0.66	2.13					
3470-30	23-Dec-99	800	404	0.51	1.62	24-Dec-99	1300	360	0.28	0.89	05-Jan-00	2150	843	0.39	1.25					
3470-31	26-May-00	1000	768	0.77	2.46	28-May-00	2200	978	0.44	1.42	02-Jun-00	2600	1539	0.59	1.89	07-Jun-00	4000	1919	0.48	1.54
3470-32	05-Jul-99	1150	537	0.47	1.49	07-Jul-99	1200	644	0.54	1.72	09-Jul-99	6150	2086	0.34	1.08					
3470-33	14-Feb-00	1350	949	0.7	2.24	15-Feb-00	1500	498	0.33	1.06	18-Feb-00	2850	1102	0.39	1.24	28-Feb-00	5300	2014	0.38	1.35
3470-34	02-Jun-99	1000	598	0.6	1.91	07-Jun-99	1600	462	0.29	0.92	10-Jun-99	4150	2171	0.52	1.67					
3470-35	14-Apr-00	1100	1038	0.94	3.3	17-Apr-00	2150	823	0.38	1.34	21-Apr-00	3800	2369	0.6	2.18					
3470-36	10-Aug-99	950	433	0.46	1.46	12-Aug-99	1500	458	0.31	1.07	16-Aug-99	1950	965	0.49	1.58	19-Aug-99	6000	3433	0.57	1.83
3440 horizon																				
3440-31	21-Feb-00	500	612	1.22	3.9	25-Feb-00	400	249	0.62	1.99	28-Feb-00	1300	969	0.74	2.38					
3440-32	12-Jan-99	500	403	0.81	2.5	15-Jan-99	1350	1100	0.81	2.53										
3440-33	10-Sep-99	500	423	0.85	2.71	17-Sep-99	1800	633	0.35	1.12	21-Sep-99	3600	1657	0.46	1.61					
3440-34	12-Mar-99	1050	739	0.7	2.06	16-Mar-99	1500	713	0.48	1.52	19-Mar-99	3800	1515	0.4	1.28					
3440-35	01-Nov-99	900	513	0.57	1.82	05-Nov-99	2000	835	0.41	1.32	10-Nov-99	4100	1610	0.39	1.26					
3440-36	09-Apr-99	900	405	0.45	1.94	13-Apr-99	900	434	0.48	1.54	16-Apr-99	2350	837	0.36	1.14					
3440-37	01-Mar-02	600	355	0.59	1.9	15-Mar-02	1200	700	0.58	1.87	25-Mar-02	2600	1657	0.64	2.04					

Table B2.3 Zone 3-1 stope blasting details, 3380m and 3410m horizon stopes

	Blasting Details																			
	Blast #1					Blast #2					Blast #3					Blast #4				
STOPE NAME	Date Blast #1	Tonnes Blasted	Tonnes Powder (kg)	PF (kg/TM)	Powder Factor (kg/m3)	Date Blast #2	Tonnes Blasted	Tonnes Powder	PF (kg/TM)	Powder Factor (kg/m3)	Date Blast #3	Tonnes Blasted	Tonnes Powder	PF (kg/TM)	Powder Factor (kg/m3)	Date Blast #4	Tonnes Blasted	Tonnes Powder	PF (kg/TM)	Powder Factor (kg/m3)
3410 horizon																				
3410-32	08-Oct-02	450	350	0.8	2.55	10-Oct-02	500	250	0.5	1.6	11-Oct-02	1000	1105	1.1	3.54					
3410-33	08-Apr-02	400	445	0.59	1.9	10-Apr-02	750	539	0.71	2.3	12-Apr-02	1250	1027	0.82	2.63					
3410-34	30-Oct-01	700	516	0.74	2.35	05-Nov-01	850	398	0.47	1.5	13-Nov-01	1500	1051	0.7	2.24					
3410-35	01-Aug-01	900	526	0.58	1.86	07-Aug-01	700	344	0.49	1.57	10-Aug-01	1850	916	0.5	1.58					
3410-36	23-Mar-01	600	417	0.7	2.22	30-Mar-01	800	479	0.6	1.92	no record									
3410-37	10-Jan-02	700	503	0.72	2.3	25-Jan-02	4150	1779	0.46	1.47										
3410-38	26-Jun-01	850	510	0.6	1.92	29-Jun-01	1400	398	0.28	0.92	04-Jul-01	1300	601	0.46	1.48					
3410-39	03-May-02	1000	442	0.44	1.41	06-May-02	1300	525	0.4	1.29	09-May-02	2200	925	0.42	1.35					
3410-40	30-Nov-01	250	174	0.7	2.23	06-Dec-01	300	274	0.91	2.92	07-Dec-01	600	310	0.52	1.65	17-Dec-01	1400	640	0.46	1.46
3380 horizon																				
3380-33	21-Sep-01	450	474	1.05	3.37	28-Sep-01	500	318	0.64	2.04	01-Oct-01	1150	782	0.68	2.17					
3380-34	18-May-01	150	185	1.23	3.95	23-May-01	450	238	0.53	1.69	30-May-01	850	598	0.7	2.25					
3380-35	31-Jan-01	150	159	1.06	3.2	01-Feb-01	500	349	0.69	2.23	05-Feb-01	2200	966	0.43	1.41					
3380-36	08-Dec-00	550	340	0.61	1.98	15-Dec-00	800	498	0.62	1.97	18-Dec-00	1850	607	0.33	1.05					
3380-37	25-Oct-01	1500	1153	0.77	2.46	30-Oct-01	2500	571	0.23	0.73	05-Nov-01	3800	1788	0.47	1.51					
3380-38	27-Apr-01	1700	914	0.54	1.72	04-May-01	800	303	0.38	1.21	11-May-01	3000	1566	0.52	1.67					
3380-39	11-Feb-02	950	582	0.61	1.96	15-Feb-02	1750	819	0.47	1.5	19-Feb-02	2750	1087	0.4	1.26					
3380-40	30-Aug-01	1000	651	0.65	2.08	04-Sep-01	1000	303	0.3	0.97	07-Sep-01	2200	1065	0.48	1.55	14-Oct-01	4800	3042	0.63	2.02
3380-41	03-Jun-02	1600	945	0.59	1.89	20-Jun-02	1400	528	0.38	1.21	27-Jun-02	2800	1876	0.67	2.14	01-Jul-02	2000	862	0.43	1.38

APPENDIX B3

Bousquet database details - summarized results

Table B3.1 Orientation of stope strike

Azimuth	3-1 Zone	% of all cases	Block 5	% of all cases
80			1	1
81			1	1
82			0	0
83			0	0
84			0	0
85			1	1
86			2	2
87			3	3
88	0		5	5
89	0		3	3
90	3	4	10	10
91	0	0	3	3
92	1	1	5	5
93	7	9	5	5
94	9	12	3	3
95	9	12	3	3
96	3	4	16	16
97	12	16	10	10
98	8	11	6	6
99	7	9	4	4
100	10	13	3	3
101	6	8	1	1
102	0	0	6	6
103	0	0	2	2
104	0	0	1	1
105	1	1	1	1
106				0
107				0
108				0
109				0
110				0
111				0
112			1	1
113				0
114				0
115			1	1

Table B3.2 Stope strike length

Length (m)	3-1 Zone	% of all cases	Block 5	% of all cases
8	1	1		
8.5	5	7		
9	5	7		
9.5	1	1		
10	38	51	0	
10.5	2	3	1	1
11	11	15	3	3
11.5	7	9	2	2
12	2	3	3	3
12.5	2	3	2	2
13	0	0	8	8
13.5	1	1	3	3
14			9	9
14.5			10	10
15			42	43
15.5			2	2
16			8	8
16.5			1	1
17			2	2
17.5			0	0
18			0	0
18.5			0	0
19			1	1

Table B3.3 Stope hanging-wall hydraulic radius

Hydraulic Radius	3-1 Zone	% of all cases	Block 5	% of all cases
3.2	1	1		
3.3	2	3		
3.4	3	4		
3.5	4	5		
3.6	1	1		
3.7	14	19		
3.8	20	27		
3.9	7	9		
4	2	3	1	1
4.1	10	13	3	3
4.2	3	4	2	2
4.3	3	4	2	2
4.4	2	3	2	2
4.5	2	3	3	3
4.6	0	0	3	3
4.7	0	0	6	6
4.8	1	1	2	2
4.9			12	12
5			18	19
5.1			30	31
5.2			4	4
5.3			4	4
5.4			3	3
5.5			0	0
5.6			1	1
5.7			0	0
5.8			0	0
5.9			0	0
6			1	1

Table B3.4 True height of hanging-wall (m)

Height	3-1 Zone	% of all cases	Block 5	% of all cases
≤ 28.5	6	8		0
≤ 29	6	8	6	6
≤ 29.5	3	4	8	8
≤ 30	11	15	4	4
≤ 30.5	2	3	10	10
≤ 31	10	13	5	5
≤ 31.5	11	15	13	13
≤ 32	5	7	15	15
≤ 32.5	6	8	18	19
≤ 33	4	5	13	13
≤ 33.5	1	1	3	3
≤ 34	4	5	1	1
≤ 34.5	4	5		0
≤ 35	1	1		0
≤ 35.5	0	0		0
≤ 36	1	1		0
≤ 36.5	0	0		0
≤ 37				0
≤ 37.5				0
≤ 38				0
≤ 38.5				0
≤ 39				0
≤ 39.5				0
≤ 40			0	0
≤ 40.5			1	1

Table B3.5 Hanging-wall dip angle (degrees from horizontal)

Dip Angle	3-1 Zone	% of all cases	Block 5	% of all cases
72	2	3	8	8
73	0	0	5	5
74	1	1	7	7
75	4	5	12	12
76	3	4	11	11
77	2	3	10	10
78	2	3	8	8
79	4	5	3	3
80	10	13	13	13
81	4	5	0	0
82	5	7	6	6
83	7	9	3	3
84	6	8	2	2
85	3	4	7	7
86	3	4	1	1
87	3	4	1	1
88	7	9		
89	1	1		
90	1	1		
91	3	4		
92	0	0		
93	3	4		
94	1	1		
95	0			
96				

Table B3.6 Stope size (tones blasted)

from (tonnes)	to (tonnes)	3-1 Zone	% of all cases	Block 5	% of all cases
1000	1999	5	7		
2000	2999	16	22		
3000	3999	14	19	3	3
4000	4999	11	15	8	8
5000	5999	11	15	5	5
6000	6999	2	3	9	9
7000	7999	3	4	10	10
8000	8999	2	3	13	13
9000	9999	6	8	6	6
10000	10999	2	3	0	0
11000	11999	0	0	8	8
12000	12999	0	0	2	2
13000	13999	1	1	3	3
14000	14999			5	5
15000	15999			1	1
16000	16999			2	2
17000	17999			3	3
18000	18999			2	2
19000	19999			6	6
20000	20999			5	5
21000	21999			2	2
22000	22999			1	1
23000	23999			0	0
24000	24999			0	0
25000	25999			0	0
26000	26999			1	1
27000	27999			0	0
28000	28999			0	0
29000	29999			0	0
30000	30999			1	1
31000	31999			0	0
32000	32999			1	1

Table B3.7 Stope type

Stope type	3-1 Zone		Block 5	
	# Cases	% of all cases	# Cases	% of all cases
P1	14	19	12	12
P2	9	12	13	13
P3	11	15	16	16
S1	15	20	20	21
S2	26	35	36	37

Table B3.8 Stope drill pattern

Drill pattern	3-1 Zone		Block 5	
	# Cases	% of all cases	# Cases	% of all cases
Parallel holes	25	33	34	35
Fanned or angled holes	34	45	54	56
Longitudinal stope (narrow zone pattern)	16	21	9	9

Table B3.9 Hanging-wall dilution density (DD_{cms}) per mining zone

from (m)	to (m)	3-1 Zone	% of all cases	Block 5	% of all cases
0	0.5	20	29.0	10	10.9
0.51	1	23	33.3	17	18.5
1.01	1.5	11	15.9	11	12.0
1.51	2	10	14.5	12	13.0
2.01	2.5	5	7.2	16	17.4
2.51	3			12	13.0
3.01	3.5			7	7.6
3.51	4			2	2.2
4.01	4.5			2	2.2
4.51	5			1	1.1
5.01	5.5			1	1.1
5.51	6			0	0.0
6.01	6.5			0	0.0
6.51	7			0	0.0
7.01	7.5			0	0.0
7.51	8			0	0.0
8.01	8.5			0	0.0
8.51	9			0	0.0
9.01	9.5			0	0.0
9.51	10			1	1.1

Table B3.10 Hanging-wall dilution density (DD_{cms}) per stope type

from (m)	to (m)	3-1 Zone	Block 5	3-1 Zone	Block 5	3-1 Zone	Block 5	3-1 Zone	Block 5	3-1 Zone	Block 5
		P1	P1	P2	P2	P3	P3	S1	S1	S2	S2
0	0.5	5	2	4		3	0	5	1	3	7
0.51	1	7	2	1	3	5	3	3	6	7	3
1.01	1.5	1	2	1		2	1	2	3	5	5
1.51	2	2	1	1	3		3	3	2	4	3
2.01	2.5		5	1	3		1	1	4	3	3
2.51	3				1		4		1		6
3.01	3.5				2		2		1		2
3.51	4				1		0		0		1
4.01	4.5						1		1		
4.51	5								1		
5.01	5.5										1
5.51	6										
6.01	6.5										
6.51	7										
7.01	7.5										
7.51	8										
8.01	8.5										
8.51	9										
9.01	9.5										
9.51	10										1
	# cases	15	12	8	13	10	15	14	20	22	32

Table B3.11 Hanging-wall dilution density (DD_{cms}) per stope type

Block 5

	Stope type					
hanging-wall DD	P1	P2	P3	all Primary	S1	S2
	1.5	4	2.7	1.5	2.2	3.4
	2.3	1.8	2.6	2.3	4.1	2.6
	0.6	1.7	1.6	0.6	3.3	
	2.1	3.5	4.5	2.1	1.4	2.4
	2.5	3.2	2.6	2.5	2.0	2.6
	1.2	2.3	1.8	1.2	1.1	1.1
	2.2	2.4	2	2.2	4.7	9.8
	2	1	1	2	3.0	2.8
	0.3	2.2	0.6	0.3	0.8	3.4
	0.4	2.6	3.1	4	0.7	3.7
	0.8	1.9	0.6	1.8	0.6	5.2
	2.1	0.7	3.1	1.7	0.6	1.1
		0.8	2.9	3.5	0.8	0.9
			2.3	2.3	2.1	0.4
			1.4	3.2	2.3	2.5
				2.3	0.5	1.4
AVERAGE	**1.50**	**2.16**	**2.19**	2.4		2.9
Std Deviation	0.8	1.0	1.1	1		2.0
# stopes	12	13	15	2.2		
				2.6		
				1.9		
				0.7		0.4
				0.8		1.0
				2.7		2.0
				2.6		1.1
				1.6		0.2
				4.5		
				2.6		0.3
				1.8		0.4
				2		2.6
				1		
				0.6		1.9
				3.1		1.0
				0.6		1.2
				3.1		
				0.4		
				0.8		
				2.1		
				2.9		
				1.4		
			AVERAGE	**1.97**	**1.89**	**2.15**
			Std Deviation	1.0	1.3	1.9
			# stopes	40	16	28

Zone 3-1

	Stope type					
hanging-wall DD	P1	P2	P3	all Primary	S1	S2
	0.8	0.4	0.5	0.8	1	1.9
	0.3	0.5	1.2	0.3	0.3	0.6
	0.4	1.1	1	0.4	0.6	0.6
	0.8	0.7	1.1	0.8	0.6	
	1		0.8	1	1.3	0.3
	0.9	0.2	0.7	0.9	0.2	0.7
	0.8	0.3	0.5	0.8	1.6	1.1
	0.5		0.7	0.5	1.7	0.6
	1		0.2	1		2.5
	0.4		0.6	0.4		0.7
	0.1					2.2
				0.4		2.1
				0.5		1.8
				1.1		1.7
				0.7		0.2
						1.2
AVERAGE	**0.64**	**0.53**	**0.73**	0.2		1.1
Std Deviation	0.3	0.3	0.3	0.3		0.9
# stopes	11	6	10	0.5		0.9
				1.2		1.3
				1		0.3
				1.1		1.1
				0.8		
				0.7		
				0.5		
				0.7		
				0.2		
				0.6		
			AVERAGE	**0.67**	**0.91**	**1.13**
			Std Deviation	0.3	0.6	0.7
			# stopes	26	8	21

Longitudinal stopes only

Block 5

	Stope type					
hanging-wall DD	P1	P2	P3	all Primary	S1	S2
	2.1			2.1	1.7	0.3
	0.4			0.4	1.1	2.4
					0.9	
					2.3	
			AVERAGE	**1.3**	**1.5**	**1.4**
			Std Deviation	1.2	0.6	1.5
			# stopes	2	4	2

Zone 3-1

	Stope type					
hanging-wall DD	P1	P2	P3	all Primary	S1	S2
	1.9	2.1	0.6	1.9	1.2	
	0.6	1.9		0.6	2	1.9
	1.8			1.8	0.3	
	1.1			1.1	0.3	
				2.1		
				1.9	2.1	
				0.6		
			AVERAGE	**1.4**	**1.2**	**1.9**
			Std Deviation	0.6	0.9	
			# stopes	7	5	1

Table B3.12 Relationship with hanging-wall cablebolting and dilution density (DD_{cms}) per stope type, Block 5

HW CABLE DOWN

	Stope type					
HW DD	P1	P2	P3	all Primary	S1	S2
	0.6	2.6	2.3	0.6	2.0	1.1
	1.5	2.2	1	1.5	1.1	2.8
	2.1	0.7		2.1	4.7	0.3
		1.8		2.6	3.0	5.2
		3.5		2.2	0.8	0.9
		3.2		0.7	2.1	0.4
		1.7		1.8	0.9	1.1
		1.9		3.5		0.2
				3.2		3.7
				1.7		2.0
				1.9		1.0
				2.3		3.4
				1.0		
		AVERAGE DD		**1.93**	**2.09**	**1.84**

HW CABLE UP

	Stope type					
HW DD	P1	P2	P3	all Primary	S1	S2
		2.4	0.6	2.4	2.2	2.0
		4	3.1	4.0	4.1	9.8
			2	0.6	3.3	3.4
			4.5	3.1	1.4	
			2.7	2.0	0.6	1.1
			1.6	4.5	0.8	0.4
			2.9	2.7		2.6
			3.1	1.6		
			1.4	2.9		2.4
			2.6	3.1		2.6
			2.6	1.4		
			1.8	2.6		1.4
				2.6		
				1.8		2.9
		AVERAGE DD		**2.52**	**2.07**	**2.86**

APPENDIX C

Numerical modelling of Block 5 and Zone 3-1 mining sequence

- summarized results

Table C.1 Block 5 modelled sequence, stopes #1 to #32

		MODEL GEOMETRY										σ_3 contour					
Stope Name	Sequence #	Stope Type P1	P2	P3	S1	S2	Strike length	TRUE height	HW area (m2)	Hydraulic Radius	Aspect ratio strike/height	$\sigma_3=\sigma_t$ DD (m)	σ_3=0 DD (m)	σ_3=+2MPa DD (m)	σ_3=+4MPa DD (m)	σ_3=+6MPa DD (m)	σ_3=+8MPa DD (m)	σ_3=+10MPa DD (m)
9-0-4	1	x					14.5	29	420.5	4.8	0.5	0	0.00	0.87	1.31	1.67	2.01	2.36
9-0-12	2	x					16	29	464	5.2	0.6	0	0.00	0.63	1.08	1.47	1.75	1.89
9-1-4	3		x				14.5	31	449.5	4.9	0.5	0.69	0.74	1.11	1.54	1.73	2.06	2.28
10-3-10	4	x					13.2	30	396	4.6	0.4	0	0.00	0.79	1.21	1.61	1.92	2.29
9-1-12	5		x				16	31	496	5.3	0.5	0.17	0.22	0.86	1.40	1.72	2.12	2.26
9-0-5	6				x		15.3	29	443.7	5.0	0.5	0	0.00	1.22	1.62	2.08	2.51	2.91
9-0-3	7				x		15.4	29	446.6	5.0	0.5	0.73	0.96	1.38	1.71	2.11	2.57	2.89
10-3-13	8	x					14.1	30	423	4.8	0.5	0	0.00	0.92	1.34	1.75	2.09	2.44
9-0-10	9		x				13.2	29	382.8	4.5	0.5	0.31	0.45	0.78	1.10	1.39	1.64	1.86
9-1-2	10	x					14.8	31	458.8	5.0	0.5	0	0.00	0.75	1.29	1.62	1.90	2.21
9-0-6	11				x		14.9	29	432.1	4.9	0.5	0.45	0.62	1.30	1.75	2.06	2.43	2.62
9-2-1	12	x					10.5	31	325.5	3.9	0.3	0	0.00	0.43	0.68	0.90	1.08	1.27
9-0-13	13				x		14.1	29	408.9	4.7	0.5	0.37	0.56	1.14	1.55	1.86	2.18	2.50
10-3-15	14	x					14.5	30	435	4.9	0.5	0	0.00	0.40	1.03	1.31	1.65	1.98
9-1-10	15			x			13.2	31	409.2	4.6	0.4	0.19	0.22	0.73	0.97	1.20	1.41	1.68
9-2-12	16		x				16	31	496	5.3	0.5	0.23	0.41	1.06	1.38	1.68	1.94	2.20
10-3-11	17				x		16.1	30	483	5.2	0.5	1.12	1.32	1.98	2.43	2.85	3.24	3.66
9-1-3	18					x	15.4	31	477.4	5.1	0.5	0.44	0.52	1.38	1.80	2.17	2.53	2.89
9-0-15	19		x				14.5	29	420.5	4.8	0.5	0	0.00	0.57	0.87	1.21	1.48	1.75
10-3-9	20				x		15	30	450	5.0	0.5	0.34	0.32	1.24	1.62	2.27	2.65	3.07
9-3-1	21		x				10.5	31	325.5	3.9	0.3	0.07	0.14	0.57	0.84	1.07	1.25	1.44
10-3-17	22	x					15	30	450	5.0	0.5	0	0.00	0.65	1.20	1.58	1.94	2.26
9-1-13	23				x		14.1	31	437.1	4.8	0.5	0.85	0.98	1.44	1.75	2.10	2.45	2.79
10-3-14	24					x	15.6	30	468	5.1	0.5	0.54	0.75	1.37	1.79	2.18	2.53	2.91
9-0-11	25					x	16.1	29	466.9	5.2	0.6	1.72	1.78	2.23	2.46	3.01	3.31	3.71
9-2-10	26		x				13.2	31	409.2	4.6	0.4	0.55	0.58	0.90	1.15	1.42	1.67	1.83
9-1-15	27		x				14.5	31	449.5	4.9	0.5	0.09	0.18	0.63	0.92	1.20	1.42	1.67
10-3-8	28				x		14.8	30	444	5.0	0.5	0.46	0.58	1.07	1.43	1.91	2.24	2.50
9-2-3	29	x					15.4	31	477.4	5.1	0.5	0	0.10	0.72	1.04	1.39	1.55	1.89
9-3-12	30			x			16	31	496	5.3	0.5	1.18	1.29	1.58	1.77	2.00	2.24	2.49
10-3-12	31					x	16	30	480	5.2	0.5	1.41	1.50	1.83	2.21	2.56	2.95	3.29
9-3-3	32		x				15.4	31	477.4	5.1	0.5	0.71	0.81	1.17	1.55	1.85	2.10	2.34

Table C.1 Block 5 modelled sequence, stopes #33 #64

		MODEL GEOMETRY										σ_3 contour						
Stope Name	Sequence #	Stope Type P1	P2	P3	S1	S2	Strike length	TRUE height	HW area (m2)	Hydraulic Radius	Aspect ratio strike/height	$\sigma_3=\sigma_t$ DD (m)	σ_3=0 DD (m)	σ_3=+2MPa DD (m)	σ_3=+4MPa DD (m)	σ_3=+6MPa DD (m)	σ_3=+8MPa DD (m)	σ_3=+10MPa DD (m)
9-0-17	33		x				15	29	435	4.9	0.5	0	0.00	0.64	1.05	1.41	1.74	2.00
9-3-10	34			x			13.2	31	409.2	4.6	0.4	0.76	0.81	1.13	1.45	1.72	1.91	2.21
9-0-8	35	x					14.8	29	429.2	4.9	0.5	0	0.00	0.77	1.22	1.50	1.86	2.17
9-1-11	36					x	16.1	31	499.1	5.3	0.5	1.3	1.59	1.36	2.50	2.85	3.23	3.61
9-1-17	37			x			15	31	465	5.1	0.5	0	0.00	0.80	1.16	1.51	1.79	2.19
9-1-8	38		x				14.8	31	458.8	5.0	0.5	0.23	0.26	0.90	1.21	1.45	1.65	1.91
9-2-2	39					x	14.8	31	458.8	5.0	0.5	1.17	1.22	1.60	2.09	2.39	2.75	3.27
9-0-14	40					x	15.6	29	452.4	5.1	0.5	1.92	1.97	2.29	2.97	3.06	3.39	3.95
9-1-5	41				x		15.3	31	474.3	5.1	0.5	1.2	1.24	1.65	2.02	2.32	2.75	3.06
9-3-2	42					x	14.8	31	458.8	5.0	0.5	0.98	1.03	1.45	1.78	2.18	2.47	2.83
9-2-11	43					x	16.1	31	499.1	5.3	0.5	2.03	2.07	2.37	2.79	3.13	3.47	3.80
9-0-9	44					x	15	29	435	4.9	0.5	2.03	2.09	2.21	2.57	2.89	3.30	3.57
10-3-19	45	x					12.5	30	375	4.4	0.4	0	0.00	0.62	1.01	1.35	1.62	2.02
9-3-11	46					x	16.1	31	499.1	5.3	0.5	1.98	2.08	2.19	2.54	2.64	2.92	3.13
9-0-7	47					x	15.7	29	455.3	5.1	0.5	1.74	1.90	2.15	2.47	2.76	3.00	3.34
9-0-19	48		x				12.5	29	362.5	4.4	0.4	0	0.00	0.29	0.72	0.98	1.29	1.52
9-2-8	49		x				14.8	31	458.8	5.0	0.5	0.53	0.79	1.17	1.48	1.76	2.06	2.30
9-2-4	50				x		14.5	31	449.5	4.9	0.5	0.59	0.62	1.23	1.60	1.91	2.23	2.57
9-0-16	51					x	15.2	29	440.8	5.0	0.5	1.32	1.41	1.80	2.19	2.52	2.87	3.21
9-2-13	52				x		14.1	31	437.1	4.8	0.5	1.20	1.25	1.52	1.82	2.08	2.35	2.67
9-3-4	53				x		14.5	31	449.5	4.9	0.5	1.44	1.48	1.73	1.97	2.34	2.52	2.75
9-1-9	54					x	15	31	465	5.1	0.5	1.25	1.29	1.60	1.91	2.14	2.51	2.79
9-3-13	55				x		14.1	31	437.1	4.8	0.5	1.70	1.75	1.82	2.05	2.16	2.36	2.5
9-3-8	56			x			14.8	31	458.8	5.0	0.5	0.96	0.98	1.20	1.40	1.57	1.76	1.94
10-3-18	57					x	15.9	30	477	5.2	0.5	0.82	0.85	1.72	2.24	2.71	3.12	3.56
9-1-6	58				x		14.9	31	461.9	5.0	0.5	0.69	0.73	0.97	0.85	1.49	1.87	2.16
9-2-15	59					x	14.5	31	449.5	4.9	0.5	0.15	0.25	0.99	1.42	1.75	2.07	2.38
9-2-5	60				x		15.3	31	474.3	5.1	0.5	0.65	0.70	1.41	1.82	2.20	2.51	2.83
9-1-14	61					x	15.6	31	483.6	5.2	0.5	2.29	2.37	2.76	3.16	3.56	3.99	4.39
10-3-16	62					x	15.2	30	456	5.0	0.5	0.94	0.97	1.47	1.87	2.28	2.69	3.01
10-3-21	63	x					15	30	450	5.0	0.5	0.00	0.00	0.79	1.38	1.83	2.21	2.56
9-3-15	64			x			14.5	31	449.5	4.9	0.5	0.71	0.84	0.93	1.20	1.40	1.55	1.7

Table C.1 Block 5 modelled sequence, stopes #65 to #97

		MODEL GEOMETRY										σ_3 contour						
Stope	Sequence	Stope Type					Strike	TRUE	HW	Hydraulic	Aspect ratio	$\sigma_3=\sigma_1$	σ_3=0	σ_3=+2MPa	σ_3=+4MPa	σ_3=+6MPa	σ_3=+8MPa	σ_3=+10MPa
Name	#	P1	P2	P3	S1	S2	length	height	area (m2)	Radius	strike/height	DD (m)	DD (m)	DD (m)	DD (m)	DD (m)	DD (m)	DD (m)
9-2-9	65			x			15	31	465	5.1	0.5	1.15	1.20	1.51	1.74	2.02	2.20	2.44
9-3-5	66				x		15.3	31	474.3	5.1	0.5	1.75	1.80	2.07	2.29	2.56	2.78	3.03
9-1-7	67					x	15.7	31	486.7	5.2	0.5	1.50	1.55	1.87	2.19	2.48	2.78	3.08
9-3-9	68					x	15	31	465	5.1	0.5	1.01	1.05	1.24	1.43	1.59	1.75	1.87
9-1-19	69			x			12.5	31	387.5	4.5	0.4	0.00	0.00	0.44	0.72	0.97	1.23	1.40
9-2-17	70			x			15	31	465	5.1	0.5	0.00	0.00	0.32	0.70	1.06	1.31	1.48
9-0-21	71		x				15	29	435	4.9	0.5	0.00	0.00	0.14	0.85	1.18	1.55	1.81
9-2-6	72				x		14.9	31	461.9	5.0	0.5	1.54	1.60	1.88	2.17	2.40	2.64	3.00
9-1-16	73					x	15.2	31	471.2	5.1	0.5	2.19	2.24	2.66	3.07	3.48	3.93	4.33
9-0-18	74					x	15.9	29	461.1	5.1	0.5	2.00	2.06	2.32	2.69	3.12	3.60	4.23
9-3-17	75			x			15	31	465	5.1	0.5	0.41	0.48	0.82	0.99	1.15	1.28	1.40
9-3-6	76				x		14.9	31	461.9	5.0	0.5	1.67	1.71	1.95	2.18	2.38	2.59	2.78
10-3-20	77					x	15	30	450	5.0	0.5	1.68	1.74	2.18	2.56	2.94	3.33	3.79
9-2-14	78					x	15.6	31	483.6	5.2	0.5	2.44	2.52	2.82	3.26	3.54	3.82	4.16
9-2-7	79					x	15.7	31	486.7	5.2	0.5	2.07	2.12	2.31	2.59	2.72	3.12	3.32
9-3-14	80					x	15.6	31	483.6	5.2	0.5	0.80	0.83	1.22	1.53	1.71	1.90	2.07
9-3-7	81					x	15.7	31	486.7	5.2	0.5	1.24	1.28	1.45	1.58	1.72	1.86	2.00
10-3-22	82				x		15	30	450	5.0	0.5	0.60	0.68	1.47	1.88	2.27	2.62	2.96
9-2-19	83			x			12.5	31	387.5	4.5	0.4	0.02	0.12	0.57	0.74	0.91	1.14	1.29
9-1-21	84		x				15	31	465	5.1	0.5	0.00	0.00	0.00	0.66	0.82	1.30	1.66
9-1-18	85					x	15.9	31	492.9	5.3	0.5	0.00	0.00	0.76	1.31	1.69	2.02	2.33
9-0-20	86					x	15	29	435	4.9	0.5	0.92	0.96	1.36	1.72	2.04	2.28	2.60
9-3-19	87			x			12.5	31	387.5	4.5	0.4	0.50	0.54	0.74	0.83	1.00	1.12	1.30
9-2-16	88					x	15.2	31	471.2	5.1	0.5	0.00	0.00	0.99	1.46	1.78	2.09	2.35
9-3-16	89					x	15.2	31	471.2	5.1	0.5	0.00	0.38	1.45	1.10	1.31	1.53	1.74
9-2-21	90			x			15	31	465	5.1	0.5	0.00	0.00	0.73	1.14	1.51	1.84	2.18
9-2-18	91					x	15.9	31	492.9	5.3	0.5	1.41	1.47	1.88	2.24	2.55	2.81	3.20
9-3-18	92					x	15.9	31	492.9	5.3	0.5	1.27	1.34	1.58	1.83	2.10	2.35	2.63
9-1-20	93					x	15	31	465	5.1	0.5	0.00	0.09	0.66	1.02	1.39	1.69	2.04
9-2-20	94					x	15	31	465	5.1	0.5	0.34	0.35	1.07	1.49	1.85	2.21	2.56
9-2-22	95				x		15	31	465	5.1	0.5	0.00	0.26	0.93	1.30	1.62	2.00	2.41
9-3-21	96	x					15	31	465	5.1	0.5	0.00	0.00	0.36	0.91	1.15	1.37	1.55
9-3-20	97					x	15	31	465	5.1	0.5	0.74	0.78	1.07	1.37	1.60	1.88	2.10

Table C.2 Zone 3-1 modelled sequence, stopes #1 to #37

		MODEL GEOMETRY									σ_3 contour						
Stope Name	Sequence #	Stope Type P1	P2	P3	S1	S2	Strike length	TRUE height	HW area (m2)	Hydraulic Radius	Aspect ratio strike/height	$\sigma_3=\sigma_1$ DD (m)	σ_3=0 DD (m)	σ_3=+2MPa DD (m)	σ_3=+4MPa DD (m)	σ_3=+6MPa DD (m)	σ_3=+8MPa DD (m)	σ_3=+10MPa DD (m)
3440-32	1	x					10	30	300	3.8	0.3	0.00	0.00	0.16	0.50	0.79	0.95	1.09
3440-34	2	x					10	30	300	3.8	0.3	0.00	0.00	0.24	0.49	0.74	0.89	1.03
3440-36	3	x					10	30	300	3.8	0.3	0.00	0.00	0.25	0.54	0.71	0.86	1.02
3470-34	4		x				10	30	300	3.8	0.3	0.11	0.16	0.43	0.68	0.85	1.03	1.17
3470-32	5		x				10	30	300	3.8	0.3	0.05	0.12	0.36	0.52	0.64	0.80	0.93
3470-36	6		x				10	30	300	3.8	0.3	0.00	0.00	0.28	0.51	0.73	0.88	1.01
3440-33	7					x	10	30	300	3.8	0.3	0.86	0.89	1.10	1.30	1.53	1.71	1.91
3500-34	8			x			10	30	300	3.8	0.3	0.02	0.05	0.44	0.70	0.95	1.15	1.29
3440-35	9					x	10	30	300	3.8	0.3	0.57	0.69	0.94	1.18	1.41	1.63	1.82
3500-32	10			x			10	30	300	3.8	0.3	0.06	0.10	0.41	0.58	0.70	0.86	0.99
3470-30	11	x					10	30	300	3.8	0.3	0.00	0.00	0.37	0.61	0.76	0.96	1.09
3500-36	12			x			10	30	300	3.8	0.3	0.00	0.00	0.28	0.54	0.77	0.91	1.07
3470-33	13					x	10	30	300	3.8	0.3	1.20	1.24	1.44	1.67	1.92	2.06	2.28
3440-31	14				x		10	30	300	3.8	0.3	0.00	0.05	0.34	0.76	0.90	1.11	1.27
3500-30	15			x			10	30	300	3.8	0.3	0.00	0.04	0.37	0.58	0.75	0.88	1.02
3470-35	16					x	10	30	300	3.8	0.3	0.62	0.66	0.91	1.10	1.29	1.52	1.7
3500-28	17	x					10	30	300	3.8	0.3	0.00	0.00	0.22	0.47	0.67	0.83	0.99
3470-31	18					x	10	30	300	3.8	0.3	0.54	0.59	0.86	1.05	1.25	1.43	1.6
3530-30	19			x			10	30	300	3.8	0.3	0.00	0.00	0.27	0.47	0.63	0.78	0.92
3530-32	20		x				10	30	300	3.8	0.3	0.05	0.09	0.45	0.63	0.83	1.01	1.13
3470-29	21				x		10	30	300	3.8	0.3	0.00	0.00	0.53	0.83	1.04	1.20	1.38
3530-28	22		x				10	30	300	3.8	0.3	0.00	0.00	0.30	0.51	0.70	0.86	1.02
3530-34	23		x				8.8	30	264	3.4	0.3	0.14	0.17	0.45	0.73	0.89	1.08	1.21
3500-29	24					x	10	30	300	3.8	0.3	0.53	0.57	0.81	1.01	1.19	1.39	1.58
3380-36	25	x					9.2	26	239.2	3.4	0.4	0.00	0.00	0.24	0.53	0.79	0.93	1.15
3500-35	26					x	10	30	300	3.8	0.3	0.84	0.95	1.08	1.36	1.54	1.72	1.95
3500-31	27					x	10	30	300	3.8	0.3	0.55	0.60	0.87	1.06	1.24	1.43	1.61
3380-35	28				x		9.6	26	249.6	3.5	0.4	0.00	0.04	0.55	0.82	1.07	1.29	1.5
3500-33	29					x	10	30	300	3.8	0.3	0.59	0.63	0.90	1.10	1.31	1.49	1.7
3500-26	30	x					10	30	300	3.8	0.3	0.00	0.00	0.00	0.20	0.57	0.77	0.95
3410-36	31	x					10	26	260	3.6	0.4	0.00	0.20	0.51	0.79	0.99	1.18	1.36
3530-33	32					x	10	30	300	3.8	0.3	0.94	1.00	1.29	1.49	1.72	2.02	2.25
3380-38	33	x					10	30	300	3.8	0.3	0.00	0.00	0.32	0.55	0.73	0.91	1.05
3530-26	34		x				10	30	300	3.8	0.3	0.00	0.00	0.30	0.51	0.68	0.85	1.02
3380-34	35				x		10	26	260	3.6	0.4	0.02	0.16	0.48	0.67	0.85	1.01	1.17
3410-38	36		x				10	30	300	3.8	0.3	0.00	0.00	0.29	0.62	0.85	1.01	1.19
3530-24	37	x					7.7	30	231	3.1	0.3	0.00	0.00	0.00	0.00	0.20	0.38	0.47

Table C.2 Zone 3-1 modelled sequence, stopes #38 to #75

		MODEL GEOMETRY										σ_3 contour					
Stope Name	Sequence #	Stope Type P1	P2	P3	S1	S2	Strike length	TRUE height	HW area (m2)	Hydraulic Radius	Aspect ratio strike/height	$\sigma_3=\sigma_1$ DD (m)	σ_3=0 DD (m)	σ_3=+2MPa DD (m)	σ_3=+4MPa DD (m)	σ_3=+6MPa DD (m)	σ_3=+8MPa DD (m)	σ_3=+10MPa DD (m)
3560-26	38			x			10	30	300	3.8	0.3	0.00	0.00	0.36	0.58	0.77	0.92	1.09
3410-35	39			x			10	26	260	3.6	0.4	0.16	0.39	0.71	0.95	1.12	1.32	1.46
3560-28	40			x			10	30	300	3.8	0.3	0.00	0.00	0.44	0.60	0.75	0.91	1.05
3380-40	41	x					10	30	300	3.8	0.3	0.00	0.00	0.28	0.55	0.74	0.93	1.08
3560-24	42			x			10	30	300	3.8	0.3	0.00	0.00	0.38	0.59	0.79	0.95	1.1
3380-33	43				x		8.4	26	218.4	3.2	0.3	0.14	0.29	0.55	0.74	0.94	1.05	1.2
3380-37	44					x	11	30	330	4.0	0.4	0.55	0.71	0.86	0.98	1.25	1.33	1.59
3410-34	45				x		10	26	260	3.6	0.4	0.67	0.75	0.88	1.04	1.20	1.41	1.56
3530-27	46					x	10	30	300	3.8	0.3	0.74	0.81	1.04	1.22	1.41	1.59	1.8
3410-40	47		x				9.2	30	276	3.5	0.3	0.00	0.00	0.00	0.29	0.47	0.65	0.79
3590-24	48			x			10	30	300	3.8	0.3	0.00	0.00	0.36	0.56	0.74	0.93	1.08
3560-22	49	x					10	30	300	3.8	0.3	0.00	0.00	0.10	0.47	0.66	0.84	1.01
3410-37	50					x	10	30	300	3.8	0.3	0.54	0.58	0.88	1.10	1.31	1.52	1.73
3530-25	51					x	10	30	300	3.8	0.3	0.42	0.47	0.71	0.94	1.07	1.27	1.44
3590-19	52	x					10	30	300	3.8	0.3	0.00	0.00	0.05	0.39	0.59	0.74	0.91
3380-39	53					x	10	30	300	3.8	0.3	0.54	0.59	0.94	1.10	1.27	1.47	1.72
3530-31	54					x	10	30	300	3.8	0.3	0.95	1.01	1.19	1.41	1.61	1.83	2.06
3590-28	55			x			10	30	300	3.8	0.3	0.00	0.00	0.15	0.55	0.75	0.91	1.08
3440-37	56				x		10	30	300	3.8	0.3	0.83	0.96	1.09	1.28	1.42	1.64	1.77
3560-21	57				x		10	30	300	3.8	0.3	0.00	0.00	0.57	0.79	0.99	1.17	1.35
3410-33	58				x		10	26	260	3.6	0.4	0.36	0.51	0.75	0.92	1.12	1.31	1.51
3590-22	59		x				10	30	300	3.8	0.3	0.00	0.00	0.30	0.51	0.66	0.82	0.96
3590-26	60		x				10	30	300	3.8	0.3	0.00	0.00	0.42	0.65	0.80	0.95	1.1
3410-39	61					x	10	30	300	3.8	0.3	0.35	0.57	0.80	1.03	1.22	1.39	1.61
3560-32	62	x					10	30	300	3.8	0.3	0.00	0.00	0.17	0.65	0.84	1.00	1.17
3530-29	63					x	10	30	300	3.8	0.3	0.81	0.86	1.04	1.21	1.40	1.58	1.8
3590-20	64				x		10	30	300	3.8	0.3	0.22	0.30	0.76	0.94	1.14	1.33	1.49
3380-41	65				x		10	30	300	3.8	0.3	0.00	0.00	0.51	0.91	1.02	1.38	1.42
3560-23	66					x	10	30	300	3.8	0.3	0.68	0.74	0.92	1.12	1.31	1.52	1.7
3560-27	67					x	10	30	300	3.8	0.3	0.73	0.78	0.96	1.14	1.32	1.49	1.67
3560-25	68					x	10	30	300	3.8	0.3	0.60	0.64	0.84	1.00	1.15	1.34	1.48
3560-31	69				x		10	30	300	3.8	0.3	0.65	0.70	0.85	1.00	1.17	1.33	1.46
3590-23	70					x	10	30	300	3.8	0.3	0.70	0.76	0.98	1.19	1.36	1.57	1.78
3590-27	71					x	10	30	300	3.8	0.3	0.75	0.79	1.00	1.19	1.38	1.58	1.79
3590-21	72					x	10	30	300	3.8	0.3	0.35	0.45	0.82	1.01	1.20	1.38	1.58
3410-32	73				x		7.8	26	202.8	3.0	0.3	0.22	0.24	0.30	0.35	0.42	0.48	0.53
3560-29	74				x		10	30	300	3.8	0.3	0.71	0.75	0.92	1.06	1.22	1.36	1.53
3590-25	75					x	10	30	300	3.8	0.3	0.48	0.58	0.82	1.01	1.16	1.33	1.51